ROLE OF BK CHANNELS IN HIPPOCAMPAL SYNAPTIC PLASTICITY DURING NEONATAL DEVELOPMENT

Tesis entregada a
LA UNIVERSIDAD DE VALPARAÍSO

en Cumplimiento Parcial de los requisitos para optar al grado de
Doctor en Ciencias con Mención en Neurociencia

Facultad De Ciencias

Por
Carlos Felipe Ancatén González
Junio, 2025

Dirigida por: Dr. Andrés E. Chávez Navarrete

FACULTAD DE CIENCIAS

UNIVERSIDAD DE VALPARAÍSO

I N F O R M E D E A P R O B A C I O N

T E S I S D E D O C T O R A D O

Se informa a la Facultad de Ciencias que la Tesis de Doctorado presentada por:

CARLOS FELIPE ANCATÉN GONZÁLEZ

Ha sido aprobada por la comisión de Evaluación de la tesis como requisito para optar al grado de Doctor en Ciencias con mención en Neurociencia, en el examen de Defensa de Tesis rendido el día 26 del Mes de junio de 2025.

Director/a de Tesis:

Dr. Andrés E. Chávez

Comisión de Evaluación de la Tesis

Dr. Ramon Latorre

Dra. Chiayu Q Chiu

Dr. Pablo E. Castillo

TABLE OF CONTENTS

ii. **DEDICATION**

iii. **ACKNOWLEDGEMENTS**

1. **SUMMARY……..6**
   - **1.1 RESUMEN……7**
2. **INTRODUCTION……8**
   - **2.1 Hippocampus……10**
   - **2.2 Long-term synaptic plasticity……10**
   - **2.3 Lipid signaling in synaptic plasticity……11**
   - **2.4 BK channels in synaptic function and plasticity……12**
3. **HYPOTHESIS & OBJECTIVES……13**
4. **MATERIALS AND METHODS……14**
5. **RESULTS……17**
   - **5.1 BK channels mediate a presynaptic form of mGluR-LTD in the neonatal hippocampus……17**
   - **5.2 BK-mediated LTD during hippocampal development and its underlying Mechanisms……44**
6. **DISCUSSION……64**
7. **Supplementary Figures and tables……69**
8. **CONCLUSIONS……74**
9. **REFERENCES……75**

APPENDIX……93

DEDICATION

To God and my family.

ACKNOWLEDGEMENTS

I would like to thank all the people who accompanied me during this process and made the development of my thesis possible.

I would also like to especially thank my tutor Dr Andrés Chávez for having me into his laboratory and accompanying me from the beginning of my career as a scientist, generously sharing his knowledge and encouraging me to continue growing on this path. For all his support I will always be thankful.

To my lab colleagues, especially to Rodrigo Meza, Alejandro Alcaíno and Sebastián Estay, for sharing their knowledge and patiently help me when I required it.

To Dr Mario Penzo for kindly allowing me to stay in his lab for 5 months supporting my career development and for fueling my desire to learn more. Also I would like to thank the members of Penzo´s Lab in National Institutes of Health, USA, for their support and help.

To Dra Chiayu Chiu, Dr Pablo Castillo and Dr Ramón Latorre for their helpful commentaries and discussions about our results that allow to strength our work and achieve the publication of part of my thesis. I consider each of one an inspiration to follow their careers and I deeply admire them as scientists, so I feel fortunate to have shared scientific discussion with all of you.

To the Doctoral Program of Science, mention in Neuroscience belonging to University of Valparaíso, especially to the director Dra Ana María Cárdenas for all the support during all these years.

To CINV for its support and help to assist to different meetings to share my results.

1. SUMMARY

Calcium- and voltage-activated potassium channels (BK) can control neuronal function, but their functional relevance in activity-dependent changes of synaptic function remains elusive. In this thesis work, we discuss and present experimental evidence demonstrating that BK channels participate in a form of synaptic plasticity during early stage of hippocampal development in mice. At excitatory Schaffer collateral inputs to CA1 pyramidal neuron (SCh-CA1 synapse), we report that repetitive low-frequency stimulation activates BK channels, but not TRPV1, through 12(S)HPETE, an arachidonic acid metabolite, produced downstream of postsynaptic metabotropic glutamate receptors (mGluRs) to trigger long-term depression (LTD) in hippocampal slices from P7–P10 mice. Notably, activation of BK channels is subunit specific, as paxilline but not iberiotoxin blocked mGluR-LTD. Moreover, 12(S) HPETE does not change the electrophysiological properties of the BK channel when the BKα subunit is expressed alone but increases the channel open probability when the BKα is co-expressed with the β4-subunit. The activation of $BK_{\beta4}$ channels is only required for the induction but not the expression of LTD, a form of plasticity that also involve calcineurin and protein synthesis. This form of neonatal BK-mediated plasticity is absent in mature animals (P20-P30), probably due to changes in BK subunit composition. Finally, we also present evidence that $BK_{\beta4}$ channel-mediated LTD in neonatal hippocampus coexists with another form of presynaptic LTD (CB1-dependent LTD) at SCh-CA1 synapse in early stage of the development, whose mechanism also changes as hippocampal synapse development continues. Thus, our findings reveal different cellular mechanisms that regulate synaptic strength during postnatal development at central synapses, highlighting the contribution of BK channels to the activity dependent regulation of synaptic efficacy and its activation by lipid messengers to regulate synaptic function in a long-term manner at SCh-CA1 synapse in the neonatal hippocampus.

1.1 RESUMEN

Los canales de potasio activados por calcio y voltaje (BK) pueden controlar la función neuronal, pero su relevancia funcional en cambios que dependen de actividad de la función sináptica permanece inconclusa. En esta tesis, nosotros discutimos y presentamos evidencia experimental que demuestra que los canales BK participan en una forma de plasticidad sináptica durante la etapa temprana del desarrollo de hipocampo en ratones. En las entradas excitatorias de las colaterales de Schaffer a las neuronas piramidales de CA1 (Sch-CA1), nosotros reportamos que la estimulación a baja frecuencia repetitiva activa a los canales BK, pero no los canales TRPV1, a través de 12(S)HPETE, un metabolito derivado del ácido araquidónico, producido río debajo de los receptores metabotrópicos de glutamato (mGluRs) para gatillar la depresión a largo plazo (LTD) en la sinapsis CA3-CA1 en rebanadas de hipocampo de ratones de P7-P10 de edad, pero no animales maduros (P20-P30). De manera notable, la activación de los canales BK es específica de subunidad, ya que la paxilina, pero no la iberiotoxina, bloquearon la depresión mediada por mGluRs. Además, 12(S)HPETE no cambia las propiedades electrofisiológicas del canal BK cuando la subunidad BKα es expresada sola, pero incrementa la probabilidad de apertura del canal cuando la BKα es co-expresada con la subunidad β4. La activación de los canales BK b4 es solo requerida para la inducción, pero no para la expresión de la LTD, una forma de plasticidad que también involucra la activación de calcineurina y síntesis de proteínas. Finalmente, nosotros presentamos evidencia que la LTD mediada por los canales BK b4 coexiste con otra forma de LTD presináptica (LTD dependiente de CB1) en la sinapsis Sch-CA1 en etapa temprana de desarrollo, cuyo mecanismo también cambia en cuanto el desarrollo sináptico hipocampal continúa. Así, nuestros hallazgos revelan diferentes mecanismos celulares que regulan la fuerza sináptica durante el desarrollo posnatal en las sinapsis centrales, destacando la contribución de los canales BK a la regulación dependiente de la actividad de la eficacia sináptica y su activación por mensajeros lipídicos para regular la función sináptica a largo plazo en la sinapsis Sch-CA1 del hipocampo neonatal.

2. INTRODUCTION

Neuronal communication is the process by which neurons transmit information within the nervous system. It involves both electrical and chemical signaling mechanisms, allowing for complex coordination of bodily functions and cognitive processes. Typically, neurons generate electrical impulses known as action potential when their internal charge surpasses a threshold. These impulses travel along the axon, a long fiber extending from the neuron, toward the axon terminal. At the synapse, where two neurons communicate to each other, action potential triggers the release of neurotransmitters from vesicles in the presynaptic neuron. Neurotransmitters cross the synaptic cleft and bind to receptors on the postsynaptic neuron, eliciting either excitatory or inhibitory responses depending on the neurotransmitter and receptor type activated. Neurotransmitters and/or neuromodulators could also be released from postsynaptic neurons to presynaptic terminals in a process known as retrograde signaling (Figure 1), a bidirectional mechanism of modulation of synaptic transmission that influence neuronal development, plasticity, and brain function (Regehr et al., 2009). One of the best-characterized retrograde signaling systems in the brain is those mediated by lipid derivates including endovanilloids and endocannabinoids (eCBs), that by activating different ion channels and receptors regulate synaptic efficacy at both excitatory and inhibitory synapses (Castillo, 2012; Maki & Poo, 1998; Winters & Vaughan, 2021). In this thesis work, we will focus on the role of calcium- and voltage-activated potassium channels (BK) in controlling synaptic transmission and plasticity at excitatory Schaffer collateral inputs to CA1 pyramidal cells (Sch-CA1 synapse) during hippocampal development. As these ion channels can be activated by some lipid derivates (Hoshi et al., 2013; Sun et al., 2007; Vaithianathan et al., 2008), we will test the possibility that BK channels could be part of a retrograde signaling that modulate synaptic strength at Sch-CA1 synapse in the hippocampus. In addition, we will also test whether another form of lipophilic retrograde signal mediated by eCB signaling could also regulate synaptic function by activating BK channels at hippocampal synapses (Y. Li, Zhang, et al., 2019; Sade et al., 2006). Finally, we present some additional evidence, from our collaborative work, regarding different mechanisms and signaling pathways that can regulate synaptic efficacy at central synapse (see annexes).

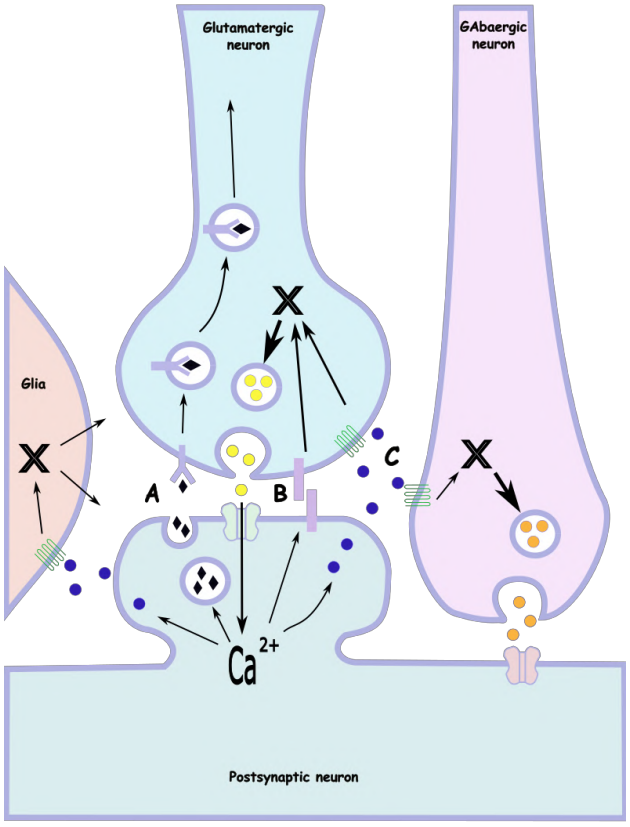


Figure 1. Schematic diagram of neuronal communication. *Excitatory (e.g,. glutamate, yellow circles) or inhibitory (e.g,. GABA or glycine, orange circles) neurotransmitters released from presynaptic terminals diffuse into the synaptic cleft and activate synaptic receptors in the postsynaptic neuron. There, an increase in calcium (Ca^{2+}) concentration occurs after the activation of excitatory postsynaptic receptors that triggers the production of retrograde. These retrograde messengers are released back into the synaptic cleft to modulate homosynaptic and heterosynaptic synapses as well as glial cells (represented by X) and thus, profoundly impact neurotransmitter release from presynaptic terminals. Three types of retrograde signaling have been described: A) exocytic secretion of soluble factors, B) modulation of presynaptic proteins through connection with postsynaptic proteins, and C) production of membrane-permeant diffusible factors* (Castillo, 2012; Maki & Poo, 1998).

2.1 Hippocampus

The hippocampus, a key brain structure involved in cognitive processing such as episodic memory, spatial function and navigation (Bird & Burgess, 2008; Rolls & Treves, 2024), is composed by a characteristic anatomical circuitry known as the "trisynaptic loop". The entorhinal cortex provides the major cortical input to the hippocampus through its strongest projection via the perforant path to the dentate gyrus (DG). Neurons from DG project to the CA3 region via the mossy fiber pathway. Then, CA3 pyramidal neurons project to the CA1 region via the Schaffer Collateral (SC) pathway. Finally, CA1 pyramidal neurons project back to the entorhinal cortex closing the loop (Knierim, 2015). Interestingly, CA3 pyramidal neurons send collaterals that connect with other CA3 neurons, making a close loop circuitry (Rebola et al., 2017). The hippocampus is known to be vulnerable to adverse environmental factors such as hypoxia, stress, toxins and malnutrition, and plays relevant role in preterm children and those exposed to alcohol, toxins and drugs during fetal development (Y. Li, Shen, et al., 2019). Interestingly, structural and functional alterations in hippocampus have been related to neurodevelopmental disorders such as autism spectrum disorder (Banker et al., 2021), schizophrenia (Lieberman et al., 2018), and Rett syndrome (Baj et al., 2014), where disfunctions in glutamatergic synapses and proteins involved in synaptic transmission and plasticity has been described (Moretto et al., 2018; Zoghbi & Bear, 2012).

2.2 Long-term synaptic plasticity

Plasticity of synaptic transmission contributes to the remodeling of neuronal circuits and memory formation (Malenka & Bear, 2004), and it corresponds to the capacity of the neural activity generated by an experience to modify the neural circuit function and thus modulate a plethora of behaviors (Citri & Malenka, 2008). These modifications can occur in a small-time window from millisecond to a few minutes (short-term plasticity) or during longer periods from minutes to hours and days (long-term plasticity). Depending on the synapse types, brain structures and developmental stage diverse forms of long-term synaptic plasticity mechanisms have been described, but they can be broadly divided according to the direction of the synaptic strength change. When synaptic transmission is increased, the process is known as long-term potentiation (LTP), whereas a depression of synaptic transmission is called long-term depression (LTD). Although the mechanisms of LTD are diverse, a common cellular mechanism for its generation involves the participation of group I metabotropic glutamate receptors (mGluR-I) (Bellone et al., 2008; Heifets & Castillo, 2009; Lüscher & Huber, 2010),

whose activation can induce presynaptic and/or postsynaptic changes. For instance, a form of LTD that depends on the activation of mGluR-I receptors (mGluR-LTD) has been described in the hippocampus of neonatal mice (Bolshakov & Siegelbaum, 1994, 1995a). Neonatal mGluR-LTD has been shown to involve the activity of the enzyme lipoxygenase 12 (LO-12) to produce an arachidonic acid metabolite, known as 12(S)HPETE (Feinmark et al., 2003). Once produced, 12(S)HPETE reportedly trigger a long-term decrease in excitatory neurotransmitter release at Schaffer collateral to CA1 synapse (Feinmark et al., 2003). *However, the exact mechanism by which 12(S)HPETE induces this decrease in neurotransmitter release remains unknown and form part of the main Aim of this thesis work.*

2.3 Lipid signaling in synaptic plasticity

Arachidonic acid (AA) derivatives, including endocannabinoids (eCBs) and endovanilloids, play diverse roles in fine-tuning synaptic strength via rapid ion channel effects and orchestrating long-term plasticity through receptor-mediated signaling (Drapeau et al., 1990; Volterra et al., 1992; Williams et al., 1989). For instance, eCBs (e.g 2-AG and AEA) by regulating short- and long-term processes at both excitatory and inhibitory synapses is considered a powerful regulator of synaptic function throughout the brain (Castillo et al., 2012; Heifets & Castillo, 2009; Ohno-Shosaku & Kano, 2014). Typically, eCBs retrogradely activate type 1 cannabinoid receptors (CB1R) to mediate changes in the synaptic strength (Castillo et al., 2012), but the eCB/endovanilloid AEA could also change synaptic efficacy by activating the transient receptor potential vanilloid 1 (TRPV1) channels (Chávez et al., 2010). Likewise, endovanilloids (e.g. AEA, NADA) also play a significant role in modulating synaptic function in the central nervous system, often in concert or opposition to eCB signaling (Jamieson et al., 2022; Lee et al., 2015; Marinelli et al., 2007). Indeed, these lipophilic signal molecules represent one of the main ligands that activate TRP channels, including TRPV channels (Taberner et al., 2015; Watanabe et al., 2003) to increase or decrease synaptic efficacy throughout the brain (Chávez et al., 2010; Edwards, 2014; Grueter et al., 2010; Marinelli et al., 2007; Meza et al., 2022; Puente et al., 2011). Interestingly, a presynaptic mechanism of long-term depression at CA3 to CA1 interneuron synapse reportedly requires the activation of TRPV1 channels by the endovanilloid 12(S)HPETE to depress excitatory synaptic transmission (Gibson et al., 2008). However, *whether TRPV1 channels are involved in the neonatal LTD that occurs between CA3 terminals and CA1 pyramidal neurons is unknown and form part of the specific objective 1.*

Aside from their effect on TRP channels, lipid derivatives have been identified as potential modulators of the activity of voltage-gated ion channels, such as calcium and potassium channels (Carta et al., 2014; Huang et al., 1992). Interestingly, large-conductance voltage-gated calcium and potassium channels (BK) have been reported to be molecular targets of arachidonic acid and its metabolites in vascular and heterologous systems (Martín et al., 2014; Sun et al., 2007; Zink et al., 2001). *However, this interaction has not been described at central synapses and will be evaluated extensively in this thesis work.*

2.4 BK channels in synaptic function and plasticity

BK channels are activated by an increase in intracellular calcium and a change in membrane potential and allow the efflux of potassium ions with a high conductance (Carrasquel-Ursulaez et al., 2018; Latorre et al., 2017; Latorre & Brauchi, 2006). These channels are ubiquitously expressed throughout the body playing important roles in several physiological processes, such as regulation of blood flow, renal excretion, muscle contraction, heart rate, and hearing, among others (Latorre et al., 2017). BK channels are also abundantly expressed in both neurons and glial cells throughout the brain (Hayashi et al., 2016; Hayashi & Nakanishi, 2015; Kang et al., 1996; Niday & Bean, 2021; Ou et al., 2009; Pratt et al., 2017; Ransom et al., 2002; Sailer et al., 2006; Salzmann et al., 2010; Seidel et al., 2011; Y. Zhang et al., 2021). There, BK channels are strategically located on both membrane surfaces and intracellular compartments to regulate neuron excitability and synaptic communication, but their role in activity-dependent modulation of synaptic function remain poorly understood as we extensively discuss previously (For review see Ancatén-González et al., 2023 in Appendix).

BK channels are composed of a fundamental subunit called α subunit, which corresponds to a seven (S0-S6) transmembrane structure (Latorre et al., 2017). This α subunit can be accompanied by auxiliary subunits that modulate the activity of the channel. Two main groups of auxiliary subunits have been described until now: gamma and beta subunits (Q. Li & Yan, 2016). β-subunits are the most studied, each one corresponding to a two transmembrane structure connected by a large extracellular loop and classified into 4 subtypes: β1, β2, β3 and β4. All the b subunits modify the BK channel gating and pharmacology (Ancatén-González et al., 2023). β2 and β4 are the most expressed subunits in the CNS (Contet et al., 2016). β1, β2 and β4 increase Ca^{+2} sensitivity by stabilizing the voltage sensor in the active conformation and slowing down the activation and deactivation kinetics

(Ancatén-González et al., 2023). Additionally, β2 induces a fast and complete inactivation. The presence of β4 shifts the conductance-voltage curves leftward at all internal Ca^{+2} concentration compared to BK/α channel. Interestingly, β2 is sensitive to the BK channel blocker iberiotoxin (IBTX) (B. Wang et al., 2014), whereas b4 is IBTX-resistant (Latorre et al., 2017). However, all BK channels can be blocked by the tremorgenic fungal alkaloid paxilline (PAX) (Y. Zhou & Lingle, 2014). While the contribution BK channels subunits to regulate neuronal excitability has been reported (Brenner et al., 2005; Whitmire et al., 2017), whether and how these subunits participate in synaptic function and plasticity remains unclear (For review see Ancatén-González et al., 2023) and will be evaluated *in specific objective 1.*

3. HYPOTHESIS & OBJECTIVES

3.1 HYPOTHESIS

BK channels are involved in mGluR-dependent long-term synaptic depression in neonatal hippocampus of mouse.

3.2 Main Objective

To determine the role of BK channels in the mechanisms underlying neonatal long-term depression at the Schaffer collateral to CA1 synapses in the mouse hippocampus.

3.3 Specific Objectives

- To evaluate if BK channels are required for mGluR-LTD at excitatory synapses in the neonatal hippocampal of mice.
- To identify the nature of BK channels involved in the regulation of synaptic strength in the neonatal hippocampal of mice.
- To study the cellular mechanisms involved in BK channel-mediated plasticity in the neonatal hippocampal of mice.
- To determine developmental changes in BK channels-mediated plasticity in the hippocampus of mice.

4. MATERIALS AND METHODS

Animals

Wild-type (WT) and TRPV1 null mice (TRPV1−/−) were raised in the animal facility of the Universidad de Valparaiso and held at 20 to 25 °C under a 12-h light/dark cycle with water and food *ad libitum*. Animal handling and use followed a protocol approved by the bioethics committee of the Universidad de Valparaiso (CBC39/2022), in accordance with the bioethics and biosafety regulation of the Chilean Research Council (CONICYT).

Hippocampal Slice Electrophysiology.

Acute transverse hippocampal slices (400 μm thick) were prepared from Postnatal day (P) 7 to P13 mice of either gender as previously described (Chávez et al., 2010, 2014). Briefly, hippocampi were isolated and cutting using a DKT or Leica TS1200 vibratome in a solution containing the following (in mM): 215 sucrose, 2.5 KCl, 26 $NaHCO_3$, 1.6 NaH_2PO_4, 1 $CaCl_2$, 4 $MgCl_2$, 4 $MgSO_4$, and 20 glucose. After 30-min recovery, slices were incubated in an artificial CSF (ACSF) recording solution containing the following (in mM): 124 NaCl, 2.5 KCl, 26 $NaHCO_3$, 1 NaH_2PO_4, 2.5 $CaCl_2$, 1.3 $MgSO_4$, and 10 glucose equilibrated with 95% O_2/5% CO_2, pH 7.4. Slices were incubated for 30 min before recordings. All experiments, except where indicated, were performed at 28 ± 1 °C in a submersion-type recording chamber perfused at 1 to 2 mL/min rate with ACSF supplemented with the $GABA_A$ receptor antagonist picrotoxin (PTX; 50 μM). Extracellular field potentials (fEPSPs) were recorded with a patch pipette filled with 1 mM NaCl and placed in the CA1 stratum radiatum (100 μm deep). Whole-cell voltage-clamp recordings (Multiclamp 700B Molecular Devices, USA) were made from CA1 pyramidal neurons voltage-clamped at −60 mV using patch-type pipette electrodes (3 to 4 M) containing the following intracellular solution (in mM): 131 Cs-gluconate, 8 NaCl, 1 $CaCl_2$, 10 EGTA, 10 glucose, 10 HEPES, pH 7.2, and 292 mmol/kg osmolality. For current clamp experiments, CA1 pyramidal neurons were recorded using a KCl-based intracellular solution (in mM): 130 KCl, 5 NaCl, 1 $MgCl_2$, 0.2 EGTA, 10 HEPES, 2 MgATP, and 0.1 NaGTP (adjusted to pH 7.2 with KOH). fEPSPs and EPSCs were evoked by stimulating Schaffer collateral inputs with a monopolar electrode filled with ACSF and positioned ~100 to 150 μm away from the recording pipette. Two pulses (100 ms interstimulus interval) were used to calculate PPR that was defined as the ratio of the slope or amplitude of the second EPSP/EPSC to the slope or amplitude of the first EPSP/EPSC, respectively.

The coefficient of variation (1/CV) was calculated as the squared mean EPSP/ EPSC slope/amplitude divided by EPSP/EPSC variance. Both PPR and 1/CV were calculated 10 min before and 15 to 20 min after application of the LTD induction protocol. mGluR-LTD was evoked using a standard low-frequency stimulation (5 Hz, 900 pulses, 3 min) as previously described (Feinmark et al., 2003) or by bath application of 50 mM DHPG, a specific mGluR agonist. LFS-or DHPH-induced LTD was typically induced after 10 min of stable baseline and the magnitude of mGluR-LTD was compared 30 to 40 min after LTD protocol in the absence or presence of the pharmacological agents. Other LFS protocols including LFS at 1 Hz (900 pulses, 15 minutes), 50 Hz (900 pulses, 18 seconds) as well as high frequency stimulation (100 Hz, 100 pulses, 1 second) repeated twice (20 seconds apart) and paired-pulses LFS (PP-LFS) consisted of two stimuli separated by 50 ms delivered during 15 minutes at 1 Hz 900 times were also used. In some experiments (Fig. 4*A*), puff application of L-glutamate (1 mM, 25 ms, 1 to 2 PSI bar) onto CA1 pyramidal neurons was delivered while neurons were voltage clamped at −60 mV. Reagents were obtained from Sigma, Tocris, and Ascent Scientific, prepared in stock solutions (water or DMSO), and added to the ACSF as needed. Total DMSO in the ACSF was maintained less than 0.01%. For whole cell experiments, series resistance (range, 8 to 12 $M\Omega$) was monitored throughout the experiment with a 5 mV, 80 ms voltage step, and cells that exhibited significant change in series resistance (>20%) were excluded from analysis. Data were elicited at 15 to 20-s intervals, filtered at 2.2 kHz, and acquired at 10 kHz using a custom-made routine written in Igor Pro 6.37 (WaveMetrics, Portland, OR), whereas statistical comparisons were made using paired Student's *t* test at $P < 0.05$ significance level, using Origin 8.5 Pro software (OriginLab).

Channel Expression and Recordings

BK channels were expressed in *X. laevis* oocytes. The cDNA coding for the WT human BK _ -subunit (Gen bank U11058), the human β 2-subunit (Gen bank AF099137) without inactivation domain (β 2IR) (Wallner et al., 1999) and β 4-subunit (Gen Bank AF160967) were provided by L. Toro (University of California, Los Angeles, CA). The mRNA was prepared in vitro by using the mMESSAGE mMACHINE (Ambion) kit. The oocytes were injected with 50 ng of mRNA and incubated in an ND96 solution (96 mM NaCl, 2 mM KCl, 1.8 mM CaCl2, 1 mM MgCl2, and 5 mM HEPES, pH adjusted to 7.4 with NaOH) at 18 °C for 3 to 5 d before electrophysiological recordings. All the recordings were acquired by using the patch-clamp technique in the inside-out configuration. Data were acquired with an Axopatch 200B (Molecular Devices) amplifier and the Clampex 10 (Molecular Devices) acquisition software. Both, the voltage command, and current output were filtered at 10 kHz with

an 8-pole Bessel low-pass filter (Frequency Devices). Current signals were sampled with a 16-bit A/D converter (Digidata 1550B; Molecular Devices), using a sampling rate of 500 kHz. Unless otherwise stated, linear membrane capacitance and leak subtraction were performed based on a P/-8 protocol (Armstrong & Bezanilla, 1973) Borosilicate capillary glasses (1B150F-4, World Precision Instruments) were pulled in a horizontal pipette puller (Sutter Instruments). After fire-polishing, pipette resistance was typically 1 to 2 M Ω. An agar bridge with Cl-as the main anion was used as the ground electrode. All experiments were performed at room temperature (18 to 20 °C). Potassium currents (IK) were elicited by 10-ms voltage steps of 10 mV, except for $\alpha + \beta$2IR or $\alpha + \beta$4 channel currents, that were elicited by 40-ms pulse durations. The holding voltage was -100 mV for all channels, and the final voltage was 300 mV. The pipette and bath solutions were almost the same and typically contained 110 mM KOH, 10 mM HEPES, and 5 mM EGTA (free Ca^{2+} ~0.8 nM) (Cox et al., 1997), while the pipette external solution contained extra 2 mM MgCl2. The pH for both cases was adjusted to 7.4 with about 108 mM $HMeSO_3$. For test solutions using Ca^{2+} (3 μ M), $CaCl_2$ was added to reach the desired free [Ca^{2+}], and 2 mM EGTA was used as calcium buffer. Free calcium concentration was estimated using the WinMaxChelator Software and checked with a Ca2+-electrode (Hanna Instruments).

Data Analysis. For ionic current experiments, the instantaneous $I_{tail,i}(V)$ data for each *i* experiment were fitted by using a Boltzmann function,

$$I_{tail,i}(V) = \frac{I_{tail,i,max}}{1 + e^{\left(\frac{-z\delta F(V - V_{h,i})}{RT}\right)}}(X),$$

where $I_{tail,max}$ is the maximum tail current, $z\delta$ is the voltage dependency for channel activation, V_h is the half-activation voltage, *T* is the absolute temperature (294 K), *F* is the Faraday's constant, and *R* is the universal gas constant. The best values for $I_{tail,max}$, V_h, and $z\delta$ were determined by using the Matlab´s function *lsqnonlin*. The averaged half activation voltage ($< V_h >$) and the averaged voltage dependency ($< z\delta >$) were reported as mean ± SEM of the *n* experiments. Each individual $I_{tail,i}(V)$ curve was normalized by dividing by its specific $I_{tail,i,max}$ value and then aligned by shifting along the voltage axis by ($< V_h > - V_{h,i}$). A further shift of the $I_{tail,i}(V)$ curves was done by rounding each voltage value to the nearest ten. This procedure allowed generating an averaged $I_{tail,i}(V)$ curve with a voltage dependence representative of the n experiments (Horrigan & Aldrich, 2002).

5. RESULTS

This section describes some of the experiments carried out to address the different unknown aspects of BK channel's contribution to activity-dependent changes on synaptic efficacy in the hippocampus of mice during postnatal development. Most of the data shown below has not yet been published but since it is a follow-up from our recently published article (Ancatén-González et al., 2025; Appendix), in the next section this article is included, and the remaining results were prepared based on future publication.

5.1 BK channels mediate a presynaptic form of mGluR-LTD in the neonatal hippocampus

Summary

Presynaptic BK channels can control transmitter release, but their functional relevance in activity-dependent changes of synaptic function remains elusive. Here, we report that repetitive low-frequency stimulation retrogradely activates presynaptic BK channels through 12(S)HPETE, an arachidonic acid metabolite, produced downstream of postsynaptic metabotropic glutamate receptors (mGluRs) to trigger long-term depression (LTD) at CA3‑CA1 synapses in hippocampal slices from P7‑P10 mice. Activation of BK channels is subunit specific, as paxilline but not iberiotoxin blocked mGluR-LTD and 12(S)HPETE does not change the electrophysiological properties of the BK channel when the BK α subunit is expressed alone but increases the channel open probability when the BK α is co-expressed with the β 4-subunit. Our findings reveal a previously unknown interaction between 12(S)HPETE and BK channels to regulate synaptic strength at central synapses and increase our understanding of the mechanisms underlying mGluR-LTD in neonatal hippocampus that likely contribute to circuit maturation necessary for the learning process.

Introduction

Activity-dependent long-term depression (LTD) of excitatory synaptic strength contributes to circuit remodeling and memory formation. Although with varying mechanisms depending upon brain region and developmental progress, a common cellular mechanism for LTD is the reliance on postsynaptic activation of group I metabotropic glutamate receptors (mGluRs) to induce either pre- or postsynaptic forms of mGluR-LTD (Lüscher & Huber, 2010). In the hippocampus, neonatal LTD is

known to require mGluRs to subsequently generate a lipid-derived metabolite from arachidonic acid, known as 12(S)HPETE. Once produced, 12(S)HPETE travels retrogradely to the CA3 axon terminal to suppress glutamate release onto CA1 pyramidal neurons in a long-term manner (Bolshakov & Siegelbaum, 1994, 1995b; Feinmark et al., 2003). However, the precise downstream targets of 12(S)HPETE at presynaptic sites involved in this form of mGluR-LTD remain elusive.

Lipid derivates, including the lipoxygenase-derived 12(S)HPETE, represent one of the primary activating ligands of TRP channels (Hardie, 2007; Taberner et al., 2015). For instance, 12(S)HPETE-dependent LTD in the mature hippocampus has been reported at glutamatergic synapses onto CA1 inhibitory interneurons. This form of plasticity involves the activation of the presynaptic transient potential vanilloid 1 receptor (TRPV1) (Gibson et al., 2008). Whether TRPV1 channels are also a key player in neonatal mGluR-LTD at CA3-CA1 excitatory synapses remains unknown. Apart from their action on TRP receptors, lipid derivates are also known to modulate synaptic efficacy by directly acting on voltage-gated ion channels (Boland & Drzewiecki, 2008), including calcium (Roberts-Crowley et al., 2009) and potassium channels (Besana et al., 2005; Carta et al., 2014). Interestingly, the large-conductance, calcium- and voltage-activated potassium channels (BK), known to regulate neuronal excitability and synaptic function throughout the brain (Ancatén-González et al., 2023; Montgomery & Meredith, 2012), are reportedly regulated by different lipoxygenase-derived metabolites (Faraci et al., 2001; Zink et al., 2001). Moreover, evidence indicates that BK channels are expressed at presynaptic terminals of CA3 neurons in the mature hippocampus (Hu et al., 2001; Misonou et al., 2006; Raffaelli et al., 2004; Sailer et al., 2006), opening the possibility that BK channels are involved in mGluR-LTD. However, whether presynaptic BK channels contribute to neonatal activity-dependent mGluR-LTD remains unknown.

Here, using electrophysiological recordings in acute hippocampal slices from P7–P10 mice, we evaluate the role of TRPV1 and BK channels as potential downstream effectors of 12(S)HPETE signaling in mediating neonatal mGluR-LTD. We find that activation of presumably presynaptic BK, but not TRPV1, channels by 12(S)HPETE is required for the induction of mGluR-LTD at immature CA3–CA1 synapses. The contribution of BK channels is subunit specific, involving BK containing $\beta 4$ but not $\beta 2$ subunit. These results identify a mechanistically necessary step for the induction of mGluR-LTD during postnatal development that likely involves retrograde activation of BK channels at presynaptic terminals to impact synaptic function in a long-term manner.

Note: The text and figures in the next section have been recently published (Proc Natl Acad Sci U S A. 2025 Jan 14;122(2):e2411506122. doi: 10.1073/pnas.2411506122) and minor changes have been made to ensure continuity.

Results

12(S)HPETE Is a Key Player of Presynaptic mGluR-LTD in the Neonatal Hippocampus.

To investigate the presynaptic mechanisms involved in the induction of mGluR-LTD, we recorded field excitatory postsynaptic potentials (fEPSPs) and currents (EPSCs) from CA1 pyramidal neurons while stimulating CA3 Schaffer collateral inputs in acute hippocampal slices of neonatal (postnatal day P7–P10) mice (*Materials and Methods*). Consistent with previous reports (Bolshakov & Siegelbaum, 1994b, 1995b; Feinmark et al., 2003; Zakharenko et al., 2002), low-frequency stimulation (LFS, 5 Hz, 3 min) induced a robust LTD that required postsynaptic mGluRs as it was eliminated by the mGluR5 antagonist MTEP (10 μM, Fig. 1A). Moreover, LFS-induced LTD can also be abolished by loading CA1 pyramidal neurons with GDPβS, a broad-spectrum G protein antagonist but was normally induced when NMDA receptors were blocked with APV (SI Appendix, Fig. S1 A–C). LFS-induced LTD was also independent of GABAergic transmission as it was normally induced in the presence (Fig. 1A) or absence of the GABAA receptor antagonist picrotoxin (50 μM; SI Appendix, Fig. S1B). Similarly, mGluR-LTD could be mimicked by pharmacological activation of mGluRs with DHPG (50 μM, 10 min), an effect that was also eliminated in the continuous presence of MTEP (Fig. 1B). Importantly, both electrical and chemical forms of mGluR-LTD were accompanied by changes in the paired-pulse ratio (PPR) and coefficient of variation 1/CV2; Fig. 1 A and B), consistent with a presynaptic origin. Moreover, LFS-and DHPG-induced LTD occluded each other (SI Appendix, Fig. S1 D and E), indicating that mGluR activation by either pharmacological means or synaptic activity suppresses glutamate release in the young hippocampus through a common presynaptic mechanism.

Previous evidence indicates that presynaptic mGluR-LTD requires a postsynaptic signal pathway that involves the activation of 12-lipoxygenase and the production of the lipid metabolite 12(S) HPETE (Bolshakov & Siegelbaum, 1995b; Feinmark et al., 2003; Normandin et al., 1996). Accordingly, two independent 12-lipoxygenase inhibitors, baicalein (10 μM) and cinnamyl-3,4-dihydroxy- α-cyanocinnamate (CDC; 10 μM), were able to eliminate both LFS- (Fig. 1C) and DHPG-induced mGluR-LTD (SI Appendix, Fig. S1F). Moreover, bath application of 12(S)HPETE (100 nM), but not its metabolite 12-HETE (100 nM), was sufficient to reduce fEPSPs in a long-lasting manner in the young hippocampus (Fig. 1D). Consistent with a presynaptic mechanism, 12(S)HPETE-mediated synaptic

depression was accompanied by changes in PPR and 1/ CV2 (Fig. 1D) and occluded the induction of either LFS- or DHPG induced mGluR-LTD (SI Appendix, Fig. S2 A and B). Moreover, 12(S)HPETE had no further effect on fEPSP amplitude if applied after the induction of LFS-LTD (SI Appendix, Fig. S2C). Altogether, these results strongly support the idea that 12(S)HPETE is a key player in the induction of presynaptic mGluR-LTD in the neonatal hippocampus (Feinmark et al., 2003).

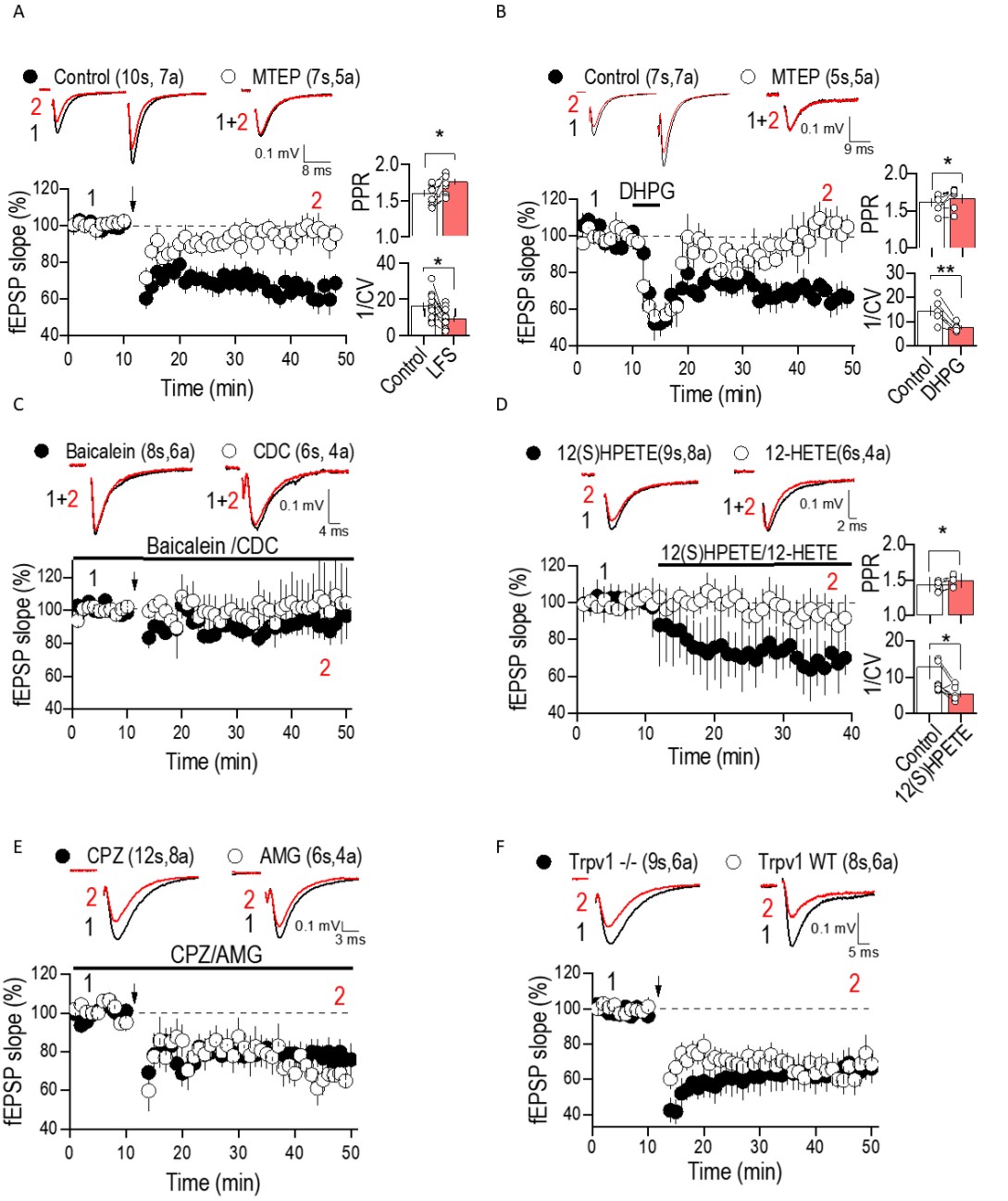


Figure 1. Arachidonic acid metabolite 12(S)HPETE is necessary to induce mGluR-LTD in the young hippocampus.

*(A) Low-frequency stimulation (LFS, 5 Hz, 3 min) induces a LTD of fEPSP (black circle) that was eliminated in the continuous presence of the mGluR antagonist MTEP (10 μM; open circle). Top, Representative traces of two consecutive fEPSP (100-ms interstimulus interval) before (black) and after (grey) LFS induction, and in the continuous presence of MTEP. Bottom, summarized graphs. (B) Representative traces (Top) and time course (Bottom) showing that bath application of the mGluR agonist DHPG (50 μM, 5 min) also induces LTD of fEPSP, an effect that was eliminated in the continuous presence of MTEP. Note that LFS-and DHPG-induced mGluR-LTD were accompanied by changes in PPR and coefficient of variation (1/CV2, Right), suggesting a presynaptic mechanism involved. In the PPR and 1/CV2 summarized plot, each open circle represents a single slice. (C) Representative traces (Top) and time course (Bottom) showing that blocking 12-lypoxigenase, and the production of 12(S)HPETE with two independent blockers (Baicalein and CDC), eliminates LFS-induced LTD. (D) Representative traces (Top) and time course (Bottom) showing that 12(S) HPETE (100 nM), but not its metabolite 12-HETE (100 nM), reduced fEPSP at CA3-CA1 synapses, an effect that was accompanied by changes in PPR and 1/CV2. (E) Representative traces (Top) and time course (Bottom) showing that LFS-induced mGluR-LTD was unaffected by two different TRPV1 antagonists Capsazepine (CPZ, 10 μM) and AMG 9810 (AMG, 10 μM). (F) Representative traces (Top) and time course (Bottom) showing that LFS-induced mGluR-LTD is similar in wild-type (TRPV1+/+) and TRPV1−/− deficient mice. In all panels, data are presented as mean ± SEM, and average sample traces taken at times indicated by numbers are shown next to each summary plot. *P <0.05, **P <0.01, and the number of slices (s) and animals (a) are indicated in parenthesis.*

mGluR-LTD at CA3-CA1 Synapses Does Not Involve the Activation of TRPV1 Channels.

What is the potential target of 12(S)HPETE at presynaptic terminals to induce mGluR-LTD? In the mature hippocampus, at excitatory CA3 to interneuron synapses, mGluR-LTD reportedly requires activation of presynaptic TRPV1 channels (Gibson et al., 2008). However, LFS-induced mGluR-LTD at immature CA3 to CA1 synapses was normally induced when TRPV1 channels were blocked with capsazepine (CPZ, 10 μM) or AMG 9810 (AMG; 10 μM Fig. 1E) or in slices from TRPV1 deficient mice (TRPV1−/−; Fig. 1F), further supporting that, unlike the excitatory CA3 to interneuron synapse (Gibson et al., 2008), TRPV1 channels are not involved in presynaptic mGluR-LTD mediated by 12(S)HPETE at excitatory CA3-CA1 synapses in the neonatal hippocampus. Consistent with this idea, 12(S)HPETE markedly reduced fEPSPs in the continuous presence of CPZ or AMG (SI Appendix, Fig. S3A) or in hippocampal slices from TRPV1−/− mice (SI Appendix, Fig. S3B), strongly suggesting that TRPV1 channels are not required for 12(S)HPETE-mediated depression in the young hippocampus. Accordingly, bath application of capsaicin (1 μM), a TRPV1 agonist, had no significant effect on basal synaptic transmission at CA3-CA1 excitatory synapses (SI Appendix, Fig. S3C), but depressed the CA3-interneuron synapses in naïve slices (SI Appendix, Fig. S3C).

BK Channels Are Required for the Induction of mGluR-LTD in the Neonatal Hippocampus.

Previous evidence suggests that BK channels regulate synaptic transmission at CA3 axon terminals (Hu et al., 2001; Raffaelli et al., 2004) and can be regulated by different lipoxygenase-derived metabolites (Faraci et al., 2001; Zink et al., 2001), but whether they play a role in regulating mGluR-LTD remains unknown. To assess their involvement in mGluR-LTD, we first applied BK channel antagonists before delivering LFS-or DHPG to induce mGluR-LTD. Blocking BK channels with iberiotoxin (100 nM) had no effect on electrical and chemical forms of mGluR-LTD (Fig. 2 A and B). However, bath application of the BK channel antagonist paxilline (1 or 10 μM) was able to abolish both forms of LTD (Fig. 2 A and B). For completeness, we also performed experiments using apamin, a blocker of the small-conductance voltage-and Ca2+-sensitive potassium (SK) channels known to regulate synaptic plasticity in the adult hippocampus (Rice & Stackman, 2024). While apamin (300 nM) was able to reduce medium afterhyperpolarization current (ImAHP) in CA1 pyramidal neurons, it failed to block LFS-induced mGluR-LTD (SI Appendix, Fig. S4 A and B). Thus, our results suggest that paxilline-sensitive BK channels are involved in mGluR-LTD. Accordingly, paxilline but not iberiotoxin eliminated 12(S) HPETE-induced depression of synaptic transmission (Fig. 2C). Importantly, paxilline had no effect on basal synaptic transmission (SI Appendix, Fig. S4C) or in synapses already expressing 12(S) HPETE-mediated depression (SI Appendix, Fig. S4D) and LFS-induced LTD was normally expressed when paxilline was applied immediately after tetanus (SI Appendix, Fig. S4E), suggesting that paxilline-sensitive BK channels are required for the induction, but not maintenance of mGluR-LTD. Moreover, bath application of the specific BK channel agonist NS11021 (3 μM) was sufficient to reduce basal synaptic transmission at CA3-CA1 synapses (Fig. 2D). This effect was accompanied by changes in PPR and 1/CV2 and was eliminated in slices preincubated with paxilline but not with iberiotoxin (Fig. 2D). Moreover, a short application of NS11021 (5 min) also induces a long-lasting and irreversible reduction of fEPSP (SI Appendix, Fig. S4F). Consistent with the idea that paxilline-sensitive BK channels are required for the induction, but not maintenance of synaptic depression at CA3-CA1 synapses, paxilline had no effect on synapses already expressing NS11021-mediated depression (SI Appendix, Fig. S4G). Moreover, in the continuous presence of NS11021, LFS and DHPG were not able to further suppress fEPSPs (Fig. 2E). Importantly, NS11021-mediated depression could not be induced at synapses already expressing 12(S)HPETE-mediated depression (Fig. 2F). Inversely, 12(S)HPETE had no effect on synapses already expressing NS11021-mediated depression (Fig. 2F). These two-way occlusion experiments indicate that 12(S)HPETE-and NS11021-mediated synaptic depression share a common mechanistic step to induce mGluR-LTD. To explore this possibility, we

delivered a subthreshold induction protocol, which by itself did not have persistent effects on fEPSPs (SI Appendix, Fig. S5A) and did not occlude further induction of LFS-LTD (SI Appendix, Fig. S5B). We tested whether such a protocol could be potentiated to trigger LTD by slightly elevating BK channel activity with the use of brief application of BK agonists 12(S)HPETE or NS11021, which does not by itself produce lasting suppression. Under these recording conditions, the subthreshold induction protocol triggered robust LTD that was blocked by paxilline (SI Appendix, Fig. S5 C and D). Altogether, these results support the idea that paxilline-sensitive BK channel activation is necessary to induce mGluR-LTD in the young hippocampus.

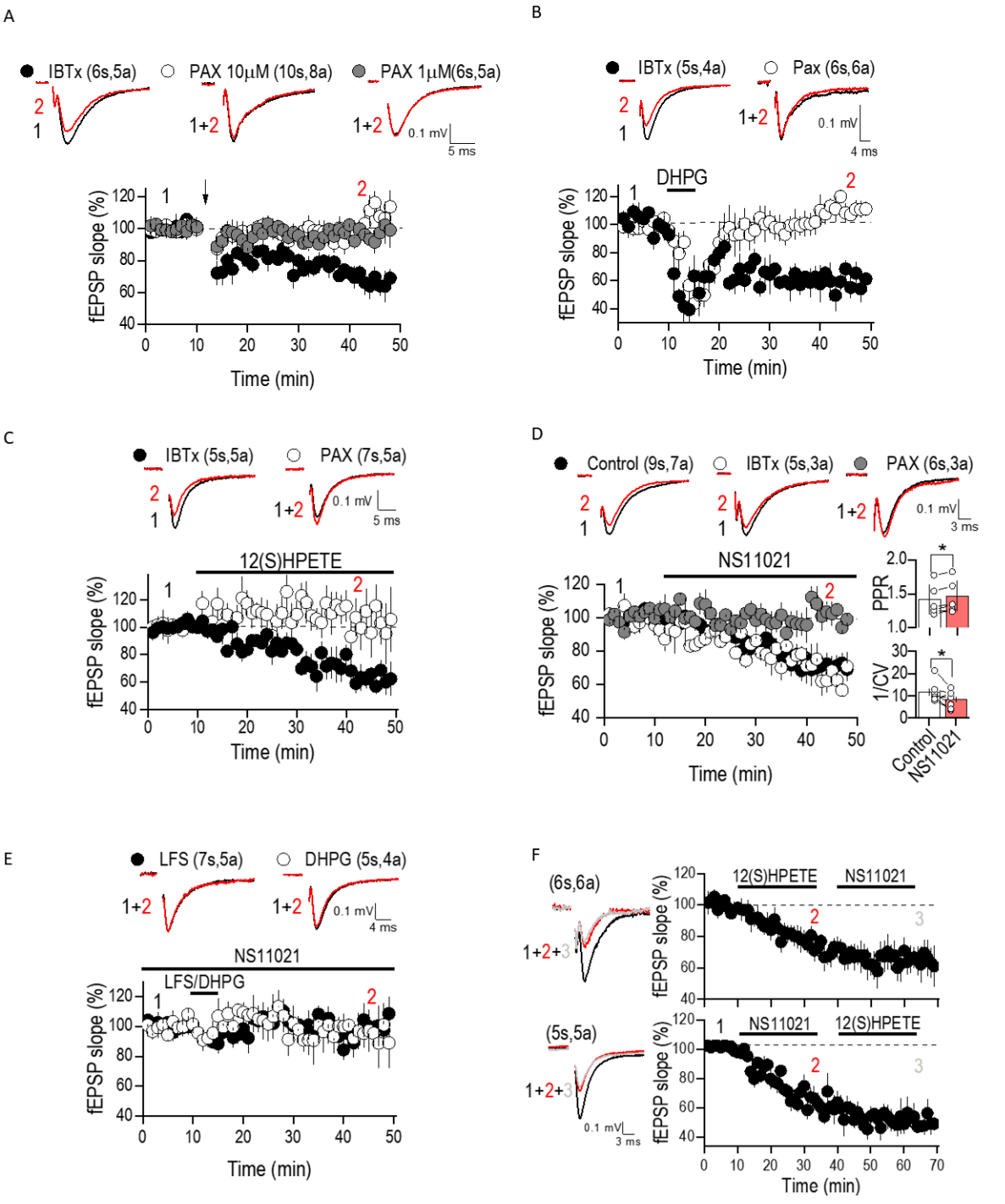

A
IBTx (6s,5a)
PAX 10μM (10s,8a)
PAX 1μM(6s,5a)
0.1 mV
5 ms
fEPSP slope (%)
Time (min)
B
IBTx (5s,4a)
Pax (6s,6a)
0.1 mV
4 ms
DHPG
C
IBTx (5s,5a)
PAX (7s,5a)
12(S)HPETE
D
Control (9s,7a)
IBTx (5s,3a)
PAX (6s,3a)
NS11021
PPR
1/CV
Control
NS11021
E
LFS (7s,5a)
DHPG (5s,4a)
NS11021
LFS/DHPG
F
(6s,6a)
(5s,5a)
12(S)HPETE
NS11021

Figure 2. Activation of BK channels containing the BKβ4 subunit is involved in mGluR-LTD.
*(A) Average traces (Top) and time course (Bottom) showing that LFS-and (B) DHPG-induced mGluR-LTD were unaffected by bath application of iberiotoxin (IBTx, 100 nM) but were eliminated in the continuous presence of Paxilline (Pax, 10 or 1 μM). (C) Average traces (Top) and time course (Bottom) showing that bath application of the 12(S)HPETE (100 nM) depresses fEPSP in the continuous presence of IBTx but had no effect in the presence of Pax. (D) Average traces (Top) and time course (Bottom) showing that bath application of NS11021 (3 μM), a BK channel agonist, depresses fEPSP in the continuous presence of IBTx but had no effect in the presence of Pax. NS1121-mediated depression of fEPSP was accompanied by changes in PPR and 1/CV, suggesting a presynaptic mechanism of action. (E) Average traces (Top) and time course (Bottom) showing that preincubation with NS11021 (3 μM) is able to block LFS-and DHPG-induced mGluR-LTD. (F) Average traces (Left) and time course (Right) showing that 12(S)HPETE-induced suppression of fEPSP occluded the NS11021-mediated depression of fEPSP at CA3-CA1 synapses (Top), and inversely, NS11021-induced depression blocks further effect of 12(S)HPETE (Bottom), suggesting a common mechanism of action. In all panels, data are presented as mean ± SEM, and averaged sample traces taken at times indicated by numbers are shown next to each summary plot, and the numbers of slices (s) and animals (a) are indicated in parentheses. *P < 0.05.*

The BK Channel Containing β4 but not the β2 Subunit Is Sensitive to 12(S)HPETE. The differential effect between iberiotoxin and paxilline on mGluR-LTD, and 12(S)HPETE-and NS11021-mediated depression, suggests that BK channels containing β4 but not β2 subunits are required for this form of LTD. To further investigate this possibility, we tested the effect of 12(S)HPETE on human BK channels formed by the , the + β2, and + β4 subunits expressed in *Xenopus laevis oocytes*. Notably, 12(S) HPETE does not change the BK channel voltage dependence when the BKα subunit is expressed alone (Fig. 3A) but strongly increases the channel open probability when the β4-subunit was coexpressed with the α subunit (Fig. 3B). The addition of 12(S)HPETE intracellularly to a final concentration of 100 nM produces a 50-mV leftward shift of the normalized BKβ4 channel open probability ($I_{tail}/I_{tailmax}$)-voltage curve (Fig. 3B). The half voltages obtained from the $I_{tail}/I_{tailmax}$ vs voltage curves were plotted against 12(S)HPETE concentration, and the data were fitted using a Hill equation (see legend of Fig. 3C). The best fit to the data was obtained with a dissociation constant of 0.98 nM and a Hill coefficient of 3 (Fig. 3C). Demonstrating that the effect of 12(S)HPETE is subunit specific, this metabolite did not modify the voltage dependence of + β2 channels (Fig. 3D). Importantly, 12(S)HPETE-mediated effect in BKβ4 channel open probability is amplified by internal Ca^{2+} given that in the presence of 3 μM internal Ca^{2+}, the probability of opening-voltage curve shifted leftward by 77 mV, twice the effect observed in the absence of internal Ca^{2+} (Fig. 3E). Moreover, cytoplasmic Ca^{2+} does not affect the binding of 12(S)HPETE to the BK channel as the equilibrium dissociation constant is close to 1 nM (Fig. 3F). These results support the idea that BK channels

formed by α and β4 subunits, but not β2-subunits, are necessary for the induction of 12(S)HPETE-mediated depression and mGluR-LTD in the young hippocampus and a tight binding accompanies this subunit specificity.

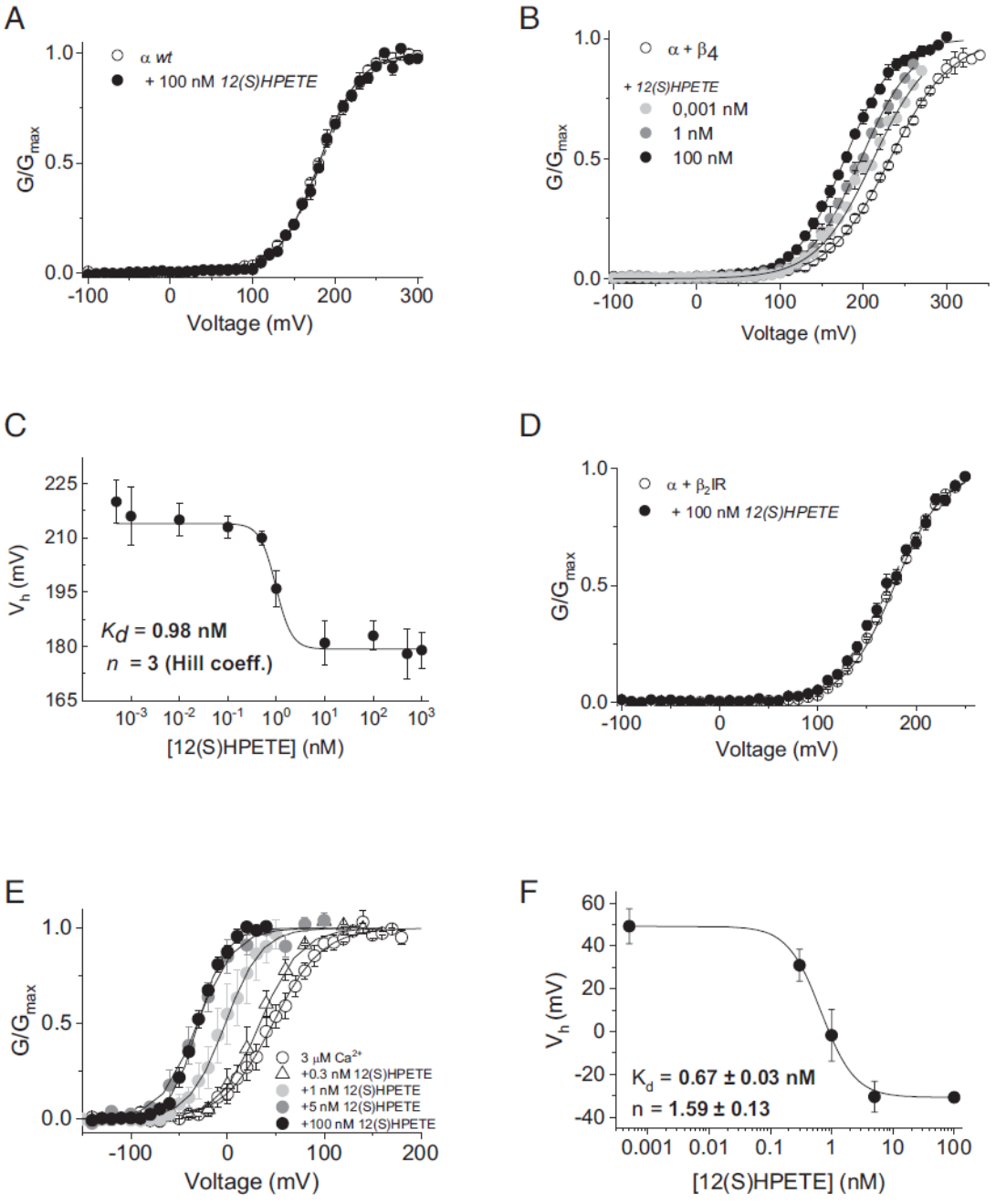


Fig. 3. BK channels containing β4 but not β2 subunit are directly activated by 12(S)HPETE. *(A) Normalized I_{tail}-V relationship (I_{tail}(V)) for BK α channels before (white diamonds) or after (black diamonds) the addition of 12(S)HPETE (100 nM) to the cytoplasmic side in 0 $[Ca^{2+}]_i$. The I_{tail}(V) data (mean ± SEM) were fitted using a Boltzmann function (Materials and Methods). Fit parameters were V_h = 180 and 182 mV; z_δ = 1.02 and 0.98 before (n = 5) and after (n = 5) the addition of 12(S) HPETE, respectively. (B) Normalized I_{tail}(V) (mean ± SEM) for BK α + β4 channels before (white hexagons) or after the addition of 12(S)HPETE at concentrations of 0.001 nM (black squares); 1 nM (black circles) or 100 nM (black triangles) to the internal side. Fit parameters were V_h = 233 mV and z_δ = 0.69, n = 7 (control); V_h = 217 mV and z_δ = 0.78, n = 4 (0.001 nM); V_h = 196 mV and z_δ = 0.81, n = 4 (1 nM); and V_h = 183 mV and z_δ = 0.76, n = 5 (100 nM). (C) Average V_h values obtained from the I_{tail}(V) curves plotted against 12(S)HPETE concentration (mean ± SEM). Data were fitted using a Hill equation where $V_h = V_{max} + (V_0 - V_{max}) \times [HPETE]^n / K^n + [HPETE]^n$ where V_{max} is the half voltage in the absence of 12(S)HPETE, V_o is the half voltage at the indicated 12(S)HPETE concentration, K the dissociation constant, and n the Hill coefficient. 12(S)HPETE binding produces a leftward shift in V_h (ΔV_h) (n = 3 to 4). (D) Normalized I_{tail}-V (mean ± SEM) for BK α + β 2 IR channels before (white diamonds) or after (black diamonds) the addition of 100 nM 12(S)HPETE to the cytoplasmic side in 0 $[Ca^{2+}]_i$. Fit parameters were V_h = 178 and 174 mV; z_δ = 0.99 and 0.90 before (n = 4) and after (n = 4) the addition of 12(S)HPETE, respectively. (E) Normalized I_{tail}(V)(mean ± SEM) for BK α + β4 channels, in the presence of 3 μM of Ca^{+2}, before (open circles) or after the addition of 12(S)HPETE at different concentrations. Data were fitted using a Boltzmann equation (Materials and Methods). The parameters were before the addition of 12(S)HPETE: V_h = 46.86 ± 1.12 mV, and z_δ = 1.00 ± 0.04 e_0 (n = 3); 0.3 nM: V_h = 33.34 ± 1.31 mV, and z_δ = 1.1 ± 0.06 e_0 (n = 3); 1 nM: V = −2.33 ± 1.25 mV, and z_δ = 1.36 ± 006 (n = 3); 5 nM: V_h = −31.18 ± 1.99 mV, and z_δ = 1.34 ± 0.12 (n = 3); 100 nM (n = 4): V = −30.33 ± 0.56 mV, and z_δ = 1.77 ± 0.06 (n = 4). (F) Average V_h values obtained from the I_{tail}(V) curves plotted against 12(S)HPETE concentration (mean ± SEM) in the presence of 3 μM of Ca^{+2}. The V_{half} -[12(S)HPETE] data were fitted to a Hill equation as described in Fig. 3C.*

Presynaptic BKβ4 Channels Likely Regulate CA3-CA1 Synapses and mGluR-LTD

Although BK channels are expressed in pre-and postsynaptic compartments in the hippocampus (Ancatén-González et al., 2023; Brenner et al., 2005; Contet et al., 2016; Hu et al., 2001; Raffaelli et al., 2004; Sailer et al., 2006) and its inhibition with either paxilline and iberiotoxin can regulate the excitability of CA1 pyramidal neurons (*SI Appendix*, Fig. S6), the changes in PPR and 1/CV2 that we observed after the induction of 12(S)HPETE-and NS11021-mediated depression as well as in mGluR-LTD (Figs. 1–3) suggest that presynaptic rather than postsynaptic BK channels are necessary for the induction of mGluR-LTD. Consistent with this idea, BK β 4 channel activation by bath application of the agonist NS11021 or 12(S) HPETE has no effect on CA1 responses elicited by brief puffs of glutamate (monitored at −60 mV), a manipulation known to shortcut glutamate release (Fig. 4*A*). Moreover, bath application of the BK channel agonist NS11021 depressed isolated NMDA receptor

(NMDAR)-mediated EPSCs (*Materials and Methods*) to an extent similar to that of AMPAR-mediated fEPSPs (Fig. 2*C*), consistent with a decrease in glutamate release (Fig. 4*B*). Additional observations further support a presynaptic localization of BK β 4 to regulate synaptic plasticity. First, when EPSCs and fast afterhyperpolarization current (IfAHP) were recorded from the same CA1 pyramidal neuron, bath application of 12(S)HPETE induced depression of EPSC but had no effect on postsynaptic IfAHP (Fig. 4*C*). Second, 12(S)HPETE-induced LTD was associated with an increase in failure rate in minimal stimulation experiments (Fig. 4*D*), an effect that was eliminated in the continuous presence of paxilline (Fig. 4*E*). Third, loading CA1 pyramidal cells with the BK channel blocker paxilline through the patch pipette, a manipulation known to reduce the excitability of CA1 pyramidal neurons (J. Zhang et al., 2018; Y. Zhou & Lingle, 2014)(*SI Appendix*, Fig. S6 *A*–*C*), does not affect synaptic depression induced by either NS11021 or 12(S)HPETE (Fig. 4*F* and *SI Appendix*, Fig. S6*D*). Additionally, bath-applied paxilline abolished LFS-induced mGluR-LTD, but intracellularly loaded paxilline (Fig. 4*G*) or cesium to block BK channels failed to prevent LTD (*SI Appendix*, Fig. S6*E*). Altogether, these results strongly suggest that presynaptic rather than postsynaptic BK channels are necessary for the induction of mGluR-LTD.

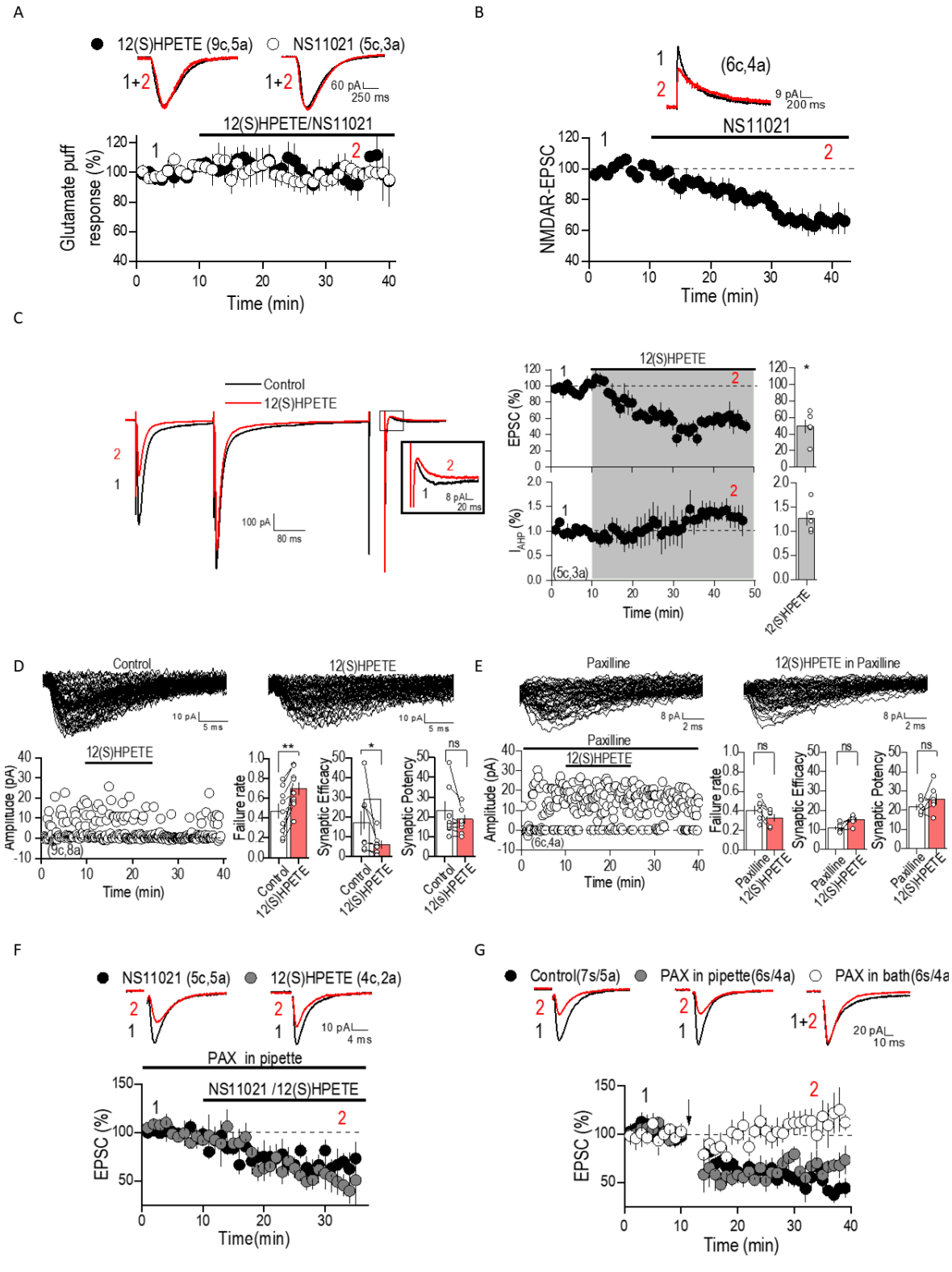

A
12(S)HPETE (9c,5a)
NS11021 (5c,3a)
1+2
60 pA
250 ms
12(S)HPETE/NS11021
Glutamate puff response (%)
Time (min)
B
(6c,4a)
9 pA
200 ms
NS11021
NMDAR-EPSC
Time (min)
C
Control
12(S)HPETE
100 pA
80 ms
8 pA
20 ms
12(S)HPETE
EPSC (%)
I_AHP (%)
(5c,3a)
Time (min)
12(S)HPETE
D
Control
12(S)HPETE
10 pA
5 ms
12(S)HPETE
Amplitude (pA)
(9c,8a)
Time (min)
Failure rate
Synaptic Efficacy
Synaptic Potency
Control
12(S)HPETE
E
Paxilline
12(S)HPETE in Paxilline
8 pA
2 ms
Paxilline
12(S)HPETE
Amplitude (pA)
(6c,4a)
Time (min)
Failure rate
Synaptic Efficacy
Synaptic Potency
Paxilline
12(S)HPETE
F
NS11021 (5c,5a)
12(S)HPETE (4c,2a)
10 pA
4 ms
PAX in pipette
NS11021 /12(S)HPETE
EPSC (%)
Time(min)
G
Control(7s/5a)
PAX in pipette(6s/4a)
PAX in bath(6s/4a)
20 pA
10 ms
EPSC (%)
Time (min)

Fig. 4. Activation of BK β 4 is required for mGluR-LTD.
*(A) Average traces (Top) and time course (Bottom) showing that postsynaptic response to exogenous glutamate puff application (1 mM, 25 ms) was unaffected by bath application of BK channel agonist 12(S)HPETE (100 nM) and NS11021 (3 μM). (B) Average trace (Top) and time course (Bottom) showing that NS11021 induces a depression of isolated NMDAR-mediated currents in a similar way as to AMPAR-mediated currents. (C) Average trace (Left) and summarized graph (Right) showing that 12(S)HPETE (100 nM) decrease presynaptic neurotransmission (EPSC; Top) without affecting postsynaptic excitability (I_{fAHP}; Bottom) recorded at the same time from neonatal CA1 pyramidal neuron. (D) Individual traces (Top) and summarized graphs (Bottom) showing that 12(S)HPETE (100 nM) increased failure rate and decreased synaptic efficacy but had no effect on synaptic potency of minimal stimulation experiments in the CA1 area of the hippocampus, supporting a presynaptic mechanism of action. (E) Individual traces (Top) and time course (Bottom) showing that bath application of paxilline (10 μM) eliminated 12(S)HPETE-mediated increase in failure rate and decrease in synaptic efficacy, supporting that 12(S) HPETE effect is mediated by presynaptic BK β4 channels. (F) Representative traces (Top) and time course (Bottom) showing that loading CA1 pyramidal neuron with paxilline (Pax; 10 μM) was not able to block NS11021-and 12(S)HPETE-induced synaptic depression. (G) Representative traces (Top) and time course (Bottom) showing that Pax in bath, but not intracellularly applied, is able to block LFS-induced LTD in the neonatal hippocampus. In all panels, data are presented as mean $\pm$ SEM, and averaged sample traces taken at times indicated by numbers are shown next to each summary plot and the numbers of cells (c) and animals (a) are indicated in parentheses. ns, no significant; * P < 0.05, ** P < 0.01.*

Discussion

So far, our findings reveal that BK β 4 channels are a crucial substrate involved in classical mGluR-LTD in the neonatal hippocampus and identify a form of lipids-derived retrograde modulation of synaptic function that involves an interaction between 12(S)HPETE and BK channels at central synapses. Notably, this modulation of synaptic strength mediated by BK channels is subunit specific as BK β 4, but not BK β 2, is activated in an activity-dependent manner to depress in a long-term manner CA3-CA1 excitatory synaptic transmission in the young hippocampus.

Multiple forms of retrograde signaling mediated by lipid messengers, including endocannabinoids and endovanilloids/eicosanoids, are known to modulate synaptic function and plasticity at central synapses, mainly by activating CB1 and TRPV1 receptors, respectively (Castillo et al., 2012; Regehr et al., 2009). Now, we add to this repertoire that the lipoxygenase product from arachidonic acid, 12(S)HPETE, can directly bind and activate presumably presynaptic BK channels containing β 4 subunit generating a long-lasting depression of transmitter release at CA3-CA1 excitatory synapses in the young hippocampus (*SI Appendix*, Fig. S7). Thus, our data, together with those indicating that retrograde regulation of potassium channels by arachidonic acid metabolites regulate synaptic plasticity at the CA3 area of the hippocampus (Carta et al., 2014), support the idea that lipid-derived

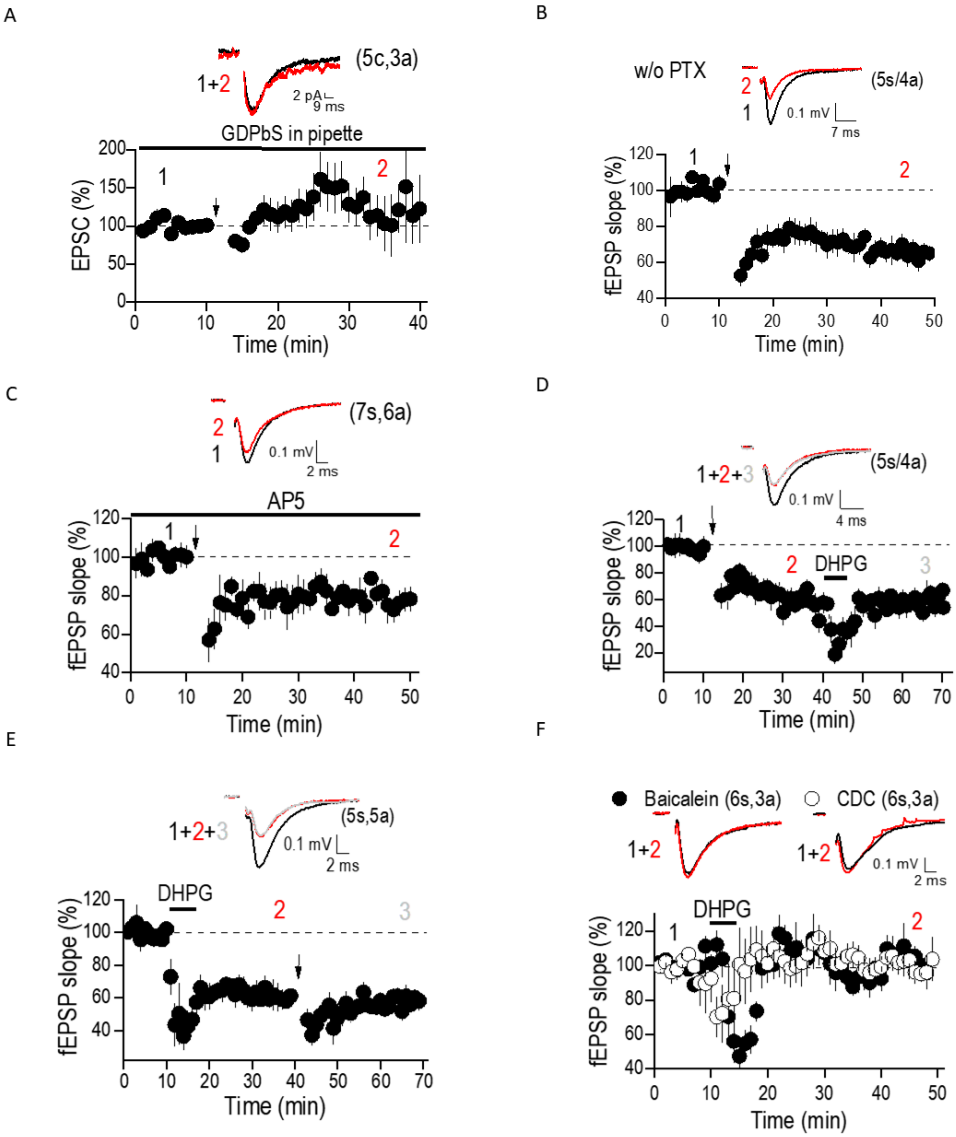
metabolites and potassium channels interaction might play an important role in the mechanisms underlying hippocampal synaptic plasticity. An additional observation of our results is the input-specific effect of the retrograde modulation mediated by 12(S)HPETE in the hippocampus. While at excitatory CA3 to interneuron synapses, 12(S)HPETE acts through TRPV1 channels to regulate synaptic plasticity (Gibson et al., 2008), our results demonstrated that at excitatory CA3-CA1 synapses BK β 4, but not TRPV1 channels are required to regulate synaptic plasticity. The differential reliance on BK β 4 versus TRPV1 depending on whether the postsynaptic target is pyramidal versus interneurons suggests that CA3 axon terminals may express specific receptor subtypes depending on the postsynaptic partner (*SI Appendix*, Fig. S3*C*). In addition, it is also unclear whether the retrograde modulation mediated by 12(S) HPETE could also be expressed at other synapses type within the neonatal brain and in the adult hippocampus. Interestingly, a functional interaction between TRPV1 and BK channels has been suggested in the peripheral nervous system (Y. Wu et al., 2013). Whether this functional interaction also regulates central synapses remains unclear, and further investigation is necessary to understand when and how retrograde modulation by 12(S)HPETE regulates synaptic function through TRPV1 or BK β 4 channels.

Consistent with a retrograde modulation of synaptic function, we demonstrated that 12(S)HPETE acts on presynaptic BK channels (Fig. 4) despite their expression in postsynaptic compartments where they are known to regulate neuronal excitability (Brenner et al., 2005; Hunsberger & Mynlieff, 2020). While the differential activation of pre- vs postsynaptic BK channels by this lipid-derived remains unclear, it could be due to different β -subunits expressed in both neuronal compartments. For instance, it has been proposed that β 4 subunits are present in CA3 pyramidal neurons(Deng et al., 2013; Shruti et al., 2012) and dentate granule cells in the dentate gyrus (Brenner et al., 2005), whereas β 2 are present in CA1 pyramidal neurons (Shao et al., 1999). Moreover, some reports indicate that subtypes of the BK channel, depending on their β subunits, can be differentially activated by lipids (Dopico & Bukiya, 2014; Hoshi et al., 2013) and also some hormones (King et al., 2006). Consistent with this idea, our results using heterologous expression demonstrate that BK β 4, but not a- and or BK β 2 channel, is directly modulated by 12(S)HPETE. Moreover, 12(S)HPETE-mediated retrograde suppression of synaptic function was blocked by paxilline but not by iberiotoxin, which blocks BK β 2 and aBK but not BK β 4 channels. Interestingly, at mature hippocampal synapses, the role of presynaptic BK channels can only be unmasked by blocking Kv

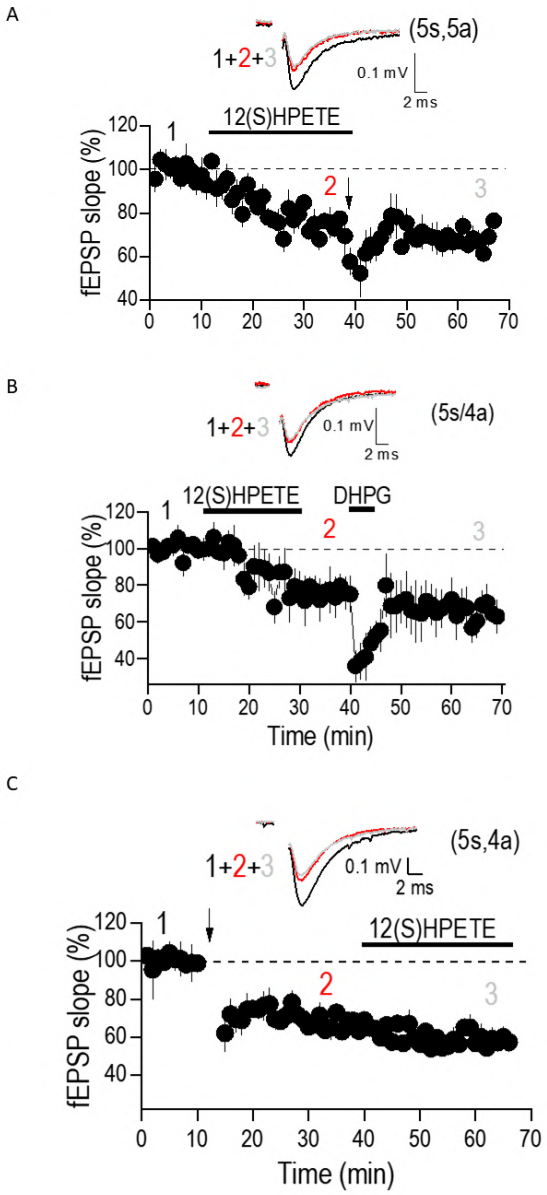
channels and BK channels become sensitive to iberiotoxin (Hu et al., 2001), opening the possibility that developmental changes in the expression or quantity of β 4 subunits may occur at presynaptic terminals during postnatal development to regulate synaptic function.

BK channels have been involved in some forms of short-term plasticity (Deng et al., 2013; Zaman et al., 2017), and our present results demonstrated their involvement in long-lasting depression in the neonatal hippocampus. While the exact mechanisms by which BK channels can generate a LTD vs a short-term plasticity is unknown, it is possible that the localization of BK β 4 at the presynaptic nerve terminal likely modulates both the amplitude and duration of depolarization evoked calcium influx limiting vesicle fusion at active zones and decreased neurotransmitter release (Hu et al., 2001; Raffaelli et al., 2004) in a long-term manner. It is also possible that changes in kinase/phosphatase balance downstream of BK activation might also be involved (Ancatén-González et al., 2023; Castillo, 2012; Leenders & Sheng, 2005). Another possibility is the transient presence of some molecular mediator or pathway that interacts with the β 4 auxiliary unit of the BK channel, as has been reported for some proteins in the postsynaptic domain (Lohmann & Kessels, 2014). While further investigations are required to fully understand the contribution of presynaptic BK channels to regulate short vs long-term synaptic plasticity, it has been suggested that synaptic plasticity mechanisms have been implicated to synaptic maturation and circuitry formation (Chaudhury et al., 2016). Particularly, LTD has been related to structural changes and a decrease in synaptic contacts (Becker et al., 2008; Piochon et al., 2016). Thus, a functional relevance of this BK-mediated plasticity can be related to the circuitry wiring, where LTD has been associated with pruning and a decrease in synaptic contacts (Becker et al., 2008; Piochon et al., 2016). Thus, synaptic plasticity could be relevant for establishing the hippocampal circuit, and BK channels could play a key role in its development, acting as a frequency filter, allowing high transmission rates to propagate but suppressing synapses that rely on low rates of transmission. In this way, BK channels may drive neuronal wiring in early development by enabling active synapses to undergo synaptic potentiation. However, whether BK channels' contribution to synaptic plasticity plays a role in synaptic wiring requires further investigations.

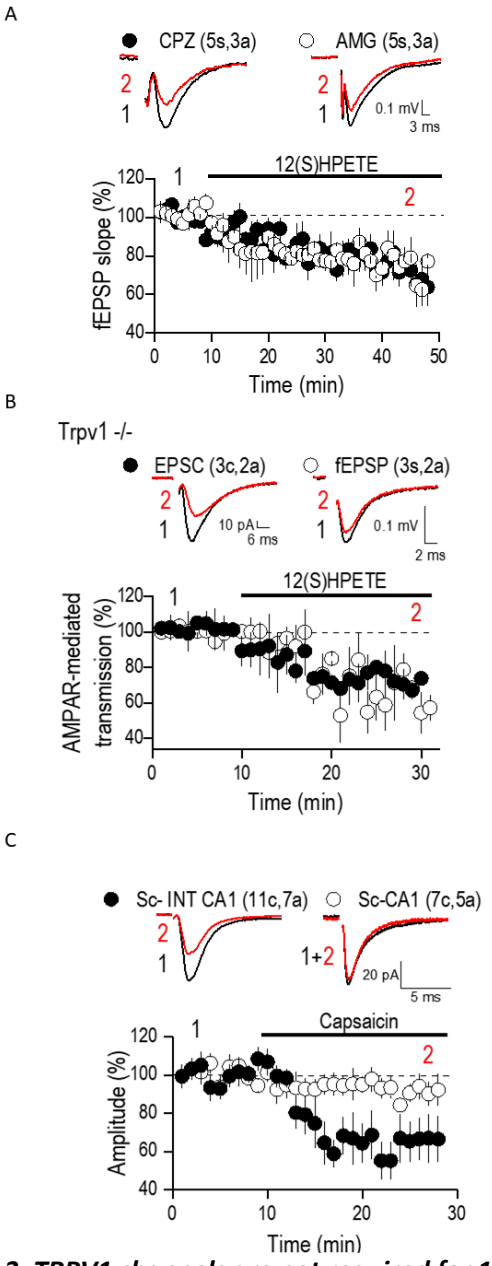
Supplementary Figures



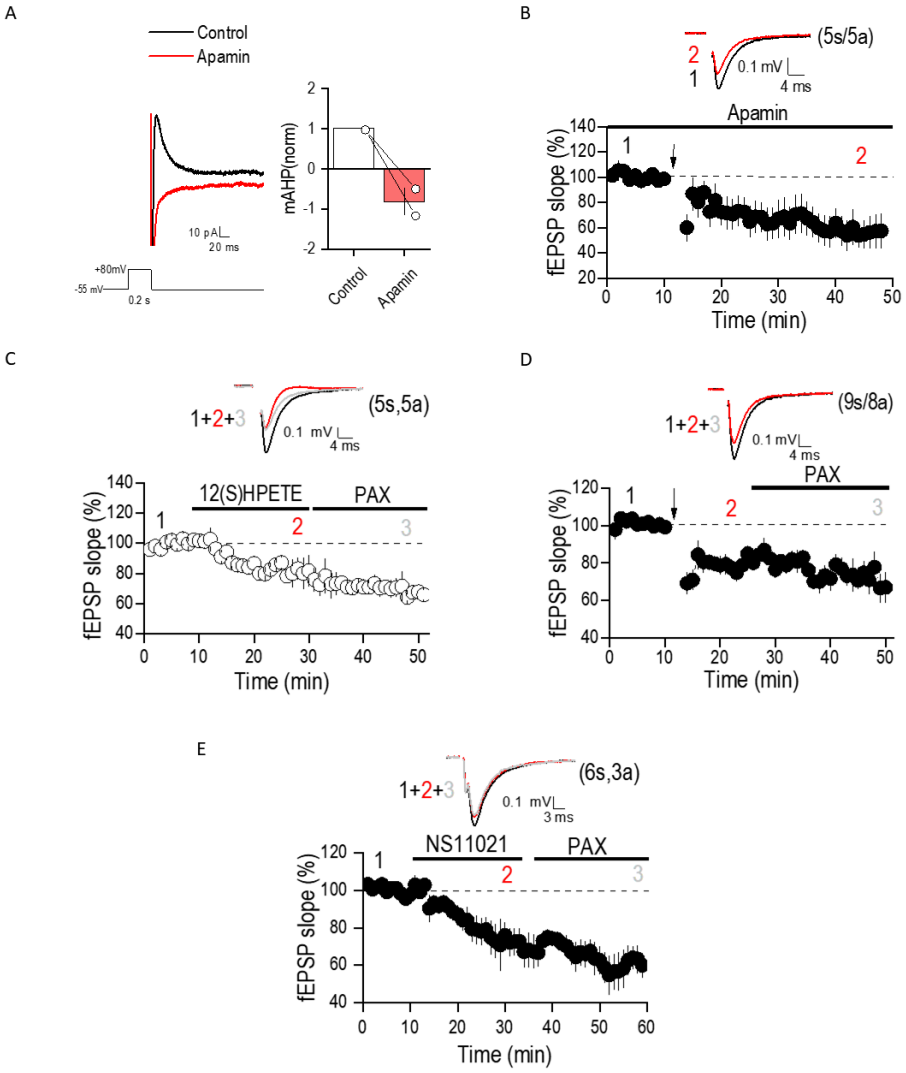
Supplementary Figure 1: Cellular mechanism involved in mGluR-LTD in neonatal hippocampus. A, *Representative traces (top) and time course (bottom) showing that loading CA1 pyramidal neurons with GDPβS (10 mM), a broad G-protein blocker, block LFS-induced mGluR-LTD.* ***B****, mGluR-LTD can be induced in the absence of GABAAR antagonist picrotoxin (PTX, 50 μM).* ***C,*** *mGluR-LTD can be also elicited in the continuous presence of the NMDAR antagonist APV, 25 μM.* ***D,*** *LFS-induced mGluR-LTD occluded further DHPG mediated effect on fEPSP.* ***E,*** *DHPG-induced LTD also occluded LFS-induced LTD, supporting the idea of a common mechanism of action.* ***F****, Slices pre-incubated with two independent 12-lypoxigenase inhibitors (baicalein (10 μM) and CDC (10 μM)) eliminated DHPG-induced mGluR-LTD. In all panels, data are presented as mean ± S.E.M and averaged sample traces taken at times indicated by numbers are shown next to each summary plot. The numbers of slices (s), cells (c) and animals (a) are indicated in parentheses.*



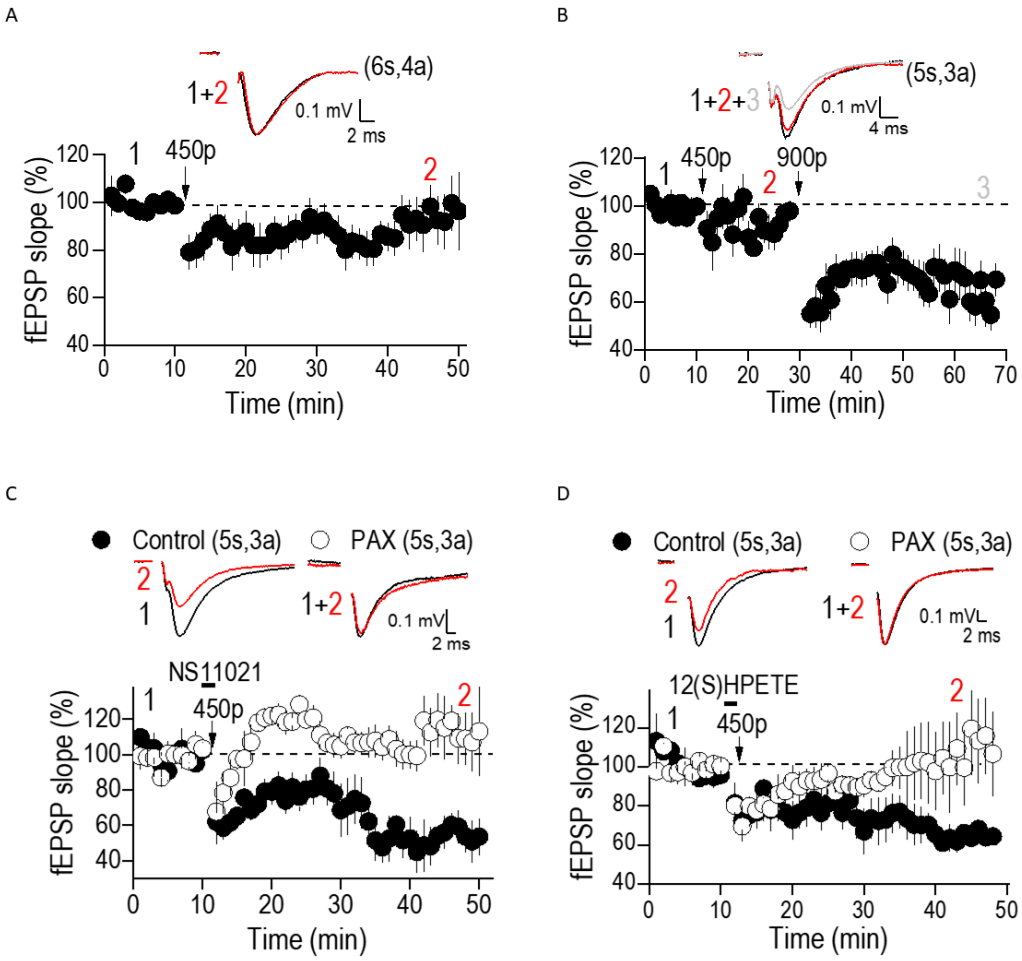
Supplementary Figure 2: The lipoxygenase metabolite 12(S)HPETE is necessary for induction of mGluR-LTD in the young hippocampus A*, 12(S)HPETE-induced reduction of fEPSP occluded LFS-induced mGluR-LTD.* ***B****, 12(S)HPETE-induced reduction of fEPSP also occluded DHPG-induced LTD, supporting the idea of a common mechanism of action of 12(S)HPETE to induce mGluR-LTD.* ***C****, 12(S)HPETE (100 nM) has no further effect when applied after the LTD induction. In all panels, data are presented as mean ± S.E.M and averaged sample traces taken at times indicated by numbers are shown next to each summary plot. The numbers of slices (s) and animals (a) are indicated in parentheses.*



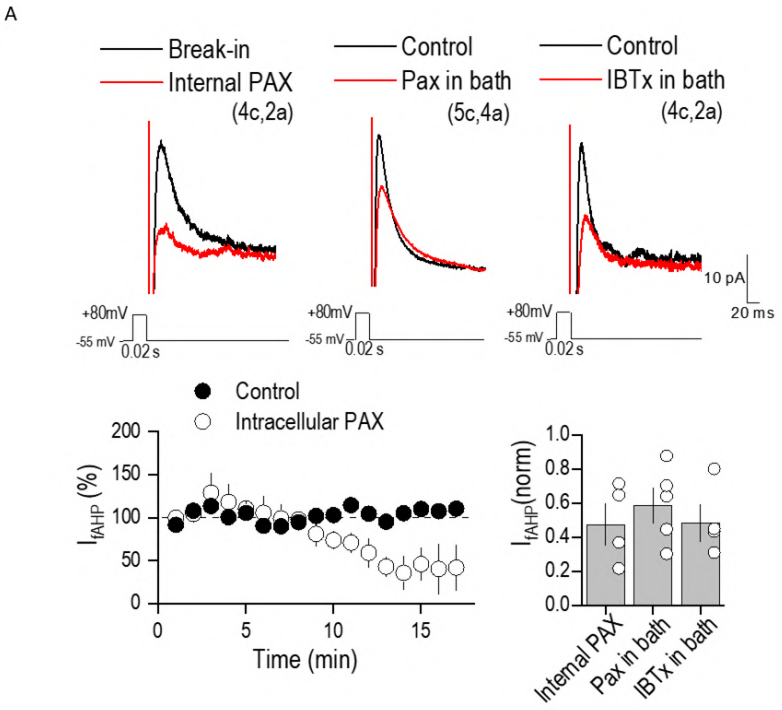
Supplementary Figure 3: TRPV1 channels are not required for 12(S)HPETE mediated depression at excitatory CA1-CA3 synapse. A, *Representative traces (top) and time course (bottom) showing that bath application of 12(S)HPETE reduces fEPSP in the continuous presence of TRPV1 antagonist capzasepine (CPZ, 10 μM) or AMG 9810 (10 μM).* ***B****, Representative traces (top) and time course (bottom) showing that bath application of 12(S)HPETE (100 nM) reduces AMPA-mediated transmission at CA3-CA1 synapses in slices obtained from TRPV1 deficient mice (TRPV1-/-).* ***C,*** *Representative traces (top) and time course (bottom) showing that bath application of capsaicin (1 μM), a TRPV1 agonist, did not affect neonatal CA3 excitatory Schaffer collateral to CA1 synapses (Sc-CA1) but markedly depress excitatory CA3 to interneuron synapses in the CA1 area of the neonatal hippocampus (SC-INT CA1). In all panels, data are presented as mean ± S.E.M and averaged sample traces taken at times indicated by numbers are shown next to each summary plot. The numbers of slices (s), cells (c) and animals (a) are indicated in parentheses.*



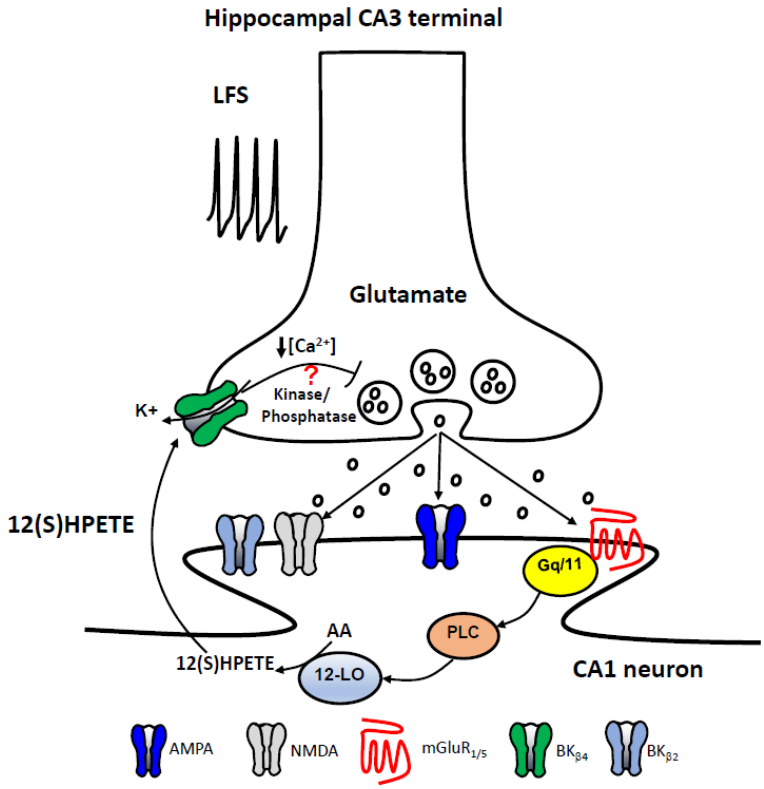
Supplementary Figure 4: BK channels are required for the induction not the maintenance of synaptic depression at CA3-CA1 synapse in the neonatal hippocampus. A, *Representative traces (left) and summary plot (right) show that the SK channel blocker Apamin (300 nM) decreases medium afterhyperpolarization current (I_{mAHP}) induced by 135 mV somatic current injection during 200 ms in CA1 pyramidal neuron.* ***B****, In the continuous presence of apamin LFS-induced mGluR-LTD was normally induced.* ***C,*** *Representative traces (top) and time course (bottom) showing that paxilline (PAX, 10 μM) had no effect on basal synaptic transmission.* ***D****, Representative traces (top) and time course (bottom) showing that PAX (10 μM) had no effect on synapses already expressing 12(S)HPETE-mediated depression.* ***E****, LFS-induced mGluR-LTD was normally expressed when PAX was applied after low frequency tetanus, suggesting that paxilline-sensitive BK channels are required for the induction, but not maintenance of mGluRLTD.* ***F****, Brief application of BK channel agonist NS11021 (5 min) produce a long-lasting and irreversible depression of fEPSP****. G****, Pax had no effect on synapses already expressing NS11021-mediated depression of fEPSP. In all panels, data is presented as mean ± S.E.M and averaged sample traces taken at times indicated by numbers are shown next to each summary plot. The numbers of slices (s), cells (c) and animals (a) are indicated in parentheses.*



Supplementary Figure 5: Brief activation of BK channels paired with subthreshold protocol induce robust LTD at CA3-CA1 synapse that were sensitive to paxilline. A, *Representative traces (top) and time course (bottom) showing that a subthreshold protocol (450 pulses) was not able to depress CA3-CA1 synaptic transmission and did occlude further induction of LFS induced LTD* ***(B)****.* ***C,*** *Representative traces (top) and time course (bottom) showing that a brief application (~2 min) of NS11021 (3 μM).* ***(C)*** *and 12(S)HPETE (100 nM)* ***(D)*** *paired with subthreshold protocol is sufficient to trigger paxilline-sensitive LTD in neonatal hippocampus. In all panels, data is presented as mean ± S.E.M and averaged sample traces taken at times indicated by numbers are shown next to each summary plot. The numbers of slices (s) and animals (a) are indicated in parentheses.*



Supplementary Figure 6: Loading CA1 pyramidal neuron with paxilline reduces afterhyperpolarization current in CA1 pyramidal neurons. A, *Representative traces (top) showing that loading CA1 pyramidal neuron with paxilline (Pax; 10 μM) or bath application of PAX or iberiotoxin (IBTx, 100 nM) decrease fast afterhyperpolarization current (I_{fAHP}) induced by 135 mV somatic injection during 20 ms in CA1 pyramidal neurons.* ***B,*** *Time course showing the effect of loading Pax on I_{fAHP}.* ***C,*** *Summarized plots showing the effect of blocking I_{fAHP} by loading Pax onto CA1 pyramidal neuron or by bath application of PAX and iberiotoxin.* ***D,*** *Representative traces (top) showing that loading CA1 pyramidal neuron with paxilline (Pax; 10 μM) for 30 min has no effect on LFS-induced mGluR-LTD.* ***E,*** *Representative traces (top) showing that loading CA1 pyramidal neuron with cesium chloride, know to block BK channels, also has no effect on LFS-induced mGluR-LTD. Data are presented as mean ± S.E.M and in the summarized plots each open circle represent a single cell.*



Supplementary Figure 7: Potential model of retrograde activation of presynaptic BK channels mediated mGluR-LTD in neonatal hippocampus. *Glutamate release during repetitive low frequency stimulation activates Gq-coupled (mGluR5) receptors, leading to the activation of phospholipase C (PLC) and 12-lipoxygenase signal pathway (12-LO), which likely triggers the biosynthesis of 12(S)HPETE, an arachidonic acid (AA) metabolite that retrogradely cross the synaptic cleft, and by activating presynaptic BKβ4 channels, suppress transmitter release in a long-term manner at excitatory CA3-CA1 synapses in the neonatal hippocampus. Solid black lines denote established signal transduction pathways. How exactly BK channels suppress transmitter release remains an open question (question mark; Decrease in intracellular calcium concentration and/or changes in kinase/phosphatase balance).*

Supplementary Table 1: Quantitative analysis of cellular mechanisms involved in mGluR-LTD in neonatal hippocampus. The table includes quantitative analyses of slice electrophysiology experiments shown in **Figs. 1, 2, and 4**. "*n*" represents number of slices (*s*), cells (*c*) and animals (*a*). PPR, paired-pulse ratio; 1/CV2 coefficient of variation; IBTX, iberitoxin; Pax, Paxilline; I_{fAHP}, Fast Afterhyperpolarization current.

Parameter	Value (mean ± s.e.m)	n	p value	Figure
LFS LFS-MTEP	62.15 ± 4.58 98.58 ± 3.56	10 s / 7a 7s / 5 a	p < 0.001 p = 0.710	1A
PPR	Pre 1.59 ± 0.05 Post 1.75 ± 0.04	10 s / 7 a 10 s / 7 a	p = 0.023	1A
$1/CV^2$	Pre 16.08 ± 2.19 Post 9.33 ± 1.54	10 s / 7 a 10 s / 7 a	p = 0.027	1A
DHPG-LTD DHPG-MTEP	68.69 ± 5.08 105.85 ± 13.68	7 s / 7 a 5 s / 5 a	p < 0.001 p = 0.698	1B
PPR	Pre 1.62 ± 0.05 Post 1.67 ± 0.06	7 s / 7 a 7 s / 7 a	p = 0.033	1B
$1/CV^2$	Pre 13.38 ± 1.31 Post 6.35 ± 0.89	7 s / 7 a 7 s / 7 a	p = 0.002	1B
LFS in Baicalein and CDC	Baicalein 96.71 ± 5.00 CDC 103.74 ± 22.00	8 s / 6 a 6 s / 4 a	p = 0.628 p = 0.872	1C
12(S)HPETE Basal Transmission	68.41 ± 8.93	9 s / 6 a	p < 0.001	1D
PPR	Pre 1.31 ± 0.12 Post 1.37 ± 0.05	9 s / 6 a 9 s / 6 a	p = 0.009	
$1/CV^2$	Pre 12.70 ± 3.10 Post 5.45 ± 0.73	9 s / 6 a 9 s / 6 a	p = 0.018	
12HETE Basal Transmission	90.05 ± 11.64	6 s / 4 a	p = 0.413	
LFS in Capsazepine (CPZ) and AMG9810 (AMG)	CPZ 79.15 ± 5.22 AMG 71.30 ± 6.61	12 s / 8 a 6 s / 4 a	p < 0.001 p = 0.001	1E
LFS in WT and TRPV1 KO mice	WT 60.95 ± 5.03 TRPV1 KO 63.78 ± 4.87 WT vs TRPV1 KO	9 s / 6 a 8 s / 6 a	p < 0.001 p < 0.001 p = 0.531	1F
LFS-IBTx Pax 10 μM Pax 1 μM	72.31 ± 5.13 104.94 ± 1.82 97.80 ± 4.31	6 s / 5 a 10 s / 8 a 6 s / 5 a	p = 0.001 p = 0.200 p = 0.561	2A
DHPG + IBTx DHPG + Pax	61.18 ± 7.85 100.73 ± 6.15	5 s / 4a 6 s / 6 a	p = 0.038 p = 0.985	2B
12(S)HPETE + IBTx 12(S)HPETE + Pax	61.18 ± 7.85 100.73 ± 6.15	5 s / 4a 6 s / 6 a	p = 0.038 p = 0.985	2C
NS11021 PPR $1/CV^2$	71.80 ± 5.90 Pre 1.30 ± 0.09 Post 1.33 ± 0.10 Pre 11.62 ± 1.61 Post 8.21 ± 1.31	9 s / 7 a 9 s / 7 a 9 s / 7 a 9 s / 7 a 9 s / 7 a	p = 0.007 p = 0.023 p = 0.023	2D

NS11021 + IBTx NS11021 + Pax	74.51 ± 7.44 96.33 ± 5.28	5 s / 3a 6 s / 3 a	p = 0.027 p = 0.517	
In NS11021 LFS DHPG	 89.94 ± 5.60 92.86 ± 6.73	 7 s / 5a 5 s / 4 a	 p = 0.188 p = 0.399	2E
12(S)HPETE-NS11021	12(S)HPETE 69.49 ± 6.97 NS11021 66.01 ± 8.90	6 s / 6 a 6 s / 6 a	p = 0.715	2F
NS11021-12(S)HPETE	NS11021 54.39 ± 5.01 12(S)HPETE 50.31 ± 4.74	5 s / 5 a 5 s / 5 a	p = 0.571	2F
Glutamate puff 12(S)HPETE NS11021	 103.38 ± 6.06 99.81 ± 4.85	 9 c / 5 a 5 c/ 3 a	 p = 0.594 p = 0.970	4A
NMDA-mediated EPSC + NS11021	66.64 ± 5.47	6 c/ 4 a	p < 0.001	4B
12(S)HPETE EPSC I_{fAHP}	 49.40 ± 8.01 1.26 ± 0.14	 5 c / 3 a	 p = 0.003 p = 0.091	4C
Minimal Stimulation Failure rate Synaptic efficacy Synaptic Potency	 Pre 0.46 ± 0.08 Post 0.69 ± 0.07 Pre 17.09 ± 6.06 Post 6.15 ± 1.97 Pre 23.26 ± 4.71 Post 18.81 ± 2.28	9 c / 8 a	 p < 0.001 p = 0.021 p = 0.641	4D
Minimal Stimulation in Pax Failure rate Synaptic efficacy Synaptic Potency	 Pre 0.41 ± 0.05 Post 0.33 ± 0.04 Pre 11.00 ± 0.97 Post 15.13 ± 1.06 Pre 21.53 ± 1.59 Post 25.77 ± 2.93	6 c / 4 a	 p = 0.432 p = 0.091 p = 0.252	4E
Pax in pipette NS11021 12(S)HPETE	 69.94 ± 8.04 57.60 ± 7.77	 5 c / 5 a 4 c / 2 a	 p = 0.020 p = 0.012	4F
LFS Control Pax in pipette Pax in bath	 45.33 ± 2.55 57.60 ± 7.77 108.25 ± 9.87	 7 c / 5 a 6 c / 4 a 6 c / 4 a	 p < 0.001 p = 0.004 p = 0.441	4G

Supplementary Table 2: Quantitative analysis of cellular mechanisms involved in mGluR-LTD in neonatal hippocampus. The table includes quantitative analyses of experiments shown in **Supplementary Figures 1 to 6.** "*n*" represents number of slices (*s*), cells (*c*) and animals (*a*). PTX, picrotoxin; I_{fAHP}, Fast Afterhyperpolarization current; I_{mAHP}, medium afterhyperpolarization current; Pax, Paxilline; IBTx, iberiotoxin; SC, Schaffer collateral; INT, Interneuron.

Parameter	Value (mean ± s.e.m)	n	p value	Supplementary Figure
LFS				
GDPβS	105.04 ± 18.01	5 c / 3 a	p = 0.786	1A
Without PTX	64.94 ± 4.92	5 s / 4 a	p = 0.002	1B
AP5	83.36 ± 6.20	7 s / 6 a	p = 0.043	1C
LFS-DHPG	59.33 ± 6.68	5 s / 4 a		1D
	56.62 ± 6.29		p = 0.805	
DHPG-LFS	61.65 ± 5.29	5 s / 5 a		1E
	57.61 ± 3.66		p = 0.582	
DHPG Baicalein	99.01 ± 5.46	5 s / 3 a	p = 0.868	1F
DHPG CDC	103.12 ± 12.05	5 s / 3 a	p = 0.419	
12(S)HPETE-LFS	72.83 ± 3.94			
	68.39 ± 3.59	5 s / 5 a	p = 0.429	2A
12(S)HPETE-DHPG	74.37 ± 7.52			
	67.91 ± 10.18	5 s / 4 a	p = 0.302	2B
LFS	59.33 ± 6.69			
12(S)HPETE after induction	56.62 ± 6.29	5 s / 4 a	p = 0.804	2C
12(S)HPETE in CPZ	71.34 ± 7.55	5 s / 3 a	p = 0.005	3A
12(S)HPETE in AMG	72.37 ± 8.34	5 s / 3 a	p = 0.011	
12(S)HPETE in TRPV1 KO	EPSC 71.37 ± 7.98	3 c / 2 a	p = 0.023	3B
	fEPSP 58.58 ± 9.38	3 s / 2 a	p = 0.012	
Capsaicin effect on SC-CA1 INT synapse	56.73 ± 9.20	11 c / 7 a	p < 0.001	3C
SC-CA1 synapse	97.03 ± 3.79	7 c / 5 a	p = 0.458	
I_{mAHP} in Apamin	I_{mAHP} 0.99 ± 0.001	2 c / 1 a		4A
	+Apamin -0.81 ± 0.33	2 c / 1 a	p = 0.033	
LFS in Apamin	59.42 ± 9.05	5 s / 5 a	p = 0.007	4B
Pax in basal transmission	103.95 ± 5.24	7 s / 7 a	p = 0.234	4C
12(S)HPETE-Pax	77.50 ± 4.94	5 s / 5 a	p = 0.332	4D
	72.61 ± 5.36			
LFS-Pax	77.51 ± 3.37	9 s / 8 a	p = 0.300	4E
	73.39 ± 5.85			
NS11021 short application	64.99 ± 17.08	6 c / 3a	p = 0.004	4F

NS11021-Pax	74.28 ± 7.53 62.63 ± 6.85	6 s / 3 a	p = 0.282	4G
450 pulses 450 to 900 pulses	93.93 ± 7.50 450 pulses 90.58 ± 4.14 900 pulse 67.33 ± 8.43	6 s / 4 a 5 s / 3 a	p = 0.441 p = 0.039	5A 5B
450 pulses control + NS11021 `+Pax	 62.58 ± 11.73 105.97 ± 11.23	 5 s / 3 a	 p = 0.012 p = 0.610	 5C
450 pulses control + 12(S)HPETE `+Pax	 63.52 ± 8.02 98.99 ± 10.67	 5 s / 3 a	 p = 0.001 p = 0.928	5D
I_{fAHP} Control Internal Pax Pax in the bath IBTx in the bath LFS-Internal Pax CsCl internal solution	 0.99 ± 0.00 0.47 ± 0.12 0.58 ± 0.10 0.48 ± 0.11 49.48 ± 12.32 55.37 ± 15.02	 4 c / 2 a 5 c / 4 a 4 c / 2 a 5 c / 3 a 7 c / 5 a	 p = 0.023 p = 0.004 p = 0.003 p < 0.001 p < 0.001	 6B/C 6C 6C 6D 6E

5.2 BK-mediated LTD during hippocampal development and its underlying mechanisms

Summary

BK channels play an important role in mGluR-mediated long-term depression (LTD) in the neonatal hippocampus. However, the cellular and molecular signaling underlying this form of synaptic plasticity remains unclear. It is also unknown whether BK channels also contribute to activity-dependent changes of synaptic strength at mature synapses. Here, we show that in neonatal hippocampus BK-mediated LTD involves activation of calcineurin and protein synthesis. Importantly, we found that BK channels do not contribute to mGluR-mediated LTD at mature synapses, likely by changes in BK subunit composition. Moreover, we found that BK-mediated LTD in neonatal hippocampus coexists with a form of LTD that requires endocannabinoid signaling. Together these results contribute to the understanding of cellular process occurring during hippocampus development, highlighting the role of BK channels in the neonatal stage of development and could be relevant to unveiling the mechanisms underlying neurodevelopmental disorders in which BK channels have been involved.

Introduction

Metabotropic glutamate receptors (mGluRs), particularly group I mGluRs (mGluR1 and mGluR5), are key modulators of synaptic plasticity. Their activation leads to long-term changes in synaptic strength, primarily through long-term depression (LTD) (Antion et al., 2008; Kamsler et al., 2010; Le Duigou et al., 2011; Lüscher & Huber, 2010; Speranza et al., 2022; Watabe et al., 2002) and, in some contexts, long-term potentiation (LTP) (Anwyl, 2009; Galván et al., 2008; Gubellini et al., 2003; H. Wang et al., 2016), influencing learning and memory processes (Ancatén-González et al., 2025; Bolshakov & Siegelbaum, 1994; Brager & Johnston, 2007; Gil-Sanz et al., 2008; Izumi & Zorumski, 2012; Kamsler et al., 2010; Kwag & Paulsen, 2012; C. Li et al., 2007; Perez et al., 2001; Purgert et al., 2014; Watabe et al., 2002). Although mGluR can modulate synaptic transmission and plasticity through diverse intracellular signaling cascades (Lüscher & Huber, 2010; Niswender & Conn, 2010), the exact mechanism underlying mGluR-LTD at early stage of hippocampal development have received much less attention than those occurring at mature synapses (Chaudhury et al., 2016). For instance, in the hippocampus, a developmental change in the mechanism underlying mGluR-LTD has

been reported (Nosyreva & Huber, 2005) including a decrease in AMPA receptor (AMPAR) surface expression in adult animals, whereas in neonatal animals, mGluR-LTD results in large decreases in presynaptic function. Conversely, mGluR-LTD at mature synapses results in little or no change in presynaptic function, suggesting a change from presynaptic to postsynaptic mechanism of expression of mGluR-LTD (Nosyreva & Huber, 2005). Recently, we reported that mGluR-LTD in neonatal hippocampus involves the activation of, presumably, presynaptic BK channels to decrease neurotransmitter release (results 5.1; (Ancatén-González et al., 2025)). Likewise, functional BK channels exist in the presynaptic terminal and can regulate transmitter release (Hu et al., 2001) and have been involved in the expression of LTP at mature hippocampus (Pham et al., 2023). *However, whether presynaptic BK channels are also involved in mGluR-LTD at mature hippocampus remains unknown.*

Intracellular levels of calcium (Ca^{2+}) are strictly and finely controlled in all synaptic components (Rusakov, 2006) that are involved in processes such as neurotransmitter release and synaptic plasticity (Chindemi et al., 2022; Cummings & Mulkey, 1996; Eshra et al., 2021; Singh et al., 2021). Notably, BK channels are known to be activated by intracellular rise in Ca^{2+} (Irie & Trussell, 2017; Latorre et al., 2017; Lorenzo-Ceballos et al., 2019; Oh et al., 2015; Shah et al., 2022), and its activation also reportedly induced changes in presynaptic action potential (AP) waveform that profoundly influence Ca^{2+} influx and thus neurotransmitter release (Dittman & Ryan, 2019; Hirono et al., 2015; Roshchin et al., 2018). *However, how changes in presynaptic Ca^{2+} influx impact on BK channels-mediated LTD remains unclear.* One source of Ca^{2+} that has been suggested to be involved in neonatal mGluR-LTD is the Ca^{2+} entry through L-type voltage-gated calcium channels (VGCCs) (Bolshakov & Siegelbaum, 1994). Otherwise, VGCCs involved in the synchronous release of neurotransmitters have been also reported including Cav2.1 (P/Q-type) and Cav2.2 (N-type) (Dolphin, 2020; Dolphin & Lee, 2020). *While the expression and functional role of these VGCCs in regulating synaptic transmission and synaptic plasticity at mature hippocampus has been reported* (Igelmund et al., 1996)*, its roles at early stage of hippocampal development remain elusive.*

Different synaptic signaling including phosphorylation or dephosphorylation of synaptic proteins also has been reported to be involved in the modulation of synaptic strength (Colbran, 2004; Leenders & Sheng, 2005; Sanderson et al., 2016; J.-H. Wang & Kelly, 1996), an effect that tightly depends on the intracellular Ca^{2+} concentration (Bradshaw et al., 2003). For instance, protein kinases add phosphate groups to target proteins (phosphorylation), typically activating signaling pathways

that enhance synaptic strength, whereas phosphatases remove these phosphate groups (dephosphorylation), generally acting to dampen or reverse the effects of kinases and are particularly important for LTD mechanism (Colbran, 2004; Lee, 2006). Previous evidence suggests that LTD in young hippocampus (2-4 weeks) is modulated by kinases such as diacylglycerol kinases (DGK) and Protein Kinase C (PKC) interaction (Yang et al., 2011), and CaMKII (Mayford et al., 1995), but whether these enzymes are involved in neonatal stage has not been directly tested. *While the balance between these kinases and phosphatases can define the direction of the synaptic plasticity (Neveu & Zucker, 1996), their role in regulating neonatal BK-mediated plasticity remains unknown.*

Results

Presynaptic BK channels did not contribute to mGluR-LTD at mature hippocampus.

To investigate whether presynaptic BK channels are involved in the induction of mGluR-LTD at mature synapses in the hippocampus and to determine potential changes in the underlying mechanism during postnatal development, we recorded fEPSPs while stimulating CA3 Schaffer collateral inputs in acute CA1 hippocampal slices of adult (postnatal day P20-30) mice using previously described low frequency stimulation (LFS) (Ancatén-González et al., 2025). Unlike neonatal hippocampus (Chapter 5.1), LFS protocol elicited a LTP at mature synapses that was dependent on NMDA receptor (NMDAR) activation, as bath application of the NMDAR inhibitor APV decreased LTP (Figure 5.2.1A). As LFS in adult hippocampus elicit an LTP, to evaluate whether BK channels participate on mGluR-mediated LTD, we next induced mGluR-LTD by bath application of the mGluR agonist DHPG (50 μM). Under this experimental condition, however, bath application of the BK channel blocker paxilline has no effect on DHPG-induced LTD (Figure 5.2.1B) suggesting that BK channels did not contribute significantly for mGluR-LTD at mature hippocampus. To further determine whether BK channels are indeed expressed at mature synapses, we bath apply the BK channels agonist 12(S)HPETE (100 nM) or NS11021 (3 μM) known to depress synaptic transmission in neonatal hippocampus (Ancatén-González et al., 2025) and found no effect on basal synaptic transmission (Figure 5.2.1C), suggesting that BK channels might not be expressed at mature synapses. However, previous evidence has shown that blocking voltage-gated K^+ channels with 4-aminopyridine (4-AP) to broaden the presynaptic action potential promotes BK channel activation by prolonging the depolarization and increasing the Ca^{2+} influx at synaptic terminal (Hu et al., 2001). To test this possibility, 4-AP (10 μM) was bath-applied, and the effects of BK channels agonist were

tested. While the BK channel opener NS11021 significantly reduced excitatory function in the presence of 4-AP, bath application of 12(S)HPETE did not reduce transmission (Figure 5.2.1D). As 12(S)HPETE only impacts $BK_{\beta4}$ (Ancatén-González et al., 2025), these results open the possibility that BK channels undergo to a subunit composition change at Sch-CA1 synapse during hippocampal maturation. If this were the case, we expect that blocking BK channels with both Iberiotoxin (Ibtx) and Paxilline (PAX) might increase synaptic transmission as previously reported (Hu et al., 2001). Consistent with this idea, we found that these antagonists had no effects on basal excitatory synaptic transmission under normal conditions but increased synaptic efficacy in the presence of 4-AP (1mM) (Figure 5.2.1E-F). Moreover, we found that even in the presence of 4-AP, BK channels did not contribute significantly for mGluR-LTD as LFS at mature hippocampus did not trigger a LTD (Figure 5.2.1G). Altogether these experiments suggest that in mature synapses presynaptic BK channels did not contribute to mGluR-LTD, its activation are masked by voltage-gated K^+ channels and presumably a change in subunit composition from $BK_{\beta4}$ to $BK_{\beta2}$ occurs during hippocampal postnatal development.

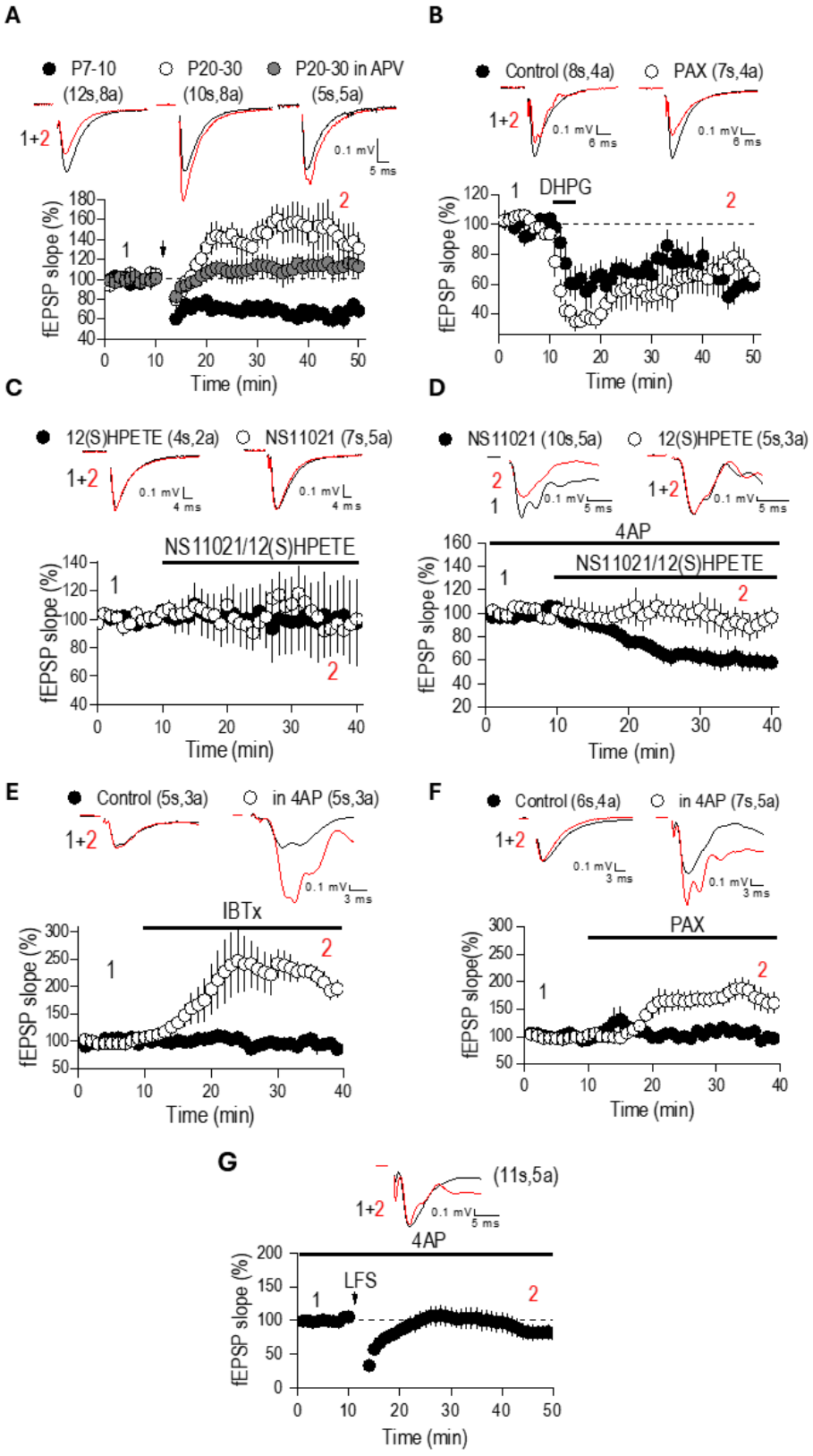

A
P7-10
(12s,8a)
P20-30
(10s,8a)
P20-30 in APV
(5s,5a)
1+2
0.1 mV
5 ms
fEPSP slope (%)
Time (min)
B
Control (8s,4a)
PAX (7s,4a)
1+2
0.1 mV
6 ms
DHPG
fEPSP slope (%)
Time (min)
C
12(S)HPETE (4s,2a)
NS11021 (7s,5a)
1+2
0.1 mV
4 ms
NS11021/12(S)HPETE
fEPSP slope (%)
Time (min)
D
NS11021 (10s,5a)
12(S)HPETE (5s,3a)
0.1 mV
5 ms
4AP
NS11021/12(S)HPETE
fEPSP slope (%)
Time (min)
E
Control (5s,3a)
in 4AP (5s,3a)
1+2
0.1 mV
3 ms
IBTx
fEPSP slope (%)
Time (min)
F
Control (6s,4a)
in 4AP (7s,5a)
1+2
0.1 mV
3 ms
PAX
fEPSP slope(%)
Time (min)
G
(11s,5a)
1+2
0.1 mV
5 ms
4AP
LFS
fEPSP slope (%)
Time (min)

Figure 5.2.1 BK channels are not required for mGluR-LTD presumably by changes in its subunit composition at mature synapses*. **A**, LFS induced mGluR-LTD in neonatal but not in adult hippocampus. This protocol instead induces a LTP that is blocked by the NMDARs antagonist APV (50μM). **B**, DHPG induced mGluR-LTD in adult hippocampus is unaffected by BK channel blocker PAX (10μM). **C**, Activation of BK channels with NS11021 (3μM) and 12(S)HPETE (100 nM) do not change the strength of synaptic function in mature animals. **D**, In the presence of 4-AP, a voltage-gated K+ channels blocker, NS11021 but not 12(S)HPETE reduces synaptic function in adult hippocampus. **E**, The BK channel blocker IBTX has no effect on basal transmission under normal conditions but increase fEPSP in the presence of 4-AP (1mM). **F**, The BK channel blocker PAX has no effect on basal transmission under normal conditions but increase fEPSP in the presence of 4-AP. **G**, Even in the presence of 4-AP LFS stimulation did not trigger a LTD in adult hippocampus. Data are presented as mean ± S.E.M and the number of slices (s) and animals (a) used are included.*

Presynaptic BK channels contribute to LTD but not to LTP at neonatal hippocampus.

As BK channels did not significantly contribute to mGluR-LTD in adult hippocampus (Figure 5.2.1), next we concentrate on understanding the cellular and molecular mechanism involved in neonatal mGluR-LTD. First, we evaluate whether BK channel contribution to synaptic plasticity is frequency-dependent in neonatal hippocampus as previously it has been suggested that LFS-induced mGluR at 1 and 5 Hz shares the same mechanism (Feinmark et al., 2003). Toward this end, we delivered electric train stimulation at different frequencies (e.g. 1 to 100 Hz) in control conditions and in presence of the BK channel blocker paxilline (PAX, 10 μM). Interestingly, LFS stimulation delivered at 1 Hz and 5 Hz induced LTD that were eliminated by PAX (Figures 5.2.2A-B), whereas higher frequencies stimulation (50 and 100 Hz) were insensitive to PAX (Figures 5.2.2C-D). These results indicate that BK channel's contribution to synaptic plasticity is indeed frequency dependent filtering synapses with high rate of transmission (Figure 5.2.2E).

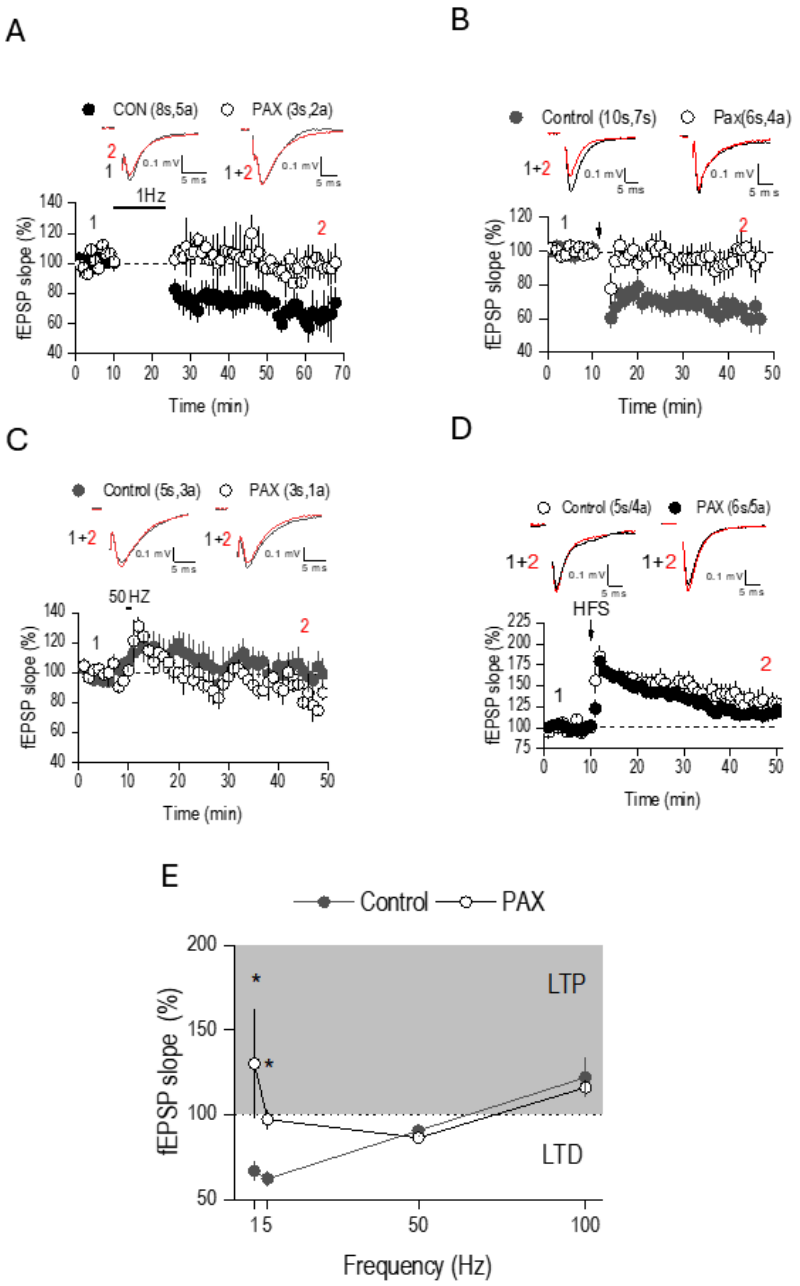


Figure 5.2.2. BK channel contribution to synaptic plasticity is frequency-dependent. *Trains of low frequency stimulation (LFS) at 1 Hz* ***(A)*** *and 5Hz* ***(B)*** *are eliminated by Paxilline (PAX,10 μM), but not at 50 Hz* ***(C)*** *or 100 Hz* ***(D)*** *stimulation, indicating that BK channels are required for LTD processes induced by LFS, but not in LTP* ***(E)****. Data are presented as mean ± S.E.M and the number of slices (s) and animals (a) used are included.*

Mechanisms underlying BK channel-mediated LTD in neonatal hippocampus.

To determine the mechanisms involved in the BK channel-mediated LTD induced by LFS in neonatal hippocampus, next we tested the participation of different biological agents involved in synaptic plasticity processes, including Ca^{2+} signal, kinases and phosphatases (Colbran, 2004; Incontro et al., 2018; Murakoshi et al., 2017; Pang et al., 2010; Stanton & Gage, 1996; J.-H. Wang & Kelly, 1996). For instance, arachidonic acid (AA) activity requires Ca^{2+} and is involved in mGluR-LTD (Bolshakov & Siegelbaum, 1995). To test whether postsynaptic Ca^{2+} is required for the induction of mGluR-LTD we load CA1 pyramidal neurons with the Ca^{2+} chelator BAPTA (10 mM) and found that LFS stimulation did not produce a mGluR-LTD (Suppl Figure 5.2A), indicating that postsynaptic Ca^{2+} is required for this form of plasticity. Importantly, when CA1 neurons were loaded with BAPTA bath application of NS11021 or 12(S)HPETE to activate BK channels induced a strong depression of synaptic function (Suppl Figure 5.2B), further supporting a presynaptic rather than a postsynaptic mechanism of action of BK channels to trigger LTD. Continuing with the source of Ca^{2+} required to produce AA metabolite, next we applied LFS stimulation in the presence of cyclopiazonic acid (CPA, 1μM), an inhibitor of intracellular Ca^{2+} stores (SERCA pump). While CPA has no effect on basal synaptic transmission (Suppl Figure 5.2C), it decreases the magnitude of LTD induced by LFS (Figure 5.2.3A), suggesting that SERCA pump might also be involved in the production of the AA metabolite involved in mGluR-LTD. In contrast, CPA did not significantly reduce NS11021-induced depression compared to control conditions (Figure 5.2.3B), supporting a role of postsynaptic SERCA pump in the induction of mGluR-LTD. Finally, we tested the role of different VGCCs in the magnitude of mGluR-LTD. As previously reported (Bolshakov & Siegelbaum, 1994) we found that the L-type VGCCs blocker Nimodipine significatively decreased LFS-induced LTD (Figure 5.2.3C). Nimodipine (10 μM), however, was unable to decrease NS11021-induced depression observed in control conditions (Figure 5.2.3D), suggesting that L-type VGCCs are involved in mGluR-LTD induction but not after BK channel activation. Moreover, we found that mibefradil (10 μM), a T-type Ca^{2+} channel blocker has no effect on LFS- and NS11021-induced depression (Figure 5.2.3E-F), indicating that this type of VGCCs do not participate in the hippocampal neonatal LTD. The participation of other VGCCs were also tested using specific blockers, including the N-type blocker ω- Conotoxin MVIIA (100 nM), P/Q-type blocker ω-Agatoxin IVA (100 nM), and the R-type blocker SNX-488(100 nM). While all of them were able to decrease

excitatory, a higher effect was observed with N and P/Q blocker (Figures 5.2.3G). Importantly, blocking R-type decreased LFS-induced LTD but not blocking N- and P/Q type (Figure 5.2.3H), suggesting the participation of R- type VGCCs in the mechanism underlying mGluR-LTD.

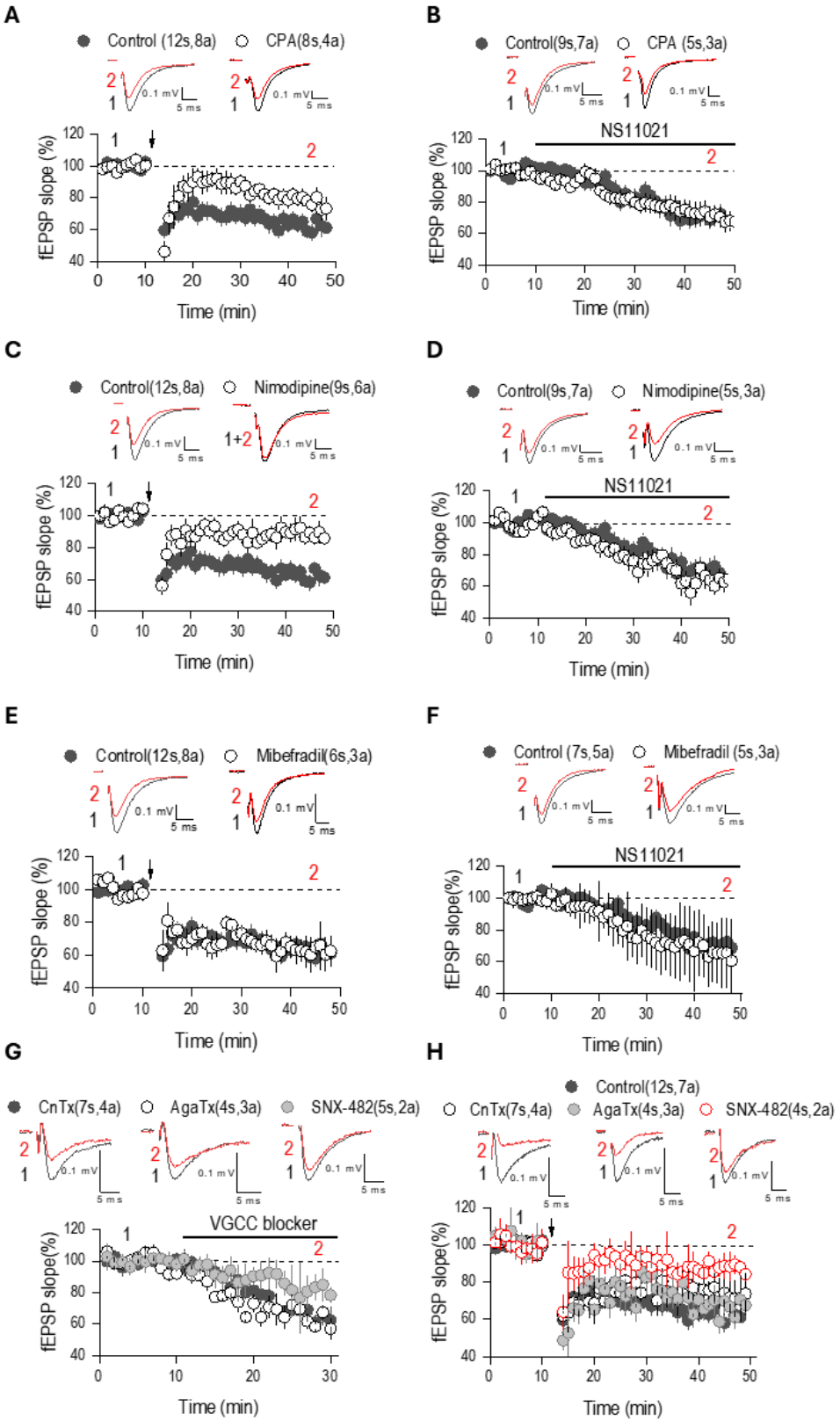

A
Control (12s,8a)
CPA(8s,4a)
fEPSP slope (%)
Time (min)
B
Control(9s,7a)
CPA (5s,3a)
NS11021
C
Control(12s,8a)
Nimodipine(9s,6a)
D
Control(9s,7a)
Nimodipine(5s,3a)
E
Control(12s,8a)
Mibefradil(6s,3a)
F
Control (7s,5a)
Mibefradil (5s,3a)
G
CnTx(7s,4a)
AgaTx(4s,3a)
SNX-482(5s,2a)
VGCC blocker
H
Control(12s,7a)
CnTx(7s,4a)
AgaTx(4s,3a)
SNX-482(4s,2a)

***Figure 5.2.3. L- but not T-type Ca^{2+} contributes to the induction of mGluR-LTD**. **A**, Cyclopiazonic acid (5μM), a SERCA pump blocker decreased magnitude of LFS-induced LTD **(B)** but not NS11021-induced LTD. **C**, Nimodipine(10μM) a L-type VGCC blocker decreased LFS-induced LTD, but not NS11021-induced LTD **(D)**. **E**, Blocking T-type Ca^{2+} channels with Mibefradil (10 μM) has no effects on LFS- and NS11021-induced LTD (**F**). Blockers for N-,P/Q-, and R- type VGCCs (ω–Conotoxin MVIIA, ω- Agatoxin IVA and SNX-482, respectively) decrease basal excitatory transmission **(G)**, but only SNX-482 reduced LFS-induced LTD **(H)**. Data are presented as mean ± S.E.M and the number of slices (s) and animals (a) used are included.*

As our results strongly suggest that increases in postsynaptic Ca^{2+} are required to induce neonatal LTD in the hippocampus, next we tested the contribution of presynaptic Ca^{2+} to induce LTD. Toward this end, we delivered LFS stimulation protocol and/or BK channel agonists in the presence of the cell membrane-permeable Ca^{2+} chelator with different binding kinetics including the fast chelator BAPTA-AM and the slow chelator EGTA-AM. Consistent with this idea, BAPTA-AM reduces basal excitatory transmission, whereas EGTA-AM did not (Suppl Figure 5.2D). Moreover, in slices pre-treated with BAPTA-AM, we found that both LFS- and DHPG-induced LTD were eliminated (Suppl Figure 5.2E) consistent with a fast requirement for Ca^{2+} changes in the induction of LTD. Importantly, 12(S)HPETE- and NS11021-induced LTD, two different forms of synaptic depression not affected by loading postsynaptic CA1 neuron with BAPTA (Suppl Figure 5.2B), were eliminated in the presence of BAPTA-AM (Suppl Figure 5.2E), strongly suggesting that fast presynaptic Ca^{2+} signal are required for BK-mediated LTD. In contrast, we found that EGTA-AM also eliminated LFS-induce LTD (Suppl Figure 5.2F) but had no effect on NS11021-induced LTD (Suppl Figure 5.2G). Given the differences in kinetics of BAPTA-AM and EGTA-AM, these results suggest that the presynaptic source required to induce BK-mediated depression should be closed to BK channels in the presynaptic terminal.

As changes in intracellular Ca^{2+} concentration modify the activity of phosphatases and kinases (Colbran, 2004; J.-H. Wang & Kelly, 1996) and different protein kinases are present in presynaptic terminal including cyclic-AMP-dependent protein kinase A (PKA), Ca+2/ calmodulin -dependent kinase II (CaMKII), and protein kinase C (PKC) (Leenders & Sheng, 2005), next we tested the identity of kinases and phosphatases involved in mGluR-LTD in neonatal hippocampus using specific pharmacology. First, we tested the contribution of PKA by applying the PKA inhibitor H89 (10 μM) which by itself did not significatively changed the basal transmission (Supp Figure 5.4A) and had no effect on the magnitude of mGluR-LTD induced by LFS stimulation (Figure 5.2.4A). Moreover, we found that the activation of adenylyl cyclase with Forskolin, which by itself increased excitatory synaptic strength (Suppl Figure 5.4B) also had no effect on LFS-induced LTD (Figure 5.2.4A), indicating that cAMP and PKA are not involved in this form of plasticity.

Second, we tested the participation of PKC, through the PKC inhibitor chelerythrine chloride (5 μM), which interestingly depressed basal transmission when was applied to the bath (Suppl Figure 5.4C). In the presence of the PCK inhibitor, NS11021 was able to depress excitatory CA3-CA1 synapse (Figure 5.2.4B), suggesting that PKC is not required for the BK channel-mediated depression of glutamate release.

Third, we tested the involvement of CaMKII, a well-known protein kinase involved in hippocampal synaptic plasticity and also in BK channel regulation (Coultrap & Bayer, 2012; Ninan & Arancio, 2004; Shibata et al., 2021; Z. W. Wang, 2008) , in the neonatal LTD. To this end, we delivered LFS stimulation protocol in two different conditions, one in the presence of the CaMKII inhibitor KN93, and another in presence of the inactive form of KN93, KN92. In both conditions a synaptic depression was observed, but the magnitude of the LTD evoked in presence of KN 93 was smaller than those observed in presence of K92 (Figure 5.2.4C), suggesting a small, but significant involvement of CaMKII in the neonatal LTD. More importantly, when the peptide inhibitor CaMKII 290-309 (Nelson et al., 2005) was loaded in CA1 pyramidal cells no effect on the magnitude of LFS-LTD was found (Figure 5.2.4D), suggesting that presynaptic rather than postsynaptic CaMKII is involved in the neonatal LTD.

Fourth, we evaluated the participation of the phosphatase calcineurin (CaN), which has been previously involved in other form of presynaptic LTD in the hippocampus (Heifets et al., 2008; Jensen

& Edwards, 2012; Lin et al., 2003; Reyes-García & Escobar, 2021; Sanderson et al., 2016; Zhuo et al., 1999). To this end, we bath-applied the CaN inhibitor FK506 (1μM) and then delivered the LFS stimulation protocol and found a full block of LFS-induced LTD (Figure 5.2.4E). Likewise, FK506 was also able to block NS11021-induced LTD (Figure 5.2.4F), strongly suggesting that CaN plays an important role in regulating BK channel mediated LTD.

Finally, we also evaluated whether protein synthesis could be also involved in mGluR-LTD in neonatal hippocampus as previously shown in other forms of LTD (Barnes et al., 2010; Calixto et al., 2003; Monday et al., 2020; Perrone-Capano et al., 2021; Till et al., 2011). To this end, we incubated hippocampal slices in the protein synthesis inhibitor Anisomycin (10 μM) and found that both LFS- and NS11021-induced LTD were eliminated (Figure 5.2.4G-H), suggesting that mGluR-LTD in neonatal hippocampus requires local protein synthesis.

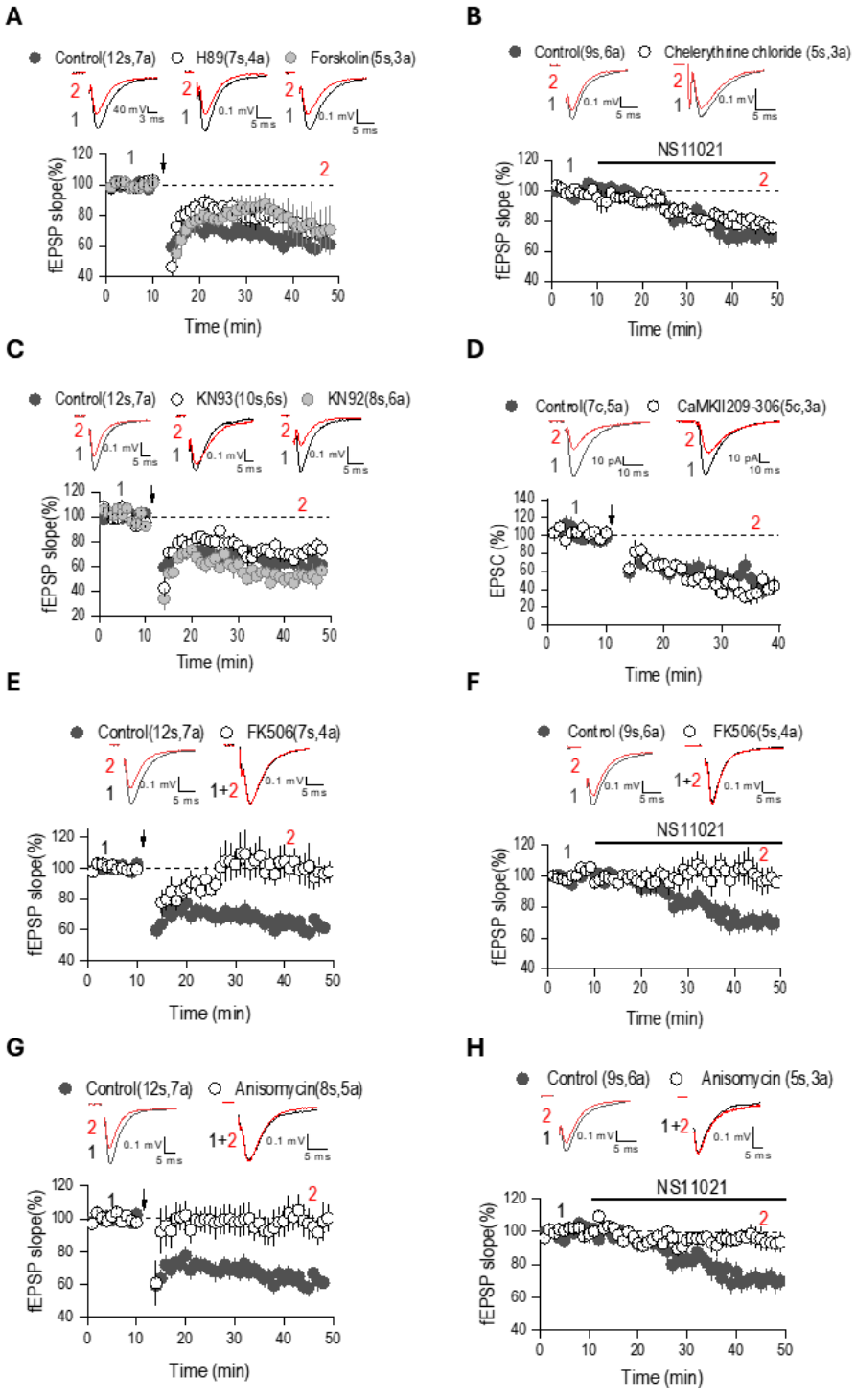

A
Control(12s,7a)
H89(7s,4a)
Forskolin(5s,3a)
fEPSP slope(%)
Time (min)
B
Control(9s,6a)
Chelerythrine chloride (5s,3a)
NS11021
fEPSP slope (%)
Time (min)
C
Control(12s,7a)
KN93(10s,6s)
KN92(8s,6a)
fEPSP slope(%)
Time (min)
D
Control(7c,5a)
CaMKII 209-306(5c,3a)
EPSC (%)
Time (min)
E
Control(12s,7a)
FK506(7s,4a)
fEPSP slope(%)
Time (min)
F
Control (9s,6a)
FK506(5s,4a)
NS11021
fEPSP slope(%)
Time (min)
G
Control(12s,7a)
Anisomycin(8s,5a)
fEPSP slope(%)
Time (min)
H
Control (9s,6a)
Anisomycin (5s,3a)
NS11021
fEPSP slope(%)
Time (min)

Figure 5.2.4. Neonatal mGluR-LTD requires presynaptic calcineurin activity and protein synthesis. ***A****, Blocking PKA with H89 or activating cAMP with forskolin did not affect LFS-induced LTD. Inhibiting PKC signaling through chelerythrine chloride (5μM) was unable to prevent NS11021-induced depression* ***(B)****. Blocking CaMKII with KN93 reduced the magnitude of LFS-induced LTD respect to the inactive form of KN93, KN92****(C)****, but blocking postsynaptic CaMKII loading the peptide CAMKII 290-309 in the postsynaptic cell did not affect LFS-induced LTD* ***(D)****. Inhibition of both calcineurin and synthesis protein were able to block LFS- and NS11021- induced LTD* ***(E-H)****. Data are presented as mean ± S.E.M and the number of slices (s), cells (c) and animals (a) used are included.*

5.3 Does BK-mediated plasticity work in concert with other types of synaptic plasticity to regulate synaptic strength in the neonatal hippocampus?

Once we have determined part of the cellular and molecular mechanisms underlying BK-mediated plasticity in neonatal hippocampus, we focus on understanding whether this form of synaptic plasticity works in concert or in opposite way with other types of synaptic plasticity to regulate synaptic strength early in hippocampal development. For instance, like endovanilloid signaling another lipid-based signaling molecules that play a crucial role in regulating synaptic transmission and plasticity throughout the brain is the endocannabinoid (eCB) system. Their modulation of synaptic function is multifaceted, involving both short- and long-term effects on excitatory and inhibitory synapses (Castillo, 2012; Lu & MacKie, 2016). Notably, eCB-mediated synaptic plasticity (eCB-LTD) often coexists with and interacts with other forms of synaptic plasticity including those involving metabotropic glutamate receptor (mGluR)-dependent LTD, sharing common signaling pathways (e.g., calcium elevation) (Meunier et al., 2017) to create a complex regulatory network that shapes neural circuit function. Interestingly, BK-mediated LTD requires activation of mGluR5 (Ancatén-González et al., 2025; Bolshakov & Siegelbaum, 1994; Feinmark et al., 2003), and requires CaN and protein synthesis, two independent mechanisms involved in different forms of eCB-mediated plasticity (Heifets et al., 2008; Monday et al., 2020), opening the possibility that BK-mediated LTD might coexist with some form of eCB-mediated plasticity at neonatal hippocampus. In support of this idea, type 1 cannabinoid receptor (CB1R), which are present at excitatory hippocampal terminals in mature animals (Kawamura et al., 2006), seem to be present also early during embryonic and neonatal development (Vitalis et al., 2008) contributing to

modulation of synaptic plasticity (Yasuda et al., 2008). *However, whether CB1R-depedent plasticity co-exist with BK-mediated LTD to regulate synaptic strength at the Sch-CA1 synapse in neonatal hippocampus remains unknown*.

To test this possibility, we applied the CB1R agonist WIN55,212-2 (WIN, 5 μM) while field EPSP were recorded in neonatal hippocampus to determine whether CB1Rs are functional expressed at excitatory Sch-CA1 synapses. Like those effects reported in mature animals (Izumi & Zorumski, 2012), we found that the activation of CB1R decreased excitatory Sch-CA1 synapses, an effect that was accompanied by an increase in PPR (Figure 5.2.5A) suggesting a presynaptic locus of action. Next, we evaluate whether LFS, known to induce BK-mediated LTD in neonatal hippocampus, is sensitive to blockage of CB1R. As shown in Figure 5.2.5B, however, LFS-induced LTD was unaffected by blocking CB1R with the inverse agonist, AM251 (4 μM). Such result is consistent with the idea that during LFS (5Hz, 3min) activation of mGluR triggers the production of the endovanilloid 12(S)HPETE (Ancatén-González et al., 2025; Bolshakov & Siegelbaum, 1994; Feinmark et al., 2003) rather than producing eCB signaling to depress in an activity-dependent manner excitatory Sch-CA1 synapses. Moreover, these results also suggest that an additional mechanism might be involved if they do not occlude each other. Accordingly, after WIN-mediated depression LFS induced an additional suppression of the excitatory transmission (Figure 5.2.5C). Inversely, activation of CB1R induced an additional depression to the LFS-induced LTD (Figure 5.2.5D), supporting the idea that CB1R- and BK channel mediated LTD require different signal pathways (induction and/or expression) to depress transmitter release at Sch-CA1 synapse in neonatal hippocampus. For instance, WIN-mediated depression is insensitive to CaN inhibitor FK506 (Figure 5.2.5E) as well as to the protein synthesis blocker anisomycin (Figure 5.2.5F), suggesting that BK channel-mediated LTD and CB1R-mediated depressing does not share the same mechanism to reduce synaptic function and coexist at immature hippocampus.

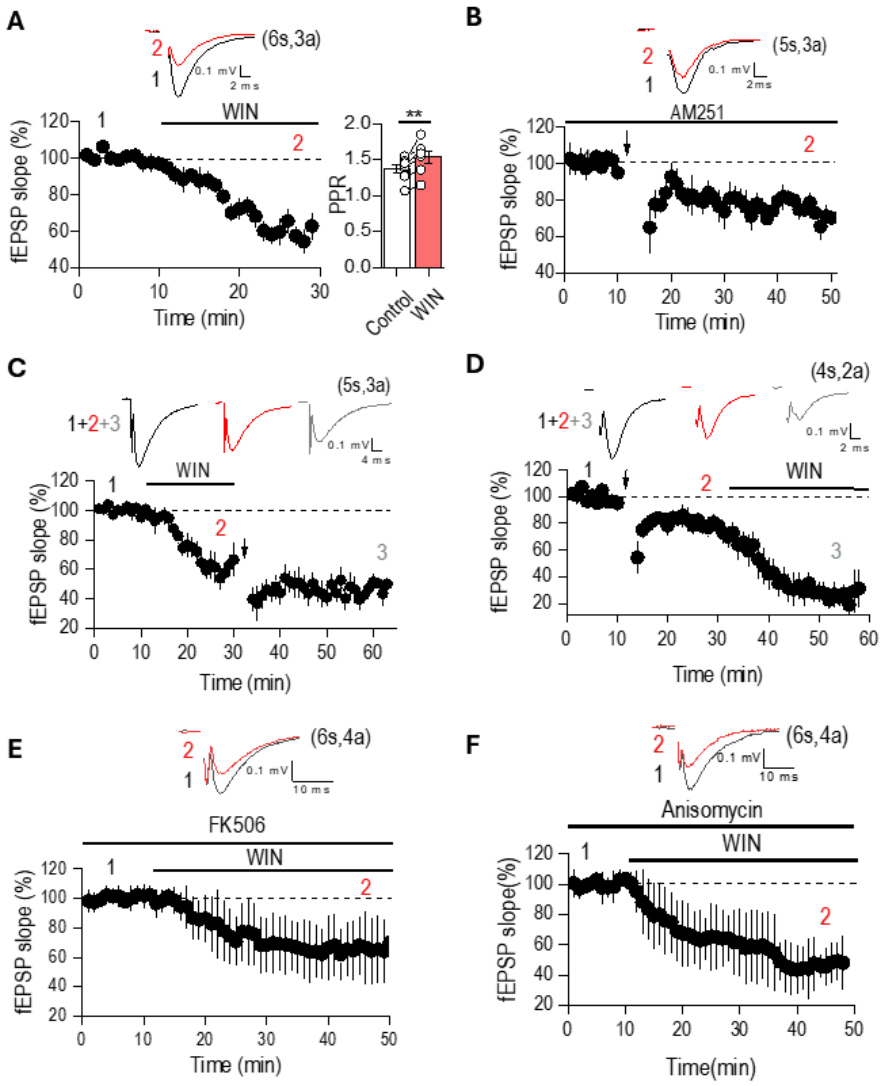


Figure 5.2.5. CB1R- and BK-dependet LTD co-exist at immature hippocampus. *Activation of CB1Rs using WIN 55,212-2 (5μM) induces a LTD which was accompanied by a change in PPR suggesting a presynaptic locus* ***(A)****. LFS-induced LTD was not affected when protocol was delivered in the presence of the CB1R inverse agonist AM251 (4μM)* ***(B)****. LFS stimulation induces an additional depression to the eCB-induced LTD* ***(C)****, and the same result is observed when the protocols are inverted* ***(D)****, suggesting different mechanisms. Activating CB1R induces a LTD that was not affected by blocking calcineurin* ***(E)*** *or protein synthesis* ***(F)****. Data are presented as mean ± S.E.M and the number of slices (s) and animals (a) used are included.*

As the activation of mGluR5 with DHPG produce an LTD that was fully blocked by the BK channel blocker paxilline (Ancatén-González et al., 2025), suggest that mGluR5 might not be the mechanism to induce eCBs production in neonatal hippocampus. To confirm that mGluR signaling does not require CB1R to depress excitatory Sch-CA1 synapse in neonatal hippocampus, we applied the group I- mGluR agonist DHPG (50μM) in presence of the CB1R inverse agonist AM251 (4μM) and found that DHPG was able to induce a long-lasting depression of fEPSP(Figure 5.2.6A), suggesting that other mechanisms for the induction of eCB-mediated plasticity might be involved. Some of the mechanisms involved in eCB-mediated LTD include astrocytic CB1Rs and NMDA receptors (NMDARs) (Han et al., 2012). For instance, an interaction between presynaptic NMDAR and CB1R to induce LTD has been described in neocortex (Sjöström et al., 2003). To evaluate if NMDAR are required for the induction of neonatal eCB-mediated LTD, we applied NMDA (50μM, 3 min) that induced a robust LTD accompanied by changes in PPR, effects that were eliminated in slices pre-incubated with the CB1R inverse agonist AM251 (Figures 5.2.6B). Moreover, NMDA-induced depression was not occluded by DHPG-induced LTD (Figure 5.2.6C), supporting the idea that mGluR- and NMDA-induced plasticity coexist at neonatal hippocampus. To test this idea, we next applied a stronger stimulation protocol (paired-pulse low frequency; PP-LFS), consisting in 900 paired stimuli at 1Hz for 15 minutes and evaluate if both mGluR- and NMDAR-dependent effects can be elicited by synaptic activity. PP-LFS induced a robust LTD that was partially reduced by bath application of the NMDARs antagonist APV (25 μM) and fully blocked by subsequent application of the mGluR5 antagonist MTEP (10μM) (Figure 5.2.7A). Notably, PP-LFS-induced LTD was also partially reduce by the BK channel antagonist paxilline or the CB1Rs inverse agonist AM251 but was eliminated in the presence of both antagonists (Figure 5.2.7B). Altogether these results further demonstrate that BK channel- and CB1R-mediated LTD coexist at neonatal hippocampus and that these forms of LTD do not share the same mechanism for induction and expression.

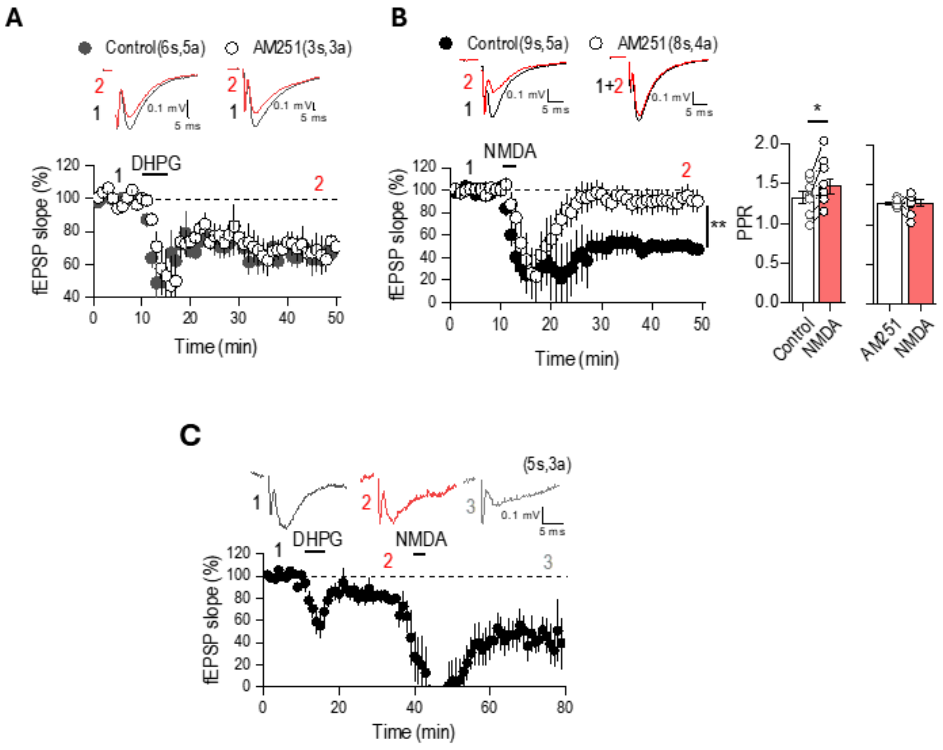


Figure 5.2.6. NMDA-mediated LTD in neonatal hippocampus requires activation of CB1R. A*, mGlur5 activation by DHPG (50μM, 5 minutes) induces robust depression in the presence of the CB1Rs inverse agonist AM251(4μM).* ***B****, NMDA (20μM, 3 minutes) induced a presynaptic form of LTD that requires CB1R activation, as this depression was blocked in presence of AM251 (4μM).* ***C****, DHPG- and NMDAR-induced LTD does not occlude to each other, suggesting different mechanisms. Data are presented as mean ± S.E.M and the number of slices (s) and animals (a) used are included.*

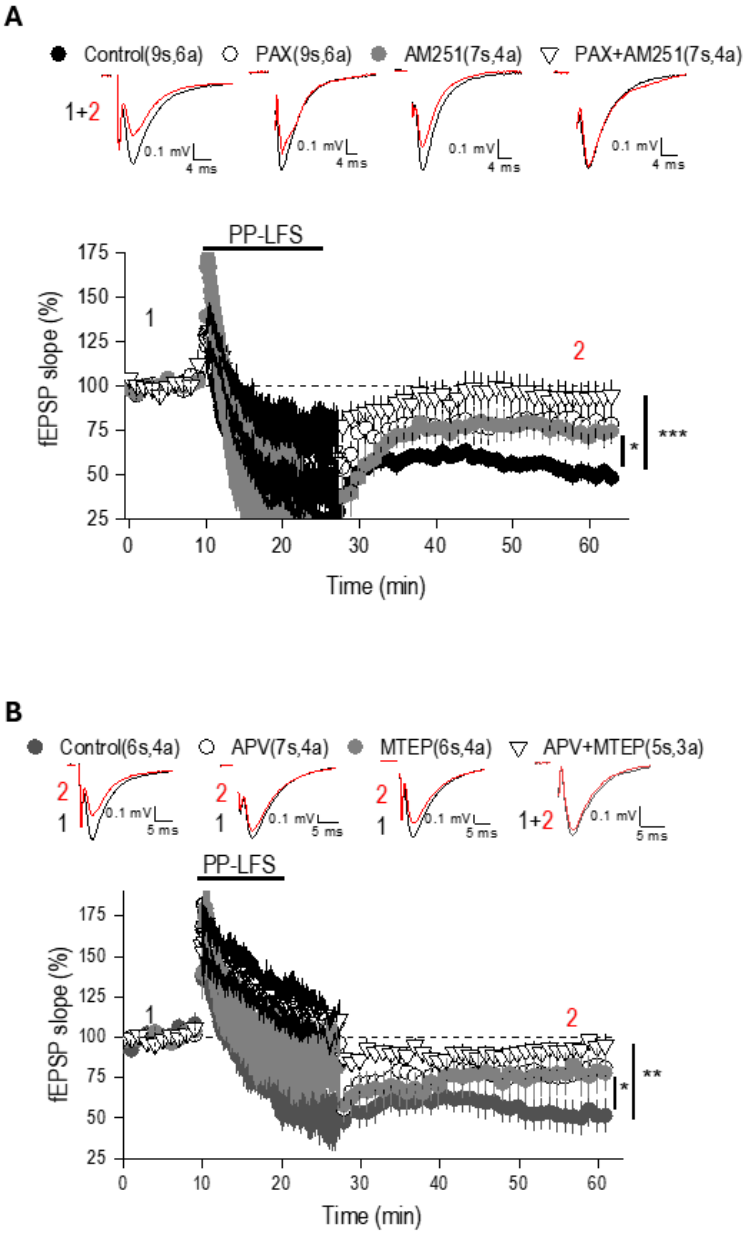


Figure 5.2.7. eCB- and BK channel-mediated LTD coexist in neonatal hippocampus. A*, Paired-pulse low frequency stimulation (PP-LFS) induces a strong depression that was partially blocked by NMDAR antagonist APV (25 μM) and subsequent application of the mGLuR5 inhibitor (MTEP 10μM) completely blocked it, indicating that PP-LFS was able to induce both mGluR- and NMDAR-induced plasticity in neonatal Sch-CA1 synapse.* ***B****, PP-LFS induced plasticity was partially blocked by Paxilline (PAX, 10 μM) or AM251 (4μM), and subsequent application of these antagonists eliminated PP-LFS-induced LTD. Data are presented as mean ± S.E.M and the number of slices (s) and animals (a) used are included.*

6. DISCUSSION

In this thesis work, we demonstrated a form of LTD in neonatal hippocampus that is mediated by mGluR5, that triggers the production of the arachidonic acid metabolite 12(S)HPETE), to activate presynaptic BK channels at Sch-CA1 synapse. Moreover, we demonstrated part of the cellular mechanisms underlying this form of plasticity, and its coexistence with an additional form of LTD mediated by NMDAR and CB1Rs, increasing our current understanding of the mechanism underlying synaptic plasticity early in the hippocampal development. Interestingly, these mechanisms change with the hippocampal development, and BK channel´s contribution to mGluR-LTD is no longer observed in mature synapses.

BK channels have been involved in some forms of short-term plasticity(Gutzmann et al., 2019) and long-term potentiation (Pham et al., 2023), but the molecular mechanisms involved in BK channel-mediated synaptic plasticity are largely unknown. Presynaptic properties such as synaptic facilitation and calcium sensitivity are lower during postnatal days (PD)7-9 than PD 12-15, producing that long-term potentiation (LTP) is strongly induced after the first postnatal week but not before (Muller et al., 1989), indicating that changes during development occur in a fine temporal window. Our results indicate that BK channel's activity changes with the hippocampal development. The LFS protocol that induces BK channel-mediated LTD during neonatal stage (p7-10) generates a slow increasing LTP, that requires NMDAR, but not BK channels. The changes in the involvement of BK channel in long-lasting depression could be due to changes in the presence or stoichiometry of β4 subunits coupled to α subunit, considering that β4 subunit changes the functional properties of BK channels such as biophysical characteristics and sensitivity to agonists (Latorre et al., 2017). Another possibility, but not exclusive, is the increase in the Kv channel activity, that can mask BK channel's activity (Hu et al., 2001). Interesting, BK channels in CA3 terminals in mature hippocampus regulate excitatory transmission on other CA3 pyramidal neurons (Raffaelli et al., 2004), but on CA1 pyramidal neurons they are masked by Kv channels (Hu et al., 2001), so the characteristics of BK channels and their role in neurotransmitter release in the same neuron could be different depending on the postsynaptic partner. While further investigations are required to fully understand the contribution of presynaptic BK channels to regulate short vs long-term synaptic plasticity, it has been suggested that synaptic plasticity mechanisms have been implicated to synaptic maturation and circuitry formation (Henson et al., 2017; Shinoda et al., 2010). Particularly, LTD has been related to structural changes and a decrease in synaptic contacts (Q. Zhou et al., 2004). Thus, a functional relevance of

this BK-mediated plasticity can be related to circuitry wiring, where LTD has been associated with pruning and a decrease in synaptic contacts(Piochon et al., 2016). Synaptic plasticity could be relevant for establishing the hippocampal circuit and further for the hippocampal-mediated behavior. In this way, BK channels could play a key role in the hippocampal development, acting as a frequency filter, allowing high transmission rates to propagate but suppressing synapses that rely on low rates of transmission, which could have in the circuit wiring by enabling active synapses to undergo synaptic potentiation late in development. In this line, we did not observe participation of BK channels in the response to high frequency stimulation in slices from P7-10 mice, which is a well-studied protocol to induce LTP (Yasuda et al., 2003). Interestingly, this BK channel-mediated mechanism disappears after neonatal stage, which is coherent with the synaptic changes proposed for presynaptic components during development (Dumas & Foster, 1995; Muller et al., 1989). However, whether BK channels' contribution to synaptic plasticity plays a role in synaptic wiring and the maturation of the presynaptic terminals requires further investigations.

The exact mechanisms by which BK channels can generate a LTD vs short-term plasticity are unknown, but it is possible that the localization of BK channels at the presynaptic nerve terminal likely modulates the calcium influx initiating activation of kinases and/or phosphatases that require calcium increases, and their activity limits vesicle fusion at active zones and decreases neurotransmitter release in a long-term manner (Leenders & Sheng, 2005). Interestingly, β4 subunit is also reported in neonatal astrocytes (Gebremedhin et al., 2003), which have been involved in some LTD mechanisms (Cavaccini et al., 2020; Durkee et al., 2021), but the glial participation in this phenomenon should be addressed. Our results also indicate that BK channel-modulated LTD requires CaN activation and protein synthesis, two processes that have been described in other forms of presynaptic plasticity (Jensen & Edwards, 2012; Rodríguez-Moreno et al., 2013). While the connection between these steps remains unclear, it is possible that activation of CaN could be a consequence of changes in calcium levels due to BK channel regulation over presynaptic calcium channels, whereas protein synthesis processes can be regulated by CaN (Lim et al., 2023; Schwartz et al., 2009), but if this occurs in neonatal BK-mediated plasticity need to be tested. However, a previous study reported that mGluR-LTD does not require protein synthesis during P8-15 rats (Nosyreva & Huber, 2005) and thus, a possible explanation for this difference is the use of different animal model (mice vs rat). As presynaptic function changes profoundly in short temporal windows during development (Muller et al., 1989; Wasling et al., 2004), another possibility is the stage of the development tested (P7-10 vs P8-P15).

Interestingly, according to our results, an eCB-mediated LTD that does not require CaN and protein synthesis coexists with the BK channel-mediated LTD. Previous eCB -mediated plasticity mechanisms have involved calcineurin and protein synthesis processes (Heifets et al., 2008; Monday et al., 2020; Puighermanal et al., 2009), so this form of plasticity is different and occurs early in the development supporting as a complement to the BK channel-induced plasticity. However, the role of CB1R in the hippocampal Sch-CA1 synapse to decrease excitatory transmission seems to be complex. CB1R is functional expressed early in this synapse (Al-Hayani & Davies, 2000), and a CB1R-mediated LTD that requires mGluR5 activation has been suggested (Péterfi et al., 2012), but other authors indicate that NMDARs and not mGluRs, are required for depressing excitatory neurotransmission in young hippocampus (Han et al., 2012). However, the latter induces a postsynaptic form of LTD, which is different to our results suggesting a presynaptic locus of the eCB-LTD. Remarkably, a heterosynaptic form of eCB-mediated LTD was reported in neonatal hippocampus (Yasuda et al., 2008), and now our result indicate that homosynaptic LTD mediated by eCBs could be also induced in neonatal synapses (Figure 7). Interestingly, a suppression of inhibitory transmission mediated by endocannabinoids required NMDAR activation in cultured hippocampal neurons (Ohno-shosaku et al., 2007), supporting that this connection can be possible. In this work we showed that a stronger protocol than typically applied LFS (e.g PP-LFS), probably increases glutamate release to a higher level than the requirement for 12(S)HPETE induction through mGluR activation and additionally induces eCB production mediated by NMDAR activation. However, a previous report did not find an effect of blocking CB1R using AM281 on the LTD evoked by PP-FLS (Nosyreva & Huber, 2005), The reason for this discrepancy is unclear but could be related to the pre-treatment and the concentration of the CB1R antagonists (AM251 4μM and AM281 1μM). Additionally, in that study rats from P8-15 were used, and we evaluated eCB-LTD in mice from P7-10. Whether changes in PP-LFS- induced LTD occur during the P10-15 developmental window or involvement of cannabinoid signaling is different between species should be addressed, but reports suggest profound modifications in small temporal windows during early development (Muller et al., 1989; Wasling et al., 2004), and differences in cannabinoid signaling between rodent species have been proposed (H. Y. Zhang et al., 2015). NMDARs can be expressed in pre- and/ or postsynaptic compartments and can be formed by different subunits composition to modulate the receptor properties (Cull-Candy et al., 2001). Indeed, reports suggest that 2A subunit is more determinant for LTD than 2B subunit in hippocampus from young animals (Bartlett et al., 2007). Also, presynaptic NMDARs have been related to LTD in cortex from neonatal stage but not in mature animals (Corlew et al., 2007), but

whether this developmental switch in the requirement of different NMDAR for the induction of specific synaptic plasticity mechanisms occur in the hippocampus should be confirmed. Interestingly, exogenous activation of endocannabinoid signaling during early development also produced negative consequences into the behavior late in the development (Higuera-Matas et al., 2015). Whether overactivation or inhibition of the synaptic processes depending on these lipid-mediated pathways produces negative consequences for the development must be demonstrated. It has been proposed that an adequate level of arachidonic acid is required for the correct development of neural networks (Weseler et al., 2008). Interestingly, lipid concentration in offspring could be easily modified by the mother´s diet (Salem & Van Dael, 2020) and endocannabinoids also are easily transported through milk to affect synaptic maturation processes (Scheyer et al., 2020). Thus, these neonatal synaptic processes could be susceptible to exogenous lipid increases or decreases but this hypothesis should be addressed.

Why are two different mechanisms for depressing excitatory synaptic transmission required in neonatal hippocampus? Gabaergic transmission is an important mechanism required to control excitatory activity to avoid detrimental consequences of excitatory overactivity but is not inhibitory in nature during early development (Ben-Ari, 2002). Thus, other mechanisms could be necessary to keep in an adequate level the excitatory signaling on pyramidal neurons, especially when circuity wiring is highly active. This idea can be in line with our result (Figure 7) in which a stronger protocol is required to induce both mechanisms, suggesting that an increase in the glutamate release by activity could lead to the production of two different, or more, signals that depress glutamate release. Indeed, this is coherent with the need of tetanic stimulation to evoke a heterosynaptic LTD mediated by eCBs (Yasuda et al., 2008). Whether these retrograde signaling mechanisms modulate the release of other neurotransmitters, such as GABA, should be tested. LTD processes have been related with destabilization in hippocampal synapses (Wiegert et al., 2018; Wiegert & Oertner, 2013) and dendritic morphological development in CA1 is highly vulnerable to changes in the synaptic activity (Groc et al., 2002), so disturbances in the mechanisms that control synaptic plasticity in neonates could generate negative consequences for the hippocampus in development and open the possibility to the appearance of neurodevelopmental disorders that involve hippocampus perturbances. In this line, previous reports indicate that prenatal and early disturbances during hippocampal development produce negative outcomes in behavior, learning and synaptic plasticity processes evaluated in mature stages (Yang et al., 2006). Importantly, most evidence showing that synaptic disturbances are involved in developmental disorders such as autism(Y. Zhang et al., 2024)

or schizophrenia (X.-L. Wu et al., 2022) are focused on mature stage, when the synapses have been established. However, we show that important processes are occurring early in the development that are different to those occurring in mature synapses, and the understanding of these mechanisms is important to evaluate if neurodevelopmental disorders are early expressed in synaptic disturbances mediated by BK channels and endocannabinoid signaling, or the further consequences of the early synaptic plasticity disruptions.

7. Supplementary Figures and tables

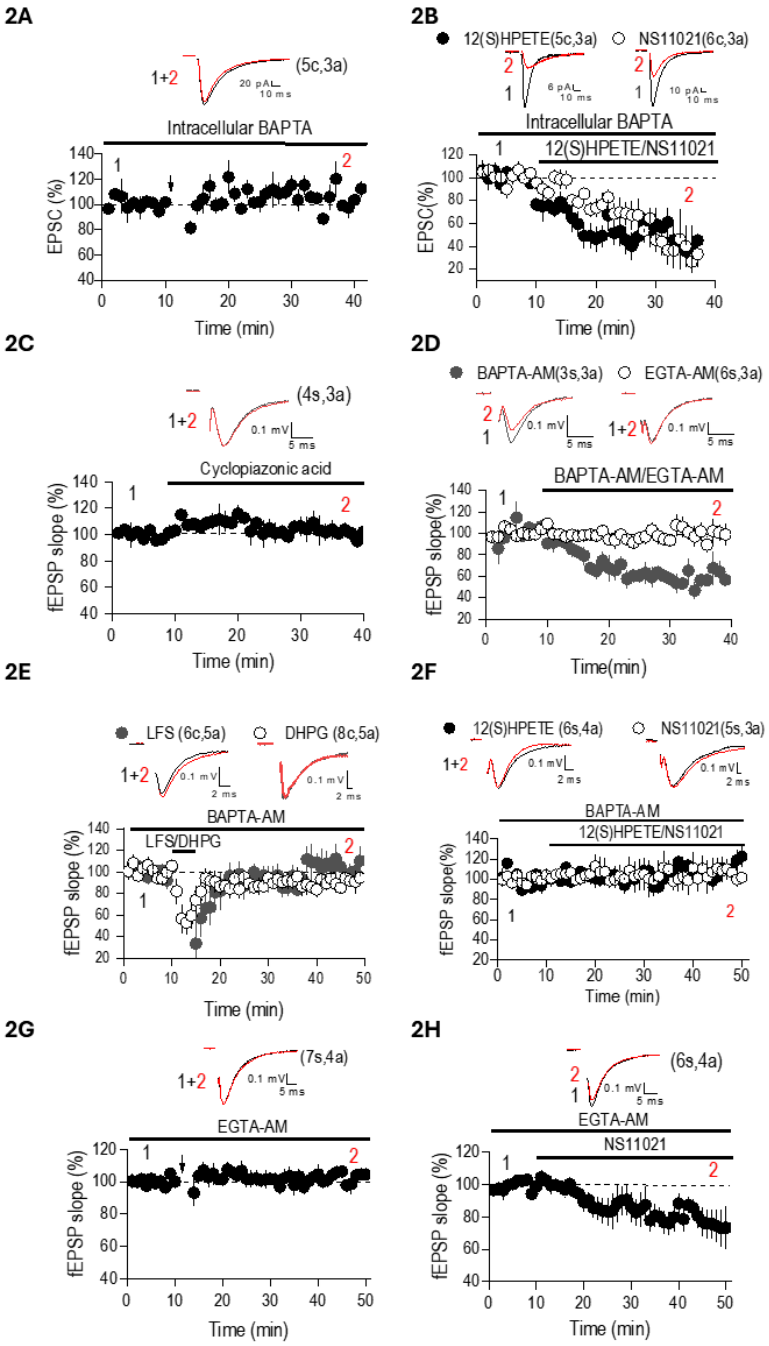


Figure Supplementary 5: *Intracellular BAPTA blocked LFS-induced LTD* ***(5.2A)*** *but not NS11021/12(S)HPETE-induced LTD* ***(5.2B)****. The inhibitor of intracellular Ca^{2+} stores (SERCA pump) Cyclopiazonic acid did not change basal transmission (****5.2C****). Fast permeable calcium chelator BAPTA-AM decreased excitatory transmission but not the slow permeable calcium chelator EGTA-AM (****5.2D****). BAPTA-AM blocked both LFS-and DHPG-induced LTD (****5.2E****) and also the NS11021/12(S)HPETE-induced LTD (****5.2F****). EGTA-AM also blocked LFS-induced LTD (****5.2G****) but no NS11021-induced LTD (****5.2H****).*

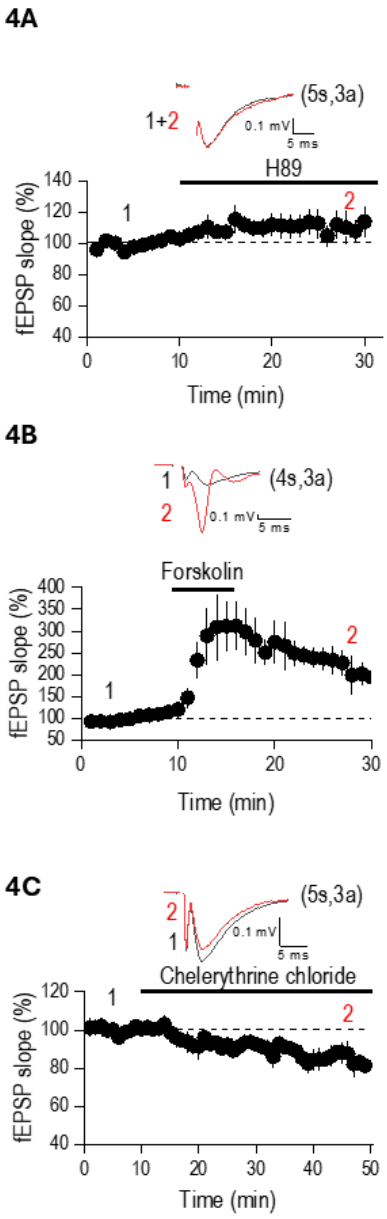


Figure Supplementary: *The PKA inhibitor h89 did not significatively change basal transmission (**5.4A**), but the cAMP activator Forskolin increased excitatory synaptic strength (**5.4B**). The PKC inhibitor Chelerythrine Chloride decreased basal excitatory transmission at Sch-CA1 synapse (**5.4C**).*

Table 1. Quantitative analysis of cellular mechanisms involved in mGluR-LTD in neonatal hippocampus. The table includes quantitative analyses of experiments shown in **Figures 5.2.1A to 5.2.6B.** "*n*" represents number of slices (*s*), cells (*c*) and animals (*a*).

Parameter	*Value (mean± SEM)*		*n (slices/cells, animals)*	*P value*	*Figure*
LFS in p7-10	*61.31*	*±4.26*	*12s/8a*	*p<0.001*	*5.2.1A*
LFS in p20-30	*153.05*	*±19.85*	*10s/8a*	*P=0.021*	
LFS in APV	*113.69*	*±11.89*	*5s/5a*	*P=0.314*	
DHPG in P20-30	*60.29*	*±7.97*	*8s/4a*	*P=0.001*	*5.2.1B*
DHPG in PAX P20-30	*68.84*	*±10.88*	*7s/4a*	*0.028*	
Post-12(S)HPETE	*122.18*	*±30.76*	*4s/2a*	*P=0.526*	*5.2.1C*
Post-NS11021	*104.49*	*±13.57*	*7s/5a*	*P=0.400*	
Post-12(S)HPETE in 4AP	*100.83*	*±10.80*	*5s/3a*	*P=0.942*	*5.2.1D*
Post-NS11021 in 4AP	*54.58*	*±6.28*	*10s/5a*	*p<0.001*	
Post-PAX in control	*102.04*	*±2.14*	*6s/4a*	*P=0.384*	*5.2.1E*
Post-PAX in 4AP	*149.12*	*±12.47*	*7s/5a*	*P=0.005*	
Post- LFS in 4AP	*90.71*	*±13.25*	*11s/5a*	*P=0.499*	*5.2.1F*
LFS Control	*61.31*	*±4.26*	*12s/8a*	*p<0.001*	*5.2.2A*
LFS in CPA	*85.18*	*±5.64*	*8s/4a*	*P=0.034*	
NS11021 Control	*71.80*	*±5.90*	*9s/7a*	*P=0.007*	*5.2.2B*
NS11021 in CPA	*71.39*	*±6.67*	*5s/3a*	*P=0.012*	
LFS Control	*61.31*	*±4.26*	*12s/8a*	*p<0.001*	*5.2.2C*
LFS in Nimodipine	*87.26*	*±6.01*	*9s/6a*	*P=0.078*	
NS11021 Control	*71.80*	*±5.90*	*9s/7a*	*P=0.007*	*5.2.2D*
NS11021 in Nimodipine	*63.33*	*±4.97*	*5s/3a*	*P=0.001*	
LFS Control	*61.31*	*±4.26*	*12s/8a*	*p<0.001*	*5.2.2E*
LFS in Mibefradil	*60.58*	*±6.29*	*6s/3a*	*P=0.001*	
NS11021 Control	*71.80*	*±5.90*	*9s/7a*	*P=0.007*	*5.2.2F*
NS11021 in Mibefradil	*65.94*	*±9.30*	*5s/3a*	*P=0.021*	
ω-conotoxin	*69.41*	*±4.06*	*7s/4a*	*p<0.001*	*5.2.2G*
ω-agatoxin	*66.27*	*±3.38*	*4s/3a*	*P=0.002*	
SNX482	*81.62*	*±5.33*	*5s/2a*	*P=0.026*	
LFS Control	*61.31*	*±4.26*	*12s/8a*	*p<0.001*	*5.2.2H*
LFS in ω-conotoxin	*72.29*	*±7.28*	*7s/4a*	*P=0.008*	
LFS in ω-agatoxin	*66.94*	*±3.58*	*4s/3a*	*P=0.002*	
LFS in SNX482	*86.91*	*±0.70*	*4s/2a*	*p<0.001*	
LFS Control	*61.31*	*±4.26*	*12s/8a*	*p<0.001*	*5.2.3A*
LFS in H89	*73.92*	*±7.72*	*7s/4a*	*P=0.189*	
LFS in Forskolin	*68.14*	*±12.63*	*5s/3a*	*P=0.065*	
NS11021 Control	*71.80*	*±5.90*	*9s/7a*	*P=0.007*	*5.2.3B*
NS11021 in Chelerythrine Chloride	*80.58*	*±1.91*	*5s/3a*	*P=0.002*	

LFS Control	*61.31*	*±4.26*	*12s/8a*	*p<0.001*	*5.2.3C*
LFS in KN93	*49.95*	*±4.84*	*8s/6a*	*p=0.005*	
LFS in KN92	*79.31*	*±5.45*	*10s/6a*	*p<0.001*	
Control WC	*45.32*	*±2.55*	*7c/5a*	*p<0.001*	*5.2.3D*
LFS with CaMKII209-306	*44.16*	*±3.50*	*5c/3a*	*p<0.001*	
LFS Control	*61.31*	*±4.26*	*12s/8a*	*p<0.001*	*5.2.3E*
LFS in FK506	*99.32*	*±8.76*	*7s/4a*	*p=0.941*	
NS11021 Control	*71.80*	*±5.90*	*9s/7a*	*P=0.007*	*5.2.3F*
NS10021 inFK506	*100.74*	*±6.11*	*5s/4a*	*P=0.909*	
LFS Control	*61.31*	*±4.26*	*12s/8a*	*p<0.001*	*5.2.3G*
LFS in Anisomycin	*94.97*	*±7.23*	*8s/5a*	*p=0.509*	
NS11021 Control	*71.80*	*±5.90*	*9s/7a*	*p=0.007*	*5.2.3H*
NS11021 in Anisomycin	*95.07*	*±3.35*	*5s/3a*	*p=0.215*	
Post-WIN	*62.55*	*±4.70*	*6s/3a*	*p<0.001*	*5.2.4A*
PPR pre WIN	*1.36*	*±0.06*			
PPR post WIN	*1.53*	*±0.08*	*6s/3a*	*p=0.005*	
LFS Control	*61.31*	*±4.26*	*12s/8a*	*p<0.001*	*5.2.4B*
LFS in AM251	*75.25*	*±3.34*	*5s/3a*	*p=0.001*	
Post-WIN	*59.099*	*±7.18*	*5s/3a*	*p=0.026*	*5.2.4C*
Post-LFS	*43.06*	*±5.17*			
Post-LFS	*74.53*	*±6.68*	*4s/2a*	*p<0.001*	*5.2.4D*
Post-WIN	*26.52*	*±7.63*			
Post-WIN in FK506	*64.93*	*±7.89*	*6s/4a*	*p=0.006*	*5.2.4E*
Post-WIN in Anisomycin	*55.71*	*±8.90*	*6s/4a*	*p=0.004*	*5.2.4F*
DHPG Control	*67.62*	*±3.71*	*6s/5a*	*p<0.001*	*5.2.5A*
DHPG in AM251	*68.48*	*±8.09*	*3s/3a*	*P=0.060*	
NMDA Control	*54.66*	*±6.00*	*9s/5a*	*p<0.001*	*5.2.5B*
NMDA in AM251	*91.71*	*±9.53*	*8s/4a*	*p=0.413*	
PPR pre NMDA control	*1.32*	*±0.07*	*9s/5a*		
post NMDA control	*1.46*	*±0.08*		*p=0.022*	
PPR pre NMDA in AM251	*1.27*	*±0.01*	*8s/4a*		
PPR post NMDA in AM251	*1.26*	*±0.04*		*p=0.915*	
Post DHPG	*83.35*	*±3.83*	*5s/3a*	*p=0.040*	*5.2.5C*
Post NMDA	*49.68*	*±11.61*			
PP-LFS Control	*58.00*	*±5.95*	*9s/6a*		*5.2.6A*
PP-LFS in PAX	*79.27*	*±8.04*	*9s/6a*	*p=0.056*	
PP-LFS in AM251	*78.28*	*±7.91*	*7s/4a*	*p=0.029*	
PP-LFS in PAX+AM251	*97.01*	*±9.32*	*7s/4a*	*p<0.001*	
PP-LFS Control	*55.98*	*±6.18*	*6s/4a*		*5.2.6B*
PP-LFS in APV	*77.48*	*±3.90*	*7s/4a*	*p=0.024*	
PP-LFS in MTEP	*76.39*	*±12.63*	*6s/4a*	*p=0.061*	
PP-LFS in APV+MTEP	*89.63*	*±3.59*	*5s/3a*	*p=0.008*	

Table 2. **Quantitative analysis of cellular mechanisms involved in mGluR-LTD in neonatal hippocampus.** The table includes quantitative analyses of experiments shown in **Supplementary Figures 5.2A to 5.4C.** "*n*" represents number of slices (*s*), cells (*c*) and animals (*a*).

Parameter	***Value (mean± SEM)***	***n (slices/cells, animals)***	***P value***	***Figure***
Post-LFS with BAPTA in pipette	*104.29 ±4.78*	*5c/3a*	*p=0.420*	*5.2A*
Post- 12(S)HPETE w/BAPTA	*51.59 ±8.62*	*5c/3a*	*p=0.004*	*5.2B*
Post-NS11021 w/BAPTA	*58.46 ±8.31*	*6c/3a*	*p=0.001*	
Post-CPA	*104.69 ±4.95*	*4s/3a*	*p=0.413*	*5.2C*
BAPTA-AM	*55.86 ±3.55*	*3s/3a*	*P=0.006*	*5.2D*
EGTA-AM	*98.12 ±6.55*	*6s/3a*	*P=0.786*	
Post-LFS in BAPTA-AM	*103.84 ±12.22*	*6s/5a*	*p=0.766*	*5.2E*
Post-DHPG in BAPTA-AM	*91.40 ±3.90*	*8s/5a*	*p=0.063*	
Post- 12(S)HPETE in BAPTA-AM	*103.90 ±7.56*	*6s/4a*	*p=0.627*	*5.2F*
Post-NS11021 in BAPTA-AM	*101.20 ±11.29*	*5s/3a*	*p=0.920*	
Post-LFS in EGTA-AM	*102.76 ±3.34*	*7s/4a*	*p=0.440*	*5.2G*
Post-NS11021 in EGTA-AM	*78.55 ±7.49*	*6s/4a*	*p=0.035*	*5.2H*
Post-H89	*110.70 ±7.42*	*5s/3a*	*p=0.222*	*5.4A*
Post-Forskolin	*211.03 ±27.47*	*4s/3a*	*p=0.015*	*5.4B*
Post-Chelethrine Chloride	*87.49 ±2.53*	*5s/3a*	*p=0.007*	*5.4C*

8. CONCLUSIONS

In conclusion our work demonstrated that:

1. BK, but not TRPV1 channels are involved in neonatal hippocampal LTD induced by low frequency stimulation
2. BK-mediated LTD involves regulation of VGGCs and requires CaN and protein synthesis
3. BK-mediated LTD are subjected to changes during development likely changes in BK subunit composition and/or expression of endovanilloid signaling.
4. BK-mediated LTD coexists with an eCB-mediated form of LTD elicited by activation of NMDARs during strong synaptic activity.

By unveiling the neonatal synaptic plasticity mechanisms, we expect to contribute to a better understanding of the hippocampal circuit formation, which is vital for the future behavioral and emotional processes, and to find possible targets for neurodevelopmental disorders involving the hippocampus.

´

9. REFERENCES

Al-Hayani, A., & Davies, S. N. (2000). Cannabinoid receptor mediated inhibition of excitatory synaptic transmission in the rat hippocampal slice is developmentally regulated. *British Journal of Pharmacology*, *131*(4), 663–665. https://doi.org/10.1038/sj.bjp.0703642

Ancatén-González, C., Meza, R. C., Gonzalez-Sanabria, N., Segura, I., Alcaino, A., Peña-Pichicoi, A., Latorre, R., Chiu, C. Q., & Chávez, A. E. (2025). BK channels mediate a presynaptic form of mGluR-LTD in the neonatal hippocampus. *Proceedings of the National Academy of Sciences of the United States of America*, *122*(2). https://doi.org/10.1073/pnas.2411506122

Ancatén-González, C., Segura, I., Alvarado-Sánchez, R., Chávez, A. E., & Latorre, R. (2023). Ca2+- and Voltage-Activated K+ (BK) Channels in the Nervous System: One Gene, a Myriad of Physiological Functions. *International Journal of Molecular Sciences 2023, Vol. 24, Page 3407*, *24*(4), 3407. https://doi.org/10.3390/IJMS24043407

Antion, M. D., Hou, L., Wong, H., Hoeffer, C. A., & Klann, E. (2008). mGluR-Dependent Long-Term Depression Is Associated with Increased Phosphorylation of S6 and Synthesis of Elongation Factor 1A but Remains Expressed in S6K-Deficient Mice. *Molecular and Cellular Biology*, *28*(9), 2996–3007. https://doi.org/10.1128/mcb.00201-08

Anwyl, R. (2009). Metabotropic glutamate receptor-dependent long-term potentiation. In *Neuropharmacology* (Vol. 56, Issue 4, pp. 735–740). https://doi.org/10.1016/j.neuropharm.2009.01.002

Armstrong, C. M., & Bezanilla, F. (1973). Currents Related to Movement of the Gating Particles of the Sodium Channels. *Nature*, *242*(5398), 459–461. https://doi.org/10.1038/242459a0

Baj, G., Patrizio, A., Montalbano, A., Sciancalepore, M., & Tongiorgi, E. (2014). Developmental and maintenance defects in Rett syndrome neurons identified by a new mouse staging system in vitro. *Frontiers in Cellular Neuroscience*, *8*(FEB). https://doi.org/10.3389/fncel.2014.00018

Banker, S. M., Gu, X., Schiller, D., & Foss-Feig, J. H. (2021). Hippocampal contributions to social and cognitive deficits in autism spectrum disorder. In *Trends in Neurosciences* (Vol. 44, Issue 10, pp. 793–807). Elsevier Ltd. https://doi.org/10.1016/j.tins.2021.08.005

Barnes, S. J., Opitz, T., Merkens, M., Kelly, T., Von Der Brelie, C., Krueppel, R., & Beck, H. (2010). Stable mossy fiber long-term potentiation requires calcium influx at the granule cell soma, protein synthesis, and microtubule-dependent axonal transport. *Journal of Neuroscience*, *30*(39), 12996–13004. https://doi.org/10.1523/JNEUROSCI.1847-10.2010

Bartlett, T. E., Bannister, N. J., Collett, V. J., Dargan, S. L., Massey, P. V., Bortolotto, Z. A., Fitzjohn, S. M., Bashir, Z. I., Collingridge, G. L., & Lodge, D. (2007). Differential roles of NR2A and NR2B-containing NMDA receptors in LTP and LTD in the CA1 region of two-week old rat hippocampus. *Neuropharmacology*, *52*(1), 60–70. https://doi.org/10.1016/j.neuropharm.2006.07.013

Becker, N., Wierenga, C. J., Fonseca, R., Bonhoeffer, T., & Nägerl, U. V. (2008). LTD Induction Causes Morphological Changes of Presynaptic Boutons and Reduces Their Contacts with Spines. *Neuron*, *60*(4), 590–597. https://doi.org/10.1016/j.neuron.2008.09.018

Bellone, C., Lüscher, C., & Mameli, M. (2008). Mechanisms of synaptic depression triggered by metabotropic glutamate receptors. *Cellular and Molecular Life Sciences*, *65*(18), 2913–2923. https://doi.org/10.1007/s00018-008-8263-3

Ben-Ari, Y. (2002). Excitatory actions of GABA during development: The nature of the nurture. *Nature Reviews Neuroscience*, *3*(9), 728–739. https://doi.org/10.1038/nrn920

Besana, A., Robinson, R. B., & Feinmark, S. J. (2005). Lipids and two-pore domain K+ channels in excitable cells. *Prostaglandins & Other Lipid Mediators*, *77*(1–4), 103–110. https://doi.org/10.1016/j.prostaglandins.2004.10.005

Bird, C. M., & Burgess, N. (2008). The hippocampus and memory: Insights from spatial processing. In *Nature Reviews Neuroscience* (Vol. 9, Issue 3, pp. 182–194). https://doi.org/10.1038/nrn2335

Boland, L. M., & Drzewiecki, M. M. (2008). Polyunsaturated Fatty Acid Modulation of Voltage-Gated Ion Channels. *Cell Biochemistry and Biophysics*, *52*(2), 59–84. https://doi.org/10.1007/s12013-008-9027-2

Bolshakov, V. Y., & Siegelbaum, S. A. (1994). Postsynaptic induction and presynaptic expression of hippocampal long-term depression. *Science*, *264*(5162), 1148–1152. https://doi.org/10.1126/science.7909958

Bolshakov, V. Y., & Siegelbaum, S. A. (1995a). Hippocampal long-term depression: Arachidonic acid as a potential retrograde messenger. *Neuropharmacology*, *34*(11), 1581–1587. https://doi.org/10.1016/0028-3908(95)00127-R

Bolshakov, V. Y., & Siegelbaum, S. A. (1995b). Regulation of hippocampal transmitter release during development and long-term potentiation. *Science*, *269*(5231), 1730–1734. https://doi.org/10.1126/science.7569903

Bradshaw, J. M., Kubota, Y., Meyer, T., & Schulman, H. (2003). An ultrasensitive Ca^{2+} /calmodulin-dependent protein kinase II-protein phosphatase 1 switch facilitates specificity in postsynaptic calcium signaling. *Proceedings of the National Academy of Sciences*, *100*(18), 10512–10517. https://doi.org/10.1073/pnas.1932759100

Brager, D. H., & Johnston, D. (2007). Plasticity of intrinsic excitability during long-term depression is mediated through mGluR-dependent changes in Ih in hippocampal CA1 pyramidal neurons. *Journal of Neuroscience*, *27*(51), 13926–13937. https://doi.org/10.1523/JNEUROSCI.3520-07.2007

Brenner, R., Chen, Q. H., Vilaythong, A., Toney, G. M., Noebels, J. L., & Aldrich, R. W. (2005). BK channel β4 subunit reduces dentate gyrus excitability and protects against temporal lobe seizures. *Nature Neuroscience*, *8*(12), 1752–1759. https://doi.org/10.1038/nn1573

Calixto, E., Thiels, E., Klann, E., & Barrionuevo, G. (2003). Early maintenance of hippocampal mossy fiber-long-term potentiation depends on protein and RNA synthesis and presynaptic granule cell integrity. *Journal of Neuroscience*, *23*(12), 4842–4849. https://doi.org/10.1523/jneurosci.23-12-04842.2003

Carrasquel-Ursulaez, W., Lorenzo, Y., Echeverria, F., Latorre, R., Carrasquel-Ursulaez, W., Lorenzo, Y., Echeverria, F., & Latorre, R. (2018). Large Conductance Potassium Channels in the Nervous System. In *The Oxford Handbook of Neuronal Ion Channels* (Issue May). https://doi.org/10.1093/oxfordhb/9780190669164.013.11

Carta, M., Lanore, F., Rebola, N., Szabo, Z., Da Silva, S. V., Lourenço, J., Verraes, A., Nadler, A., Schultz, C., Blanchet, C., & Mulle, C. (2014). Membrane lipids tune synaptic transmission by direct modulation of presynaptic potassium channels. *Neuron*, *81*(4), 787–799. https://doi.org/10.1016/j.neuron.2013.12.028

Castillo, P. E. (2012). Presynaptic LTP and LTD of excitatory and inhibitory synapses. *Cold Spring Harbor Perspectives in Biology*, *4*(2). https://doi.org/10.1101/cshperspect.a005728

Castillo, P. E., Younts, T. J., Chávez, A. E., & Hashimotodani, Y. (2012). Endocannabinoid Signaling and Synaptic Function. *Neuron*, *76*(1), 70–81. https://doi.org/10.1016/j.neuron.2012.09.020

Cavaccini, A., Durkee, C., Kofuji, P., Tonini, R., & Araque, A. (2020). Astrocyte signaling gates long-term depression at corticostriatal synapses of the direct pathway. *Journal of Neuroscience*, *40*(30), 5757–5768. https://doi.org/10.1523/JNEUROSCI.2369-19.2020

Chaudhury, S., Sharma, V., Kumar, V., Nag, T. C., & Wadhwa, S. (2016). Activity-dependent synaptic plasticity modulates the critical phase of brain development. In *Brain and Development* (Vol. 38, Issue 4, pp. 355–363). Elsevier B.V. https://doi.org/10.1016/j.braindev.2015.10.008

Chávez, A. E., Chiu, C. Q., & Castillo, P. E. (2010). TRPV1 activation by endogenous anandamide triggers postsynaptic long-term depression in dentate gyrus. *Nature Neuroscience*, *13*(12), 1511–1518. https://doi.org/10.1038/nn.2684

Chávez, A. E., Hernández, V. M., Rodenas-Ruano, A., Chan, C. S., & Castillo, P. E. (2014). Compartment-Specific Modulation of GABAergic Synaptic Transmission by TRPV1 Channels in the Dentate Gyrus. *The Journal of Neuroscience*, *34*(50), 16621–16629. https://doi.org/10.1523/JNEUROSCI.3635-14.2014

Chindemi, G., Abdellah, M., Amsalem, O., Benavides-Piccione, R., Delattre, V., Doron, M., Ecker, A., Jaquier, A. T., King, J., Kumbhar, P., Monney, C., Perin, R., Rössert, C., Tuncel, A. M., Van Geit, W., DeFelipe, J., Graupner, M., Segev, I., Markram, H., & Muller, E. B. (2022). A calcium-based plasticity model for predicting long-term potentiation and depression in the neocortex. *Nature Communications*, *13*(1). https://doi.org/10.1038/s41467-022-30214-w

Citri, A., & Malenka, R. C. (2008). Synaptic plasticity: Multiple forms, functions, and mechanisms. *Neuropsychopharmacology*, *33*(1), 18–41. https://doi.org/10.1038/sj.npp.1301559

Colbran, R. J. (2004). Protein phosphatases and calcium/calmodulin-dependent protein kinase II-dependent synaptic plasticity. *Journal of Neuroscience*, *24*(39), 8404–8409. https://doi.org/10.1523/JNEUROSCI.3602-04.2004

Contet, C., Goulding, S. P., Kuljis, D. A., & Barth, A. L. (2016). BK Channels in the Central Nervous System. In *International Review of Neurobiology* (1st ed., Vol. 128). Elsevier Inc. https://doi.org/10.1016/bs.irn.2016.04.001

Corlew, R., Wang, Y., Ghermazien, H., Erisir, A., & Philpot, B. D. (2007). Developmental switch in the contribution of presynaptic and postsynaptic NMDA receptors to long-term depression. *Journal of Neuroscience*, *27*(37), 9835–9845. https://doi.org/10.1523/JNEUROSCI.5494-06.2007

Coultrap, S. J., & Bayer, K. U. (2012). CaMKII regulation in information processing and storage. *Trends in Neurosciences*, *35*(10), 607–618. https://doi.org/10.1016/j.tins.2012.05.003

Cox, D. H., Cui, J., & Aldrich, R. W. (1997). Separation of Gating Properties from Permeation and Block in *mslo* Large Conductance Ca-activated K+ Channels. *The Journal of General Physiology*, *109*(5), 633–646. https://doi.org/10.1085/jgp.109.5.633

Cull-Candy, S., Brickley, S., & Farrant, M. (2001). NMDA receptor subunits: Diversity, development and disease. *Current Opinion in Neurobiology*, *11*(3), 327–335. https://doi.org/10.1016/S0959-4388(00)00215-4

Cummings, J. A., & Mulkey, R. M. (1996). Ca 2 Signaling Requirements for Long-Term Depression in the Hippocampus. In *Neuron* (Vol. 16).

Deng, P. Y., Rotman, Z., Blundon, J. A., Cho, Y., Cui, J., Cavalli, V., Zakharenko, S. S., & Klyachko, V. A. (2013). FMRP Regulates Neurotransmitter Release and Synaptic Information Transmission by Modulating Action Potential Duration via BK Channels. *Neuron*, *77*(4), 696–711. https://doi.org/10.1016/j.neuron.2012.12.018

Dittman, J. S., & Ryan, T. A. (2019). The control of release probability at nerve terminals. *Nature Reviews Neuroscience*, *20*(3), 177–186. https://doi.org/10.1038/s41583-018-0111-3

Dolphin, A. C. (2020). Functions of Presynaptic Voltage-gated Calcium Channels. *Function*, *2*(1), 1–10. https://doi.org/10.1093/function/zqaa027

Dolphin, A. C., & Lee, A. (2020). Presynaptic calcium channels: specialized control of synaptic neurotransmitter release. *Nature Reviews Neuroscience*, *21*(4), 213–229. https://doi.org/10.1038/s41583-020-0278-2

Dopico, A. M., & Bukiya, A. N. (2014). Lipid regulation of BK channel function. In *Frontiers in Physiology: Vol. 5 AUG*. Frontiers Research Foundation. https://doi.org/10.3389/fphys.2014.00312

Drapeau, C., Pellerin, L., Wolfe, L. S., & Avoli, M. (1990). Long-term changes of synaptic transmission induced by arachidonic acid in the CA1 subfield of the rat hippocampus. *Neuroscience Letters*, *115*(2–3), 286–292. https://doi.org/10.1016/0304-3940(90)90470-T

Dumas, T. C., & Foster, T. C. (1995). Developmental increase in CA3-CA1 presynaptic function in the hippocampal slice. *Journal of Neurophysiology*, *73*(5), 1821–1828. https://doi.org/10.1152/jn.1995.73.5.1821

Durkee, C., Kofuji, P., Navarrete, M., & Araque, A. (2021). Astrocyte and neuron cooperation in long-term depression. *Trends in Neurosciences*, 1–12. https://doi.org/10.1016/j.tins.2021.07.004

Edwards, J. G. (2014). TRPV1 in the Central Nervous System: Synaptic Plasticity, Function, and Pharmacological Implications. In *Capsaicin as a Therapeutic Molecule* (pp. 77–104). Springer Basel. https://doi.org/10.1007/978-3-0348-0828-6_3

Eshra, A., Schmidt, H., Eilers, J., & Hallermann, S. (2021). Calcium dependence of neurotransmitter release at a high fidelity synapse. *ELife*, *10*. https://doi.org/10.7554/eLife.70408

Faraci, F. M., Sobey, C. G., Chrissobolis, S., Lund, D. D., Heistad, D. D., & Weintraub, N. L. (2001). Arachidonate dilates basilar artery by lipoxygenase-dependent mechanism and activation of K+ channels. *American Journal of Physiology - Regulatory Integrative and Comparative Physiology*, *281*(1 50-1), 246–253. https://doi.org/10.1152/ajpregu.2001.281.1.r246

Feinmark, S. J., Begum, R., Tsvetkov, E., Goussakov, I., Funk, C. D., Siegelbaum, S. A., & Bolshakov, V. Y. (2003). 12-Lipoxygenase Metabolites of Arachidonic Acid Mediate Metabotropic Glutamate Receptor-Dependent Long-Term Depression at Hippocampal CA3-CA1 Synapses. *Journal of Neuroscience*, *23*(36), 11427–11435. https://doi.org/10.1523/jneurosci.23-36-11427.2003

Galván, E. J., Calixto, E., & Barrionuevo, G. (2008). Bidirectional hebbian plasticity at hippocampal mossy fiber synapses on CA3 interneurons. *Journal of Neuroscience*, *28*(52), 14042–14055. https://doi.org/10.1523/JNEUROSCI.4848-08.2008

Gebremedhin, D., Yamaura, K., Zhang, C., Bylund, J., Koehler, R. C., & Harder, D. R. (2003). Metabotropic glutamate receptor activation enhances the activities of two types of Ca2+-activated K+ channels in rat hippocampal astrocytes. *Journal of Neuroscience*, *23*(5), 1678–1687. https://doi.org/10.1523/jneurosci.23-05-01678.2003

Gibson, H. E., Edwards, J. G., Page, R. S., Van Hook, M. J., & Kauer, J. A. (2008). TRPV1 Channels Mediate Long-Term Depression at Synapses on Hippocampal Interneurons. *Neuron*, *57*(5), 746–759. https://doi.org/10.1016/j.neuron.2007.12.027

Gil-Sanz, C., Delgado-García, J. M., Fairén, A., & Gruart, A. (2008). Involvement of the mGluR1 receptor in hippocampal synaptic plasticity and associative learning in behaving mice. *Cerebral Cortex*, *18*(7), 1653–1663. https://doi.org/10.1093/cercor/bhm193

Groc, L., Petanjek, Z., Gustafsson, B., Ben-Ari, Y., Hanse, E., & Khazipov, R. (2002). In vivo blockade of neural activity alters dendritic development of neonatal CA1 pyramidal cells. *European Journal of Neuroscience*, *16*(10), 1931–1938. https://doi.org/10.1046/j.1460-9568.2002.02264.x

Grueter, B. A., Brasnjo, G., & Malenka, R. C. (2010). Postsynaptic TRPV1 triggers cell type–specific long-term depression in the nucleus accumbens. *Nature Neuroscience*, *13*(12), 1519–1525. https://doi.org/10.1038/nn.2685

Gubellini, P., Saulle, E., Centonze, D., Costa, C., Tropepi, D., Bernardi, G., Conquet, F., & Calabresi, P. (2003). Corticostriatal LTP requires combined mGluR1 and mGluR5 activation. *Neuropharmacology*, *44*(1), 8–16. https://doi.org/10.1016/S0028-3908(02)00214-9

Gutzmann, J. J., Lin, L., & Hoffman, D. A. (2019). Functional coupling of cav2.3 and BK potassium channels regulates action potential repolarization and short-term plasticity in the mouse hippocampus. *Frontiers in Cellular Neuroscience*, *13*(February), 1–14. https://doi.org/10.3389/fncel.2019.00027

Han, J., Kesner, P., Metna-Laurent, M., Duan, T., Xu, L., Georges, F., Koehl, M., Abrous, D. N., Mendizabal-Zubiaga, J., Grandes, P., Liu, Q., Bai, G., Wang, W., Xiong, L., Ren, W., Marsicano, G., & Zhang, X. (2012). Acute cannabinoids impair working memory through astroglial CB 1 receptor modulation of hippocampal LTD. *Cell*, *148*(5), 1039–1050. https://doi.org/10.1016/j.cell.2012.01.037

Hardie, R. C. (2007). TRP channels and lipids: From Drosophila to mammalian physiology. In *Journal of Physiology* (Vol. 578, Issue 1, pp. 9–24). https://doi.org/10.1113/jphysiol.2006.118372

Hayashi, Y., Morinaga, S., Zhang, J., Satoh, Y., Meredith, A. L., Nakata, T., Wu, Z., Kohsaka, S., Inoue, K., & Nakanishi, H. (2016). BK channels in microglia are required for morphine-induced hyperalgesia. *Nature Communications*, *7*(May), 1–7. https://doi.org/10.1038/ncomms11697

Hayashi, Y., & Nakanishi, H. (2015). BK channel in microglia as a potent therapeutic molecular target for neuropathic pain. *Journal of Oral Biosciences*, *57*(3), 131–134. https://doi.org/10.1016/j.job.2015.03.001

Heifets, B. D., & Castillo, P. E. (2009). Endocannabinoid Signaling and Long-Term Synaptic Plasticity. *Annual Review of Physiology*, *71*(1), 283–306. https://doi.org/10.1146/annurev.physiol.010908.163149

Heifets, B. D., Chevaleyre, V., & Castillo, P. E. (2008). Interneuron activity controls endocannabinoid-mediated presynaptic plasticity through calcineurin. *Proceedings of the National Academy of Sciences of the United States of America*, *105*(29), 10250–10255. https://doi.org/10.1073/pnas.0711880105

Henson, M. A., Tucker, C. J., Zhao, M., & Dudek, S. M. (2017). Long-term depression-associated signaling is required for an in vitro model of NMDA receptor-dependent synapse pruning. *Neurobiology of Learning and Memory*, *138*, 39–53. https://doi.org/10.1016/j.nlm.2016.10.013

Higuera-Matas, A., Ucha, M., & Ambrosio, E. (2015). Long-term consequences of perinatal and adolescent cannabinoid exposure on neural and psychological processes. In *Neuroscience and Biobehavioral Reviews* (Vol. 55, pp. 119–146). Elsevier Ltd. https://doi.org/10.1016/j.neubiorev.2015.04.020

Hirono, M., Ogawa, Y., Misono, K., Zollinger, D. R., Trimmer, J. S., Rasband, M. N., & Misonou, H. (2015). BK channels localize to the paranodal junction and regulate action potentials in myelinated axons of cerebellar Purkinje cells. *Journal of Neuroscience*, *35*(18), 7082–7094. https://doi.org/10.1523/JNEUROSCI.3778-14.2015

Horrigan, F. T., & Aldrich, R. W. (2002). Coupling between voltage sensor activation, Ca2+ binding and channel opening in large conductance (BK) potassium channels. *Journal of General Physiology*, *120*(3), 267–305. https://doi.org/10.1085/jgp.20028605

Hoshi, T., Tian, Y., Xu, R., Heinemann, S. H., & Hou, S. (2013). Mechanism of the modulation of BK potassium channel complexes with different auxiliary subunit compositions by the omega-3 fatty acid DHA. *Proceedings of the National Academy of Sciences of the United States of America*, *110*(12), 4822–4827. https://doi.org/10.1073/pnas.1222003110

Hu, H., Shao, L. R., Chavoshy, S., Gu, N., Trieb, M., Behrens, R., Laake, P., Pongs, O., Knaus, H. G., Ottersen, O. P., & Storm, J. F. (2001). Presynaptic Ca2+-activated K+channels in glutamatergic hippocampal terminals and their role in spike repolarization and regulation of transmitter release. *Journal of Neuroscience*, *21*(24), 9585–9597. https://doi.org/10.1523/jneurosci.21-24-09585.2001

Huang, J. M., Xian, H., & Bacaner, M. (1992). Long-chain fatty acids activate calcium channels in ventricular myocytes. *Proceedings of the National Academy of Sciences*, *89*(14), 6452–6456. https://doi.org/10.1073/pnas.89.14.6452

Hunsberger, M. S., & Mynlieff, M. (2020). BK potassium currents contribute differently to action potential waveform and firing rate as rat hippocampal neurons mature in the first postnatal week. *Journal of Neurophysiology*, *124*(3), 703–714. https://doi.org/10.1152/jn.00711.2019

Igelmund, P., Zhao U Heinemann, Y. Q., Igelmund, R., Zhao, Y. Q., & Heinemann, U. (1996). Effects of T-type, L-type, N-type, P-type, and Q-type calcium channel blockers on stimulus-induced pre-and postsynaptic calcium fluxes in rat hippocampal slices. In *Exp Brain Res* (Vol. 109). Springer-Verlag.

Incontro, S., Díaz-Alonso, J., Iafrati, J., Vieira, M., Asensio, C. S., Sohal, V. S., Roche, K. W., Bender, K. J., & Nicoll, R. A. (2018). The CaMKII/NMDA receptor complex controls hippocampal synaptic transmission by kinase-dependent and independent mechanisms. *Nature Communications*, *9*(1), 1–21. https://doi.org/10.1038/s41467-018-04439-7

Irie, T., & Trussell, L. O. (2017). Double-Nanodomain Coupling of Calcium Channels, Ryanodine Receptors, and BK Channels Controls the Generation of Burst Firing. *Neuron*, *96*(4), 856-870.e4. https://doi.org/10.1016/j.neuron.2017.10.014

Izumi, Y., & Zorumski, C. F. (2012). NMDA receptors, mGluR5, and endocannabinoids are involved in a cascade leading to hippocampal long-term depression. *Neuropsychopharmacology*, *37*(3), 609–617. https://doi.org/10.1038/npp.2011.243

Jamieson, B. B., Kim, J. S., & Iremonger, K. J. (2022). Cannabinoid and vanilloid pathways mediate opposing forms of synaptic plasticity in corticotropin-releasing hormone neurons. *Journal of Neuroendocrinology*, *34*(4). https://doi.org/10.1111/jne.13084

Jensen, T., & Edwards, J. G. (2012). Calcineurin is required for TRPV1-induced long-term depression of hippocampal interneurons. *Neuroscience Letters*, *510*(2), 82–87. https://doi.org/10.1016/j.neulet.2012.01.006

Kamsler, A., McHugh, T. J., Gerber, D., Huang, S. Y., & Tonegawa, S. (2010). Presynaptic m1 muscarinic receptors are necessary for mGluR long-term depression in the hippocampus. *Proceedings of the National Academy of Sciences of the United States of America*, *107*(4), 1618–1623. https://doi.org/10.1073/pnas.0912540107

Kang, J., Huguenard, J. R., & Prince, D. A. (1996). Development of BK channels in neocortical pyramidal neurons. *Journal of Neurophysiology*, *76*(1), 188–198. https://doi.org/10.1152/jn.1996.76.1.188

Kawamura, Y., Fukaya, M., Maejima, T., Yoshida, T., Miura, E., Watanabe, M., Ohno-Shosaku, T., & Kano, M. (2006). The CB1 cannabinoid receptor is the major cannabinoid receptor at excitatory presynaptic sites in the hippocampus and cerebellum. *Journal of Neuroscience*, *26*(11), 2991–3001. https://doi.org/10.1523/JNEUROSCI.4872-05.2006

King, J. T., Lovell, P. V., Rishniw, M., Kotlikoff, M. I., Zeeman, M. L., & McCobb, D. P. (2006). β2 and β4 subunits of BK channels confer differential sensitivity to acute modulation by steroid hormones. *Journal of Neurophysiology*, *95*(5), 2878–2888. https://doi.org/10.1152/jn.01352.2005

Knierim, J. J. (2015). The hippocampus. *Current Biology*, *25*(23), R1116–R1121. https://doi.org/10.1016/j.cub.2015.10.049

Kwag, J., & Paulsen, O. (2012). Gating of NMDA receptor-mediated hippocampal spike timing-dependent potentiation by mGluR5. *Neuropharmacology*, *63*(4), 701–709. https://doi.org/10.1016/j.neuropharm.2012.05.021

Latorre, R., & Brauchi, S. (2006). Large conductance Ca2+-activated K+ (BK) channel: Activation by Ca2+ and voltage. *Biological Research*, *39*(3), 385–401. https://doi.org/10.4067/S0716-97602006000300003

Latorre, R., Castillo, K., Carrasquel-Ursulaez, W., Sepulveda, R. V., Gonzalez-Nilo, F., Gonzalez, C., & Alvarez, O. (2017). Molecular determinants of BK channel functional diversity and functioning. *Physiological Reviews*, *97*(1), 39–87. https://doi.org/10.1152/physrev.00001.2016

Le Duigou, C., Holden, T., & Kullmann, D. M. (2011). Short- and long-term depression at glutamatergic synapses on hippocampal interneurons by group i mGluR activation. *Neuropharmacology*, *60*(5), 748–756. https://doi.org/10.1016/j.neuropharm.2010.12.015

Lee, H.-K. (2006). Synaptic plasticity and phosphorylation. *Pharmacology & Therapeutics*, *112*(3), 810–832. https://doi.org/10.1016/j.pharmthera.2006.06.003

Lee, S. H., Ledri, M., Tóth, B., Marchionni, I., Henstridge, C. M., Dudok, B., Kenesei, K., Barna, L., Szabó, S. I., Renkecz, T., Oberoi, M., Watanabe, M., Limoli, C. L., Horvai, G., Soltesz, I., & Katona, I. (2015). Multiple forms of endocannabinoid and endovanilloid signaling regulate the

tonic control of GABA release. *Journal of Neuroscience*, *35*(27), 10039–10057. https://doi.org/10.1523/JNEUROSCI.4112-14.2015

Leenders, A. G. M., & Sheng, Z. H. (2005). Modulation of neurotransmitter release by the second messenger-activated protein kinases: Implications for presynaptic plasticity. In *Pharmacology and Therapeutics* (Vol. 105, Issue 1, pp. 69–84). https://doi.org/10.1016/j.pharmthera.2004.10.012

Li, C., Li, X., Chen, W., Yu, S., Chen, J., Wang, H., & Ruan, D. (2007). The different roles of cyclinD1-CDK4 in STP and mGluR-LTD during the postnatal development in mice hippocampus area CA1. *BMC Developmental Biology*, *7*, 1–9. https://doi.org/10.1186/1471-213X-7-57

Li, Q., & Yan, J. (2016). Modulation of BK Channel Function by Auxiliary Beta and Gamma Subunits. *International Review of Neurobiology*, *128*, 51–90. https://doi.org/10.1016/bs.irn.2016.03.015

Li, Y., Shen, M., Stockton, M. E., & Zhao, X. (2019). Hippocampal deficits in neurodevelopmental disorders. *Neurobiology of Learning and Memory*, *165*. https://doi.org/10.1016/j.nlm.2018.10.001

Li, Y., Zhang, L., Wu, Y., Zheng, Q., Chen, M., Qian, Z., Wei, C., Han, J., Liu, Z., Ren, W., & Liu, Y. (2019). Cannabinoids-induced peripheral analgesia depends on activation of BK channels. *Brain Research*, *1711*(January), 23–28. https://doi.org/10.1016/j.brainres.2019.01.007

Lieberman, J. A., Girgis, R. R., Brucato, G., Moore, H., Provenzano, F., Kegeles, L., Javitt, D., Kantrowitz, J., Wall, M. M., Corcoran, C. M., Schobel, S. A., & Small, S. A. (2018). Hippocampal dysfunction in the pathophysiology of schizophrenia: a selective review and hypothesis for early detection and intervention. *Molecular Psychiatry*, *23*(8), 1764–1772. https://doi.org/10.1038/mp.2017.249

Lim, D., Tapella, L., Dematteis, G., Talmon, M., & Genazzani, A. A. (2023). Calcineurin Signalling in Astrocytes: From Pathology to Physiology and Control of Neuronal Functions. *Neurochemical Research*, *48*(4), 1077–1090. https://doi.org/10.1007/s11064-022-03744-4

Lin, C. H., Lee, C. C., & Gean, P. W. (2003). Involvement of a calcineurin cascade in amygdala depotentiation and quenching of fear memory. *Molecular Pharmacology*, *63*(1), 44–52. https://doi.org/10.1124/mol.63.1.44

Lohmann, C., & Kessels, H. W. (2014). The developmental stages of synaptic plasticity. *Journal of Physiology*, *592*(1), 13–31. https://doi.org/10.1113/jphysiol.2012.235119

Lorenzo-Ceballos, Y., Carrasquel-Ursulaez, W., Castillo, K., Alvarez, O., & Latorre, R. (2019). Calcium-driven regulation of voltagesensingdomains in BK channels. *ELife*, *8*, 1–24. https://doi.org/10.7554/eLife.44934

Lu, H. C., & MacKie, K. (2016). An introduction to the endogenous cannabinoid system. In *Biological Psychiatry* (Vol. 79, Issue 7, pp. 516–525). Elsevier USA. https://doi.org/10.1016/j.biopsych.2015.07.028

Lüscher, C., & Huber, K. M. (2010). Group 1 mGluR-Dependent Synaptic Long-Term Depression: Mechanisms and Implications for Circuitry and Disease. *Neuron*, *65*(4), 445–459. https://doi.org/10.1016/j.neuron.2010.01.016

Maki, R., & Poo, M.-M. (1998). Retrograde Signaling in the Development and Modification of Synapses. In *PHYSIOLOGICAL REVIEWS* (Vol. 78, Issue 1).

Malenka, R. C., & Bear, M. F. (2004). LTP and LTD: An embarrassment of riches. *Neuron*, *44*(1), 5–21. https://doi.org/10.1016/j.neuron.2004.09.012

Marinelli, S., Di Marzo, V., Florenzano, F., Fezza, F., Viscomi, M. T., Van Der Stelt, M., Bernardi, G., Molinari, M., Maccarrone, M., & Mercuri, N. B. (2007). N-arachidonoyl-dopamine tunes synaptic transmission onto dopaminergic neurons by activating both cannabinoid and vanilloid receptors. *Neuropsychopharmacology*, *32*(2), 298–308. https://doi.org/10.1038/sj.npp.1301118

Martín, P., Moncada, M., Enrique, N., Asuaje, A., Valdez Capuccino, J. M., Gonzalez, C., & Milesi, V. (2014). Arachidonic acid activation of BKCa (Slo1) channels associated to the β1-subunit in human vascular smooth muscle cells. *Pflügers Archiv - European Journal of Physiology*, *466*(9), 1779–1792. https://doi.org/10.1007/s00424-013-1422-x

Mayford, M., Wang, J., Kandel, E. R., & O'Dell, T. J. (1995). CaMKII regulates the frequency-response function of hippocampal synapses for the production of both LTD and LTP. *Cell*, *81*(6), 891–904. https://doi.org/10.1016/0092-8674(95)90009-8

Meunier, C. N. J., Chameau, P., & Fossier, P. M. (2017). Modulation of Synaptic Plasticity in the Cortex Needs to Understand All the Players. *Frontiers in Synaptic Neuroscience*, *9*. https://doi.org/10.3389/fnsyn.2017.00002

Meza, R. C., Ancatén-González, C., Chiu, C. Q., & Chávez, A. E. (2022). Transient Receptor Potential Vanilloid 1 Function at Central Synapses in Health and Disease. *Frontiers in Cellular Neuroscience*, *16*. https://doi.org/10.3389/fncel.2022.864828

Misonou, H., Menegola, M., Buchwalder, L., Park, E. W., Meredith, A., Rhodes, K. J., Aldrich, R. W., & Trimmer, J. S. (2006). Immunolocalization of the Ca2+-activated K+ channel Slo1 in axons and nerve terminals of mammalian brain and cultured neurons. *Journal of Comparative Neurology*, *496*(3), 289–302. https://doi.org/10.1002/cne.20931

Monday, H. R., Bourdenx, M., Jordan, B. A., & Castillo, P. E. (2020). Cb1-receptor-mediated inhibitory ltd triggers presynaptic remodeling via protein synthesis and ubiquitination. *ELife*, *9*, 1–25. https://doi.org/10.7554/ELIFE.54812

Montgomery, J. R., & Meredith, A. L. (2012). Genetic activation of BK currents in vivo generates bidirectional effects on neuronal excitability. *Proceedings of the National Academy of Sciences of the United States of America*, *109*(46), 18997–19002. https://doi.org/10.1073/pnas.1205573109

Moretto, E., Murru, L., Martano, G., Sassone, J., & Passafaro, M. (2018). Glutamatergic synapses in neurodevelopmental disorders. In *Progress in Neuro-Psychopharmacology and Biological Psychiatry* (Vol. 84, pp. 328–342). Elsevier Inc. https://doi.org/10.1016/j.pnpbp.2017.09.014

Muller, D., Oliver, M., & Lynch, G. (1989). Developmental changes in synaptic properties in hippocampus of neonatal rats. *Developmental Brain Research*, *49*(1), 105–114. https://doi.org/10.1016/0165-3806(89)90063-1

Murakoshi, H., Shin, M. E., Parra-Bueno, P., Szatmari, E. M., Shibata, A. C. E., & Yasuda, R. (2017). Kinetics of Endogenous CaMKII Required for Synaptic Plasticity Revealed by Optogenetic Kinase Inhibitor. *Neuron*, *94*(1), 37-47.e5. https://doi.org/10.1016/j.neuron.2017.02.036

Nelson, A. B., Gittis, A. H., & Du Lac, S. (2005). Decreases in CaMKII activity trigger persistent potentiation of intrinsic excitability in spontaneously firing vestibular nucleus neurons. *Neuron*, *46*(4), 623–631. https://doi.org/10.1016/j.neuron.2005.04.009

Neveu, D., & Zucker, R. S. (1996). Postsynaptic Levels of [Ca 2] i Needed to Trigger LTD and LTP. In *Neuron* (Vol. 16).

Niday, Z., & Bean, B. P. (2021). BK channel regulation of afterpotentials and burst firing in cerebellar purkinje neurons. *Journal of Neuroscience*, *41*(13), 2854–2869. https://doi.org/10.1523/JNEUROSCI.0192-20.2021

Ninan, I., & Arancio, O. (2004). Presynaptic CaMKII is necessary for synaptic plasticity in cultured hippocampal neurons. *Neuron*, *42*(1), 129–141. https://doi.org/10.1016/S0896-6273(04)00143-6

Niswender, C. M., & Conn, P. J. (2010). Metabotropic Glutamate Receptors: Physiology, Pharmacology, and Disease. *Annual Review of Pharmacology and Toxicology*, *50*(1), 295–322. https://doi.org/10.1146/annurev.pharmtox.011008.145533

Normandin, M., Gagné, J., Bernard, J., Élie, R., Miceli, D., Baudry, M., & Massicotte, G. (1996). Involvement of the 12-lipoxygenase pathway of arachidonic acid metabolism in homosynaptic long-term depression of the rat hippocampus. *Brain Research*, *730*(1–2), 40–46. https://doi.org/10.1016/0006-8993(96)00428-3

Nosyreva, E. D., & Huber, K. M. (2005). Developmental switch in synaptic mechanisms of hippocampal metabotropic glutamate receptor-dependent long-term depression. *Journal of Neuroscience*, *25*(11), 2992–3001. https://doi.org/10.1523/JNEUROSCI.3652-04.2005

Oh, K. H., Abraham, L. S., Gegg, C., Silvestri, C., Huang, Y. C., Alkema, M. J., Furst, J., Raicu, D., & Kim, H. (2015). Presynaptic BK channel localization is dependent on the hierarchical organization of alpha-catulin and dystrobrevin and fine-tuned by CaV2 calcium channels. *BMC Neuroscience*, *16*(1), 1–13. https://doi.org/10.1186/s12868-015-0166-2

Ohno-shosaku, T., Hashimotodani, Y., Ano, M., Takeda, S., Tsubokawa, H., & Kano, M. (2007). Endocannabinoid signalling triggered by NMDA receptor-mediated calcium entry into rat hippocampal neurons. *Journal of Physiology*, *584*(2), 407–418. https://doi.org/10.1113/jphysiol.2007.137505

Ohno-Shosaku, T., & Kano, M. (2014). Endocannabinoid-mediated retrograde modulation of synaptic transmission. In *Current Opinion in Neurobiology* (Vol. 29, pp. 1–8). Elsevier Ltd. https://doi.org/10.1016/j.conb.2014.03.017

Ou, J. W., Kumar, Y., Alioua, A., Sailer, C., Stefani, E., & Toro, L. (2009). Ca2+- and thromboxane-dependent distribution of MaxiK channels in cultured astrocytes: From microtubules to the plasma membrane. *Glia*, *57*(12), 1280–1295. https://doi.org/10.1002/glia.20847

Pang, Z. P., Cao, P., Xu, W., & Südhof, T. C. (2010). Calmodulin controls synaptic strength via presynaptic activation of calmodulin kinase II. *Journal of Neuroscience*, *30*(11), 4132–4142. https://doi.org/10.1523/JNEUROSCI.3129-09.2010

Perez, Y., Morin, F., & Lacaille, J. C. (2001). A hebbian form of long-term potentiation dependent on mGluR1a in hippocampal inhibitory interneurons. *Proceedings of the National Academy of Sciences of the United States of America*, *98*(16), 9401–9406. https://doi.org/10.1073/pnas.161493498

Perrone-Capano, C., Volpicelli, F., Penna, E., Chun, J. T., & Crispino, M. (2021). Presynaptic protein synthesis and brain plasticity: From physiology to neuropathology. *Progress in Neurobiology*, *202*(March), 102051. https://doi.org/10.1016/j.pneurobio.2021.102051

Péterfi, Z., Urbán, G. M., Papp, O. I., Németh, B., Monyer, H., Szabó, G., Erdélyi, F., Mackie, K., Freund, T. F., Hájos, N., & Katona, I. (2012). Endocannabinoid-mediated long-term depression of afferent excitatory synapses in hippocampal pyramidal cells and GABAergic interneurons. *Journal of Neuroscience*, *32*(41), 14448–14463. https://doi.org/10.1523/JNEUROSCI.1676-12.2012

Pham, T., Hussein, T., Calis, D., Bischof, H., Skrabak, D., Cruz Santos, M., Maier, S., Spähn, D., Kalina, D., Simonsig, S., Ehinger, R., Groschup, B., Knipper, M., Plesnila, N., Ruth, P., Lukowski, R., & Matt, L. (2023). BK channels sustain neuronal Ca2+ oscillations to support hippocampal long-term potentiation and memory formation. *Cellular and Molecular Life Sciences*, *80*(12). https://doi.org/10.1007/s00018-023-05016-y

Piochon, C., Kano, M., & Hansel, C. (2016). LTD-like molecular pathways in developmental synaptic pruning. *Nature Neuroscience*, *19*(10), 1299–1310. https://doi.org/10.1038/nn.4389

Pratt, C. P., Kuljis, D. A., Homanics, G. E., He, J., Kolodieznyi, D., Dudem, S., Hollywood, M. A., Barth, A. L., & Bruchez, M. P. (2017). Tagging of Endogenous BK Channels with a Fluorogen-Activating Peptide Reveals β4-Mediated Control of Channel Clustering in Cerebellum. *Frontiers in Cellular Neuroscience*, *11*(October), 1–18. https://doi.org/10.3389/fncel.2017.00337

Puente, N., Cui, Y., Lassalle, O., Lafourcade, M., Georges, F., Venance, L., Grandes, P., & Manzoni, O. J. (2011). Polymodal activation of the endocannabinoid system in the extended amygdala. *Nature Neuroscience*, *14*(12), 1542–1547. https://doi.org/10.1038/nn.2974

Puighermanal, E., Marsicano, G., Busquets-Garcia, A., Lutz, B., Maldonado, R., & Ozaita, A. (2009). Cannabinoid modulation of hippocampal long-term memory is mediated by mTOR signaling. *Nature Neuroscience*, *12*(9), 1152–1158. https://doi.org/10.1038/nn.2369

Purgert, C. A., Izumi, Y., Jong, Y. J. I., Kumar, V., Zorumski, C. F., & O'Malley, K. L. (2014). Intracellular mGluR5 can mediate synaptic plasticity in the hippocampus. *Journal of Neuroscience*, *34*(13), 4589–4598. https://doi.org/10.1523/JNEUROSCI.3451-13.2014

Raffaelli, G., Saviane, C., Mohajerani, M. H., Pedarzani, P., & Cherubini, E. (2004). BK potassium channels control transmitter release at CA3-CA3 synapses in the rat hippocampus. *Journal of Physiology*, *557*(1), 147–157. https://doi.org/10.1113/jphysiol.2004.062661

Ransom, C. B., Liu, X., & Sontheimer, H. (2002). BK channels in human glioma cells have enhanced calcium sensitivity. *Glia*, *38*(4), 281–291. https://doi.org/10.1002/glia.10064

Rebola, N., Carta, M., & Mulle, C. (2017). Operation and plasticity of hippocampal CA3 circuits: Implications for memory encoding. In *Nature Reviews Neuroscience* (Vol. 18, Issue 4, pp. 209–221). Nature Publishing Group. https://doi.org/10.1038/nrn.2017.10

Regehr, W. G., Carey, M. R., & Best, A. R. (2009). Activity-Dependent Regulation of Synapses by Retrograde Messengers. In *Neuron* (Vol. 63, Issue 2, pp. 154–170). https://doi.org/10.1016/j.neuron.2009.06.021

Reyes-García, S. E., & Escobar, M. L. (2021). Calcineurin Participation in Hebbian and Homeostatic Plasticity Associated With Extinction. In *Frontiers in Cellular Neuroscience* (Vol. 15). Frontiers Media S.A. https://doi.org/10.3389/fncel.2021.685838

Rice, C. A., & Stackman, R. W. (2024). The small conductance Ca2+-activated K+ channel activator GW542573X impairs hippocampal memory in C57BL/6J mice. *Neuropharmacology*, *252*. https://doi.org/10.1016/j.neuropharm.2024.109960

Roberts-Crowley, M. L., Mitra-Ganguli, T., Liu, L., & Rittenhouse, A. R. (2009). Regulation of voltage-gated Ca2+ channels by lipids. In *Cell Calcium* (Vol. 45, Issue 6, pp. 589–601). Elsevier Ltd. https://doi.org/10.1016/j.ceca.2009.03.015

Rodríguez-Moreno, A., González-Rueda, A., Banerjee, A., Upton, A. L., Craig, M. T., & Paulsen, O. (2013). Presynaptic Self-Depression at Developing Neocortical Synapses. *Neuron*, *77*(1), 35–42. https://doi.org/10.1016/j.neuron.2012.10.035

Rolls, E. T., & Treves, A. (2024). A theory of hippocampal function: New developments. In *Progress in Neurobiology* (Vol. 238). Elsevier Ltd. https://doi.org/10.1016/j.pneurobio.2024.102636

Roshchin, M. V., Matlashov, M. E., Ierusalimsky, V. N., Balaban, P. M., Belousov, V. V., Kemenes, G., Staras, K., & Nikitin, E. S. (2018). A BK channel–mediated feedback pathway links single-synapse activity with action potential sharpening in repetitive firing. *Science Advances*, *4*(7), 1–9. https://doi.org/10.1126/sciadv.aat1357

Rusakov, D. A. (2006). Ca2+-dependent mechanisms of presynaptic control at central synapses. In *Neuroscientist* (Vol. 12, Issue 4, pp. 317–326). https://doi.org/10.1177/1073858405284672

Sade, H., Muraki, K., Ohya, S., Hatano, N., & Imaizumi, Y. (2006). Activation of large-conductance, Ca2+-activated K+ channels by cannabinoids. *American Journal of Physiology - Cell Physiology*, *290*(1). https://doi.org/10.1152/ajpcell.00482.2004

Sailer, C. A., Kaufmann, W. A., Kogler, M., Chen, L., Sausbier, U., Ottersen, O. P., Ruth, P., Shipston, M. J., & Knaus, H. G. (2006). Immunolocalization of BK channels in hippocampal pyramidal neurons. *European Journal of Neuroscience*, *24*(2), 442–454. https://doi.org/10.1111/j.1460-9568.2006.04936.x

Salem, N., & Van Dael, P. (2020). Arachidonic acid in human milk. In *Nutrients* (Vol. 12, Issue 3). MDPI AG. https://doi.org/10.3390/nu12030626

Salzmann, M., Seidel, K. N., Bernard, R., Prüss, H., Veh, R. W., & Derst, C. (2010). BKβ1 subunits contribute to BK channel diversity in rat hypothalamic neurons. *Cellular and Molecular Neurobiology*, *30*(6), 967–976. https://doi.org/10.1007/s10571-010-9527-7

Sanderson, J. L., Gorski, J. A., & Dell'Acqua, M. L. (2016). NMDA Receptor-Dependent LTD Requires Transient Synaptic Incorporation of Ca2+-Permeable AMPARs Mediated by AKAP150-Anchored PKA and Calcineurin. *Neuron*, *89*(5), 1000–1015. https://doi.org/10.1016/j.neuron.2016.01.043

Scheyer, A. F., Borsoi, M., Pelissier-Alicot, A. L., & Manzoni, O. J. J. (2020). Maternal exposure to the cannabinoid agonist WIN 55,12,2 during lactation induces lasting behavioral and synaptic alterations in the rat adult offspring of both sexes. *ENeuro*, *7*(5), 1–11. https://doi.org/10.1523/ENEURO.0144-20.2020

Schwartz, N., Schohl, A., & Ruthazer, E. S. (2009). Neural Activity Regulates Synaptic Properties and Dendritic Structure In Vivo through Calcineurin/NFAT Signaling. *Neuron*, *62*(5), 655–669. https://doi.org/10.1016/j.neuron.2009.05.007

Seidel, K. N., Derst, C., Salzmann, M., Höltje, M., Priller, J., Markgraf, R., Heinemann, S. H., Heilmann, H., Skatchkov, S. N., Eaton, M. J., Veh, R. W., & Prüss, H. (2011). Expression of the voltage- and Ca2+-dependent BK potassium channel subunits BKβ1 and BKβ4 in rodent astrocytes. *Glia*, *59*(6), 893–902. https://doi.org/10.1002/glia.21160

Shah, K. R., Guan, X., & Yan, J. (2022). Structural and Functional Coupling of Calcium-Activated BK Channels and Calcium-Permeable Channels Within Nanodomain Signaling Complexes. *Frontiers in Physiology*, *12*(January), 1–16. https://doi.org/10.3389/fphys.2021.796540

Shao, L. R., Halvorsrud, R., Borg-Graham, L., & Storm, J. F. (1999). The role of BK-type Ca2+-dependent K+ channels in spike broadening during repetitive firing in rat hippocampal pyramidal cells. *Journal of Physiology*, *521*(1), 135–146. https://doi.org/10.1111/j.1469-7793.1999.00135.x

Shibata, A. C. E., Ueda, H. H., Eto, K., Onda, M., Sato, A., Ohba, T., Nabekura, J., & Murakoshi, H. (2021). Photoactivatable CaMKII induces synaptic plasticity in single synapses. *Nature Communications*, *12*(1), 1–15. https://doi.org/10.1038/s41467-021-21025-6

Shinoda, Y., Tanaka, T., Tominaga-Yoshino, K., & Ogura, A. (2010). Persistent Synapse Loss Induced by Repetitive LTD in Developing Rat Hippocampal Neurons. *PLoS ONE*, *5*(4), e10390. https://doi.org/10.1371/journal.pone.0010390

Shruti, S., Urban-Ciecko, J., Fitzpatrick, J. A., Brenner, R., Bruchez, M. P., & Barth, A. L. (2012). The brain-specific beta4 subunit downregulates BK channel cell surface expression. *PLoS ONE*, *7*(3). https://doi.org/10.1371/journal.pone.0033429

Singh, N., Bartol, T., Levine, H., Sejnowski, T., & Nadkarni, S. (2021). Presynaptic endoplasmic reticulum regulates short-term plasticity in hippocampal synapses. *Communications Biology*, *4*(1), 1–29. https://doi.org/10.1038/s42003-021-01761-7

Sjöström, P. J., Turrigiano, G. G., & Nelson, S. B. (2003). Neocortical LTD via Coincident Activation of Presynaptic NMDA and Cannabinoid Receptors. *Neuron*, *39*(4), 641–654. https://doi.org/10.1016/S0896-6273(03)00476-8

Speranza, L., Inglebert, Y., De Sanctis, C., Wu, P. Y., Kalinowska, M., McKinney, R. A., & Francesconi, A. (2022). Stabilization of Spine Synaptopodin by mGluR1 Is Required for mGluR-LTD. *Journal of Neuroscience*, *42*(9), 1666–1678. https://doi.org/10.1523/JNEUROSCI.1466-21.2022

Stanton, P. K., & Gage, A. T. (1996). Distinct synaptic loci of Ca2+/calmodulin-dependent protein kinase II necessary for long-term potentiation and depression. *Journal of Neurophysiology*, *76*(3), 2097–2101. https://doi.org/10.1152/jn.1996.76.3.2097

Sun, X., Zhou, D., Zhang, P., Moczydlowski, E. G., & Haddad, G. G. (2007). β-subunit-dependent modulation of hSlo BK current by arachidonic acid. *Journal of Neurophysiology*, *97*(1), 62–69. https://doi.org/10.1152/jn.00700.2006

Taberner, F. J., Fernández-Ballester, G., Fernández-Carvajal, A., & Ferrer-Montiel, A. (2015). TRP channels interaction with lipids and its implications in disease. In *Biochimica et Biophysica Acta - Biomembranes* (Vol. 1848, Issue 9, pp. 1818–1827). Elsevier B.V. https://doi.org/10.1016/j.bbamem.2015.03.022

Till, S. M., Li, H. L., Miniaci, M. C., Kandel, E. R., & Choi, Y. B. (2011). A presynaptic role for FMRP during protein synthesis-dependent long-term plasticity in Aplysia. *Learning and Memory*, *18*(1), 39–48. https://doi.org/10.1101/lm.1958811

Vaithianathan, T., Bukiya, A., Liu, J., Liu, P., Asuncion-Chin, M., Fan, Z., & Dopico, A. (2008). Direct regulation of BK channels by phosphatidylinositol 4,5-bisphosphate as a novel signaling pathway. *Journal of General Physiology*, *132*(1), 13–28. https://doi.org/10.1085/jgp.200709913

Vitalis, T., Lainé, J., Simon, A., Roland, A. B., Leterrier, C., Lenkei, Z., & Roland, A. (2008). The type 1 cannabinoid receptor is highly expressed in embryonic cortical projection neurons and negatively regulates neurite growth in vitro. *European Journal of Neuroscience*, *28*(9), 1705–1718. https://doi.org/10.1111/j.1460-9568.2008.06484.xï

Volterra, A., Trotti, D., Cassutti, P., Tromba, C., Galimberti, R., Lecchi, P., & Racagni, G. (1992). *A Role for The Arachidonic Acid Cascade In Fast Synaptic Modulation: Ion Channels and Transmitter Uptake Systems As Target Proteins* (pp. 147–158). https://doi.org/10.1007/978-1-4615-3426-6_13

Wallner, M., Meera, P., & Toro, L. (1999). Molecular basis of fast inactivation in voltage and Ca $^{2+}$ -activated K $^{+}$ channels: A transmembrane β-subunit homolog. *Proceedings of the National Academy of Sciences*, *96*(7), 4137–4142. https://doi.org/10.1073/pnas.96.7.4137

Wang, B., Jaffe, D. B., & Brenner, R. (2014). Current understanding of iberiotoxin-resistant BK channels in the nervous system. *Frontiers in Physiology*, *5*(OCT), 1–11. https://doi.org/10.3389/fphys.2014.00382

Wang, H., Ardiles, A. O., Yang, S., Tran, T., Posada-Duque, R., Valdivia, G., Baek, M., Chuang, Y. A., Palacios, A. G., Gallagher, M., Worley, P., & Kirkwood, A. (2016). Metabotropic glutamate receptors induce a form of LTP controlled by translation and arc signaling in the hippocampus. *Journal of Neuroscience*, *36*(5), 1723–1729. https://doi.org/10.1523/JNEUROSCI.0878-15.2016

Wang, J.-H., & Kelly, P. T. (1996). *The Balance between Postsynaptic Ca 2+-dependent Protein Kinase and Phosphatase Activities Controlling Synapti¢ Strength*.

Wang, Z. W. (2008). Regulation of synaptic transmission by presynaptic CAMKII and BK channels. *Molecular Neurobiology*, *38*(2), 153–166. https://doi.org/10.1007/s12035-008-8039-7

Wasling, P., Hanse, E., & Gustafsson, B. (2004). *Developmental Changes in Release Properties of the CA3-CA1 Glutamate Synapse in Rat Hippocampus*. https://doi.org/10.1152/jn.00464

Watabe, A. M., Carlisle, H. J., & O'Dell, T. J. (2002). Postsynaptic induction and presynaptic expression of group 1 mGluR-dependent LTD in the hippocampal CA1 region. *Journal of Neurophysiology*, *87*(3), 1395–1403. https://doi.org/10.1152/jn.00723.2001

Watanabe, H., Vriens, J., Prenen, J., Droogmans, G., Voets, T., & Nilius, B. (2003). Anandamide and arachidonic acid use epoxyeicosatrienoic acids to activate TRPV4 channels. *Nature*, *424*(6947), 434–438. https://doi.org/10.1038/nature01807

Weseler, A. R., Dirix, C. E. H., Bruins, M. J., & Hornstra, G. (2008). Dietary arachidonic acid dose-dependently increases the arachidonic acid concentration in human milk. *Journal of Nutrition*, *138*(11), 2190–2197. https://doi.org/10.3945/jn.108.089318

Whitmire, L. E., Ling, L., Bugay, V., Carver, C. M., Timilsina, S., Chuang, H. H., Jaffe, D. B., Shapiro, M. S., Cavazos, J. E., & Brenner, R. (2017). Downregulation of KCNMB4 expression and changes in BK channel subtype in hippocampal granule neurons following seizure activity. *PLoS ONE*, *12*(11), 1–20. https://doi.org/10.1371/journal.pone.0188064

Wiegert, J. S., & Oertner, T. G. (2013). Long-Term depression triggers the selective elimination of weakly integrated synapses. *Proceedings of the National Academy of Sciences of the United States of America*, *110*(47). https://doi.org/10.1073/pnas.1315926110

Wiegert, J. S., Pulin, M., Gee, C. E., & Oertner, T. G. (2018). The fate of hippocampal synapses depends on the sequence of plasticity-inducing events. *ELife*, *7*. https://doi.org/10.7554/eLife.39151

Williams, J. H., Errington, M. L., Lynch, M. A., & Bliss, T. V. P. (1989). Arachidonic acid induces a long-term activity-dependent enhancement of synaptic transmission in the hippocampus. *Nature*, *341*(6244), 739–742. https://doi.org/10.1038/341739a0

Winters, B. L., & Vaughan, C. W. (2021). Mechanisms of endocannabinoid control of synaptic plasticity. In *Neuropharmacology* (Vol. 197). Elsevier Ltd. https://doi.org/10.1016/j.neuropharm.2021.108736

Wu, X.-L., Yan, Q.-J., & Zhu, F. (2022). Abnormal synaptic plasticity and impaired cognition in schizophrenia. *World Journal of Psychiatry*, *12*(4), 541–557. https://doi.org/10.5498/wjp.v12.i4.541

Wu, Y., Liu, Y., Hou, P., Yan, Z., Kong, W., Liu, B., Li, X., Yao, J., Zhang, Y., Qin, F., & Ding, J. (2013). TRPV1 Channels Are Functionally Coupled with BK(mSlo1) Channels in Rat Dorsal Root Ganglion (DRG) Neurons. *PLoS ONE*, *8*(10), 1–12. https://doi.org/10.1371/journal.pone.0078203

Yang, J., Han, H., Cao, J., Li, L., & Xu, L. (2006). Prenatal stress modifies hippocampal synaptic plasticity and spatial learning in young rat offspring. *Hippocampus*, *16*(5), 431–436. https://doi.org/10.1002/hipo.20181

Yang, J., Seo, J., Nair, R., Han, S., Jang, S., Kim, K., Han, K., Paik, S. K., Choi, J., Lee, S., Bae, Y. C., Topham, M. K., Prescott, S. M., Rhee, J. S., Choi, S. Y., & Kim, E. (2011). DGKl regulates presynaptic release during mGluR-dependent LTD. *EMBO Journal*, *30*(1), 165–180. https://doi.org/10.1038/emboj.2010.286

Yasuda, H., Barth, A. L., Stellwagen, D., & Malenka, R. C. (2003). A developmental switch in the signaling cascades for LTP induction. *Nature Neuroscience*, *6*(1), 15–16. https://doi.org/10.1038/nn985

Yasuda, H., Huang, Y., & Tsumoto, T. (2008). Regulation of excitability and plasticity by endocannabinoids and PKA in developing hippocampus. *Proceedings of the National Academy of Sciences of the United States of America*, *105*(8), 3106–3111. https://doi.org/10.1073/pnas.0708349105

Zakharenko, S. S., Zablow, L., & Siegelbaum, S. A. (2002). Altered presynaptic vesicle release and cycling during mGluR-dependent LTD. *Neuron*, *35*(6), 1099–1110. https://doi.org/10.1016/S0896-6273(02)00898-X

Zaman, T., De Oliveira, C., Smoka, M., Narla, C., Poulter, M. O., & Schmid, S. (2017). BK channels mediate synaptic plasticity underlying habituation in rats. *Journal of Neuroscience*, *37*(17), 4540–4551. https://doi.org/10.1523/JNEUROSCI.3699-16.2017

Zhang, H. Y., Bi, G. H., Li, X., Li, J., Qu, H., Zhang, S. J., Li, C. Y., Onaivi, E. S., Gardner, E. L., Xi, Z. X., & Liu, Q. R. (2015). Species differences in cannabinoid receptor 2 and receptor responses to cocaine self-administration in mice and rats. *Neuropsychopharmacology*, *40*(4), 1037–1051. https://doi.org/10.1038/npp.2014.297

Zhang, J., Guan, X., Li, Q., Meredith, A. L., Pan, H. L., & Yan, J. (2018). Glutamate-activated BK channel complexes formed with NMDA receptors. *Proceedings of the National Academy of Sciences of the United States of America*, *115*(38), E9006–E9014. https://doi.org/10.1073/pnas.1802567115

Zhang, Y., Li, Z., Zhang, Y., Zhang, H., Lu, C., & Vreugdenhil, M. (2021). The Control of Rat Hippocampal Gamma Oscillation Strength by BK Channel Activity. *Neuroscience*, *475*(September), 220–228. https://doi.org/10.1016/j.neuroscience.2021.09.002

Zhang, Y., Tang, R., Hu, Z.-M., Wang, X.-H., Gao, X., Wang, T., & Tang, M.-X. (2024). Key Synaptic Pathology in Autism Spectrum Disorder: Genetic Mechanisms and Recent Advances. *Journal of Integrative Neuroscience*, *23*(10). https://doi.org/10.31083/j.jin2310184

Zhou, Q., Homma, K. J., & Poo, M. M. (2004). Shrinkage of dendritic spines associated with long-term depression of hippocampal synapses. *Neuron*, *44*(5), 749–757. https://doi.org/10.1016/j.neuron.2004.11.011

Zhou, Y., & Lingle, C. J. (2014). Paxilline inhibits BK channels by an almost exclusively closed-channel block mechanism. *Journal of General Physiology*, *144*(5), 415–440. https://doi.org/10.1085/jgp.201411259

Zhuo, M., Zhang, W., Son, H., Mansuy, I., Sobel, R. A., Seidman, J., & Kandel, E. R. (1999). A selective role of calcineurin Aα in synaptic depotentiation in hippocampus. *Proceedings of the National Academy of Sciences of the United States of America*, *96*(8), 4650–4655. https://doi.org/10.1073/pnas.96.8.4650

Zink, M. H., Oltman, C. L., Lu, T., Katakam, P. V. G., Kaduce, T. L., Lee, H. C., Dellsperger, K. C., Spector, A. A., Myers, P. R., & Weintraub, N. L. (2001). 12-Lipoxygenase in porcine coronary microcirculation: Implications for coronary vasoregulation. *American Journal of Physiology - Heart and Circulatory Physiology*, *280*(2 49-2). https://doi.org/10.1152/ajpheart.2001.280.2.h693

Zoghbi, H. Y., & Bear, M. F. (2012). Synaptic dysfunction in neurodevelopmental disorders associated with autism and intellectual disabilities. *Cold Spring Harbor Perspectives in Biology*, *4*(3). https://doi.org/10.1101/cshperspect.a009886

APPENDIX

International Journal of
Molecular Sciences

MDPI

Review

Ca^{2+}- and Voltage-Activated K^+ (BK) Channels in the Nervous System: One Gene, a Myriad of Physiological Functions

Carlos Ancatén-González [1,2], Ignacio Segura [1], Rosangelina Alvarado-Sánchez [1,3], Andrés E. Chávez [1,*,†] and Ramon Latorre [1,*,†]

1 Centro Interdisciplinario de Neurociencia de Valparaíso (CINV), Instituto de Neurociencias, Universidad de Valparaíso, Valparaíso 2340000, Chile
2 Programa de Doctorado en Ciencias, Mención Neurociencia, Universidad de Valparaíso, Valparaíso 2340000, Chile
3 Doctorado en Ciencias Mención Biofísica y Biología Computacional, Universidad de Valparaíso, Valparaíso 2340000, Chile
* Correspondence: andres.chavez@uv.cl (A.E.C.); ramon.latorre@uv.cl (R.L.)
† These authors contributed equally to this work.

Abstract: BK channels are large conductance potassium channels characterized by four pore-forming α subunits, often co-assembled with auxiliary β and γ subunits to regulate Ca^{2+} sensitivity, voltage dependence and gating properties. BK channels are abundantly expressed throughout the brain and in different compartments within a single neuron, including axons, synaptic terminals, dendritic arbors, and spines. Their activation produces a massive efflux of K^+ ions that hyperpolarizes the cellular membrane. Together with their ability to detect changes in intracellular Ca^{2+} concentration, BK channels control neuronal excitability and synaptic communication through diverse mechanisms. Moreover, increasing evidence indicates that dysfunction of BK channel-mediated effects on neuronal excitability and synaptic function has been implicated in several neurological disorders, including epilepsy, fragile X syndrome, mental retardation, and autism, as well as in motor and cognitive behavior. Here, we discuss current evidence highlighting the physiological importance of this ubiquitous channel in regulating brain function and its role in the pathophysiology of different neurological disorders.

Keywords: K+ channels; BK channels; neurobiology; ion-channels; nervous system; neuronal excitability; synapsis

check for updates

Citation: Ancatén-González, C.; Segura, I.; Alvarado-Sánchez, R.; Chávez, A.E.; Latorre, R. Ca^{2+}- and Voltage-Activated K^+ (BK) Channels in the Nervous System: One Gene, a Myriad of Physiological Functions. *Int. J. Mol. Sci.* **2023**, *24*, 3407. https://doi.org/10.3390/ijms24043407

Academic Editor: Marco Colombini

Received: 19 December 2022
Revised: 18 January 2023
Accepted: 21 January 2023
Published: 8 February 2023

Copyright: © 2023 by the authors. Licensee MDPI, Basel, Switzerland. This article is an open access article distributed under the terms and conditions of the Creative Commons Attribution (CC BY) license (https://creativecommons.org/licenses/by/4.0/).

1. Introduction

Large-conductance calcium (Ca^{2+})- and voltage-activated potassium (K^+) channels (BK, also known as Maxi-K or Slo1) are ubiquitously expressed in the body playing important roles in blood flow regulation, renal excretion, muscle contraction, circadian rhythm, and hearing [1–3]. BK channels are also abundantly expressed throughout the central nervous system in the cortex, basal ganglia, hippocampus, thalamus, and cerebellum, among other areas (Table 1) [4–6]. There, BK channels are strategically positioned on the plasma membrane and intracellular compartments in both neurons and glial cells [7–13]. Typically, activation of BK channels leads to a massive efflux of K^+ ions that hyperpolarizes cellular membrane potential to regulate neuronal excitability and synaptic function, and, ultimately, motor and cognitive behavior [14–17]. Within a single neuron, BK channels are known to be expressed within different compartments, accomplishing different functions [18], including somatic regulation of action potentials [10,19] and regulation of neurotransmitter release at synaptic terminals [16,20–24]. BK channels are also present in dendritic compartments and neuronal spines [25], where they can limit the postsynaptic potential [25–27] or dendritic Ca^{2+} signals [25,28]. Although BK channels are also localized in nuclei, lysosomes, and mitochondria [11], their contribution to regulating neuronal function remains elusive.

While increasing evidence supports a critical role for BK channels in regulating neuronal excitability, their ability to act as a coincidence detector for changes in intracellular Ca^{2+} concentration suggests that BK channels are also well-positioned to control synaptic communication by exerting either negative [23,24] or positive [29] regulation of Ca^{2+} influx through voltage-activated Ca^{2+} channels (for review see Griguoli et al., 2016 [16]). However, the mechanisms by which BK regulate neuronal function and behavior in the brain remain far from being completely understood.

2. BK Biophysical and Structural Characteristics

Coded for by a single gene (*Slo1, KCNMA1*), BK channels have been proven, from the very beginning, to show a complex, albeit very attractive behavior. Their large conductance (≈250 pS in symmetrical 100 mM K^+) near the limit of the diffusional process of K^+ in solution is accompanied by an exquisite K^+ selectivity, making them unique in the large family of different K^+ channels [30–32]. Cloning of BK channels showed their similarity to voltage-dependent K^+ channels in which each subunit contains six transmembrane domains, including a well-defined voltage sensor (S1–S4) and a pore domain (S5–S6) [33,34]. However, later studies showed that the channel-forming protein contained an extra segment (S0) placing the N-terminus on the extracellular side [35]. In addition, BK possess a large C-terminus, composed of two regulators of K^+ conductance (RCK1 and RCK2), where the high-affinity Ca^{2+}-binding sites reside [36–39].

Once single-channel, macroscopic, and gating currents records were available, one of the main challenges was to combine BK voltage dependence and channel activation by Ca^{2+} in one gating-kinetics scheme. From the start, it became clear that BK gating kinetics are intricate. One big step ahead was achieved by the group of Magleby [40], who identified that the several open and closed states present in the single-channel current records were correlated and inversely related. Shorter open intervals were followed by long closed intervals and vice versa. These observations made linear gating-kinetics models as those proposed, for example, for shaker K^+ channels, unlikely. Instead, they suggested a progression of closed states of decreasing duration connected to open states of increasing lifetimes. More importantly, these findings hinted that the gating in BK channels is allosteric. Another important piece of information was that treatment of BK channels with *N*-bromoacetamide rendered BK voltage-dependent channels insensitive to internal Ca^{2+}, a clear indication that voltage sensors and Ca^{2+}-binding sites were in different regions of the channel-forming protein [41]. These early discoveries allowed us to define BK channels from the start as modular proteins with allosteric gating before knowing their well-defined structure.

The BK channel gating characteristics have been summarized in a two-tiered kinetic model [42,43]. Considering the tetrameric nature of BK channels in this allosteric gating-kinetics model, the four voltage sensor domains (VSD) undergo a transition between resting (R) and active states (A). The transition R–A is defined by a voltage-dependent equilibrium constant *J*. The VSDs allosterically interact with the pore opening through the allosteric factor *D* (Figure 1A). The model considers the existence of four Ca^{2+}-binding sites, each of which includes a Ca^{2+}-binding mediated transition between an empty site (U) and a Ca^{2+}-bound site (BCa^{2+}) with an equilibrium constant $K = [Ca^{2+}]/K_D$. In this case, the allosteric interaction with the pore opening is determined by the allosteric factor *C*. On the other hand, the strength of allosteric interaction between voltage sensors and Ca^{2+} binding is determined by the allosteric factor *E*. It is important to note here that the closed–open (C–O) reaction defined by the equilibrium constant *L* can proceed in the absence of voltage-sensor activation and of internal Ca^{2+}, albeit with a very low probability of opening (Figure 1B). Figure 2B shows that Ca^{2+} alone can increase the open probability (Po) by about four orders of magnitude. Since Po increases with depolarizing voltages and internal Ca^{2+} concentrations, and BK has large conductance, BK channels are the perfect damping machine to brake excitatory processes mediated by internal Ca^{2+}.

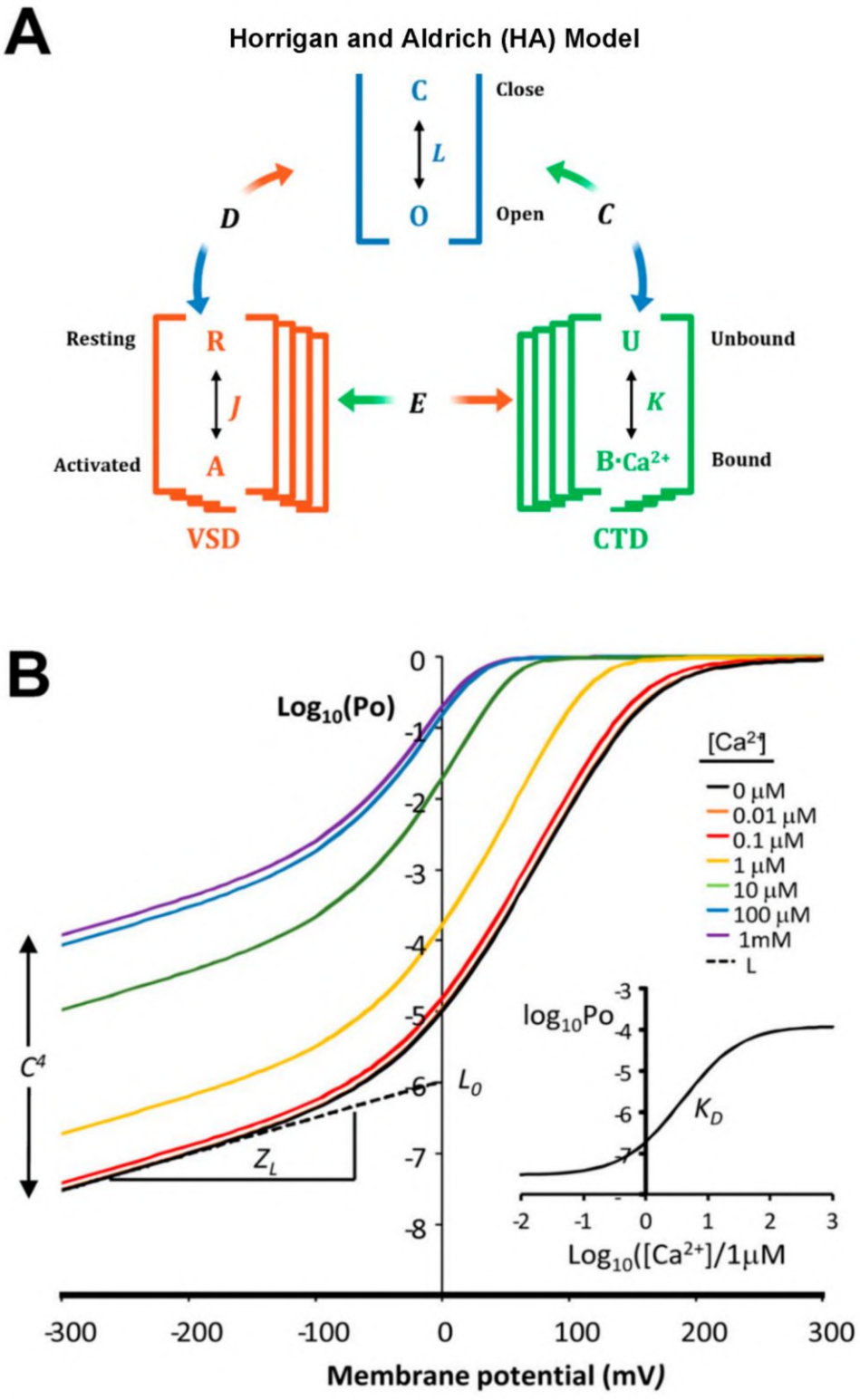


Figure 1. BK Channel allosteric gating mechanism. (**A**) H–A allosteric model [43]. Voltage sensor (R–A), Ca^{2+} binding, and C–O transitions are defined by the equilibrium constants *J*, *K*, and *L*, respectively. Voltage sensors and Ca^{2+} sensors are coupled to the pore by allosteric factors D and C, respectively, and coupling between sensors is performed by *E*. (**B**) Simulated data of the Log10 of the probability of opening vs. voltage obtained using the H–A model. Notice that when all the voltage sensors are at rest the parameters *L*, *zL*, and *C* can be obtained.

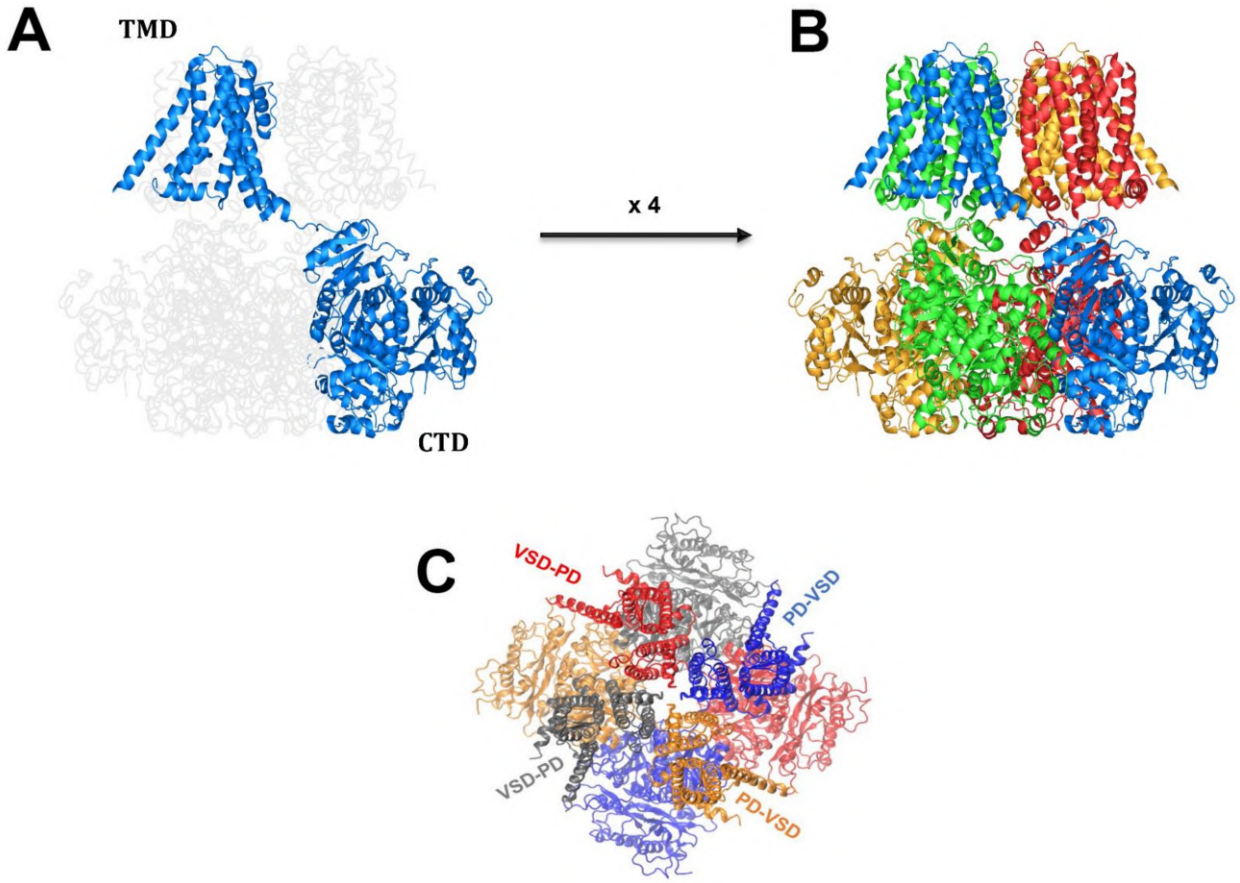


Figure 2. Structural characteristics of the BK channel. (**A**) The α subunit is formed by a transmembrane domain (TMD) composed of seven α helices (S0–S7) and a large carboxy terminal (CTD) containing two regulatory potassium conductance domains. (**B**) The BK channel is a tetramer formed by 4 α subunits in which the CTD acquires a swapped conformation and the 4 CTDs form the gating ring. (**C**) Top view of the BK channel. The voltage sensor domain (VSD) and the pore domain (PD) have been colored to highlight the non-swapped configuration of the VSD and the PD.

There is a strong coupling between the Ca^{2+} binding sites and the voltage sensors. At saturating Ca^{2+} concentrations, the equilibrium constant *J* that defines the resting–active equilibrium of the voltage sensor (Figure 1A) increases 26-fold [44,45]. This result implies that the free energy necessary to activate the BK channel voltage sensor decreases by about 8 kJ/mol at saturating internal Ca^{2+} concentrations (100 μM).

The modular nature of BK channels was confirmed when the first BK structures were determined using cryo-microscopy [38,46]. As voltage-dependent K^+ (Kv) channels, BK channels are tetramers composed of four identical α subunits (Figure 2A), but unlike Kv channels, BK channels have a non-swapped configuration. The VSD of one subunit (S1–S4) contacts the pore domain (S5–Pore domain–S6) of the same subunit (Figure 2 A, C). Although the work of Ma et al. [47] suggested the presence of a decentralized VSD in which the gating charges were spread across S2, S3, and S4, more recent work gave strong evidence that the gating charges are two arginines contained in S4 (R210 and R213) located in a septum devoid of water [48]. The movements of the charges during BK-VSD activation are small, with only a modest (≈2 Å) displacement of S4. It is unclear at present how the electrical energy is transformed into opening of the pore. However, the gating ring probably mediates the coupling between VSDs and the pore [38,45,46].

The two RCK domains form a gating ring (Figure 1B) containing the two high-affinity Ca^{2+}-binding domains that can be distinguished structurally by their selectivity to divalent ions. The divalent cation-binding site in RCK1 preferentially binds Ca^{2+} and Cd^{2+}, whereas in RCK2, the preferred divalent cations are Ca^{2+} and Ba^{2+} [38,49,50]. The binding of Ca^{2+}

promotes an expansion of the gating ring, which, by pulling the linker that connects the gating ring to S6, causes this transmembrane segment to adopt a configuration that leads to channel opening [46]. It is unclear at present where the gate that defines the closed–open transition is located (Figure 1A). The BK structures show that there is only a modest decrease in the radius of the internal BK vestibule when the channel closes, which varies between 1 and 4 Å [38]. The diameter of the narrowest part of the vestibule is 12 Å. If there is no well-defined structure hindering ions' passage through the BK channel, the following question arises: Where is the gate? Blockade mediated by large quaternary ammonium ions gave the first hint suggesting that, similarly to other channels [51,52], the BK gate resides in a selectivity filter [53–55]. However, simulations of molecular dynamics using BK structures in the absence and the presence of Ca^{2+} indicated that the actual decrease in diameter of the internal cavity of the BK channel during closed state is larger than the one shown by the BK structure obtained in the absence of Ca^{2+} [56]. The final diameter of the cavity was 6–8 Å, and its walls became more hydrophobic, creating a region devoid of water. Due to its low dielectric constant, it produces an energy barrier unsurmountable to ions.

3. BK Auxiliary Subunits

The four auxiliary β subunits (β1–β4) in BK are characterized by a common structure consisting of two transmembrane segments connected by a large extracellular loop (~148 aa residues) and cytoplasmic COOH and NH2 termini. Although to a different degree, all β subunits modify BK channel gating and pharmacology (reviewed in [10,57,58]), β1, β2, and β4 increase Ca^{2+} sensitivity by stabilizing the voltage sensor's active conformation and slowing down the activation and deactivation kinetics. Mediated by its NH_2 terminus, β2 also induces a fast and complete inactivation. Four isoforms are generated by splicing the β3 gene (*kcnmb3*; β3a–d). β3 subunits do not modify BK channel Ca^{2+} sensitivity, but three of them (β3a–c) produce a fast and incomplete inactivation. Importantly, β subunits have different pharmacological profiles, as β2 is iberiotoxin (IBTX)-sensitive, whereas β4 is IBTX-resistant. However, BK channels consisting of the complexes α/β2 or α/β4 can be blocked by paxilline [10,57,59,60]. β4 slows down the activation and deactivation kinetics at all Ca^{2+} concentrations. In symmetrical K^+-concentration conditions, β4 promotes a leftward shift of the BK conductance–voltage curve only at Ca^{2+} concentrations >10 μM compared to BK channels formed by the α subunit alone [61,62]. However, here it is essential to highlight the fact that under physiological conditions—low external K^+—BK/β4 channels shift the conductance–voltage curves leftward at all internal Ca^{2+} concentrations compared to BK/α channels [63,64].

When characterizing the different types of Ca^{2+}-activated channels in the brain plasma membrane vesicles, Reinhart et al. [65] detected two types of high-conductance BK channels. One type showed fast gating and was blocked by charybdotoxin (ChTX) (type I), and the other was ChTX-resistant and exhibited slow gating (type II). Cloning of the different β subunits (β1–β4) showed that the toxin resistance of some BK channels in the brain was most probably due to the formation of complexes between the pore-forming α and the β4 subunit [60,66,67]. Swapping the long external loop connecting TM1 and TM2 between β4 and β1 and neutralization of some of its basic residues showed that this region of the β4 subunit hinders the binding of iberiotoxin (IBTX) by blocking access of the toxin to the BK external vestibule [60,68]. The cryo-structures of the α/β4 BK channel show a 1:1 stoichiometry between α and β4 subunits in which the four external loops of the β4 give origin to a crown-like structure [69]. The crown impedes both access to and toxin release from the binding site, explaining the extremely slow ON and OFF rates of IBTX-inhibition kinetics [70].

β4 is the most abundant auxiliary subunit expressed in the nervous system [66,71]. β4 is found in the thalamus, brainstem, posterior pituitary terminals, pyramidal neurons of the cortex, CA3 pyramidal neurons in the hippocampus, hippocampal dentate granule cells, olfactory bulb, and Purkinje cerebellar neurons [64,72–75] (Table 1). β2 is also extensively

expressed in the brain, albeit at lower levels than β4 [66,71]. β1 on the other hand, is almost absent in the brain, but it has been detected in the hypothalamus, paraventricular neurons, and cerebellar Purkinje cells [76–78]. Interestingly, these hypothalamic neurons reportedly express β1 subunits on the soma and dendrites, while the axon terminals mainly contain the β4 subunit [79]. Such specific distribution of β subunits within the same neurons may have important functional significance in understanding how BK channels differentially contribute to the regulation of somatic and nerve terminal compartments.

The physiological role of the α/β4 BK channels in the brain was first elucidated by Brenner et al. [72], who showed that this type of BK channel (type II) is present in the dentate gyrus granular cells regulating their excitability. Knockout of the β4 converted type II into type I (fast) BK channels [72]. Type I channels reduce, and type II BK channels increase the duration of action potentials [63,72]. Interestingly, in pathological conditions, such as a neuropathic pain model, β4 seems to be upregulated in anterior cingulate cortex pyramidal neurons [73], suggesting that the expression of BK channel subunits could be modulated in an activity-dependent and cellular-specific fashion. Moreover, evidence suggests that the fragile mental retardation protein (FMRP), by interacting with the β4 subunit, shortens the action potential, thus regulating neurotransmitter release in CA3 pyramidal neurons [15]. Single-channel recording in CA3 pyramidal neurons showed that the α/β4 BK channel open probability is reduced by about 50% in neurons from *fmpr* knockout mice increasing the inter-burst interval [80]. However, a recent study showed that FMPR modulates both α/β4 BK and α BK channels [81]. The degree of importance in modulating synaptic activity via interaction of FMPR with α/β4 BK or α BK channels is currently unclear.

Inactivating BK currents have been detected in mammalian auditory hair cells, rat lateral amygdala neurons, and hippocampal CA1 neurons [82–84]. In CA1 and dorsal root ganglion neurons, inactivation is removed when the inner membrane surface is treated with trypsin, suggesting that BK channels are formed by the α/β2 complex [84,85]. Consistent with this idea, in rat dorsal root ganglion neurons, α/β2 BK channels are blocked by IBTX, resulting in increasing firing frequency, broadening of the action potential, and reducing afterhyperpolarization [85]. The spontaneous firing rate in the suprachiasmatic nucleus (SCN) exhibits daily oscillations that determine the normal circadian timing of behavior in mammals. The intrinsic circadian clock in the SCN controls the daily expression of BK. Consistently, BK currents are lower during the day and high at night [86–88], thus determining the daily SCN rate of firing. Moreover, inactivating BK currents are predominant during the day and are reduced at night with an increase in steady-state BK currents [86]. Importantly, in the SCN, BK inactivation is mediated by the β2 subunit, and β2 knockout mice show a lack of diurnal variation in BK currents and SCN firing rate [86].

4. BK Channel Coupling with Ca^{2+}-Permeable Channels

Ca_V and BK Nanodomains: Critical for the feedback control of Ca^{2+} influx and cell excitability in the nervous system, BK channels co-localize with voltage-dependent Ca^{2+} (Ca_V) channels and N-methyl-D-aspartate receptors (NMDAR; reviewed in [89,90]). Due to the low affinity of BK for Ca^{2+} (Kd $\geq$ 3 μM; [91]), co-localization with Ca^{2+}-permeable channels provides BK channels with an effective local Ca^{2+} concentration for their activation and function [92,93]. Indeed, BK channels have been reported to form nanodomains with L-type, P/Q, N-type, R-type, or T-type Ca_V [94–98].

Ca^{2+} chelator EGTA and fast chelator BAPTA differ in their Ca^{2+}-binding rates but have similar Ca^{2+} affinities. They have been a powerful tool for determining the diffusion distance for Ca^{2+} from calcium channels to BK channels. BK channel activity was abolished when using BAPTA as the internal Ca^{2+} buffer, but not with EGTA, revealing the close spatial proximity (~10 to 20 nm) in the nanodomains between BK channels and voltage-sensitive calcium (Ca_V) channels [96,99,100]. More recently, a mathematical model revealed the coexistence of L-type and BK-type Ca_V channels and suggested that they are grouped in nanodomains spatially separated 30 nm from each other [101].

Activation of BK channels mediated by the influx of Ca^{2+} through Ca_V channels decreases the action potential duration, promotes fast hyperpolarization potentials, decreases the time of Ca^{2+} influx, and limits the release of neurotransmitters [99,102,103]. The activation of Ca_V channels modifies the voltage dependency, current amplitude, and kinetics of BK channel activation, causing functional variability in BK dependent on the expression pattern of Ca_V channels [96,104]. The pharmacological blockade of BK channels using IBTX, ChTX, or paxilline has also demonstrated the functional coupling between BK and Ca_V channels. The application of these toxins increases the amplitude of the action potential and Ca^{2+} entry through Ca_V channels as well as the release of neurotransmitters [99,102,105–108]. On the other hand, the specific blockade of a subset of Ca_V channels suppresses the hyperpolarization that is provided by the flow of K^+ ions from active BK channels [96,97,102,105,106,109,110]. One example that illustrates the importance of Ca_V and BK localization is the functional and spatial localization of $Ca_V1.3$ and BK channels in rat hippocampal and sympathetic neurons [104]. $Ca_V1.3$ activates at low voltages, and when co-expressed with BK, the latter started activating at about −50 mV. In hippocampal and sympathetic neurons, $Ca_V1.3$ and BK are localized as clusters of $Ca_V1.3$ encircling clusters of BK channels, forming a multi-channel complex. Since BK channels activate at voltages near the action potential threshold in these complexes, they enable the modulation of neuronal excitability.

BK and NMDAR Complexes: BK channels and NMDARs are widely expressed in the brain, and subcellular distribution variations are caused by the appearance of distinct BK channel auxiliary subunits and NMDAR subunit composition. So far, the BK–GluN1 complex has been functionally described on granule cells of the olfactory bulb [111], on mature dentate granule cells in the hippocampus [27], and in a subset of layer 5 pyramidal neurons of the barrel cortex and visual cortex [25]. Moreover, pulling-down assays demonstrated that this complex is also present in the cerebellum, cortex, thalamus, and striatum [27].

Functional coupling between NMDARs and BK channels was first demonstrated in outside-out patches from the cell bodies of granule cells, where the glutamate-induced outward currents were abolished after applying TEA, paxilline, or IBTX [111]. Distinctively, in the BK–GluN1 complex, the BK S0–S1 loop interacts with the C-terminal domain of the NMDARs. NMDAR activation by glutamate produced robust BK outward currents in whole-cell voltage-clamp recordings on mature dentate gyrus granule cells [27]. The application of NMDAR antagonist (2R)-amino-5-phosphonovaleric acid (AP5) and the pore-blocker MK-801 inhibited the outward currents, confirming the tight association of the BK–GluN1 complex. BK channel outward currents were also elicited by NMDAR activation in neocortex pyramidal neurons [112], those BK currents were also eliminated by AP5, confirming that NMDAR activation is needed to trigger the opening of BK channels. Likewise, $ZnCl_2$ and ifenprodil (IFEN) were used to inhibit GluN2A or GluN2B-containing NMDARs, respectively, to assess the selective coupling between BK channels and different NMDAR subunit compositions. Nevertheless, these compounds only partially suppressed the BK outward currents, suggesting that GluN2A or GluN2B might also be a part of the functional coupling between BK channels and NMDARs in the brain.

NMDAR–BK coupling efficiency with the different NMDAR subunits was also tested in HEK cells expressing BK and GluN1/GluN2A or GluN1/GluN2B using a proximity ligation assay. In agreement with the pharmacological data, BK channels showed no preference for different NMDAR subunits [112]. To further evaluate the degree of coupling between BK channel activation and NMDAR, the Ca^{2+} chelators EGTA and BAPTA were used to determine the relative distance between BK channels and NMDARs in granule cell bodies [111]. The BK channel outward currents induced by glutamate were insensitive to the applied intracellular EGTA. In contrast, BAPTA abolished the BK currents induced by the activation of NMDARs. BK–NMDAR coupling has also been tested in hippocampal and pyramidal neurons using Ca^{2+} chelators [27,112]. In both cases, the results show that BK is

robustly activated by the Ca^{2+} influx mediated by NMDAR, suggesting a short coupling distance.

Other Sources of Ca^{2+} for BK Channel Activation: Co-localization of BK channels with Ca_V channels may form a dynamic and reversible channel complex between the plasma membrane and the endoplasmic reticulum. In neurons of the cerebellum, hippocampus, and suprachiasmatic nucleus, the Ca^{2+} influx mediated by Ca_V channels activates the ryanodine receptors (RyR) present on a nanodomain of the endoplasmic reticulum. RyR release sparks caused by Ca^{2+} immediately below the plasmatic membrane, result in generating rapid activation of the BK channels, forming a complex commonly named a Ca_V–RyR–BK triad [113–115]. This triad allows control over action potential firing patterns on a millisecond time scale [113,114]. Moreover, interaction of BK channels with transient receptor potential vanilloid receptor 1 (TRPV1) channels has also been demonstrated in rat dorsal root ganglion neurons and in heterologous systems where both channels were co-expressed. Using electrophysiological recordings and co-immunoprecipitation assays showed that BK channels are activated by Ca^{2+} influx through TRPV1 channels, with which they associate in complexes in a largely EGTA-insensitive manner [116].

5. BK Post-Translational Modifications

In addition to the diversity of subunits controlling BK function, extensive post-translational modifications significantly modify channel function [117–120]. These post-translational modifications impact the contribution of BK channels to the control of neuronal function. One of the most studied modifications is the addition of phosphate groups to functionally essential residues (Ser/Thr/Tyr) present within the BK α subunit [9], where at least 30 Ser/Thr phosphorylation sites have been identified. Changes in phosphorylation status differentially modulate the voltage and Ca^{2+}-dependent activation [118]. This effect seems to be developmentally regulated [121] as phosphorylation by protein kinase A (PKA) and protein kinase C (PKC) are inversely predominant during fetal and adult stages [117]. While phosphorylation can suppress BK currents induced by an action potential [122], inhibition of phosphatases or mutation in Ser/Thr phosphorylation sites hinders the slow-down of the BK gating kinetics induced by the β4 subunit [123]. These post-translational modifications of BK channels imply that different functions might arise depending on their phosphorylation status. For instance, in medial vestibular nucleus neurons, BK channels contribute to afterhyperpolarization in a CaMKII-dependent manner [124]. In contrast, PKC decreases BK channel activity [125]. In cerebellar Purkinje neurons, PKA can activate non-inactivating BK channels with low activity but inhibits channels with higher activity [126]. PKCγ on the other hand, negatively modulates BK currents resulting in attenuation of the electrical signal and significant alterations of the complex spike waveform [127]. In presynaptic terminals, activation of BK channels and their subsequent phosphorylation by CaMKII modulates neurotransmitter release [119,128], synaptic depression underlying habituation [129], and input-specific spike-timing-dependent long-term depression at thalamostriatal, but not at corticostriatal synapses [28]. Similar to kinases, phosphatases can also regulate the function of BK channels mainly through an inhibitory control of the channel [106,130–132]. Accordingly, type I BK channels lacking β4 can increase neuronal excitability in dentate granule cells in response to reduced phosphatase activity [133].

6. BK Channels Differentially Contribute to Control of Brain Function

The BK α subunit is highly expressed during late embryonic and early postnatal development [14]. As development progresses, BK currents undergo an abrupt increase during the first weeks after birth in neocortical pyramidal neurons, substantia nigra dopamine neurons, and cochlear inner hair cells [134–136]. Similarly, BK channel expression in hippocampal neurons is likely to be developmentally regulated, differentially contributing to the repolarization of single action potentials during the first postnatal week [137], suggesting that BK channels contribute to shaping the properties of mature neuronal firing. One of the clearest roles of BK channels in regulating neural activity comes from electrophysio-

logical studies of neuronal firing. Several reports showed that BK channels control action potential shape by contributing to repolarization and fast afterhyperpolarization (fAHP) currents in multiple neuronal types. These include cerebellar Purkinje cells [102,138–140], hippocampal pyramidal cells [141–143], cortical pyramidal neurons [144,145], and striatal medium spiny neurons [146,147] (Table 1). As discussed above, the strategic co-localization of BK with Cav channels allows BK channels to control Ca^{2+} influx during action potential repolarization and fAHP, even in spontaneously firing neurons [34], suggesting that BK channels act as a feedback regulator to control neuronal excitability. While the BK–Cav channel coupling indicates that BK channels participate during the repolarization phase of the action potential, their coupling with the RyR contributes to the free Ca^{2+} necessary for BK channel activation during the fAHP [148]. However, recent evidence in CA1 pyramidal neurons indicates that the BK channel–Cav2.3 complex regulates somatic excitability by controlling fAHP rather than repolarization. Cav2.3 KO mice showed increased excitability with a decreased fAHP [103]. Such differences may arise from the non-homogenous distribution of BK channels in clustered or scattered pools. While clustered pools may be involved in slower events triggered by Ca^{2+} released by intracellular domains, scattered pools could be involved in transient events such as spike repolarization [139]. Adding to the complexity of BK channel function regulating neuronal firing, evidence indicates that BK channels could also increase neuronal firing [142]. By accelerating membrane repolarization and limiting sodium channel inactivation, BK channels can promote repetitive spiking [149]. An enhanced fAHP can also increase neuronal firing by promoting sodium-channel recovery from inactivation [150].

Table 1. Functional expression of BK channels in the central nervous system.

CNS Area and Neuronal Type	Site of Neuronal Expression	Function	Subunit and/or Pharmacology	References
Prefrontal cortex pyramidal neurons	Pre- (AIS and axon) and postsynaptic (soma)	Limit AP broadening and allow high-frequency firing.	IBTX-sensitive	[151,152]
			Pax-sensitive	[153]
Visual cortex pyramidal neurons	Postsynaptic (basal dendrites)	Reduce EPSPs in small-headed spines.	α subunit, Chtx-sensitive	[25]
Somatosensorial layer 5 pyramidal neurons	Postsynaptic (soma and dendrites)	Reduce influx of ions through NMDAR and increase threshold for plasticity. Modulate dendritic Na^+ and Ca^{2+} spikes.	IBTX and Pax-sensitive	[154]
			Pax-sensitive	[112,155,156]
Hippocampal CA1 pyramidal neuron	Pre- (axon) and Postsynaptic (soma and apical dendrites)	Limit repetitive firing of dendritic calcium spikes. AP repolarization and fAHP.	α subunit	[141,157]
			Chtx-sensitive	[158,159]
			Pax and IBTX-sensitive	[160]
			IBTX-sensitive	[137,142]
Hippocampal CA3 pyramidal neuron	Pre- (Axonal terminals) and postsynaptic (soma)	Decrease glutamate release. Regulate neuronal excitability.	α subunit	[161]
			β4 subunit	[15,162]
			Chtx-sensitive	[163]
			IBTX-sensitive	[23]
			IBTX and Pax-sensitive	[24]
Hippocampal dentate gyrus granule cells	Pre- (mossy fiber boutons and perforant path terminals) and postsynaptic (soma and dendrites)	Control perforant path induce EPSP. Regulate excitability. At mossy fiber boutons contribute to AP repolarization when Kv channels are blocked.	α subunit	[161]
			β2 and β4 subunits	[164]
			β4 subunit	[72]
			Pax-, Chtx- and IBTX-sensitive	[99]
			Pax-sensitive	[27]
Piriform cortex pyramidal neuron	Postsynaptic (soma)	Reduce excitability modulating odor perception.	Pax-sensitive	[165]
Anterior cingulate cortex pyramidal neurons	Pre- (axonal terminals) and postsynaptic (soma)	Reduce hyperexcitability induced by neuropathic pain state.	β4 subunit.	[73]
Somatosensorial SOM+ interneurons	Pre- (axon) and postsynaptic (soma)	Contribute to AP repolarization.	IBTX-sensitive	[166]

Table 1. *Cont.*

CNS Area and Neuronal Type	Site of Neuronal Expression	Function	Subunit and/or Pharmacology	References
Amygdala central nucleus gabaergic neurons	Presynaptic	Limit GABA release.	β2 and β4 subunits	[12]
Substantia nigra pars reticulata gabaergic neurons	Postsynaptic (soma)	Contribute to hyperpolarization.	Chtx- and Pax-sensitive	[167]
Substantia nigra dopaminergic neurons	Postsynaptic (soma)	Not tested.	IBTX-senstive	[134]
Infragranular pyramidal neurons	Postsynaptic (soma and apical dendrites)	Not tested.	Chtx-sensitive	[135]
Lateral habenula nucleus neurons	Postsynaptic (soma)	fAHP increased by corticotropin-releasing factor activation.	IBTX-sensitive	[168]
Medial habenula nucleus neurons	Not described	Not tested.	LRRC55 γ subunit	[169]
Cerebellum Purkinje neurons	Presynaptic (paranodal junctions of axons) Postsynaptic (soma and dendrites)	Decrease dendritic Ca^{2+} spikes avoiding DSE propagation. Regulate afterdepolarization. In myelinated axons allow high-fidelity firing of AP.	α subunit	[161]
			β4 subunit	[170]
			Penitrem A sensitive.	[171]
			IBTX-sensitive	[172]
			IBTX–sensitive + IBTX-insensitive component	[138]
			IBTX and Pax-sensitive.	[102]
			Pax-sensitive	[173]
Cerebellar basket cells	Presynaptic (axonal terminals)	Not tested.	α subunit	[161]
Cerebellar granule cells	Postsynaptic (soma)	Contribute to hyperpolarization and AHP.	IBTX-sensitive	[170]
Suprachiasmatic nucleus neurons	Postsynaptic (soma)	Increase neuronal firing at night but decrease firing during day.	β4 subunit	[174]
			β2 subunit	[86]
Supraoptic nucleus neurons	Pre- and postsynaptic (dendrites, soma and nerve terminals)	β4 but not β1 allows potentiation by ethanol.	β1 subunit in soma and dendrites; β4 in nerve terminals	[79]
Medial vestibular nucleus neurons	Postsynaptic (soma)	Contribute to excitability. Can be activated by CaMKII and inhibited by PKC.	Not tested	[125]
Dorsal cochlear nucleus cartwheel cells	Postsynaptic (soma and dendrites)	Control EPSP.	IBTX-sensitive	[113,175]
Retinal ganglion cells	Postsynaptic (soma)	Regulate cell excitability.	IBTX-sensitive	[176]
A17 amacrine cells	Postsynaptic (varicosities)	Limit Cav channel activation and GABA release.	β2 subunit, IBTX-sensitive	[22]

Abbreviations: AIS: axonal initial segment; IBTX: iberiotoxin; Pax: paxilline; Chtx: charybdotoxin; EPSP: excitatory postsynaptic potential; AP: action potential; AHP: afterhyperpolarization; DSE: depolarization-induced suppression of excitation.

In some neurons, such as Purkinje [177] and vestibular neurons [178], inhibiting BK channels speeds up action potential firing accompanied by a reduction in afterhyperpolarization. Paradoxically, in substantia nigra dopaminergic neurons, inhibiting BK channels increased spike width. This effect was accompanied by an increase in afterhyperpolarization current, likely involving an enhancement of the slowly deactivating K_{v2} current [179]. Similarly, in vestibular nucleus neurons, the fastest firing neurons express Kv3 channels, predominantly to repolarize the neuronal membrane during an AP train. However, in slower-firing neurons, BK channels are responsible for repolarization [180]. This evidence supports the idea that the functional role of BK channels cannot be defined in isolation but critically depends on the context of the other conductances in the cell, as well as their precise localization and composition.

As for principal cells, BK channels also have been reported to control excitability of GABAergic interneurons, but in a lesser extension. For example, in the cortex, action potential repolarization is governed by BK channels in somatostatin (SST)- but not Parvalbumin (PV)-positive interneurons [166]. Interestingly, in the striatum, SST enhances BK currents [146]. If SST released from SST-positive interneurons could act in an autocrine manner to regulate BK channels and control their excitability remains unknown. It is noteworthy, however, that in isolated retinal bipolar cells, SST inhibits BK channels [181]. BK channels also regulate action potential repolarization in striatal cholinergic interneurons [21], regulate firing properties of GABAergic vestibular nucleus neurons [182], and contribute to fAHP in cholinergic neurons of the pontine laterodorsal tegmentum [183]. In the retina, BK channels suppress activation of Ca^{2+} channels to regulate GABAergic A17 amacrine cell signaling [22]. On the other hand, in fast-spiking stellate cerebellar interneurons, blocking BK channels increases action potential width and Ca^{2+} influx [184], further supporting a role for BK in regulating GABAergic interneurons function.

BK channels regulate dendritic excitability: In addition to controlling somatic excitability, increasing evidence indicates that BK channels are also present in dendritic compartments [5], where they exert an additional level of control by modulating dendritic excitability. For example, in the somatosensory cortex, BK channels are present in apical dendrites [154], exerting a suppressive effect on the Ca^{2+} channel to regulate Ca^{2+} spikes and dendritic excitability [18,144,185]. This control is activity-dependent, as a single action potential or a train of low-frequency action potentials could not activate BK channels [156]. In contrast, a high-frequency train of action potentials can activate BK channels [185]. BK channels also restrict dendritic Ca^{2+} spikes in CA1 pyramidal cells, thereby generating an inhibitory effect over synaptic potentiation [186] although dendritic BK channels are not activated by backpropagating action potentials [158,187]. Inhibition of BK channels was also shown to improve dendritic Ca^{2+} spikes in cerebellar Purkinje neurons, thereby facilitating short-term synaptic plasticity mediated by endocannabinoids at distal spines [171] or signal propagation from dendrites to the soma [127]. BK channels also control the magnitude of excitatory potentials in cerebellar Purkinje dendrites [172]. BK-mediated effects for dendritic spike generation could depend on the spine size where they are expressed. For example, in basal dendrites of pyramidal neurons of layer V in the visual cortex, BK channels are activated only in small-head spines, where they suppress excitatory postsynaptic potentials [25]. This effect requires a BK–NMDA receptor complex rather than coupled BK–Cav channels, as Ca^{2+} influx through NMDAR is required to activate BK channels [25]. A similar coupling between NMDAR and BK channels was also observed in basal dendrites of layer V pyramidal neurons in the barrel cortex, where they avoid the induction of spike-timing-dependent plasticity [188]. However, the BK–NMDAR complex is not observed in all basal dendrites from cortical neurons, where coupling between SK channels and NMDARs to regulate dendritic excitability has also been described [185]. Interestingly, BK-mediated regulation of dendritic excitability in layer 5 neocortical neurons is impaired in mice lacking FMRP [151], thereby suggesting that BK channels might play a role in the pathophysiology of mental deficiency.

BK channels regulate synaptic transmission: BK channels also appear to be essential regulators of neurotransmitter release when expressed at synaptic terminals within different brain circuits [14,16]. Their localization in the active zone appears to be regulated by different synaptic proteins, including RIM-binding proteins [189], synapsin [190], α-catulin [191], and dystrobrevin [191,192]. In the brain, the function of presynaptic BK channels in regulating neurotransmitter release may vary from synapse to synapse [23,24]. For example, BK channels regulate excitatory glutamate-release probability, an effect associated with broadening a presynaptic action potential at CA3–CA3 connections [24]. In contrast, at Schaffer collaterals to CA1 synapses, BK channels contribute to transmitter release only after action potential broadening with 4-aminopyridine, and thus, it has been suggested that BK channels act as 'emergency brakes' to exert a protective effect against synaptic hyperactivity [23]. A similar effect was observed at glutamatergic mossy fiber

boutons in rat hippocampal slices, where the contribution of BK channels to presynaptic action potential repolarization was not observed under basal conditions due to the presence of a subtype of fast-activating Kv3 channels [164]. Moreover, evidence suggests that postsynaptic BK channels in mature dentate granule cells [27] and thalamocortical circuits [112], could also regulate synaptic transmission via NMDAR-mediated channel activation. Interestingly, NMDARs could be localized at some presynaptic terminals, where their activation regulates transmitter release and plasticity [193–195]. Whether a similar BK–NMDA complex is present at presynaptic terminals, thereby regulating transmitter release, remains unknown.

BK-mediated control of synaptic transmission also has been described in rod photoreceptors in the salamander retina [29], and in the brainstem, where they regulate paired-pulse ratio and depression induced by trains of high-frequency stimulation [129]. Although a preferential control exerted by BK channels on excitatory versus inhibitory synapses has been suggested [196,197], it has become clear that BK channels could also control GABA release in different neuronal circuits. For example, in the retina [22] BK channels contribute to GABA release from A17 amacrine cells. In the cortex BK control GABA release from fast-spiking interneurons to II/III layer pyramidal neurons [21] and at GABAergic synapses in the central amygdala [12]. Likewise, BK channels regulate inhibitory glycine release in the spinal cord [198] and acetylcholine release from efferent terminals from the medial olivocochlear system to inner hair cells [199]. These results suggest that by regulating excitatory and inhibitory transmitter release, BK channels might contribute to the excitatory–inhibitory balance necessary for normal brain function. Consistent with this idea, it has been observed that cereblon, a protein related to intellectual disability, downregulates BK channel activity at hippocampal CA3 terminals affecting paired-pulse ratio and short-term plasticity, but not long-term plasticity [200].

Glial BK channels: In addition to being present in neurons, BK channels are also localized in astrocytes [201], where their activation reportedly modulates blood pressure [202,203] and generates vasodilation [204]. Interestingly, astrocytic BK channels mainly express the β4 subunit during neonatal development [12,205], thereby regulating voltage gradients and K^+ homeostasis [12], but their contribution to regulating synaptic function remains unclear. In glioblastoma, the most invasive and aggressive primary brain tumor, astrocytic BK channels are likely upregulated to induce water loss and reduce cellular volume [206]. More recently, an interaction between BK channels and the GABA transporter type 3 (GAT3) has also been reported, suggesting that BK channels could regulate GABA homeostasis and signaling by regulating astrocyte function [207]. However, the role of astrocyte BK channels in regulating glutamatergic and GABAergic synaptic function remains unknown.

BK channels are also localized in the spinal cord [208] and cortical microglia [209]. In the spinal cord, BK can induce microglial hyperactivity related to neuropathic pain [210] and potentiate spinal synapses in lamina I spinal neurons [8]. In the brain, evidence suggests that microglial BK channels might participate in BDNF release and induce microglial phagocytosis [209]. BK channels have also been identified in microglial cells of the hippocampus [211,212], which, unlike neuronal BK, might not be developmentally regulated [213]. Whether microglial BK channels may contribute to regulate neuronal excitability and synaptic transmission within selective brain circuits remains unknown.

Lastly, BK channels also seem to be present in oligodendrocyte precursors [214,215] and to a lesser extent in mature oligodendrocytes [214]. In multiple sclerosis lesions, the β4-subunit coding gene KCNMB4, is upregulated in oligodendrocytes [216], but its role is largely unknown.

Could BK channels be activated by endogenous ligands to regulate neuronal function? In addition to being activated by voltage and Ca^{2+}, increasing evidence suggests that different molecules can directly bind to BK channels to regulate their function. For instance, 17β-estradiol activates BK channels via a process that requires the presence of the β1 subunit [217]. Moreover, β4 confers BK channel sensitivity to corticosterone [218].

While evidence suggests that estradiol could regulate hippocampal excitability [219] and regulate glutamatergic synaptic transmission and plasticity in the hippocampus [220] and primary auditory cortex [221], whether these effects are directly mediated by targeting BK channels remains unclear.

Different lipid ligands interact directly with BK channels. For example, the omega-3 fatty acid DHA activates β1 and β4, with minimal effect on β2-containing BK channels [222]. Similarly, arachidonic acid (AA) increases BK channel currents in the presence of β2 subunits [223] and AA metabolites produced by a COX-mediated pathway are responsible for BK channel activation in microglia [8]. In vascular tissues, lipoxygenase (LOX)-metabolites have also been shown to activate BK [224]. In particular, BK channels from coronary artery smooth muscle, which contains β1 and β4 subunits, are activated by AA-lipoxygenase metabolites [225].

The endocannabinoid anandamide and its stable analog, methanandamide, also activate BK currents [226,227]. Moreover, a direct interaction between cannabinoid signaling and the BK channel appears to be involved in the effect of cannabinoids suppressing peripherical firing in injured fibers [228]. However, it is unknown whether endocannabinoids can regulate brain function by targeting BK channels.

7. BK Channel Dysfunction in Neurological Disorders

Given the critical role of BK channels in regulating neuronal excitability and synaptic function, it is not surprising that dysfunction of BK channels has been implicated in several neurological disorders. These include epilepsy, fragile X syndrome, mental retardation, autism, movement disorders, and chronic pain [229]. The use of BK channels in animal models of BK loss-of-function (LOF) and gain-of-function (GOF) mutants has increased our current understanding of the role of BK channels in the etiology of these disturbances. For example, GOF mutations are more common than LOF alleles for patients with paroxysmal non-kinesigenic dyskinesia (PNKD), while non-PKND movement disorders were observed in LOF mutations [230]. In a GOF knock-in murine model carrying a human BK-D434G mutation, mice showed increased susceptibility to generalized seizures and motor deficits related to hyperexcitability in cortical pyramidal and cerebellar Purkinje neurons. Importantly, blocking BK channels with paxilline suppressed seizures, motor disturbances, and neuronal hyperexcitability [155]. Similarly, a D434G mutation that produces an increase in Ca^{2+} sensitivity that potentiates BK channel activity [231] was described in individuals affected by epileptic seizures and/or PNKD [232]. Moreover, a rare disease called KCNMA1-linked channelopathy, is also characterized by seizures and abnormal movements associated with the clinical detection of a KCNMA1 variant [232]. Another mutation, the N995S variant, is present in individuals with epilepsy but not PNKD. Such a mutation in the RCK2 domain increases BK channel currents by increasing voltage sensitivity but does not affect Ca^{2+}-dependent activation. In BK-N995S/β4 channels, the effect of the mutation is slightly more pronounced [233]. However, in a mouse model with the N995S mutation, PNKD-like symptoms could appear after stress exposure [232].

We recall here that targeted deletion of the *KCNMB4* gene coding for β4 subunits narrows action potentials and increases firing in dentate granule cells of the hippocampus, possibly leading to an enhancement of transmitter release and temporal lobe seizures [72]. Consistent with the involvement of the β4 subunit in epilepsy, pilocarpine-induced seizures generated a decrease in β4 subunits in dentate gyrus granular cells and a reduction in type II BK channels [234]. While β4 subunits seem to play an important role in epilepsy, a mutation in the gene encoding the accessory β3 subunits (KCNMB3b β3b-truncation) have also been frequently observed in patients affected by idiopathic generalized epilepsy [235].

Functional alterations of BK channel expression are also linked to neuropathic pain. A downregulation of BK channels in dorsal root ganglions and the spinal dorsal horn is accompanied by neuropathic pain [236–238]. Nerve injury promotes an increase in N-type Ca^{2+} channels in the spinal dorsal horn mediated by an upregulation of Cav2δ subunits, increasing pain signaling. Expressing the BK channel N-terminus, a domain

that binds the Cav2δ subunit, promotes a reduction in the expression of N-type Ca^{2+} channels and analgesia [239]. Additionally, the pharmacological blockade of spinal BK channels with iberiotoxin produces mechanical hyperalgesia. In contrast, activation of the BK channel reduces tactile allodynia and mechanical and thermal hyperalgesia, in nerve-ligated rats [236]. Similarly, decreasing spinal β3 subunit expression reportedly attenuated neuropathic pain produced by nerve injury in mice [240], further supporting a role for BK channels in regulating pain.

BK channels are also involved in motor and cognitive diseases. For instance, in homozygous mice lacking α subunits, muscular tremors, muscular weakness, and gait disturbances have been reported. However, in an open field test, these animal models showed normal distance for locomotor behavior. In addition, these mice also display deficits in learning, with a delay in acquiring a new task but not in memory once the task was learned [241]. Similarly, a mutation (BKG354S) in the α subunit has recently been reported in a child with congenital and progressive cerebellar ataxia with cognitive impairment. This mutation dramatically reduced single-channel conductance and ion selectivity and reduced neurite outgrowth, cell viability, and mitochondrial content [242].

Besides humans, GOF mutations are also present in *Drosophila.* There, the SLO E366G mutation (equivalent to the human mutation D434G) generates motor disturbances in both larvae and adult stages [243]. In *C.elegans*, deleting the Shank gene Shn-1, a synaptic scaffolding protein related to autism, produces a decrease in BK channel currents and clustering at muscles and neurons [244]. Interestingly, BK channels may play a role in the physiopathology of fragile X syndrome [245] as accessory β4 subunits interact with FMRP proteins, whose loss causes the fragile X syndrome, characterized by intellectual disabilities associated with language deficits, hyperactivity, autistic behavior, and seizures. In the absence of β4 subunits, FMRP decrease channel activation and deactivation rates, but in the presence of β4, FMRP increase channel opening [81]. BK channel agonists have a major impact on rescuing social and cognitive impairments [246]. However, the diversity of BK channel expression within different neuronal populations and brain circuits and the poor selectivity of drugs, suggest that one should take the use of these compounds in clinical practice with caution.

A role for BK channels in modulating learning and memory processes also has been suggested [160,247–249]. For example, if a methyl-donor-rich diet is supplied to mice before mating, the offspring show disturbances in hippocampus-related memory tasks and long-term potentiation of synaptic transmission related to decreased β2 subunit expression in the hippocampus [250]. Additionally, anxiety and cognitive disturbances induced by thalidomide were correlated to increased BK channel activity. These alterations can be rescued by the BK channel blocker paxilline [251]. Similarly, BK channel currents are reduced in pyramidal neurons of the anterior cingulate cortex in a mechanical allodynia model generating anxiety behaviors in mice. Upregulated expression of β4 subunits in presynaptic and postsynaptic domains and increased neuronal excitability and presynaptic neurotransmitter release accompanied this phenomenon. BK channel activation with NS1619 reversed anxiety-like behaviors and the mechanical pain threshold [73]. Last but not least, a genome-wide association study reported that a single-nucleotide polymorphism (SNP) in the gene encoding α subunits (*KCNMA1*, rs16934131) was associated with late-onset Alzheimer's disease (AD) risk in humans [252].

On the other hand, an SNP in the gene encoding β2 (*KCNMB2*, rs9637454) was strongly associated with hippocampal sclerosis, a comorbid neuropathological feature of AD [253]. While the functional consequence of these point mutations is unknown, rodent AD models have shed some light on how BK channels may contribute to AD pathogenesis. For example, in TgCRND8 mice; a mouse model for AD which overexpresses the amyloid precursor protein due to containing a double human amyloid precursor protein mutation; a decreased basal transmission associated with a reduced decay of afferent volleys has been reported. This difference was recovered when blockers for BK channels were present [254]. Moreover, intracellular injection of amyloid-β1–42 (Aβ1–42) peptides into neocortical pyramidal cells

suppresses BK channel activity, which broadens evoked AP spike width and indirectly enhances Ca^{2+} influx [255]. Similarly, Ab42 oligomers, stimulate spontaneous transient Ca^{2+} release from RyRs. RyRs activate presynaptic BK channels and reduce AMPA-mediated neurotransmission in hippocampal neurons [256]. Conversely, in the triple transgenic AD mouse model 3xTg, increased basal transmission and pyramidal excitability and decreased synaptic plasticity at the hippocampal CA1 area were related to a hypofunction of BK channels. 3xTg also displayed poor performance in non-spatial and spatial memory tasks, a dysfunction that was improved when a BK channel activator was delivered through ventricular injection [257]. While this evidence suggests a potential role of BK channels in the pathophysiology of AD, a direct link between Aβ42 oligomers and BK channel activation at the early stages of AD remains to be identified.

8. Conclusions and Future Directions

Increasing evidence indicates that, in addition to its well-known role in regulating neuronal excitability, BK channels also regulate dendritic excitability and synaptic transmission in different brain circuits. Their presynaptic and postsynaptic expression within a specific synapse suggests they are also well positioned to regulate synaptic function of excitatory and inhibitory neurons. This effect may vary from synapse to synapse (i.e., either increase or decrease) and might also regulate synaptic plasticity. While indirect evidence suggests that BK channels can regulate long-term potentiation and depression, whether BK channels play a pivotal role in the induction or expression of a different form of synaptic plasticity needs further investigation. Similarly, their expression in glial cells has yet to be entirely understood. For instance, the role of BK channels regulating gliotransmission, thereby modulating synaptic brain function, remains largely unexplored. Future work will expand our understanding of the role of glial BK channels, particularly their contribution to regulating GABA homeostasis and signaling, as they have been reported to directly interact with the GABA transporter in astrocytes [207]. Notably, lipid molecules, including AA derivates and endocannabinoids, are known to stimulate BK channels in heterologous and peripheral systems. However, whether these lipids regulate brain function and behavior in a BK-dependent manner remains unknown. Given the ubiquitous expression of BK channels throughout the brain, it is not surprising that they have been implicated in several neurological disorders, such as epilepsy, mental retardation, autism, AD, anxiety, movement disorders, and chronic pain [229]. Using LOF or GOF animal models has increased our current understanding of the role of BK channels in the etiology of these disturbances. However, further work is required for better development of novel therapeutic strategies and interventions that may ameliorate these devastating disorders.

Author Contributions: C.A.-G., I.S. and R.A.-S., original draft preparation, Tables and Figures. A.E.C. and R.L. guided the research and wrote the paper. All authors have read and agreed to the published version of the manuscript.

Funding: This work was supported by the Chilean government through FONDECYT Regular #1201848 (A.E.C.), #1190203 (R.L.), and by ANID Millennium Science Initiative Program (ACE210014 to A.E.C. and R.L.). C.A.G. and R.A.S. were supported by a PhD fellowship from ANID #21201603 (C.A.G.) and #21221040 (R.A.S.). We apologize to those authors whose work we could not cite due to space limitations.

Conflicts of Interest: The authors declare no conflict of interest.

References

1. Pyott, S.; Duncan, R. BK Channels in the Vertebrate Inner Ear. *Int. Rev. Neurobiol.* **2016**, *128*, 369–399. [CrossRef] [PubMed]
2. Krishnamoorthy-Natarajan, G.; Koide, M. BK Channels in the Vascular System. *Int. Rev. Neurobiol.* **2016**, *128*, 401–438. [CrossRef] [PubMed]
3. Harvey, J.R.M.; Plante, A.E.; Meredith, A.L. Ion Channels Controlling Circadian Rhythms in Suprachiasmatic Nucleus Excitability. *Physiol. Rev.* **2020**, *100*, 1415–1454. [CrossRef]

4. Knaus, H.; Schwarzer, C.; Koch, R.; Eberhart, A.; Kaczorowski, G.; Glossmann, H.; Wunder, F.; Pongs, O.; Garcia, M.; Sperk, G. Distribution of high-conductance Ca(2+)-activated K+ channels in rat brain: Targeting to axons and nerve terminals. *J. Neurosci.* **1996**, *16*, 955–963. [CrossRef] [PubMed]
5. Sausbier, U.; Sausbier, M.; Sailer, C.A.; Arntz, C.; Knaus, H.-G.; Neuhuber, W.; Ruth, P. Ca^{2+}-activated K+ channels of the BK-type in the mouse brain. *Histochem. Cell Biol.* **2006**, *125*, 725–741. [CrossRef]
6. Wanner, S.G.; Koch, R.O.; Koschak, A.; Trieb, M.; Garcia, M.L.; Kaczorowski, G.J.; Knaus, H.-G. High-Conductance Calcium-Activated Potassium Channels in Rat Brain: Pharmacology, Distribution, and Subunit Composition. *Biochemistry* **1999**, *38*, 5392–5400. [CrossRef]
7. González-Sanabria, N.; Echeverría, F.; Segura, I.; Alvarado-Sánchez, R.; Latorre, R. BK in Double-Membrane Organelles: A Biophysical, Pharmacological, and Functional Survey. *Front. Physiol.* **2021**, *12*, 761474. [CrossRef]
8. Hayashi, Y.; Morinaga, S.; Zhang, J.; Satoh, Y.; Meredith, A.; Nakata, T.; Wu, Z.; Kohsaka, S.; Inoue, K.; Nakanishi, H. BK channels in microglia are required for morphine-induced hyperalgesia. *Nat. Commun.* **2016**, *7*, 11697. [CrossRef]
9. Kyle, B.D.; Braun, A.P. The regulation of BK channel activity by pre- and post-translational modifications. *Front. Physiol.* **2014**, *5*, 316. [CrossRef]
10. Latorre, R.; Castillo, K.; Carrasquel-Ursulaez, W.; Sepulveda, R.V.; Gonzalez-Nilo, F.; Gonzalez, C.; Alvarez, O. Molecular Determinants of BK Channel Functional Diversity and Functioning. *Physiol. Rev.* **2017**, *97*, 39–87. [CrossRef]
11. Li, B.; Gao, T.-M. Functional Role of Mitochondrial and Nuclear BK Channels. *Int. Rev. Neurobiol.* **2016**, *128*, 163–191. [CrossRef]
12. Seidel, K.N.; Derst, C.; Salzmann, M.; Höltje, M.; Priller, J.; Markgraf, R.; Heinemann, S.H.; Heilmann, H.; Skatchkov, S.N.; Eaton, M.J.; et al. Expression of the voltage- and Ca2+-dependent BK potassium channel subunits BKβ1 and BKβ4 in rodent astrocytes. *Glia* **2011**, *59*, 893–902. [CrossRef]
13. Seifert, G.; Henneberger, C.; Steinhäuser, C. Diversity of astrocyte potassium channels: An update. *Brain Res. Bull.* **2018**, *136*, 26–36. [CrossRef]
14. Contet, C.; Goulding, S.P.; Kuljis, D.A.; Barth, A.L. BK channel sin the CNS. *Int. Rev. Neurobiol.* **2016**, *128*, 281–342.
15. Deng, P.-Y.; Rotman, Z.; Blundon, J.A.; Cho, Y.; Cui, J.; Cavalli, V.; Zakharenko, S.; Klyachko, V.A. FMRP Regulates Neurotransmitter Release and Synaptic Information Transmission by Modulating Action Potential Duration via BK Channels. *Neuron* **2013**, *77*, 696–711. [CrossRef]
16. Griguoli, M.; Sgritta, M.; Cherubini, E. Presynaptic BK channels control transmitter release: Physiological relevance and potential therapeutic implications. *J. Physiol.* **2016**, *594*, 3489–3500. [CrossRef]
17. Sausbier, M.; Hu, H.; Arntz, C.; Feil, S.; Kamm, S.; Adelsberger, H.; Sausbier, U.; Sailer, C.A.; Feil, R.; Hofmann, F.; et al. Cerebellar ataxia and Purkinje cell dysfunction caused by Ca^{2+}-activated K+channel deficiency. *Proc. Natl. Acad. Sci. USA* **2004**, *101*, 9474–9478. [CrossRef]
18. Bock, T.; Stuart, G.J. The Impact of BK Channels on Cellular Excitability Depends on their Subcellular Location. *Front. Cell. Neurosci.* **2016**, *10*, 206. [CrossRef]
19. Storm, J.F. Understanding the Brain Through the Hippocampus the Hippocampal Region as a Model for Studying Brain Structure and Function. *Prog. Brain Res.* **1990**, *83*, 161–187.
20. Bielefeldt, K.; Jackson, M.B. A calcium-activated potassium channel causes frequency-dependent action-potential failures in a mammalian nerve terminal. *J. Neurophysiol.* **1993**, *70*, 284–298. [CrossRef]
21. Goldberg, J.A.; Wilson, C.J. Control of spontaneous firing patterns by the selective coupling of calcium currents to calcium-activated potassium currents in striatal cholinergic interneurons. *J. Neurosci.* **2005**, *25*, 10230–10238. [CrossRef]
22. Grimes, W.N.; Li, W.; Chávez, A.E.; Diamond, J.S. BK channels modulate pre- and postsynaptic signaling at reciprocal synapses in retina. *Nat. Neurosci.* **2009**, *12*, 585–592. [CrossRef] [PubMed]
23. Hu, H.; Shao, L.-R.; Chavoshy, S.; Gu, N.; Trieb, M.; Behrens, R.; Laake, P.; Pongs, O.; Knaus, H.G.; Ottersen, O.P.; et al. Presynaptic Ca^{2+}-Activated K^{+}Channels in Glutamatergic Hippocampal Terminals and Their Role in Spike Repolarization and Regulation of Transmitter Release. *J. Neurosci.* **2001**, *21*, 9585–9597. [CrossRef] [PubMed]
24. Raffaelli, G.; Saviane, C.; Mohajerani, M.H.; Pedarzani, P.; Cherubini, E. BK potassium channels control transmitter release at CA3-CA3 synapses in the rat hippocampus. *J. Physiol.* **2004**, *557*, 147–157. [CrossRef]
25. Tazerart, S.; Blanchard, M.G.; Miranda-Rottmann, S.; Mitchell, D.E.; Pina, B.N.; Thomas, C.I.; Kamasawa, N.; Araya, R. Selective activation of BK channels in small-headed dendritic spines suppresses excitatory postsynaptic potentials. *J. Physiol.* **2022**, *600*, 2165–2187. [CrossRef] [PubMed]
26. Guo, Y.-Y.; Liu, S.-B.; Cui, G.-B.; Ma, L.; Feng, B.; Xing, J.-H.; Yang, Q.; Li, X.-Q.; Wu, Y.-M.; Xiong, L.-Z.; et al. Acute stress induces down-regulation of large-conductance Ca^{2+}-activated potassium channels in the lateral amygdala. *J. Physiol.* **2012**, *590*, 875–886. [CrossRef]
27. Zhang, J.; Guan, X.; Li, Q.; Meredith, A.L.; Pan, H.-L.; Yan, J. Glutamate-activated BK channel complexes formed with NMDA receptors. *Proc. Natl. Acad. Sci. USA* **2018**, *115*, E9006–E9014. [CrossRef]
28. Cavaccini, A.; Gritti, M.; Giorgi, A.; Locarno, A.; Heck, N.; Migliarini, S.; Bertero, A.; Mereu, M.; Margiani, G.; Trusel, M.; et al. Serotonergic Signaling Controls Input-Specific Synaptic Plasticity at Striatal Circuits. *Neuron* **2018**, *98*, 801–816.e7. [CrossRef]
29. Xu, J.W.; Slaughter, M.M. Large-Conductance Calcium-Activated Potassium Channels Facilitate Transmitter Release in Salamander Rod Synapse. *J. Neurosci.* **2005**, *25*, 7660–7668. [CrossRef]

30. Eisenman, G.; Latorre, R.; Miller, C. Multi-ion conduction and selectivity in the high-conductance Ca++-activated K+ channel from skeletal muscle. *Biophys. J.* **1986**, *50*, 1025–1034. [CrossRef]
31. Latorre, R.; Miller, C. Conduction and selectivity in potassium channels. *J. Membr. Biol.* **1983**, *71*, 11–30. [CrossRef]
32. Yellen, G. Ionic permeation and blockade in Ca2+-activated K+ channels of bovine chromaffin cells. *J. Gen. Physiol.* **1984**, *84*, 157–186. [CrossRef]
33. Adelman, J.P.; Shen, K.-Z.; Kavanaugh, M.P.; Warren, R.A.; Wu, Y.-N.; Lagrutta, A.; Bond, C.T.; North, R.A. Calcium-activated potassium channels expressed from cloned complementary DNAs. *Neuron* **1992**, *9*, 209–216. [CrossRef]
34. Butler, A.; Tsunoda, S.; McCobb, D.P.; Wei, A.; Salkoff, L. mSlo, a complex mouse gene encoding "maxi" calcium-activated potassium channels. *Science* **1993**, *261*, 221–224. [CrossRef]
35. Meera, P.; Wallner, M.; Song, M.; Toro, L. Large conductance voltage- and calcium-dependent K+ channel, a distinct member of voltage-dependent ion channels with seven N-terminal transmembrane segments (SO-S6), an extracellular N terminus, and an intracellular (S9-S10) C terminus. *Proc. Natl. Acad. Sci. USA* **1997**, *94*, 14066–14071. [CrossRef]
36. Bao, L.; Rapin, A.M.; Holmstrand, E.C.; Cox, D.H. Elimination of the BKCa Channel's High-Affinity Ca2+ Sensitivity. *J. Gen. Physiol.* **2002**, *120*, 173–189. [CrossRef]
37. Salkoff, L.; Butler, A.; Ferreira, G.; Santi, C.; Wei, A. High-conductance potassium channels of the SLO family. *Nat. Rev. Neurosci.* **2006**, *7*, 921–931. [CrossRef]
38. Tao, X.; Hite, R.K.; MacKinnon, R. Cryo-EM structure of the open high-conductance Ca^{2+}-activated K+ channel. *Nature* **2016**, *541*, 46–51. [CrossRef]
39. Xia, X.-M.; Zeng, X.; Lingle, C.J. Multiple regulatory sites in large-conductance calcium-activated potassium channels. *Nature* **2002**, *418*, 880–884. [CrossRef]
40. McManus, O.B.; Blatz, A.L.; Magleby, K.L. Inverse relationship of the durations of adjacent open and shut intervals for Cl and K channels. *Nature* **1985**, *317*, 625–627. [CrossRef]
41. Pallotta, B.S. Calcium-activated potassium channels in rat muscle inactivate from a short-duration open state. *J. Physiol.* **1985**, *363*, 501–516. [CrossRef] [PubMed]
42. Rothberg, B.S.; Magleby, K.L. Voltage and Ca2+ Activation of Single Large-Conductance Ca2+-Activated K+ Channels Described by a Two-Tiered Allosteric Gating Mechanism. *J. Gen. Physiol.* **2000**, *116*, 75–100. [CrossRef] [PubMed]
43. Horrigan, F.T.; Aldrich, R.W. Coupling between Voltage Sensor Activation, Ca2+ Binding and Channel Opening in Large Conductance (BK) Potassium Channels. *J. Gen. Physiol.* **2002**, *120*, 267–305. [CrossRef] [PubMed]
44. Carrasquel-Ursulaez, W.; Contreras, G.F.; Sepúlveda, R.V.; Aguayo, D.; González-Nilo, F.; González, C.; Latorre, R. Hydrophobic interaction between contiguous residues in the S6 transmembrane segment acts as a stimuli integration node in the BK channel. *J. Gen. Physiol.* **2014**, *145*, 61–74. [CrossRef]
45. Lorenzo-Ceballos, Y.; Carrasquel-Ursulaez, W.; Castillo, K.; Alvarez, O.; Latorre, R. Calcium-driven regulation of voltagesensing-domains in BK channels. *Elife* **2019**, *8*, 1–24. [CrossRef]
46. Hite, R.K.; Tao, X.; MacKinnon, R. Structural basis for gating the high-conductance Ca2+-activated K+ channel. *Nature* **2016**, *541*, 52–57. [CrossRef]
47. Ma, Z.; Lou, X.J.; Horrigan, F.T. Role of Charged Residues in the S1–S4 Voltage Sensor of BK Channels. *J. Gen. Physiol.* **2006**, *127*, 309–328. [CrossRef]
48. Carrasquel-Ursulaez, W.; Segura, I.; Díaz-Franulic, I.; Echeverría, F.; Lorenzo-Ceballos, Y.; Espinoza, N.; Rojas, M.; Garate, J.A.; Perozo, E.; Alvarez, O. Mechanism of voltage sensing in Ca^{2+}- and voltage-activated K+ (BK) channels. *Proc. Natl. Acad. Sci. USA* **2022**, *119*, 1–11. [CrossRef]
49. Zeng, X.-H.; Xia, X.-M.; Lingle, C.J. Divalent Cation Sensitivity of BK Channel Activation Supports the Existence of Three Distinct Binding Sites. *J. Gen. Physiol.* **2005**, *125*, 273–286. [CrossRef]
50. Zhou, Y.; Zeng, X.-H.; Lingle, C.J. Barium ions selectively activate BK channels via the Ca^{2+} -bowl site. *Proc. Natl. Acad. Sci. USA* **2012**, *109*, 11413–11418. [CrossRef]
51. Lee, C.-H.; MacKinnon, R. Structures of the Human HCN1 Hyperpolarization-Activated Channel. *Cell* **2017**, *168*, 111–120.e11. [CrossRef]
52. Wang, W.; MacKinnon, R. Cryo-EM Structure of the Open Human Ether-à-go-go -Related K + Channel hERG. *Cell* **2017**, *169*, 422–430.e10. [CrossRef]
53. Tang, Q.-Y.; Zeng, X.-H.; Lingle, C.J. Closed-channel block of BK potassium channels by bbTBA requires partial activation. *J. Gen. Physiol.* **2009**, *134*, 409–436. [CrossRef]
54. Thompson, J.; Begenisich, T. Selectivity filter gating in large-conductance Ca2+-activated K+ channels. *J. Gen. Physiol.* **2012**, *139*, 235–244. [CrossRef]
55. Wilkens, C.M.; Aldrich, R.W. State-independent Block of BK Channels by an Intracellular Quaternary Ammonium. *J. Gen. Physiol.* **2006**, *128*, 347–364. [CrossRef]
56. Jia, Z.; Yazdani, M.; Zhang, G.; Cui, J.; Chen, J. Hydrophobic gating in BK channels. *Nat. Commun.* **2018**, *9*, 3408. [CrossRef]
57. Torres, Y.P.; Granados, S.T.; Latorre, R. Pharmacological consequences of the coexpression of BK channel α and auxiliary β subunits. *Front Physiol.* **2014**, *5*, 383. [CrossRef]
58. Orio, P.; Rojas, P.; Ferreira, G.; Latorre, R. New Disguises for an Old Channel: MaxiK Channel β-Subunits. *Physiology* **2002**, *17*, 156–161. [CrossRef]

59. Zhou, Y.; Lingle, C.J. Paxilline inhibits BK channels by an almost exclusively closed-channel block mechanism. *J. Gen. Physiol.* **2014**, *144*, 415–440. [CrossRef]
60. Meera, P.; Wallner, M.; Toro, L. A neuronal β subunit (KCNMB4) makes the large conductance, voltage- and Ca^{2+} -activated K + channel resistant to charybdotoxin and iberiotoxin. *Proc. Natl. Acad. Sci. USA* **2000**, *97*, 5562–5567. [CrossRef]
61. Ha, T.S.; Heo, M.-S.; Park, C.-S. Functional Effects of Auxiliary β4-Subunit on Rat Large-Conductance Ca2+-Activated K+ Channel. *Biophys. J.* **2004**, *86*, 2871–2882. [CrossRef] [PubMed]
62. Wang, B.; Rothberg, B.S.; Brenner, R. Mechanism of β4 Subunit Modulation of BK Channels. *J. Gen. Physiol.* **2006**, *127*, 449–465. [CrossRef] [PubMed]
63. Jaffe, D.; Wang, B.; Brenner, R. Shaping of action potentials by type I and type II large-conductance Ca^{2+}-activated K+ channels. *Neuroscience* **2011**, *192*, 205–218. [CrossRef] [PubMed]
64. Wang, B.; Jaffe, D.B.; Brenner, R. Current understanding of iberiotoxin-resistant BK channels in the nervous system. *Front. Physiol.* **2014**, *5*, 382. [CrossRef]
65. Reinhart, P.H.; Chung, S.; Levitan, I.B. A family of calcium-dependent potassium channels from rat brain. *Neuron* **1989**, *2*, 1031–1041. [CrossRef]
66. Behrens, R.; Nolting, A.; Reimann, F.; Schwarz, M.; Waldschütz, R.; Pongs, O. hKCNMB3 and hKCNMB4, cloning and characterization of two members of the large-conductance calcium-activated potassium channel β subunit family. *FEBS Lett.* **2000**, *474*, 99–106. [CrossRef]
67. Lippiat, J.D.; Standen, N.B.; Harrow, I.D.; Phillips, S.C.; Davies, N.W. Properties of BKCa channels formed by bicistronic expression of hSloα and β1-4 subunits in HEK293 cells. *J. Membr. Biol.* **2003**, *192*, 141–148.
68. Gan, G.; Yi, H.; Chen, M.; Sun, L.; Li, W.; Wu, Y.; Ding, J. Structural Basis for Toxin Resistance of β4-Associated Calcium-activated Potassium (BK) Channels. *J. Biol. Chem.* **2008**, *283*, 24177–24184. [CrossRef]
69. Tao, X.; Mackinnon, R. Molecular structures of the human slo1 k+ channel in complex with b4. *Elife* **2019**, *8*, e51409. [CrossRef]
70. Candia, S.; Garcia, M.; Latorre, R. Mode of action of iberiotoxin, a potent blocker of the large conductance Ca(2+)-activated K+ channel. *Biophys. J.* **1992**, *63*, 583–590. [CrossRef]
71. Weiger, T.M.; Holmqvist, M.H.; Levitan, I.B.; Clark, F.T.; Sprague, S.; Huang, W.-J.; Ge, P.; Wang, C.; Lawson, D.; Jurman, M.E.; et al. A Novel Nervous System β Subunit that Downregulates Human Large Conductance Calcium-Dependent Potassium Channels. *J. Neurosci.* **2000**, *20*, 3563–3570. [CrossRef]
72. Brenner, R.; Chen, Q.H.; Vilaythong, A.; Toney, G.M.; Noebels, J.; Aldrich, R.W. BK channel β4 subunit reduces dentate gyrus excitability and protects against temporal lobe seizures. *Nat. Neurosci.* **2005**, *8*, 1752–1759. [CrossRef]
73. Zhao, H.; Xue, Q.; Li, C.; Wang, Q.; Han, S.; Zhou, Y.; Yang, T.; Xie, Y.; Fu, H.; Lu, C.; et al. Upregulation of Beta4 subunit of BKCa channels in the anterior cingulate cortex contributes to mechanical allodynia associated anxiety-like behaviors. *Mol. Brain* **2020**, *13*, 1–18. [CrossRef]
74. Piwonska, M.; Wilczek, E.; Szewczyk, A.; Wilczynski, G. Differential distribution of Ca2+-activated potassium channel β4 subunit in rat brain: Immunolocalization in neuronal mitochondria. *Neuroscience* **2008**, *153*, 446–460. [CrossRef]
75. Benton, M.D.; Lewis, A.H.; Bant, J.; Raman, I.M. Iberiotoxin-sensitive and -insensitive BK currents in Purkinje neuron somata. *J. Neurophysiol.* **2013**, *109*, 2528–2541. [CrossRef]
76. Jiang, Z.; Wallner, M.; Meera, P.; Toro, L. Human and Rodent MaxiK Channel β-Subunit Genes: Cloning and Characterization. *Genomics* **1999**, *55*, 57–67. [CrossRef]
77. Salzmann, M.; Seidel, K.N.; Bernard, R.; Prüss, H.; Veh, R.W.; Derst, C. BKβ1 Subunits Contribute to BK Channel Diversity in Rat Hypothalamic Neurons. *Cell. Mol. Neurobiol.* **2010**, *30*, 967–976. [CrossRef]
78. Tseng-Crank, J.; Godinot, N.; Johansen, T.E.; Ahring, P.K.; Strøbæk, D.; Mertz, R.; Foster, C.D.; Olesen, S.P.; Reinhart, P.H. Cloning, expression, and distribution of a Ca2+-activated K+ channel β-subunit from human brain. *Proc. Natl. Acad. Sci. USA* **1996**, *93*, 9200–9205. [CrossRef]
79. Wynne, P.M.; Puig, S.I.; Martin, G.E.; Treistman, S.N. Compartmentalized β subunit distribution determines characteristics and ethanol sensitivity of somatic, dendritic, and terminal large-conductance calcium-activated potassium channels in the rat central nervous system. *J. Pharmacol. Exp. Ther.* **2009**, *329*, 978–986. [CrossRef]
80. Deng, P.-Y.; Klyachko, V.A. Genetic upregulation of BK channel activity normalizes multiple synaptic and circuit defects in a mouse model of fragile X syndrome. *J. Physiol.* **2015**, *594*, 83–97. [CrossRef]
81. Kshatri, A.; Cerrada, A.; Gimeno, R.; Bartolomé-Martín, D.; Rojas, P.; Giraldez, T. Differential regulation of BK channels by fragile X mental retardation protein. *J. Gen. Physiol.* **2020**, *152*, e201912502. [CrossRef] [PubMed]
82. Pyott, S.; Glowatzki, E.; Trimmer, J.S.; Aldrich, R.W. Extrasynaptic Localization of Inactivating Calcium-Activated Potassium Channels in Mouse Inner Hair Cells. *J. Neurosci.* **2004**, *24*, 9469–9474. [CrossRef] [PubMed]
83. Faber, E.S.L.; Sah, P. Ca^{2+} -activated K+ (BK) channel inactivation contributes to spike broadening during repetitive firing in the rat lateral amygdala. *J Physiol.* **2003**, *552*, 483–497. [CrossRef] [PubMed]
84. Hicks, G.A.; Marrion, N.V. Ca^{2+}-dependent inactivation of large conductance Ca^{2+}-activated K+ (BK) channels in rat hippocampal neurones produced by pore block from an associated particle. *J. Physiol.* **1998**, *508*, 721–734. [CrossRef]
85. Li, W.; Gao, S.-B.; Lv, C.-X.; Wu, Y.; Guo, Z.-H.; Ding, J.-P.; Xu, T. Characterization of voltage-and Ca2+-activated K+ channels in rat dorsal root ganglion neurons. *J. Cell. Physiol.* **2007**, *212*, 348–357. [CrossRef]

86. Whitt, J.P.; Montgomery, J.R.; Meredith, A.L. BK channel inactivation gates daytime excitability in the circadian clock. *Nat. Commun.* **2016**, *7*, 10837. [CrossRef]
87. Meredith, A.L.; Wiler, S.W.; Miller, B.H.; Takahashi, J.S.; Fodor, A.A.; Ruby, N.F.; Aldrich, R.W. BK calcium-activated potassium channels regulate circadian behavioral rhythms and pacemaker output. *Nat. Neurosci.* **2006**, *9*, 1041–1049. [CrossRef]
88. Pitts, G.R.; Ohta, H.; McMahon, D.G. Daily rhythmicity of large-conductance Ca^{2+}-activated K+ currents in suprachiasmatic nucleus neurons. *Brain Res.* **2006**, *1071*, 54–62. [CrossRef]
89. Berkefeld, H.; Fakler, B.; Schulte, U. Ca^{2+}-activated K^+ channels: From protein complexes to function. *Physiol. Rev.* **2010**, *90*, 1437–1459. [CrossRef]
90. Shah, K.R.; Guan, X.; Yan, J. Structural and Functional Coupling of Calcium-Activated BK Channels and Calcium-Permeable Channels Within Nanodomain Signaling Complexes. *Front. Physiol.* **2022**, *12*, 2556. [CrossRef]
91. Sweet, T.B.; Cox, D.H. Measurements of the BK Ca channel's high-affinity Ca 2+ binding constants: Effects of membrane voltage. *J. Gen. Physiol.* **2008**, *132*, 491–505. [CrossRef]
92. Fakler, B.; Adelman, J.P. Control of KCa Channels by Calcium Nano/Microdomains. *Neuron* **2008**, *59*, 873–881. [CrossRef]
93. Naraghi, M.; Neher, E. Linearized Buffered Ca^{2+}Diffusion in Microdomains and Its Implications for Calculation of [Ca^{2+}] at the Mouth of a Calcium Channel. *J. Neurosci.* **1997**, *17*, 6961–6973. [CrossRef]
94. Bellono, N.W.; Leitch, D.B.; Julius, D. Molecular basis of ancestral vertebrate electroreception. *Nature* **2017**, *543*, 391–396. [CrossRef]
95. Berkefeld, H.; Fakler, B. Repolarizing Responses of BKCa-Cav Complexes Are Distinctly Shaped by Their Cav Subunits. *J. Neurosci.* **2008**, *28*, 8238–8245. [CrossRef]
96. Berkefeld, H.; Sailer, C.A.; Bildl, W.; Rohde, V.; Thumfart, J.O.; Eble, S.; Klugbauer, N.; Reisinger, E.; Bischofberger, J.; Oliver, D.; et al. BKCa-Cav channel complexes mediate rapid and localized Ca 2+-activated K+ signaling. *Science* **2006**, *314*, 615–620. [CrossRef]
97. Marrion, N.V.; Tavalin, S.J. Selective activation of Ca^{2+}-activated K^+ channels by co-localized Ca^{2+} channels in hippocampal neurons. *Nature* **1998**, *395*, 900–905. [CrossRef]
98. Rehak, R.; Bartoletti, T.M.; Engbers, J.D.T.; Berecki, G.; Turner, R.W.; Zamponi, G.W. Low Voltage Activation of KCa1.1 Current by Cav3-KCa1.1 Complexes. *PLoS ONE* **2013**, *8*, e61844. [CrossRef]
99. Müller, A.; Kukley, M.; Uebachs, M.; Beck, H.; Dietrich, D. Nanodomains of single Ca2+ channels contribute to action potential repolarization in cortical neurons. *J. Neurosci.* **2007**, *27*, 483–495. [CrossRef]
100. Gola, M.; Crest, M. Colocalization of active KCa channels and Ca^{2+} channels within Ca^{2+} Domains in helix neurons. *Neuron* **1993**, *10*, 689–699. [CrossRef]
101. Monreal, M.R.; Pérez, J.Q.; Escalera, M.P.; Lazalde, A.R.; Bonilla, M.E.P. Development of the L-type CaV/BK Complex Simulator (II): Estimation of the distance between the channels. *South Florida J. Dev.* **2021**, *2*, 1258–1265. [CrossRef]
102. Edgerton, J.R.; Reinhart, P.H. Distinct contributions of small and large conductance Ca2+- activated K+ channels to rat Purkinje neuron function. *J. Physiol.* **2003**, *548*, 53–69. [CrossRef] [PubMed]
103. Gutzmann, J.J.; Lin, L.; Hoffman, D.A. Functional Coupling of Cav2.3 and BK Potassium Channels Regulates Action Potential Repolarization and Short-Term Plasticity in the Mouse Hippocampus. *Front. Cell. Neurosci.* **2019**, *13*, 27. [CrossRef] [PubMed]
104. Vivas, O.; Moreno, C.M.; Santana, L.F.; Hille, B. Proximal clustering between BK and CaV1.3 channels promotes functional coupling and BK channel activation at low voltage. *Elife* **2017**, *6*, e28029. [CrossRef]
105. Smith, M.R.; Nelson, A.B.; du Lac, S. Regulation of Firing Response Gain by Calcium-Dependent Mechanisms in Vestibular Nucleus Neurons. *J. Neurophysiol.* **2002**, *87*, 2031–2042. [CrossRef]
106. Loane, D.J.; Hicks, G.A.; Perrino, B.A.; Marrion, N.V. Inhibition of BKCa channel activity by association with calcineurin in rat brain. *Eur. J. Neurosci.* **2006**, *24*, 433–441. [CrossRef]
107. Sun, X.; Gu, X.Q.; Haddad, G.G. Calcium Influx via L- and N-Type Calcium Channels Activates a Transient Large-Conductance Ca^{2+}-Activated K^+Current in Mouse Neocortical Pyramidal Neurons. *J. Neurosci.* **2003**, *23*, 3639–3648. [CrossRef]
108. Plante, A.E.; Whitt, J.P.; Meredith, A.L. BK channel activation by L-type Ca^{2+} channels $Ca_V1.2$ and $Ca_V1.3$ during the subthreshold phase of an action potential. *J. Neurophysiol.* **2021**, *126*, 427–439. [CrossRef]
109. Davies, P.J.; Ireland, D.R.; McLachlan, E.M. Sources of Ca^{2+} for different Ca^{2+}-activated K^+ conductances in neurones of the rat superior cervical ganglion. *J. Physiol.* **1996**, *495*, 353–366. [CrossRef]
110. Womack, M.D.; Chevez, C.; Khodakhah, K. Calcium-Activated Potassium Channels Are Selectively Coupled to P/Q-Type Calcium Channels in Cerebellar Purkinje Neurons. *J. Neurosci.* **2004**, *24*, 8818–8822. [CrossRef]
111. Isaacson, J.S.; Murphy, G. Glutamate-Mediated Extrasynaptic Inhibition: Direct Coupling of NMDA Receptors to Ca2+-Activated K+ Channels. *Neuron* **2001**, *31*, 1027–1034. [CrossRef]
112. Gómez, R.; Maglio, L.E.; Gonzalez-Hernandez, A.J.; Rivero-Pérez, B.; Bartolomé-Martín, D.; Giraldez, T. NMDA receptor–BK channel coupling regulates synaptic plasticity in the barrel cortex. *Proc. Natl. Acad. Sci. USA* **2021**, *118*, e2107026118. [CrossRef]
113. Irie, T.; Trussell, L.O. Double-Nanodomain Coupling of Calcium Channels, Ryanodine Receptors, and BK Channels Controls the Generation of Burst Firing. *Neuron* **2017**, *96*, 856–870.e4. [CrossRef]
114. Wang, B.; Bugay, V.; Ling, L.; Chuang, H.H.; Jaffe, D.B.; Brenner, R. Knockout of the BK β4-subunit promotes a functional coupling of BK channels and ryanodine receptors that mediate a fAHP-induced increase in excitability. *J. Neurophysiol.* **2016**, *116*, 456–465. [CrossRef]

115. Whitt, J.P.; McNally, B.A.; Meredith, A.L. Differential contribution of Ca2+ sources to day and night BK current activation in the circadian clock. *J. Gen. Physiol.* **2017**, *150*, 259–275. [CrossRef]
116. Wu, Y.; Liu, Y.; Hou, P.; Yan, Z.; Kong, W.; Liu, B.; Li, X.; Yao, J.; Zhang, Y.; Qin, F.; et al. TRPV1 Channels Are Functionally Coupled with BK(mSlo1) Channels in Rat Dorsal Root Ganglion (DRG) Neurons. *PLoS ONE* **2013**, *8*, e78203. [CrossRef]
117. Lin, M.T.; Hessinger, D.A.; Pearce, W.J.; Longo, L.D. Modulation of BK channel calcium affinity by differential phosphorylation in developing ovine basilar artery myocytes. *Am. J. Physiol. Circ. Physiol.* **2006**, *291*, H732–H740. [CrossRef]
118. Yan, J.; Olsen, J.V.; Park, K.-S.; Li, W.; Bildl, W.; Schulte, U.; Aldrich, R.W.; Fakler, B.; Trimmer, J.S. Profiling the Phospho-status of the BKCa Channel α Subunit in Rat Brain Reveals Unexpected Patterns and Complexity. *Mol. Cell. Proteom.* **2008**, *7*, 2188–2198. [CrossRef]
119. Wang, Z.-W. Regulation of Synaptic Transmission by Presynaptic CaMKII and BK Channels. *Mol. Neurobiol.* **2008**, *38*, 153–166. [CrossRef]
120. Wang, J.; Zhou, Y.; Wen, H.; Levitan, I.B. Simultaneous Binding of Two Protein Kinases to a Calcium-Dependent Potassium Channel. *J. Neurosci.* **1999**, *19*, RC4. [CrossRef]
121. Lin, M.T.; Longo, L.D.; Pearce, W.J.; Hessinger, D.A. Ca^{2+}-activated K^+ channel-associated phosphatase and kinase activities during development. *Am. J. Physiol.-Hear Circ. Physiol.* **2005**, *289*, 414–425. [CrossRef] [PubMed]
122. Shelley, C.; Whitt, J.P.; Montgomery, J.R.; Meredith, A.L. Phosphorylation of a constitutive serine inhibits BK channel variants containing the alternate exon "SRKR". *J. Gen. Physiol.* **2013**, *142*, 585–598. [CrossRef] [PubMed]
123. Jin, P.; Weiger, T.M.; Wu, Y.; Levitan, I.B. Phosphorylation-dependent Functional Coupling of hSlo Calcium-dependent Potassium Channel and Its hβ4 Subunit. *J. Biol. Chem.* **2002**, *277*, 10014–10020. [CrossRef] [PubMed]
124. Nelson, A.B.; Gittis, A.; du Lac, S. Decreases in CaMKII Activity Trigger Persistent Potentiation of Intrinsic Excitability in Spontaneously Firing Vestibular Nucleus Neurons. *Neuron* **2005**, *46*, 623–631. [CrossRef]
125. van Welie, I.; du Lac, S. Bidirectional control of BK channel open probability by CAMKII and PKC in medial vestibular nucleus neurons. *J. Neurophysiol.* **2011**, *105*, 1651–1659. [CrossRef]
126. Widmer, H.A.; Rowe, I.C.M.; Shipston, M.J.; D'Antona, G.; Pellegrino, M.A.; Adami, R.; Rossi, R.; Carlizzi, C.N.; Canepari, M.; Saltin, B.; et al. Conditional protein phosphorylation regulates BK channel activity in rat cerebellar Purkinje neurons. *J. Physiol.* **2003**, *552*, 379–391. [CrossRef]
127. Watanave, M.; Takahashi, N.; Hosoi, N.; Konno, A.; Yamamoto, H.; Yasui, H.; Kawachi, M.; Horii, T.; Matsuzaki, Y.; Hatada, I.; et al. Protein kinase Cγ in cerebellar Purkinje cells regulates Ca2+-activated large-conductance K+ channels and motor coordination. *Proc. Natl. Acad. Sci. USA* **2022**, *119*, 1–11. [CrossRef]
128. Liu, Q.; Chen, B.; Ge, Q.; Wang, Z.W. Presynaptic Ca^{2+}/calmodulin-dependent protein kinase II modulates neurotransmitter release by activating BK channels at Caenorhabditis elegans neuromuscular junction. *J. Neurosci.* **2007**, *27*, 10404–10413. [CrossRef]
129. Zaman, T.; De Oliveira, C.; Smoka, M.; Narla, C.; Poulter, M.O.; Schmid, S. BK Channels Mediate Synaptic Plasticity Underlying Habituation in Rats. *J. Neurosci.* **2017**, *37*, 4540–4551. [CrossRef]
130. Sansom, S.C.; Stockand, J.D.; Hall, D.; Williams, B. Regulation of Large Calcium-activated Potassium Channels by Protein Phosphatase 2A. *J. Biol. Chem.* **1997**, *272*, 9902–9906. [CrossRef]
131. Tian, L.; Knaus, H.-G.; Shipston, M. Glucocorticoid Regulation of Calcium-activated Potassium Channels Mediated by Serine/Threonine Protein Phosphatase. *J. Biol. Chem.* **1998**, *273*, 13531–13536. [CrossRef]
132. Zhou, X.-B.; Ruth, P.; Schlossmann, J.; Hofmann, F.; Korth, M. Protein Phosphatase 2A Is Essential for the Activation of Ca2+-activated K+ Currents by cGMP-dependent Protein Kinase in Tracheal Smooth Muscle and Chinese Hamster Ovary Cells. *J. Biol. Chem.* **1996**, *271*, 19760–19767. [CrossRef]
133. Petrik, D.; Wang, B.; Brenner, R. Modulation by the BK accessory β4 subunit of phosphorylation-dependent changes in excitability of dentate gyrus granule neurons. *Eur. J. Neurosci.* **2011**, *34*, 695–704. [CrossRef]
134. Ramírez-Latorre, J.A. Functional Upregulation of Ca2+ -Activated K+ Channels in the Development of Substantia Nigra Dopamine Neurons. *PLoS ONE* **2012**, *7*, e51610. [CrossRef]
135. Kang, J.; Huguenard, J.R.; Prince, D.A. Development of BK channels in neocortical pyramidal neurons. *J. Neurophysiol.* **1996**, *76*, 188–198. [CrossRef]
136. Kros, C.J.; Ruppersberg, J.P.; Rüsch, A. Expression of a potassium current in inner hair cells during development of hearing in mice. *Nature* **1998**, *394*, 281–284. [CrossRef]
137. Hunsberger, M.S.; Mynlieff, M. BK potassium currents contribute differently to action potential waveform and firing rate as rat hippocampal neurons mature in the first postnatal week. *J. Neurophysiol.* **2020**, *124*, 703–714. [CrossRef]
138. Niday, Z.; Bean, B.P. BK Channel Regulation of Afterpotentials and Burst Firing in Cerebellar Purkinje Neurons. *J. Neurosci.* **2021**, *41*, 2854–2869. [CrossRef]
139. Kaufmann, W.; Kasugai, Y.; Ferraguti, F.; Storm, J. Two distinct pools of large-conductance calcium-activated potassium channels in the somatic plasma membrane of central principal neurons. *Neuroscience* **2010**, *169*, 974–986. [CrossRef]
140. Womack, M.D.; Khodakhah, K. Characterization of large conductance Ca^{2+}-activated K^+ channels in cerebellar Purkinje neurons. *Eur. J. Neurosci.* **2002**, *16*, 1214–1222. [CrossRef]
141. Sánchez-Aguilera, A.; Monedero, G.; Colino, A.; Vicente-Torres, M. Development of Action Potential Waveform in Hippocampal CA1 Pyramidal Neurons. *Neuroscience* **2020**, *442*, 151–167. [CrossRef] [PubMed]

142. Gu, N.; Vervaeke, K.; Storm, J.F. BK potassium channels facilitate high-frequency firing and cause early spike frequency adaptation in rat CA1 hippocampal pyramidal cells. *J. Physiol.* **2007**, *580*, 859–882. [CrossRef] [PubMed]
143. Shao, L.R.; Halvorsrud, R.; Borg-Graham, L.; Storm, J.F. The role of BK-type Ca^{2+}-dependent K^+ channels in spike broadening during repetitive firing in rat hippocampal pyramidal cells. *J. Physiol.* **1999**, *521*, 135–146. [CrossRef] [PubMed]
144. Benhassine, N.; Berger, T. Large-conductance calcium-dependent potassium channels prevent dendritic excitability in neocortical pyramidal neurons. *Pflügers Arch.-Eur. J. Physiol.* **2008**, *457*, 1133–1145. [CrossRef]
145. Kurowski, P.; Grzelka, K.; Szulczyk, P. Ionic Mechanism Underlying Rebound Depolarization in Medial Prefrontal Cortex Pyramidal Neurons. *Front. Cell. Neurosci.* **2018**, *12*, 93. [CrossRef]
146. Galarraga, E.; Vilchis, C.; Tkatch, T.; Salgado, H.; Tecuapetla, F.; Perez-Rosello, T.; Perez-Garci, E.; Hernandez-Echeagaray, E.; Surmeier, D.; Bargas, J. Somatostatinergic modulation of firing pattern and calcium-activated potassium currents in medium spiny neostriatal neurons. *Neuroscience* **2007**, *146*, 537–554. [CrossRef]
147. Vilchis, C.; Bargas, J.; Ayala, G.; Galván, E.; Galarraga, E. Ca2+ channels that activate Ca^{2+}-dependent K^+ currents in neostriatal neurons. *Neuroscience* **1999**, *95*, 745–752. [CrossRef]
148. Wang, H.; Ardiles, A.O.; Yang, S.; Tran, T.; Posada-Duque, R.; Valdivia, G.; Baek, M.; Chuang, Y.-A.; Palacios, A.G.; Gallagher, M.; et al. Metabotropic Glutamate Receptors Induce a Form of LTP Controlled by Translation and Arc Signaling in the Hippocampus. *J. Neurosci.* **2016**, *36*, 1723–1729. [CrossRef]
149. Kohashi, T.; Carlson, B.A. A fast BK-type KCa current acts as a postsynaptic modulator of temporal selectivity for communication signals. *Front. Cell. Neurosci.* **2014**, *8*, 286. [CrossRef]
150. Klyachko, V.A.; Ahern, G.P.; Jackson, M.B. cGMP-mediated facilitation in nerve terminals by enhancement of the spike afterhyperpolarization. *Neuron* **2001**, *31*, 1015–1025. [CrossRef]
151. Zhang, Y.; Bonnan, A.; Bony, G.; Ferezou, I.; Pietropaolo, S.; Ginger, M.; Sans, N.; Rossier, J.; Oostra, B.; LeMasson, G.; et al. Dendritic channelopathies contribute to neocortical and sensory hyperexcitability in Fmr1-/y mice. *Nat. Neurosci.* **2014**, *17*, 1701–1709. [CrossRef]
152. Roshchin, M.V.; Matlashov, M.E.; Ierusalimsky, V.N.; Balaban, P.M.; Belousov, V.V.; Kemenes, G.; Staras, K.; Nikitin, E.S. A BK channel–mediated feedback pathway links single-synapse activity with action potential sharpening in repetitive firing. *Sci. Adv.* **2018**, *4*, 1–9. [CrossRef]
153. Książek, A.; Ładno, W.; Szulczyk, B.P.; Grzelka, K.; Szulczyk, P.J. Properties of BK-type Ca++-dependent K+ channel currents in medial prefrontal cortex pyramidal neurons in rats of different ages. *Front. Cell. Neurosci.* **2013**, *7*, 185. [CrossRef]
154. Benhassine, N.; Berger, T. Homogeneous distribution of large-conductance calcium-dependent potassium channels on soma and apical dendrite of rat neocortical layer 5 pyramidal neurons. *Eur. J. Neurosci.* **2005**, *21*, 914–926. [CrossRef]
155. Dong, P.; Zhang, Y.; Hunanyan, A.S.; Mikati, M.A.; Cui, J.; Yang, H. Neuronal mechanism of a BK channelopathy in absence epilepsy and dyskinesia. *Proc. Natl. Acad. Sci. USA* **2022**, *119*, e2200140119. [CrossRef]
156. Grewe, B.F.; Bonnan, A.; Frick, A. Back-propagation of physiological action potential output in dendrites of slender-tufted L5A pyramidal neurons. *Front. Cell. Neurosci.* **2010**, *4*, 13. [CrossRef]
157. Sailer, C.A.; Kaufmann, W.A.; Kogler, M.; Chen, L.; Sausbier, U.; Ottersen, O.P.; Ruth, P.; Shipston, M.J.; Knaus, H.-G. Immunolocalization of BK channels in hippocampal pyramidal neurons. *Eur. J. Neurosci.* **2006**, *24*, 442–454. [CrossRef]
158. Golding, N.L.; Jung, H.-Y.; Mickus, T.; Spruston, N. Dendritic Calcium Spike Initiation and Repolarization Are Controlled by Distinct Potassium Channel Subtypes in CA1 Pyramidal Neurons. *J. Neurosci.* **1999**, *19*, 8789–8798. [CrossRef]
159. Shanley, L.J.; Irving, A.J.; Rae, M.G.; Ashford, M.L.; Harvey, J. Leptin inhibits rat hippocampal neurons via activation of large conductance calcium-activated K+ channels. *Nat. Neurosci.* **2002**, *5*, 299–300. [CrossRef]
160. Springer, S.J.; Burkett, B.J.; Schrader, L.A. Modulation of BK channels contributes to activity-dependent increase of excitability through MTORC1 activity in CA1 pyramidal cells of mouse hippocampus. *Front. Cell. Neurosci.* **2015**, *8*, 451. [CrossRef]
161. Misonou, H.; Menegola, M.; Buchwalder, L.; Park, E.W.; Meredith, A.; Rhodes, K.J.; Aldrich, R.W.; Trimmer, J.S. Immunolocalization of the Ca^{2+}-activated K^+channel Slo1 in axons and nerve terminals of mammalian brain and cultured neurons. *J. Comp. Neurol.* **2006**, *496*, 289–302. [CrossRef] [PubMed]
162. Shruti, S.; Urban-Ciecko, J.; Fitzpatrick, J.A.; Brenner, R.; Bruchez, M.P.; Barth, A.L. The brain-specific beta4 subunit downregulates BK channel cell surface expression. *PLoS ONE* **2012**, *7*, e33429. [CrossRef]
163. Jalini, S.; Ye, H.; Tonkikh, A.A.; Charlton, M.P.; Carlen, P.L. Raised Intracellular Calcium Contributes to Ischemia-Induced Depression of Evoked Synaptic Transmission. *PLoS ONE* **2016**, *11*, e0148110. [CrossRef] [PubMed]
164. Alle, H.; Kubota, H.; Geiger, J.R.P. Sparse But Highly Efficient Kv3 Outpace BKCa Channels in Action Potential Repolarization at Hippocampal Mossy Fiber Boutons. *J. Neurosci.* **2011**, *31*, 8001–8012. [CrossRef]
165. Wang, D.; Wang, X.; Liu, P.; Jing, S.; Du, H.; Zhang, L.; Jia, F.; Li, A. Serotonergic afferents from the dorsal raphe decrease the excitability of pyramidal neurons in the anterior piriform cortex. *Proc. Natl. Acad. Sci. USA* **2020**, *117*, 3239–3247. [CrossRef]
166. Casale, A.E.; Foust, A.J.; Bal, T.; McCormick, D.A. Cortical Interneuron Subtypes Vary in Their Axonal Action Potential Properties. *J. Neurosci.* **2015**, *35*, 15555–15567. [CrossRef]
167. Ji, J.J.; Chen, L.; Duan, X.; Song, X.; Su, W.; Zhang, P.; Li, L.; Bai, S.; Sun, Y.; Inagaki, N. BK Channels Reveal Novel Phosphate Sensitivity in SNr Neurons. *PLoS ONE* **2012**, *7*, e52148. [CrossRef]
168. Authement, M.E.; Langlois, L.D.; Shepard, R.D.; Browne, C.A.; Lucki, I.; Kassis, H.; Nugent, F.S. A role for corticotropin-releasing factor signaling in the lateral habenula and its modulation by early-life stress. *Sci. Signal.* **2018**, *11*, eaan6480. [CrossRef]

169. Zhang, Y.Y.; Han, X.; Liu, Y.; Chen, J.; Hua, L.; Ma, Q.; Huang, Y.Y.X.; Tang, Q.Y.; Zhang, Z. +MRNA expression of LRRC55 protein (leucine-rich repeat-containing protein 55) in the adult mouse brain. *PLoS ONE* **2018**, *13*, e0191749.
170. Ster, J.; De Bock, F.; Guérineau, N.C.; Janossy, A.; Barrère-Lemaire, S.; Bos, J.L.; Bockaert, J.; Fagni, L. Exchange protein activated by cAMP (Epac) mediates cAMP activation of p38 MAPK and modulation of Ca2+-dependent K+ channels in cerebellar neurons. *Proc. Natl. Acad. Sci. USA* **2007**, *104*, 2519–2524. [CrossRef]
171. Rancz, E.A.; Häusser, M. Dendritic calcium spikes are tunable triggers of cannabinoid release and short-term synaptic plasticity in cerebellar purkinje neurons. *J. Neurosci.* **2006**, *26*, 5428–5437. [CrossRef]
172. Ouares, K.A.; Filipis, L.; Tzilivaki, A.; Poirazi, P.; Canepari, M. Two Distinct Sets of Ca^{2+} and K^{+} Channels Are Activated at Different Membrane Potentials by the Climbing Fiber Synaptic Potential in Purkinje Neuron Dendrites. *J. Neurosci.* **2019**, *39*, 1969–1981. [CrossRef]
173. Hirono, M.; Ogawa, Y.; Misono, K.; Zollinger, D.R.; Trimmer, J.S.; Rasband, M.N.; Misonou, H. BK Channels Localize to the Paranodal Junction and Regulate Action Potentials in Myelinated Axons of Cerebellar Purkinje Cells. *J. Neurosci.* **2015**, *35*, 7082–7094. [CrossRef]
174. Montgomery, J.R.; Meredith, A.L. Genetic activation of BK currents in vivo generates bidirectional effects on neuronal excitability. *Proc. Natl. Acad. Sci. USA* **2012**, *109*, 18997–19002. [CrossRef]
175. He, S.; Wang, Y.-X.; Petralia, R.S.; Brenowitz, S.D. Cholinergic Modulation of Large-Conductance Calcium-Activated Potassium Channels Regulates Synaptic Strength and Spine Calcium in Cartwheel Cells of the Dorsal Cochlear Nucleus. *J. Neurosci.* **2014**, *34*, 5261–5272. [CrossRef]
176. Garaycochea, J.; Slaughter, M.M. GABAB receptors enhance excitatory responses in isolated rat retinal ganglion cells. *J. Physiol.* **2016**, *594*, 5543–5554. [CrossRef]
177. Womack, M.; Hoang, C.; Khodakhah, K. Large conductance calcium-activated potassium channels affect both spontaneous firing and intracellular calcium concentration in cerebellar Purkinje neurons. *Neuroscience* **2009**, *162*, 989–1000. [CrossRef]
178. Nelson, A.B.; Krispel, C.M.; Sekirnjak, C.; du Lac, S. Long-Lasting Increases in Intrinsic Excitability Triggered by Inhibition. *Neuron* **2003**, *40*, 609–620. [CrossRef]
179. Kimm, T.; Khaliq, Z.M.; Bean, B.P. Differential Regulation of Action Potential Shape and Burst-Frequency Firing by BK and Kv2 Channels in Substantia Nigra Dopaminergic Neurons. *J. Neurosci.* **2015**, *35*, 16404–16417. [CrossRef]
180. Gittis, A.; Moghadam, S.H.; Du Lac, S. Mechanisms of Sustained High Firing Rates in Two Classes of Vestibular Nucleus Neurons: Differential Contributions of Resurgent Na, Kv3, and BK Currents. *J. Neurophysiol.* **2010**, *104*, 1625–1634. [CrossRef]
181. Petrucci, C.; Resta, V.; Fieni, F.; Bigiani, A.; Bagnoli, P. Modulation of potassium current and calcium influx by somatostatin in rod bipolar cells isolated from the rabbit retina via sst2 receptors. *Naunyn-Schmiedeberg's Arch. Pharmacol.* **2001**, *363*, 680–694. [CrossRef] [PubMed]
182. Gittis, A.H.; Lac, S. Firing Properties of GABAergic Versus Non-GABAergic Vestibular Nucleus Neurons Conferred by a Differential Balance of Potassium Currents. *J. Neurophysiol.* **2007**, *2003*, 3986. [CrossRef] [PubMed]
183. Kohlmeier, K.A.; Christensen, M.H.; Kristensen, M.P.; Kristiansen, U. Pharmacological evidence of functional inhibitory metabotrophic glutamate receptors on mouse arousal-related cholinergic laterodorsal tegmental neurons. *Neuropharmacology* **2013**, *66*, 99–113. [CrossRef] [PubMed]
184. Liu, Y.; Savtchouk, I.; Acharjee, S.; Liu, S.J. Inhibition of Ca^{2+}-activated large-conductance K^{+} channel activity alters synaptic AMPA receptor phenotype in mouse cerebellar stellate cells. *J. Neurophysiol.* **2011**, *106*, 144–152. [CrossRef]
185. Bock, T.; Stuart, G.J. Impact of calcium-activated potassium channels on NMDA spikes in cortical layer 5 pyramidal neurons. *J. Neurophysiol.* **2016**, *115*, 1740–1748. [CrossRef]
186. Golding, N.L.; Staff, N.P.; Spruston, N. Dendritic spikes as a mechanism for cooperative long-term potentiation. *Nature* **2002**, *418*, 326–331. [CrossRef]
187. Poolos, N.P.; Johnston, D. Calcium-Activated Potassium Conductances Contribute to Action Potential Repolarization at the Soma But Not the Dendrites of Hippocampal CA1 Pyramidal Neurons. *J. Neurosci.* **1999**, *19*, 5205–5212. [CrossRef]
188. Egaña-Huguet, J.; Saumell-Esnaola, M.; Achicallende, S.; Soria-Gomez, E.; Río, I.B.-D.; del Caño, G.G.; Barrondo, S.; Sallés, J.; Gerrikagoitia, I.; Puente, N.; et al. Lack of the Transient Receptor Potential Vanilloid 1 Shifts Cannabinoid-Dependent Excitatory Synaptic Plasticity in the Dentate Gyrus of the Mouse Brain Hippocampus. *Front. Neuroanat.* **2021**, *15*, 701573. [CrossRef]
189. Sclip, A.; Acuna, C.; Luo, F.; Südhof, T.C. RIM-binding proteins recruit BK-channels to presynaptic release sites adjacent to voltage-gated Ca^{2+} -channels. *EMBO J.* **2018**, *37*, 1–14. [CrossRef]
190. Brenes, O.; Vandael, D.; Carbone, E.; Montarolo, P.; Ghirardi, M. Knock-down of synapsin alters cell excitability and action potential waveform by potentiating BK and voltage-gated Ca2+ currents in Helix serotonergic neurons. *Neuroscience* **2015**, *311*, 430–443. [CrossRef]
191. Oh, K.H.; Abraham, L.S.; Gegg, C.; Silvestri, C.; Huang, Y.-C.; Alkema, M.J.; Furst, J.; Raicu, D.; Kim, H. Presynaptic BK channel localization is dependent on the hierarchical organization of alpha-catulin and dystrobrevin and fine-tuned by CaV2 calcium channels. *BMC Neurosci.* **2015**, *16*, 1–13. [CrossRef]
192. Chen, B.; Liu, P.; Zhan, H.; Wang, Z.-W. Dystrobrevin Controls Neurotransmitter Release and Muscle Ca2+ Transients by Localizing BK Channels in Caenorhabditis elegans. *J. Neurosci.* **2011**, *31*, 17338–17347. [CrossRef]

193. Abrahamsson, T.; Chou, C.Y.C.; Li, S.Y.; Mancino, A.; Costa, R.P.; Brock, J.A.; Nuro, E.; Buchanan, K.A.; Elgar, D.; Blackman, A.V.; et al. Differential Regulation of Evoked and Spontaneous Release by Presynaptic NMDA Receptors. *Neuron* **2017**, *96*, 839–855.e5. [CrossRef]
194. Banerjee, A.; Larsen, R.; Philpot, B.D.; Paulsen, O. Roles of Presynaptic NMDA Receptors in Neurotransmission and Plasticity. *Trends Neurosci.* **2015**, *39*, 26–39. [CrossRef]
195. Lituma, P.J.; Kwon, H.-B.; Alviña, K.; Luján, R.; Castillo, P.E. Presynaptic NMDA receptors facilitate short-term plasticity and BDNF release at hippocampal mossy fiber synapses. *Elife* **2021**, *10*, e66612. [CrossRef]
196. Martire, M.; Barrese, V.; D'Amico, M.; Iannotti, F.A.; Pizzarelli, R.; Samengo, I.; Viggiano, D.; Ruth, P.; Cherubini, E.; Taglialatela, M. Pre-synaptic BK channels selectively control glutamate versus GABA release from cortical and hippocampal nerve terminals. *J. Neurochem.* **2010**, *115*, 411–422. [CrossRef]
197. Samengo, I.; Curro', D.; Barrese, V.; Taglialatela, M.; Martire, M. Large Conductance Calcium-Activated Potassium Channels: Their Expression and Modulation of Glutamate Release from Nerve Terminals Isolated from Rat Trigeminal Caudal Nucleus and Cerebral Cortex. *Neurochem. Res.* **2014**, *39*, 901–910. [CrossRef]
198. Shoudai, K.; Nonaka, K.; Maeda, M.; Wang, Z.-M.; Jeong, H.-J.; Higashi, H.; Murayama, N.; Akaike, N. Effects of various K+ channel blockers on spontaneous glycine release at rat spinal neurons. *Brain Res.* **2007**, *1157*, 11–22. [CrossRef]
199. De San Martín, J.Z.; Pyott, S.; Ballestero, J.; Katz, E. Ca^{2+} and Ca^{2+}-activated K+ channels that support and modulate transmitter release at the olivocochlear efferent-inner hair cell synapse. *J. Neurosci.* **2010**, *30*, 12157–12167. [CrossRef]
200. Choi, T.-Y.; Lee, S.-H.; Kim, Y.-J.; Bae, J.R.; Lee, K.M.; Jo, Y.; Kim, S.-J.; Lee, A.-R.; Choi, S.; Choi, L.-M.; et al. Cereblon Maintains Synaptic and Cognitive Function by Regulating BK Channel. *J. Neurosci.* **2018**, *38*, 3571–3583. [CrossRef]
201. Price, D.L.; Ludwig, J.W.; Mi, H.; Schwarz, T.L.; Ellisman, M.H. Distribution of rSlo Ca2+-activated K+ channels in rat astrocyte perivascular endfeet. *Brain Res.* **2002**, *956*, 183–193. [CrossRef] [PubMed]
202. Girouard, H.; Bonev, A.D.; Hannah, R.M.; Meredith, A.; Aldrich, R.W.; Nelson, M.T. Astrocytic endfoot Ca $^{2+}$ and BK channels determine both arteriolar dilation and constriction. *Proc. Natl. Acad. Sci. USA* **2010**, *107*, 3811–3816. [CrossRef] [PubMed]
203. Kyle, B.; Mishra, R.C.; Braun, A.P. The augmentation of BK channel activity by nitric oxide signaling in rat cerebral arteries involves co-localized regulatory elements. *J. Cereb. Blood Flow Metab.* **2017**, *37*, 3759–3773. [CrossRef] [PubMed]
204. Filosa, J.A.; Bonev, A.D.; Straub, S.V.; Meredith, A.; Wilkerson, M.K.; Aldrich, R.W.; Nelson, M. Local potassium signaling couples neuronal activity to vasodilation in the brain. *Nat. Neurosci.* **2006**, *9*, 1397–1403. [CrossRef]
205. Gebremedhin, D.; Yamaura, K.; Zhang, C.; Bylund, J.; Koehler, R.C.; Harder, D.R. Metabotropic Glutamate Receptor Activation Enhances the Activities of Two Types of Ca^{2+}-Activated K^{+}Channels in Rat Hippocampal Astrocytes. *J. Neurosci.* **2003**, *23*, 1678–1687. [CrossRef]
206. Brandalise, F.; Ratto, D.; Leone, R.; Olivero, F.; Roda, E.; Locatelli, C.A.; Grazia Bottone, M.; Rossi, P. Deeper and Deeper on the Role of BK and Kir4.1 Channels in Glioblastoma Invasiveness: A Novel Summative Mechanism? *Front Neurosci.* **2020**, *14*, 1–6. [CrossRef]
207. Singh, H.; Li, M.; Hall, L.; Chen, S.; Sukur, S.; Lu, R.; Caputo, A.; Meredith, A.; Stefani, E.; Toro, L. MaxiK channel interactome reveals its interaction with GABA transporter 3 and heat shock protein 60 in the mammalian brain. *Neuroscience* **2016**, *317*, 76–107. [CrossRef]
208. Hayashi, Y.; Nakanishi, H. BK channel in microglia as a potent therapeutic molecular target for neuropathic pain. *J. Oral Biosci.* **2015**, *57*, 131–134. [CrossRef]
209. Huang, S.; Chen, T.; Suo, Q.; Shi, R.; Khan, H.; Ma, Y.; Tang, Y.; Yang, G.-Y.; Zhang, Z. BK Channel-Mediated Microglial Phagocytosis Alleviates Neurological Deficit After Ischemic Stroke. *Front. Cell. Neurosci.* **2021**, *15*, 683769. [CrossRef]
210. Hayashi, Y.; Kawaji, K.; Sun, L.; Zhang, X.; Koyano, K.; Yokoyama, T.; Kohsaka, S.; Inoue, K.; Nakanishi, H. Microglial Ca^{2+}-Activated K^{+} Channels Are Possible Molecular Targets for the Analgesic Effects of S-Ketamine on Neuropathic Pain. *J. Neurosci.* **2011**, *31*, 17370–17382. [CrossRef]
211. Bordey, A.; Spencer, D.D. Chemokine modulation of high-conductance Ca2+-sensitive K+ currents in microglia from human hippocampi. *J. FENS* **2003**, *18*, 2893–2898. [CrossRef]
212. Schilling, T.; Eder, C. Ion channel expression in resting and activated microglia of hippocampal slices from juvenile mice. *Brain Res.* **2007**, *1186*, 21–28. [CrossRef]
213. Schilling, T.; Eder, C. Microglial K^{+} channel expression in young adult and aged mice. *Glia* **2014**, *63*, 664–672. [CrossRef]
214. Buttigieg, J.; Eftekharpour, E.; Karimi-Abdolrezaee, S.; Fehlings, M.G. Molecular and electrophysiological evidence for the expression of BK channels in oligodendroglial precursor cells. *Eur. J. Neurosci.* **2011**, *34*, 538–547. [CrossRef]
215. Larson, V.A.; Zhang, Y.; Bergles, D.E. Electrophysiological properties of NG2 þ cells: Matching physiological studies with gene expression profiles. *Brain Res.* **2015**, *15*, 1853.
216. Jäkel, S.; Agirre, E.; Falcão, A.M.; van Bruggen, D.; Lee, K.W.; Knuesel, I.; Malhotra, D.; Ffrench-Constant, C.; Williams, A.; Castelo-Branco, G. Altered human oligodendrocyte heterogeneity in multiple sclerosis. *Nature* **2019**, *566*, 543–547. [CrossRef]
217. Valverde, M.A.; Rojas, P.; Amigo, J.; Cosmelli, D.; Orio, P.; Bahamonde, M.I.; Mann, G.E.; Vergara, C.; Latorre, R. Acute Activation of Maxi-K Channels (*hSlo*) by Estradiol Binding to the β Subunit. *Science* **1999**, *285*, 1929–1931. [CrossRef]
218. King, J.T.; Lovell, P.V.; Rishniw, M.; Kotlikoff, M.I.; Zeeman, M.L.; McCobb, D.P. β2 and β4 Subunits of BK Channels Confer Differential Sensitivity to Acute Modulation by Steroid Hormones. *J. Neurophysiol.* **2006**, *95*, 2878–2888. [CrossRef]

219. Teyler, T.J.; Vardaris, R.M.; Lewis, D.; Rawitch, A.B. Gonadal Steroids: Effects on Excitability of Hippocampal Pyramidal Cells. *Science* **1980**, *209*, 1017–1018. [CrossRef]
220. Oberlander, J.G.; Woolley, C.S. 17β-Estradiol Acutely Potentiates Glutamatergic Synaptic Transmission in the Hippocampus through Distinct Mechanisms in Males and Females. *J. Neurosci.* **2016**, *36*, 2677–2690. [CrossRef]
221. Soutar, C.N.; Grenier, P.; Patel, A.; Kabitsis, P.P.; Olmstead, M.C.; Bailey, C.D.C.; Dringenberg, H.C. Brain-Generated 17β-Estradiol Modulates Long-Term Synaptic Plasticity in the Primary Auditory Cortex of Adult Male Rats. *Cereb. Cortex* **2021**, *32*, 2140–2155. [CrossRef]
222. Hoshi, T.; Tian, Y.; Xu, R.; Heinemann, S.H.; Hou, S. Mechanism of the modulation of BK potassium channel complexes with different auxiliary subunit compositions by the omega-3 fatty acid DHA. *Proc. Natl. Acad. Sci. USA* **2013**, *110*, 4822–4827. [CrossRef] [PubMed]
223. Sun, X.; Zhou, D.; Zhang, P.; Moczydlowski, E.G.; Haddad, G.G. β-subunit-dependent modulation of hSlo BK current by arachidonic acid. *J. Neurophysiol.* **2007**, *97*, 62–69. [CrossRef] [PubMed]
224. Duerson, K.; White, R.E.; Jiang, F.; Schonbrunn, A.; Armstrong, D.L. Somatostatin stimulates BK(Ca) channels in rat pituitary tumor cells through lipoxygenase metabolites of arachidonic acid. *Neuropharmacology* **1996**, *35*, 949–961. [CrossRef] [PubMed]
225. Barlow, R.S.; El-Mowafy, A.M.; White, A.R.E. H_2O_2 opens BK(Ca) channels via the PLA2-arachidomic acid signaling cascade in coronary artery smooth muscle. *Am. J. Physiol.-Hear. Circ. Physiol.* **2000**, *279*, H475–H483. [CrossRef] [PubMed]
226. Bondarenko, A.I.; Panasiuk, O.; Okhai, I.; Montecucco, F.; Brandt, K.J.; Mach, F. Direct activation of Ca2+ and voltage-gated potassium channels of large conductance by anandamide in endothelial cells does not support the presence of endothelial atypical cannabinoid receptor. *Eur. J. Pharmacol.* **2017**, *805*, 14–24. [CrossRef]
227. Sade, H.; Muraki, K.; Ohya, S.; Hatano, N.; Imaizumi, Y. Activation of large-conductance, Ca^{2+}-activated K^+ channels by cannabinoids. *Am. J. Physiol.-Cell Physiol.* **2006**, *290*, C77–C86. [CrossRef]
228. Li, Y.; Zhang, L.; Wu, Y.; Zheng, Q.; Chen, M.; Qian, Z.; Wei, C.; Han, J.; Liu, Z.; Ren, W.; et al. Cannabinoids-induced peripheral analgesia depends on activation of BK channels. *Brain Res.* **2019**, *1711*, 23–28. [CrossRef]
229. Bailey, C.S.; Moldenhauer, H.J.; Park, S.M.; Keros, S.; Meredith, A.L. KCNMA1-linked channelopathy. *J. Gen. Physiol.* **2019**, *151*, 1173–1189. [CrossRef]
230. Miller, J.P.; Moldenhauer, H.J.; Keros, S.; Meredith, A.L. An emerging spectrum of variants and clinical features in *KCNMA1*-linked channelopathy. *Channels* **2021**, *15*, 447–464. [CrossRef]
231. Du, W.; Bautista, J.F.; Yang, H.; Diez-Sampedro, A.; You, S.-A.; Wang, L.; Kotagal, P.; Lüders, H.O.; Shi, J.; Cui, J.; et al. Calcium-sensitive potassium channelopathy in human epilepsy and paroxysmal movement disorder. *Nat. Genet.* **2005**, *37*, 733–738. [CrossRef]
232. Mi Park, S.; Roache, C.E.; Iffland, P.H., II; Moldenhauer, H.J.; Matychak, K.K.; Plante, A.E. BK channel properties correlate with neurobehavioral severity in three KCNMA1-linked channelopathy mouse models. *Elife* **2022**, *11*, e77953. [CrossRef]
233. Li, X.; Poschmann, S.; Chen, Q.; Fazeli, W.; Oundjian, N.J.; Snoeijen-Schouwenaars, F.M.; Fricke, O.; Kamsteeg, E.-J.; Willemsen, M.; Wang, Q.K. De novo BK channel variant causes epilepsy by affecting voltage gating but not Ca2+ sensitivity. *Eur. J. Hum. Genet.* **2018**, *26*, 220–229. [CrossRef]
234. Whitmire, L.E.; Ling, L.; Bugay, V.; Carver, C.M.; Timilsina, S.; Chuang, H.-H.; Jaffe, D.B.; Shapiro, M.S.; Cavazos, J.; Brenner, R. Downregulation of KCNMB4 expression and changes in BK channel subtype in hippocampal granule neurons following seizure activity. *PLoS ONE* **2017**, *12*, e0188064. [CrossRef]
235. Lorenz, S.; Heils, A.; Kasper, J.M.; Sander, T. Allelic association of a truncation mutation of theKCNMB3 gene with idiopathic generalized epilepsy. *Am. J. Med Genet. Part B Neuropsychiatr. Genet.* **2007**, *144B*, 10–13. [CrossRef]
236. Chen, S.R.; Cai, Y.Q.; Pan, H.L. Plasticity and emerging role of BKCa channels in nociceptive control in neuropathic pain. *J Neurochem.* **2009**, *110*, 352–362. [CrossRef]
237. Furukawa, N.; Takasusuki, T.; Fukushima, T.; Hori, Y. Presynaptic large-conductance calcium-activated potassium channels control synaptic transmission in the superficial dorsal horn of the mouse. *Neurosci. Lett.* **2008**, *444*, 79–82. [CrossRef]
238. Sarantopoulos, C.D.; McCallum, J.B.; Rigaud, M.; Fuchs, A.; Kwok, W.-M.; Hogan, Q.H. Opposing effects of spinal nerve ligation on calcium-activated potassium currents in axotomized and adjacent mammalian primary afferent neurons. *Brain Res.* **2007**, *1132*, 84–99. [CrossRef]
239. Zhang, F.-X.; Gadotti, V.M.; Souza, I.A.; Chen, L.; Zamponi, G.W. BK Potassium Channels Suppress Cavα2δ Subunit Function to Reduce Inflammatory and Neuropathic Pain. *Cell Rep.* **2018**, *22*, 1956–1964. [CrossRef]
240. Imari, K.; Harada, Y.; Zhang, J.; Mori, Y.; Hayashi, Y. KCNMB3 in spinal microglia contributes to the generation and maintenance of neuropathic pain in mice. *Int. J. Mol. Med.* **2019**, *44*, 1585–1593. [CrossRef]
241. Typlt, M.; Mirkowski, M.; Azzopardi, E.; Ruettiger, L.; Ruth, P.; Schmid, S. Mice with Deficient BK Channel Function Show Impaired Prepulse Inhibition and Spatial Learning, but Normal Working and Spatial Reference Memory. *PLoS ONE* **2013**, *8*, e81270. [CrossRef] [PubMed]
242. Du, X.; Carvalho-De-Souza, J.L.; Wei, C.; Carrasquel-Ursulaez, W.; Lorenzo, Y.; Gonzalez, N.; Kubota, T.; Staisch, J.; Hain, T.; Petrossian, N.; et al. Loss-of-function BK channel mutation causes impaired mitochondria and progressive cerebellar ataxia. *Proc. Natl. Acad. Sci. USA* **2020**, *117*, 6023–6034. [CrossRef] [PubMed]

243. Kratschmer, P.; Lowe, S.A.; Buhl, E.; Chen, K.F.; Kullmann, D.M.; Pittman, A.; Hodge, J.J.L.; Jepson, J.E.C. Impaired Pre-Motor Circuit Activity and Movement in a Drosophila Model of KCNMA1-Linked Dyskinesia. *Mov. Disord.* **2021**, *36*, 1158–1169. [CrossRef] [PubMed]
244. Gao, L.; Zhao, J.; Ardiel, E.L.; Hall, Q.; Nurrish, S.; Kaplan, J.M. Shank promotes action potential repolarization by recruiting BK channels to calcium microdomains. *Elife* **2022**, *11*, e75140. [CrossRef] [PubMed]
245. Deng, P.-Y.; Klyachko, V.A. Channelopathies in fragile X syndrome. *Nat. Rev. Neurosci.* **2021**, *22*, 275–289. [CrossRef]
246. Hébert, B.; Pietropaolo, S.; Même, S.; Laudier, B.; Laugeray, A.; Doisne, N.; Quartier, A.; Lefeuvre, S.; Got, L.; Cahard, D.; et al. Rescue of fragile X syndrome phenotypes in Fmr1KO mice by a BKCa channel opener molecule. *Orphanet. J. Rare Dis.* **2014**, *9*, 124. [CrossRef]
247. Edwards, T.; Rickard, N. Pharmaco-behavioural evidence indicating a complex role for ryanodine receptor calcium release channels in memory processing for a passive avoidance task. *Neurobiol. Learn. Mem.* **2006**, *86*, 1–8. [CrossRef]
248. Matthews, E.A.; Weible, A.P.; Shah, S.; Disterhoft, J.F. The BK-mediated fAHP is modulated by learning a hippocampus-dependent task. *Proc. Natl. Acad. Sci. USA* **2008**, *105*, 15154–15159. [CrossRef]
249. Matthews, E.A.; Disterhoft, J.F. Blocking the BK channel impedes acquisition of trace eyeblink conditioning. *Learn. Mem.* **2009**, *16*, 106–109. [CrossRef]
250. Ryan, D.P.; Henzel, K.S.; Pearson, B.L.; Siwek, M.E.; Papazoglou, A.; Guo, L.; Paesler, K.; Yu, M.; Müller, R.; Xie, K.; et al. A paternal methyl donor-rich diet altered cognitive and neural functions in offspring mice. *Mol. Psychiatry* **2017**, *23*, 1345–1355. [CrossRef]
251. Choi, T.-Y.; Lee, S.-H.; Kim, S.-J.; Jo, Y.; Park, C.-S.; Choi, S.-Y. BK channel blocker paxilline attenuates thalidomide-caused synaptic and cognitive dysfunctions in mice. *Sci. Rep.* **2018**, *8*, 17653. [CrossRef]
252. Beecham, G.W.; Schnetz-Boutaud, N.; Haines, J.L.; Pericak-Vance, M.A. *CALHM1*Polymorphism is not Associated with Late-onset Alzheimer Disease. *Ann. Hum. Genet.* **2009**, *73*, 379–381. [CrossRef]
253. Beecham, G.W.; Hamilton, K.; Naj, A.C.; Martin, E.R.; Huentelman, M.; Myers, A.J.; Corneveaux, J.J.; Hardy, J.; Vonsattel, J.-P.; Younkin, S.G.; et al. Genome-Wide Association Meta-analysis of Neuropathologic Features of Alzheimer's Disease and Related Dementias. *PLOS Genet.* **2014**, *10*, e1004606. [CrossRef]
254. Ye, H.; Jalini, S.; Mylvaganam, S.; Carlen, P. Activation of large-conductance Ca2+-activated K+ channels depresses basal synaptic transmission in the hippocampal CA1 area in APP (swe/ind) TgCRND8 mice. *Neurobiol. Aging* **2010**, *31*, 591–604. [CrossRef]
255. Yamamoto, K.; Ueta, Y.; Wang, L.; Yamamoto, R.; Inoue, N.; Inokuchi, K.; Aiba, A.; Yonekura, H.; Kato, N. Suppression of a neocortical potassium channel activity by intracellular amyloid-β and its rescue with homer1a. *J. Neurosci.* **2011**, *31*, 11100–11109. [CrossRef]
256. Gavello, D.; Calorio, C.; Franchino, C.; Cesano, F.; Carabelli, V.; Carbone, E.; Marcantoni, A. Early Alterations of Hippocampal Neuronal Firing Induced by Abeta42. *Cereb. Cortex* **2018**, *28*, 433–446. [CrossRef]
257. Wang, L.; Kang, H.; Li, Y.; Shui, Y.; Yamamoto, R.; Sugai, T.; Kato, N. Cognitive recovery by chronic activation of the large-conductance calcium-activated potassium channel in a mouse model of Alzheimer's disease. *Neuropharmacology* **2015**, *92*, 8–15. [CrossRef]

Disclaimer/Publisher's Note: The statements, opinions and data contained in all publications are solely those of the individual author(s) and contributor(s) and not of MDPI and/or the editor(s). MDPI and/or the editor(s) disclaim responsibility for any injury to people or property resulting from any ideas, methods, instructions or products referred to in the content.

PNAS RESEARCH ARTICLE | NEUROSCIENCE

BK channels mediate a presynaptic form of mGluR-LTD in the neonatal hippocampus

Carlos Ancatén-González[a,b], Rodrigo C. Meza[b], Naileth Gonzalez-Sanabria[a,b], Ignacio Segura[b], Alejandro Alcaino[a,b], Antonio Peña-Pichicoi[b], Ramón Latorre[b], Chiayu Q. Chiu[b], and Andrés E. Chávez[b,1]

Affiliations are included on p. 8.

Edited by Julie Kauer, Stanford University, Stanford, CA; received June 20, 2024; accepted December 7, 2024 by Editorial Board Member Carol A. Mason

BK channels can control neuronal function, but their functional relevance in activity-dependent changes of synaptic function remains elusive. Here, we report that repetitive low-frequency stimulation activates BK channels through 12(S)HPETE, an arachidonic acid metabolite, produced downstream of postsynaptic metabotropic glutamate receptors (mGluRs) to trigger long-term depression (LTD) at CA3–CA1 synapses in hippocampal slices from P7–P10 mice. Activation of BK channels is subunit specific, as paxilline but not iberiotoxin blocked mGluR-LTD. Also, 12(S)HPETE does not change the electrophysiological properties of the BK channel when the BKα subunit is expressed alone but increases the channel open probability when the BKα is coexpressed with the β4-subunit. Our findings reveal an interaction between 12(S)HPETE and BK channels to regulate synaptic strength at central synapses and increase our understanding of the mechanisms underlying mGluR-LTD in the neonatal hippocampus that likely contribute to circuit maturation necessary for learning.

retrograde signaling | synaptic plasticity | BK channels | hippocampus

Activity-dependent long-term depression (LTD) of excitatory synaptic strength contributes to circuit remodeling and memory formation. Although with varying mechanisms depending upon brain region and developmental progress, a common cellular mechanism for LTD is the reliance on postsynaptic activation of group I metabotropic glutamate receptors (mGluRs) to induce either pre- or postsynaptic forms of mGluR-LTD (1). In the hippocampus, neonatal LTD is known to require mGluRs to subsequently generate a lipid-derived metabolite from arachidonic acid, known as 12(S)HPETE. Once produced, 12(S)HPETE travels retrogradely to the CA3 axon terminal to suppress glutamate release onto CA1 pyramidal neurons in a long-term manner (2–4). However, the precise downstream targets of 12(S)HPETE at presynaptic sites involved in this form of mGluR-LTD remain elusive.

Lipid derivates, including the lipoxygenase-derived 12(S)HPETE, represent one of the primary activating ligands of TRP channels (5, 6). For instance, 12(S)HPETE-dependent LTD in the mature hippocampus has been reported at glutamatergic synapses onto CA1 inhibitory interneurons. This form of plasticity involves the activation of the presynaptic transient potential vanilloid 1 receptor (TRPV1) (7). Whether TRPV1 channels are also a key player in neonatal mGluR-LTD at CA3-CA1 excitatory synapses remains unknown. Apart from their action on TRP receptors, lipid derivates are also known to modulate synaptic efficacy by directly acting on voltage-gated ion channels (8), including calcium (9) and potassium channels (10, 11). Interestingly, the large-conductance, calcium- and voltage-activated potassium channels (BK), known to regulate neuronal excitability and synaptic function throughout the brain (12, 13), are reportedly regulated by different lipoxygenase-derived metabolites (14, 15). Moreover, evidence indicates that BK channels are expressed at presynaptic terminals of CA3 neurons in the mature hippocampus (16–19), opening the possibility that BK channels are involved in mGluR-LTD. However, whether presynaptic BK channels contribute to neonatal activity-dependent mGluR-LTD remains unknown.

Here, using electrophysiological recordings in acute hippocampal slices from P7–P10 mice, we evaluate the role of TRPV1 and BK channels as potential downstream effectors of 12(S)HPETE signaling in mediating neonatal mGluR-LTD. We find that activation of presumably presynaptic BK, but not TRPV1, channels by 12(S)HPETE is required for the induction of mGluR-LTD at immature CA3–CA1 synapses. The contribution of BK channels is subunit specific, involving BK containing β4 but not β2 subunit. These results identify a mechanistically necessary step for the induction of mGluR-LTD during postnatal

Significance

Calcium- and voltage-activated potassium channels (BK) are well known to regulate neuronal excitability and synaptic function throughout the brain. However, the contribution of BK channels to activity-dependent changes of synaptic efficacy remains elusive. Here, we report that an arachidonic acid–derived metabolite activates BK channels to induce long-term depression of glutamate release mediated by metabotropic glutamate receptor (mGluR-LTD) in the neonatal hippocampus. This modulation of synaptic efficacy is subunit specific, as BK channels containing the β4 but not β2 subunit are required. These results highlight the contribution of BK channels in activity-dependent regulation of synaptic efficacy and identify a subunit-dependent activation of BK channels by lipid messengers to regulate synaptic function in a long-term manner in the neonatal hippocampus.

Author contributions: C.A.-G., R.L., C.Q.C., and A.E.C. designed research; C.A.-G., R.C.M., N.G.-S., I.S., A.A., and A.P.-P. performed research; R.L. and A.E.C. contributed new reagents/analytic tools; C.A.-G., R.C.M., N.G.-S., I.S., A.A., A.P., C.Q.C., and A.E.C. analyzed data; and C.A.-G., R.L., C.Q.C., and A.E.C. wrote the paper.

The authors declare no competing interest.

This article is a PNAS Direct Submission. J.K. is a guest editor invited by the Editorial Board.

Copyright © 2025 the Author(s). Published by PNAS. This article is distributed under Creative Commons Attribution-NonCommercial-NoDerivatives License 4.0 (CC BY-NC-ND).

[1]To whom correspondence may be addressed. Email: andres.chavez@uv.cl.

This article contains supporting information online at https://www.pnas.org/lookup/suppl/doi:10.1073/pnas.2411506122/-/DCSupplemental.

Published January 8, 2025.

Downloaded from https://www.pnas.org by Andrés Eduardo Chávez on January 8, 2025 from IP address 186.78.166.3.

development that likely involves retrograde activation of BK channels at presynaptic terminals to impact synaptic function in a long-term manner.

Results

12(S)HPETE Is a Key Player of Presynaptic mGluR-LTD in the Neonatal Hippocampus. To investigate the presynaptic mechanisms involved in the induction of mGluR-LTD, we recorded field excitatory postsynaptic potentials (fEPSPs) and currents (EPSCs) from CA1 pyramidal neurons while stimulating CA3 Schaffer collateral inputs in acute hippocampal slices of neonatal (postnatal day P7–P10) mice (*Materials and Methods*). Consistent with previous reports (2, 3, 20, 21), low-frequency stimulation (LFS, 5 Hz, 3 min) induced a robust LTD that required postsynaptic mGluRs as it was eliminated by the mGluR5 antagonist MTEP (10 μM, Fig. 1*A*). Moreover, LFS-induced LTD can also be abolished by loading CA1 pyramidal neurons with GDPβS, a broad-spectrum G protein antagonist but was normally induced when NMDA receptors were blocked with APV (*SI Appendix*, Fig. S1 *A–C*). LFS-induced LTD was also independent of GABAergic transmission as it was normally induced in the presence (Fig. 1*A*) or absence of the $GABA_A$ receptor antagonist picrotoxin (50 μM; *SI Appendix*, Fig. S1*B*). Similarly, mGluR-LTD could be mimicked by pharmacological activation of mGluRs with DHPG (50 μM, 10 min), an effect that was also eliminated in the continuous presence of MTEP (Fig. 1*B*). Importantly, both electrical and chemical forms of mGluR-LTD were accompanied by changes in the paired-pulse ratio (PPR) and coefficient of variation ($1/CV^2$; Fig. 1 *A* and *B*), consistent with a presynaptic origin. Moreover,

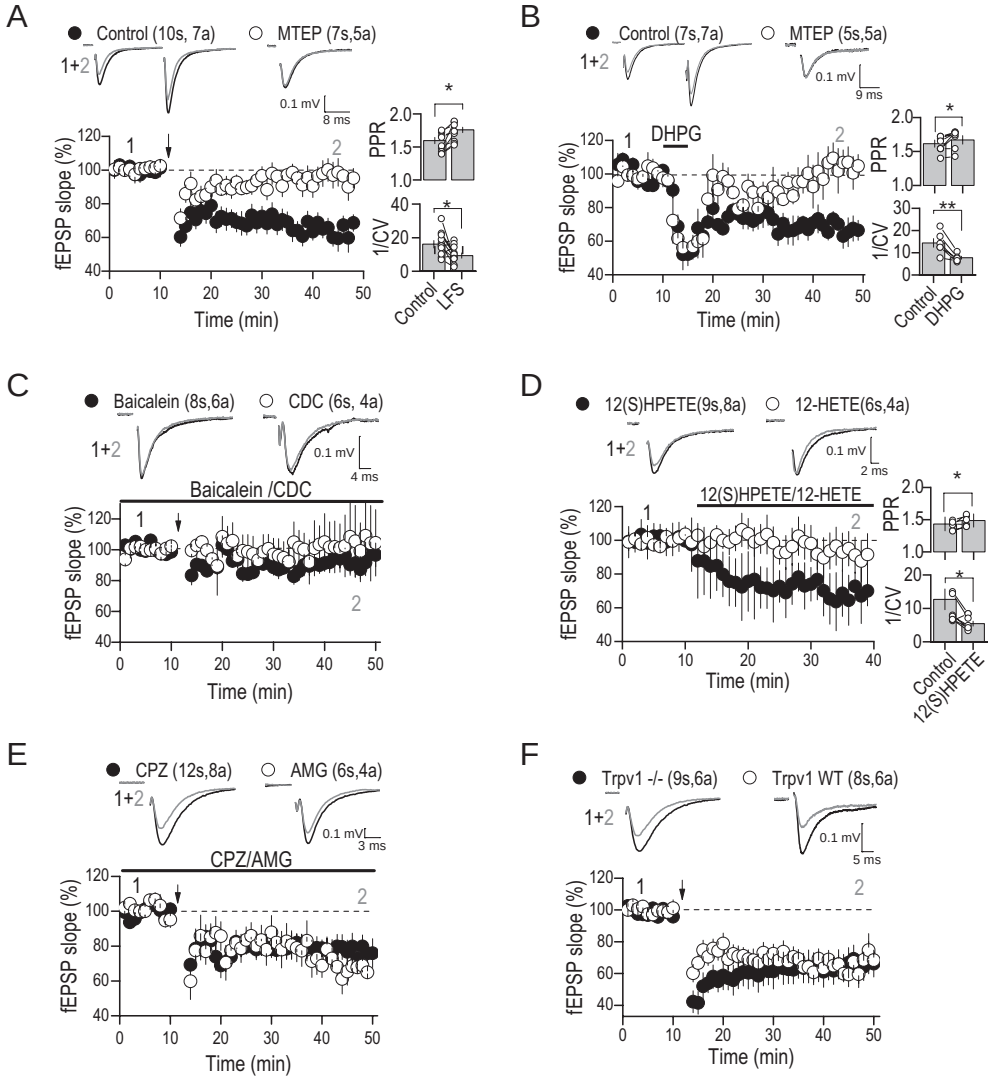


Fig. 1. Arachidonic acid metabolite 12(S)HPETE is necessary to induce mGluR-LTD in the young hippocampus. (*A*) Low-frequency stimulation (LFS, 5 Hz, 3 min) induces a LTD of fEPSP (black circle) that was eliminated in the continuous presence of the mGluR antagonist MTEP (10 μM; open circle). *Top,* Representative traces of two consecutive fEPSP (100-ms interstimulus interval) before (black) and after (grey) LFS induction, and in the continuous presence of MTEP. *Bottom*, summarized graphs. (*B*) Representative traces (*Top*) and time course (*Bottom*) showing that bath application of the mGluR agonist DHPG (50 μM, 5 min) also induces LTD of fEPSP, an effect that was eliminated in the continuous presence of MTEP. Note that LFS- and DHPG-induced mGluR-LTD were accompanied by changes in PPR and coefficient of variation ($1/CV^2$, *Right*), suggesting a presynaptic mechanism involved. In the PPR and $1/CV^2$ summarized plot, each open circle represents a single slice. (*C*) Representative traces (*Top*) and time course (*Bottom*) showing that blocking 12-lypoxigenase, and the production of 12(S)HPETE with two independent blockers (Baicalein and CDC), eliminates LFS-induced LTD. (*D*) Representative traces (*Top*) and time course (*Bottom*) showing that 12(S)HPETE (100 nM), but not its metabolite 12-HETE (100 nM), reduced fEPSP at CA3-CA1 synapses, an effect that was accompanied by changes in PPR and $1/CV^2$. (*E*) Representative traces (*Top*) and time course (*Bottom*) showing that LFS-induced mGluR-LTD was unaffected by two different TRPV1 antagonists Capsazepine (CPZ, 10 μM) and AMG 9810 (AMG, 10 μM). (*F*) Representative traces (*Top*) and time course (*Bottom*) showing that LFS-induced mGluR-LTD is similar in wild-type ($TRPV1^{+/+}$) and $TRPV1^{-/-}$ deficient mice. In all panels, data are presented as mean ± SEM, and averaged sample traces taken at times indicated by numbers are shown next to each summary plot. **P* <0.05, ***P* <0.01, and the number of slices (s) and animals (a) are indicated in parenthesis.

Downloaded from https://www.pnas.org by Andrés Eduardo Chávez on January 8, 2025 from IP address 186.78.166.3.

LFS- and DHPG-induced LTD occluded each other (*SI Appendix*, Fig. S1 *D* and *E*), indicating that mGluR activation by either pharmacological means or synaptic activity suppresses glutamate release in the young hippocampus through a common presynaptic mechanism.

Previous evidence indicates that presynaptic mGluR-LTD requires a postsynaptic signal pathway that involves the activation of 12-lipoxygenase and the production of the lipid metabolite 12(S) HPETE (2, 4, 22). Accordingly, two independent 12-lipoxygenase inhibitors, baicalein (10 μM) and cinnamyl-3,4-dihydroxy-α-cyanocinnamate (CDC; 10 μM), were able to eliminate both LFS- (Fig. 1*C*) and DHPG-induced mGluR-LTD (*SI Appendix*, Fig. S1*F*). Moreover, bath application of 12(S)HPETE (100 nM), but not its metabolite 12-HETE (100 nM), was sufficient to reduce fEPSPs in a long-lasting manner in the young hippocampus (Fig. 1*D*). Consistent with a presynaptic mechanism, 12(S)HPETE-mediated synaptic depression was accompanied by changes in PPR and $1/CV^2$ (Fig. 1*D*) and occluded the induction of either LFS- or DHPG-induced mGluR-LTD (*SI Appendix*, Fig. S2 *A* and *B*). Moreover, 12(S)HPETE had no further effect on fEPSP amplitude if applied after the induction of LFS-LTD (*SI Appendix*, Fig. S2*C*). Altogether, these results strongly support the idea that 12(S)HPETE is a key player in the induction of presynaptic mGluR-LTD in the neonatal hippocampus (2).

mGluR-LTD at CA3-CA1 Synapses Does Not Involve the Activation of TRPV1 Channels. What is the potential target of 12(S)HPETE at presynaptic terminals to induce mGluR-LTD? In the mature hippocampus, at excitatory CA3 to interneuron synapses, mGluR-LTD reportedly requires activation of presynaptic TRPV1 channels (7). However, LFS-induced mGluR-LTD at immature CA3 to CA1 synapses was normally induced when TRPV1 channels were blocked with capsazepine (CPZ, 10 μM) or AMG 9810 (AMG; 10 μM Fig. 1*E*) or in slices from TRPV1 deficient mice ($TRPV1^{-/-}$; Fig. 1*F*), further supporting that, unlike the excitatory CA3 to interneuron synapse (7), TRPV1 channels are not involved in presynaptic mGluR-LTD mediated by 12(S)HPETE at excitatory CA3-CA1 synapses in the neonatal hippocampus. Consistent with this idea, 12(S)HPETE markedly reduced fEPSPs in the continuous presence of CPZ or AMG (*SI Appendix*, Fig. S3*A*) or in hippocampal slices from $TRPV1^{-/-}$ mice (*SI Appendix*, Fig. S3*B*), strongly suggesting that TRPV1 channels are not required for 12(S)HPETE-mediated depression in the young hippocampus. Accordingly, bath application of capsaicin (1 μM), a TRPV1 agonist, had no significant effect on basal synaptic transmission at CA3-CA1 excitatory synapses (*SI Appendix*, Fig. S3*C*), but depressed the CA3-interneuron synapse in naïve slices (*SI Appendix*, Fig. S3*C*).

BK Channels Are Required for the Induction of mGluR-LTD in the Neonatal Hippocampus. Previous evidence suggests that BK channels regulate synaptic transmission at CA3 axon terminals (16, 18) and can be regulated by different lipoxygenase-derived metabolites (14, 15), but whether they play a role in regulating mGluR-LTD remains unknown. To assess their involvement in mGluR-LTD, we first applied BK channel antagonists before delivering LFS- or DHPG to induce mGluR-LTD. Blocking BK channels with iberiotoxin (100 nM) had no effect on electrical and chemical forms of mGluR-LTD (Fig. 2 *A* and *B*). However, bath application of the BK channel antagonist paxilline (1 or 10 μM) was able to abolish both forms of LTD (Fig. 2 *A* and *B*). For completeness, we also performed experiments using apamin, a blocker of the small-conductance voltage- and Ca^{2+}-sensitive potassium (SK) channels known to regulate synaptic plasticity in the adult hippocampus (23). While apamin (300 nM) was able to reduce medium afterhyperpolarization current (I_{mAHP}) in CA1 pyramidal neurons, it failed to block LFS-induced mGluR-LTD (*SI Appendix*, Fig. S4 *A* and *B*). Thus, our results suggest that paxilline-sensitive BK channels are involved in mGluR-LTD. Accordingly, paxilline but not iberiotoxin eliminated 12(S) HPETE-induced depression of synaptic transmission (Fig. 2*C*). Importantly, paxilline had no effect on basal synaptic transmission (*SI Appendix*, Fig. S4*C*) or in synapses already expressing 12(S) HPETE-mediated depression (*SI Appendix*, Fig. S4*D*) and LFS-induced LTD was normally expressed when paxilline was applied immediately after tetanus (*SI Appendix*, Fig. S4*E*), suggesting that paxilline-sensitive BK channels are required for the induction, but not maintenance of mGluR-LTD. Moreover, bath application of the specific BK channel agonist NS11021 (3 μM) was sufficient to reduce basal synaptic transmission at CA3-CA1 synapses (Fig. 2*D*). This effect was accompanied by changes in PPR and $1/CV^2$ and was eliminated in slices preincubated with paxilline but not with iberiotoxin (Fig. 2*D*). Moreover, a short application of NS11021 (5 min) also induces a long-lasting and irreversible reduction of fEPSP (*SI Appendix*, Fig. S4*F*). Consistent with the idea that paxilline-sensitive BK channels are required for the induction, but not maintenance of synaptic depression at CA3-CA1 synapses, paxilline had no effect on synapses already expressing NS11021-mediated depression (*SI Appendix*, Fig. S4*G*). Moreover, in the continuous presence of NS11021, LFS and DHPG were not able to further suppress fEPSPs (Fig. 2*E*). Importantly, NS11021-mediated depression could not be induced at synapses already expressing 12(S)HPETE-mediated depression (Fig. 2*F*). Inversely, 12(S)HPETE had no effect on synapses already expressing NS11021-mediated depression (Fig. 2*F*). These two-way occlusion experiments indicate that 12(S)HPETE- and NS11021-mediated synaptic depression share a common mechanistic step to induce mGluR-LTD. To explore this possibility, we delivered a subthreshold induction protocol, which by itself did not have persistent effects on fEPSPs (*SI Appendix*, Fig. S5*A*) and did not occlude further induction of LFS-LTD (*SI Appendix*, Fig. S5*B*). We tested whether such a protocol could be potentiated to trigger LTD by slightly elevating BK channel activity with the use of brief application of BK agonists 12(S)HPETE or NS11021, which does not by itself produce lasting suppression. Under these recording conditions, the subthreshold induction protocol triggered robust LTD that was blocked by paxilline (*SI Appendix*, Fig. S5 *C* and *D*). Altogether, these results support the idea that paxilline-sensitive BK channel activation is necessary to induce mGluR-LTD in the young hippocampus.

The BK Channel Containing β4 but not the β2 Subunit Is Sensitive to 12(S)HPETE. The differential effect between iberiotoxin and paxilline on mGluR-LTD, and 12(S)HPETE- and NS11021-mediated depression, suggests that BK channels containing β4 but not β2 subunits are required for this form of LTD. To further investigate this possibility, we tested the effect of 12(S)HPETE on human BK channels formed by the α, the α+ β2, and α+ β4 subunits expressed in *Xenopus laevis* oocytes. Notably, 12(S) HPETE does not change the BK channel voltage dependence when the BKα subunit is expressed alone (Fig. 3*A*), but strongly increases the channel open probability when the β4-subunit was coexpressed with the α subunit (Fig. 3*B*). The addition of 12(S)HPETE intracellularly to a final concentration of 100 nM produces a 50 mV leftward shift of the normalized BKβ4 channel open probability ($I_{tail}/I_{tailmax}$)-voltage curve (Fig. 3*B*). The half voltages obtained from the $I_{tail}/I_{tailmax}$ vs voltage curves were plotted against 12(S)HPETE concentration, and the data were

Downloaded from https://www.pnas.org by Andrés Eduardo Chávez on January 8, 2025 from IP address 186.78.166.3.

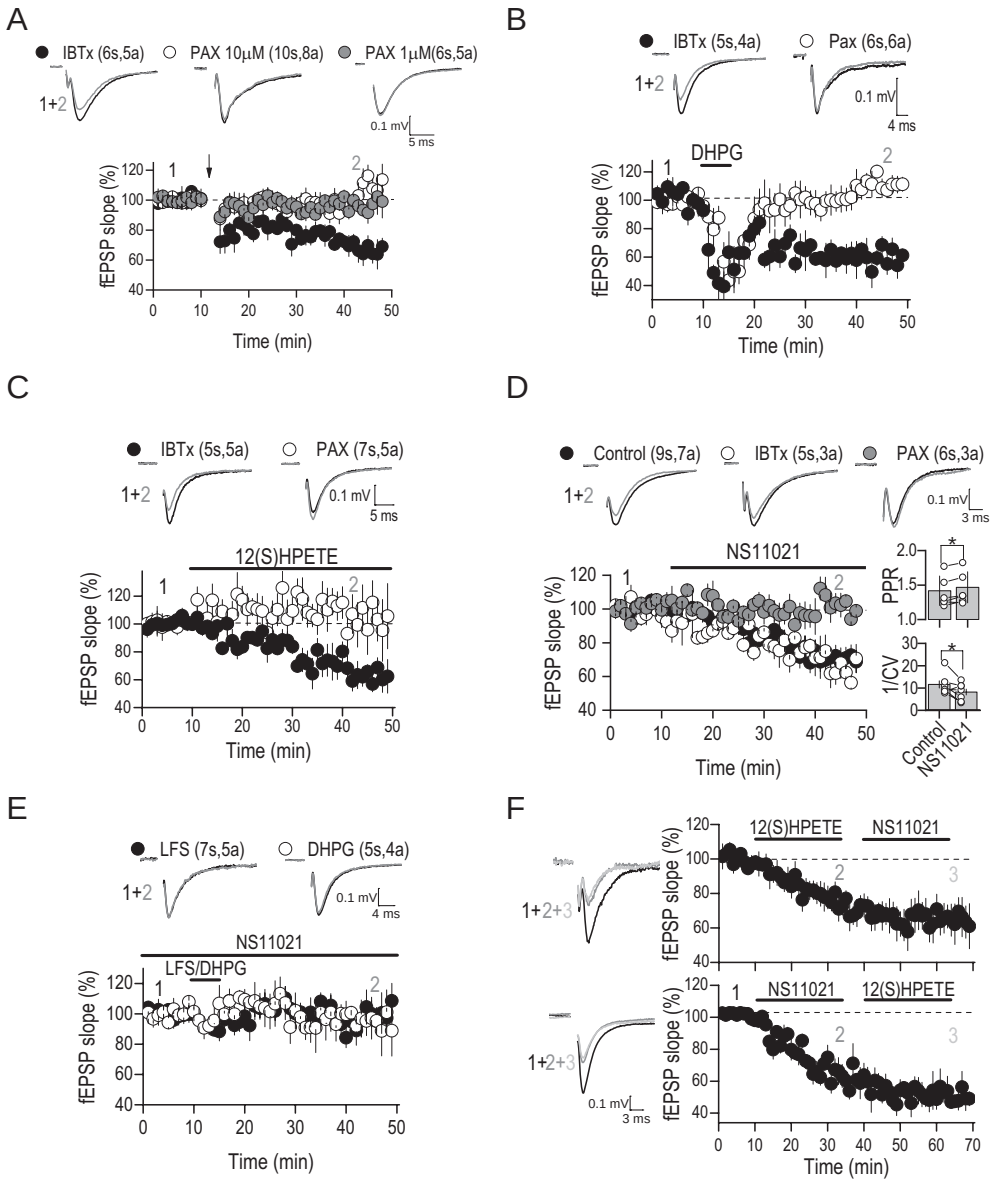


Fig. 2. Activation of BK channels containing the BKβ4 subunit is involved in mGluR-LTD. (*A*) Average traces (*Top*) and time course (*Bottom*) showing that LFS- and (*B*) DHPG-induced mGluR-LTD were unaffected by bath application of iberiotoxin (IBTx, 100 nM) but were eliminated in the continuous presence of Paxilline (Pax, 10 or 1 μM). (*C*) Average traces (*Top*) and time course (*Bottom*) showing that bath application of the 12(S)HPETE (100 nM) depresses fEPSP in the continuous presence of IBTx but had no effect in the presence of Pax. (*D*) Average traces (*Top*) and time course (*Bottom*) showing that bath application of NS11021 (3 μM), a BK channel agonist, depresses fEPSP in the continuous presence of IBTx but had no effect in the presence of Pax. NS1121-mediated depression of fEPSP was accompanied by changes in PPR and 1/CV, suggesting a presynaptic mechanism of action. (*E*) Average traces (*Top*) and time course (*Bottom*) showing that preincubation with NS11021 (3 μM) is able to block LFS- and DHPG-induced mGluR-LTD. (*F*) Average traces (*Left*) and time course (*Right*) showing that 12(S)HPETE-induced suppression of fEPSP occluded the NS11021-mediated depression of fEPSP at CA3-CA1 synapses (*Top*), and inversely, NS11021-induced depression blocks further effect of 12(S)HPETE (*Bottom*), suggesting a common mechanism of action. In all panels, data are presented as mean ± SEM, and averaged sample traces taken at times indicated by numbers are shown next to each summary plot, and the numbers of slices (s) and animals (a) are indicated in parentheses. *$P < 0.05$

fitted using a Hill equation (see legend of Fig. 3*C*). The best fit to the data was obtained with a dissociation constant of 0.98 nM and a Hill coefficient of 3 (Fig. 3*C*). Demonstrating that the effect of 12(S)HPETE is subunit specific, this metabolite did not modify the voltage dependence of α + β2 channels (Fig. 3*D*). Importantly, 12(S)HPETE-mediated effect in BKβ4 channel open probability is amplified by internal Ca^{2+} given that in the presence of 3 μM internal Ca^{2+}, the probability of opening-voltage curve shifted leftward by 77 mV, twice the effect observed in the absence of internal Ca^{2+} (Fig. 3*E*). Moreover, cytoplasmic Ca^{2+} does not affect the binding of 12(S)HPETE to the BK channel as the equilibrium dissociation constant is close to 1 nM (Fig. 3*F*). These results support the idea that BK channels formed by α and β4 subunits, but not β2-subunits, are necessary for the induction of 12(S)HPETE-mediated depression and mGluR-LTD in the young hippocampus and a tight binding accompanies this subunit specificity.

Presynaptic BKβ4 Channels Likely Regulate CA3-CA1 Synapses and mGluR-LTD. Although BK channels are expressed in pre- and postsynaptic compartments in the hippocampus (12, 16, 18, 19, 24, 25) and its inhibition with either paxilline and iberiotoxin can regulate the excitability of CA1 pyramidal neurons (*SI Appendix*, Fig. S6), the changes in PPR and $1/CV^2$ that we observed after the induction of 12(S)HPETE- and NS11021-mediated depression as well as in mGluR-LTD (Figs. 1–3) suggest that presynaptic rather than postsynaptic BK channels are necessary for the induction of mGluR-LTD. Consistent with this idea, BKβ4 channel

Downloaded from https://www.pnas.org by Andrés Eduardo Chávez on January 8, 2025 from IP address 186.78.166.3.

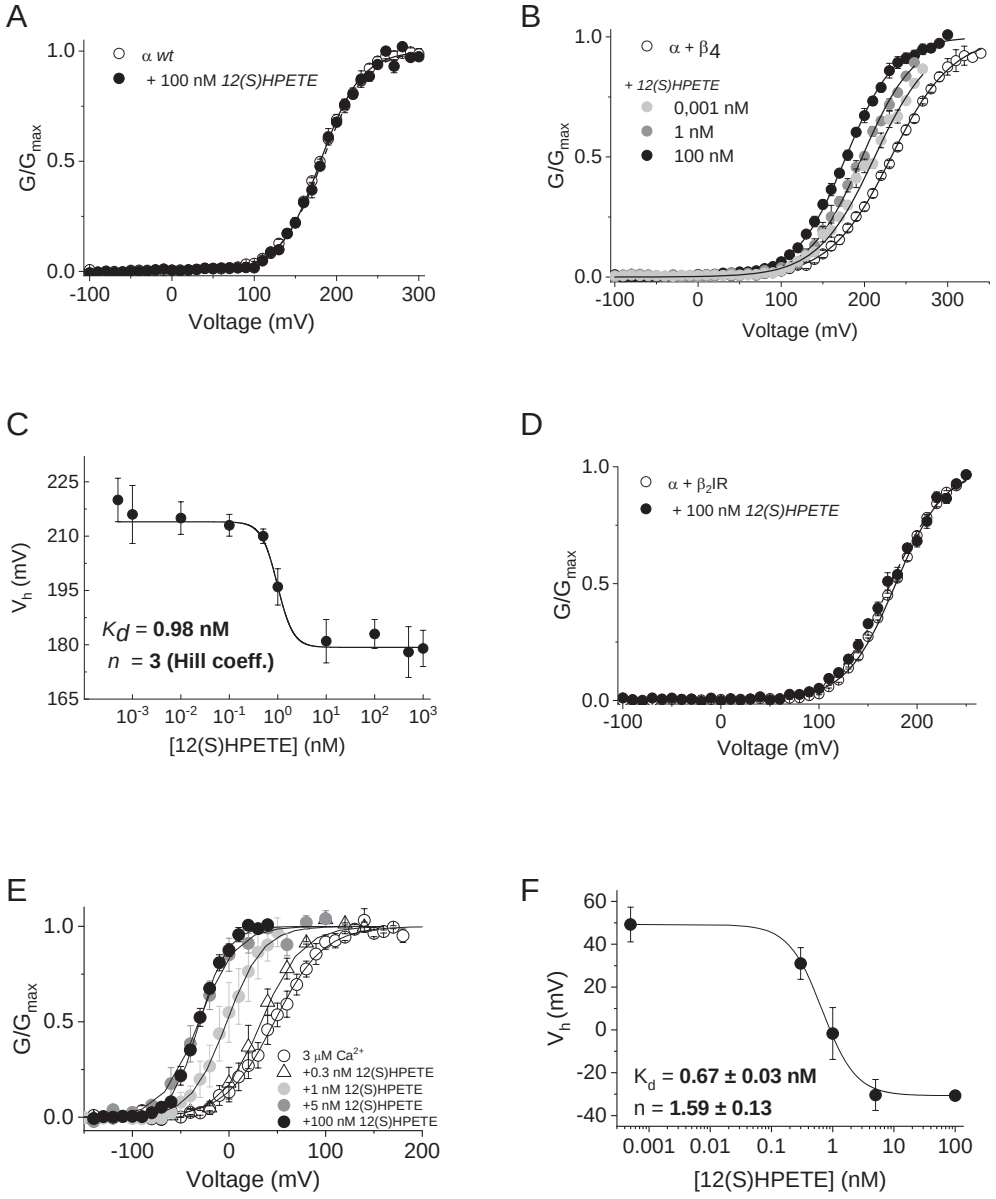


Fig. 3. BK channels containing β4 but not β2 subunit are directly activated by 12(S)HPETE. (*A*) Normalized I_{tail}-V relationship ($I_{tail}(V)$) for BK α channels before (white diamonds) or after (black diamonds) the addition of 12(S)HPETE (100 nM) to the cytoplasmic side in 0 $[Ca^{2+}]_i$. The I_{tail}(V) data (mean ± SEM) were fitted using a Boltzmann function (*Materials and Methods*). Fit parameters were V_h = 180 and 182 mV; z_δ = 1.02 and 0.98 before (n = 5) and after (n = 5) the addition of 12(S)HPETE, respectively. (*B*) Normalized $I_{tail}(V)$ (mean ± SEM) for BK $\alpha + \beta_4$ channels before (white hexagons) or after the addition of 12(S)HPETE at concentrations of 0.001 nM (black squares); 1 nM (black circles) or 100 nM (black triangles) to the internal side. Fit parameters were V_h = 233 mV and z_δ = 0.69, n = 7 (control); V_h = 217 mV and z_δ = 0.78, n = 4 (0.001 nM); V_h = 196 mV and z_δ = 0.81, n = 4 (1 nM); and V_h = 183 mV and z_δ = 0.76, n = 5 (100 nM). (*C*) Average V_h values obtained from the $I_{tail}(V)$ curves plotted against 12(S)HPETE concentration (mean ± SEM). Data were fitted using a Hill equation where $V_h = V_{max} + \frac{(V_0 - V_{max}) \times [HPETE]^n}{K^n + [HPETE]^n}$ where V_{max} is the half voltage in the absence of 12(S)HPETE, V_o is the half voltage at the indicated 12(S)HPETE concentration, K the dissociation constant, and n the Hill coefficient. 12(S)HPETE binding produces a leftward shift in V_h (ΔV_h) (n = 3 to 4). (*D*) Normalized I_{tail}-V (mean ± SEM) for BK $\alpha + \beta_2$IR channels before (white diamonds) or after (black diamonds) the addition of 100 nM 12(S)HPETE to the cytoplasmic side in 0 $[Ca^{2+}]_i$. Fit parameters were V_h = 178 and 174 mV; z_δ = 0.99 and 0.90 before (n = 4) and after (n = 4) the addition of 12(S)HPETE, respectively. (*E*) Normalized $I_{tail}(V)$ (mean ± SEM) for BK α + β4 channels, in the presence of 3 μM of Ca^{+2}, before (open circles) or after the addition of 12(S)HPETE at different concentrations. Data were fitted using a Boltzmann equation (*Materials and Methods*). The parameters were before the addition of 12(S)HPETE: V_h = 46.86 ± 1.12 mV, and zδ = 1.00 ± 0.04 e_0 (n = 3); 0.3 nM: V_h = 33.34 ± 1.31 mV, and zδ = 1.1 ± 0.06 e_0 (n = 3); 1 nM: V = −2.33 ± 1.25 mV, and zδ = 1.36 ± 006 (n = 3); 5 nM: V_h = −31.18 ± 1.99 mV, and zδ = 1.34 ± 0.12 (n = 3); 100 nM (n = 4): V = −30.33 ± 0.56 mV, and zδ = 1.77 ± 0.06 (n = 4). (*F*) Average V_h values obtained from the I_{tail}(V) curves plotted against 12(S)HPETE concentration (mean ± SEM) in the presence of 3 μM of Ca^{+2}. The V_{half} −[12(S)HPETE] data were fitted to a Hill equation as described in Fig. 3*C*.

activation by bath application of the agonist NS11021 or 12(S)HPETE has no effect on CA1 responses elicited by brief puffs of glutamate (monitored at −60 mV), a manipulation known to shortcut glutamate release (Fig. 4*A*). Moreover, bath application of the BK channel agonist NS11021 depressed isolated NMDA receptor (NMDAR)-mediated EPSCs (*Materials and Methods*) to an extent similar to that of AMPAR-mediated fEPSPs (Fig. 2*C*), consistent with a decrease in glutamate release (Fig. 4*B*). Additional observations further support a presynaptic localization of BKβ4 to regulate synaptic plasticity. First, when EPSCs and fast afterhyperpolarization current (I_{fAHP}) were recorded from the same CA1 pyramidal neuron, bath application of 12(S)HPETE induced depression of EPSC but had no effect on postsynaptic I_{fAHP} (Fig. 4*C*). Second, 12(S)HPETE-induced LTD was associated with an increase in failure rate in minimal stimulation experiments (Fig. 4*D*), an effect that was eliminated in the continuous presence

Downloaded from https://www.pnas.org by Andrés Eduardo Chávez on January 8, 2025 from IP address 186.78.166.3.

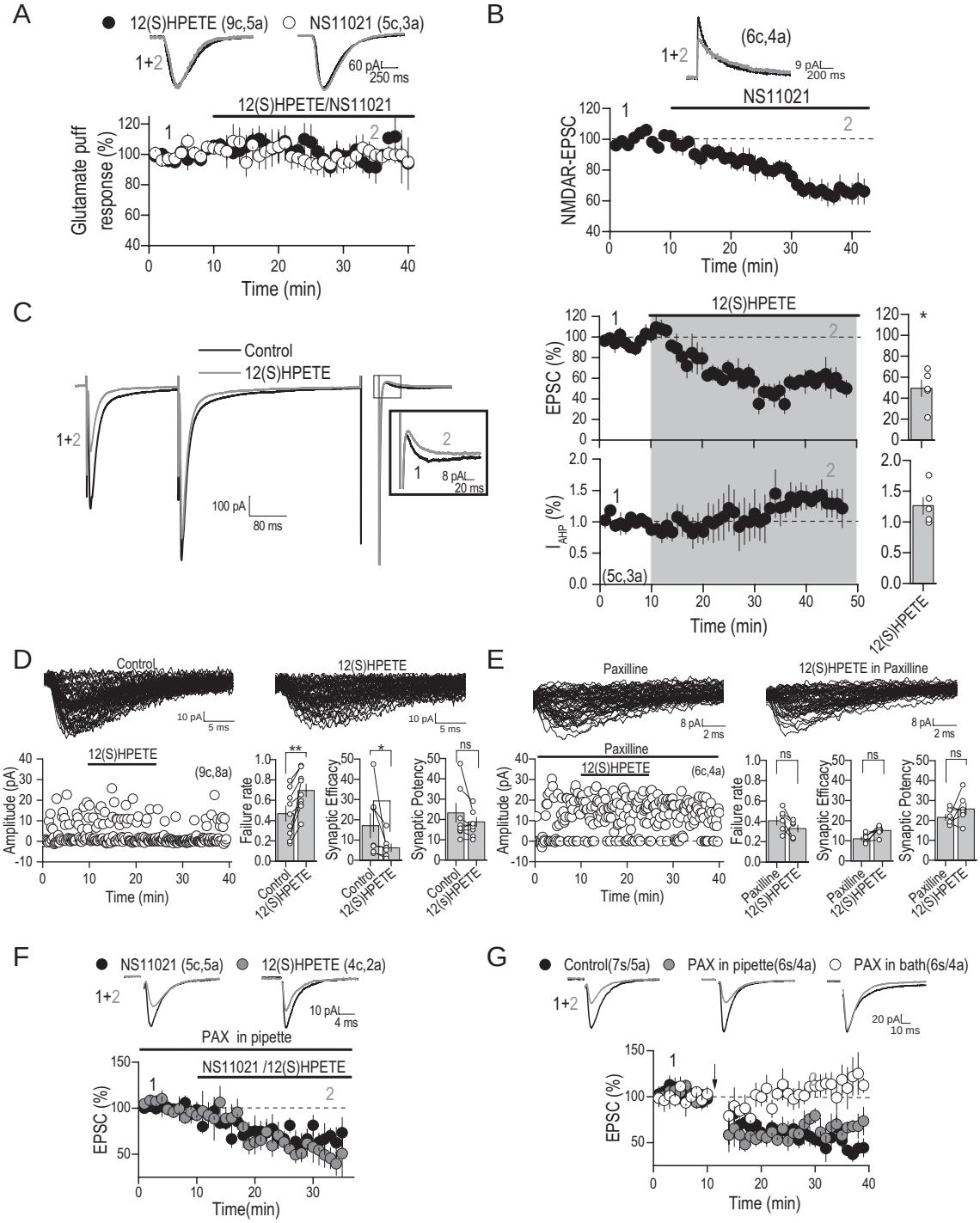


Fig. 4. Activation of BKβ4 is required for mGluR-LTD. (*A*) Average traces (*Top*) and time course (*Bottom*) showing that postsynaptic response to exogenous glutamate puff application (1 mM, 25 ms) was unaffected by bath application of BK channels agonist 12(S)HPETE (100 nM) and NS11021 (3 μM). (*B*) Average trace (*Top*) and time course (*Bottom*) showing that NS11021 induces a depression of isolated NMDAR-mediated currents in a similar way as to AMPAR-mediated currents. (*C*) Average trace (*Left*) and summarized graph (*Right*) showing that 12(S)HPETE (100 nM) decrease presynaptic neurotransmission (EPSC; *Top*) without affecting postsynaptic excitability (I_{fAHP}; *Bottom*) recorded at the same time from neonatal CA1 pyramidal neuron. (*D*) Individual traces (*Top*) and summarized graphs (*Bottom*) showing that 12(S)HPETE (100 nM) increased failure rate and decreased synaptic efficacy but had no effect on synaptic potency of minimal stimulation experiments in the CA1 area of the hippocampus, supporting a presynaptic mechanism of action. (*E*) Individual traces (*Top*) and time course (*Bottom*) showing that bath application of paxilline (10 μM) eliminated 12(S)HPETE-mediated increase in failure rate and decrease in synaptic efficacy, supporting that 12(S)HPETE effect is mediated by presynaptic BKβ4 channels. (*F*) Representative traces (*Top*) and time course (*Bottom*) showing that loading CA1 pyramidal neuron with paxilline (Pax; 10 μM) was not able to block NS11021- and 12(S)HPETE-induced synaptic depression. (*G*) Representative traces (*Top*) and time course (*Bottom*) showing that Pax in bath, but not intracellularly applied, is able to block LFS-induced LTD in the neonatal hippocampus. In all panels, data are presented as mean ± SEM, and averaged sample traces taken at times indicated by numbers are shown next to each summary plot and the numbers of cells (c) and animals (a) are indicated in parentheses. ns, no significant; * $P < 0.05$, ** $P < 0.01$.

of paxilline (Fig. 4*E*). Third, loading CA1 pyramidal cells with the BK channel blocker paxilline through the patch pipette, a manipulation known to reduce the excitability of CA1 pyramidal neurons (26, 27) (*SI Appendix*, Fig. S6 *A–C*), does not affect synaptic depression induced by either NS11021 or 12(S)HPETE (Fig. 4*F* and *SI Appendix*, Fig. S6*D*). Additionally, bath-applied

Downloaded from https://www.pnas.org by Andrés Eduardo Chávez on January 8, 2025 from IP address 186.78.166.3.

paxilline abolished LFS-induced mGluR-LTD, but intracellularly loaded paxilline (Fig. 4*G*) or cesium to block BK channels failed to prevent LTD (*SI Appendix*, Fig. S6*E*). Altogether, these results strongly suggest that presynaptic rather than postsynaptic BK channels are necessary for the induction of mGluR-LTD.

Discussion

Our findings reveal that BKβ4 channels are a crucial substrate involved in classical mGluR-LTD in the neonatal hippocampus and identify a form of lipids-derived retrograde modulation of synaptic function that involves an interaction between 12(S)HPETE and BK channels at central synapses. Notably, this modulation of synaptic strength mediated by BK channels is subunit specific as BKβ4, but not BKβ2, is activated in an activity-dependent manner to depress in a long-term manner CA3-CA1 excitatory synaptic transmission in the young hippocampus.

Multiple forms of retrograde signaling mediated by lipid messengers, including endocannabinoids and endovanilloids/eicosanoids, are known to modulate synaptic function and plasticity at central synapses, mainly by activating CB1 and TRPV1 receptors, respectively (28, 29). Now, we add to this repertoire that the lipoxygenase product from arachidonic acid, 12(S)HPETE, can directly bind and activate presumably presynaptic BK channels containing β4 subunit generating a long-lasting depression of transmitter release at CA3-CA1 excitatory synapses in the young hippocampus (*SI Appendix*, Fig. S7). Thus, our data, together with those indicating that retrograde regulation of potassium channels by arachidonic acid metabolites regulate synaptic plasticity at the CA3 area of the hippocampus (11), support the idea that lipid-derived metabolites and potassium channels interaction might play an important role in the mechanisms underlying hippocampal synaptic plasticity. An additional observation of our results is the input-specific effect of the retrograde modulation mediated by 12(S)HPETE in the hippocampus. While at excitatory CA3 to interneuron synapses, 12(S)HPETE acts through TRPV1 channels to regulate synaptic plasticity (7), our results demonstrated that at excitatory CA3-CA1 synapses BKβ4, but not TRPV1 channels are required to regulate synaptic plasticity. The differential reliance on BKβ4 versus TRPV1 depending on whether the postsynaptic target is pyramidal versus interneurons suggests that CA3 axon terminals may express specific receptor subtypes depending on the postsynaptic partner (*SI Appendix*, Fig. S3*C*). In addition, it is also unclear whether the retrograde modulation mediated by 12(S)HPETE could also be expressed at other synapse types within the neonatal brain and in the adult hippocampus. Interestingly, a functional interaction between TRPV1 and BK channels has been suggested in the peripheral nervous system (30). Whether this functional interaction also regulates central synapses remains unclear, and further investigation is necessary to understand when and how retrograde modulation by 12(S)HPETE regulates synaptic function through TRPV1 or BKβ4 channels.

Consistent with a retrograde modulation of synaptic function, we demonstrated that 12(S)HPETE acts on presynaptic BK channels (Fig. 4) despite their expression in postsynaptic compartments where they are known to regulate neuronal excitability (24, 31). While the differential activation of pre- vs postsynaptic BK channels by this lipid-derived remains unclear, it could be due to different β-subunits expressed in both neuronal compartments. For instance, it has been proposed that β4 subunits are present in CA3 pyramidal neurons (32, 33) and dentate granule cells in the dentate gyrus (24), whereas β2 are present in CA1 pyramidal neurons (34). Moreover, some reports indicate that subtypes of the BK channel, depending on their β subunits, can be differentially activated by lipids (35, 36) and also some hormones (37). Consistent with this idea, our results using heterologous expression demonstrate that BKβ4, but not a- and or BKβ2 channel, is directly modulated by 12(S)HPETE. Moreover, 12(S)HPETE-mediated retrograde suppression of synaptic function was blocked by paxilline but not by iberiotoxin, which blocks BKβ2 and aBK but not BKβ4 channels. Interestingly, at mature hippocampal synapses, the role of presynaptic BK channels can only be unmasked by blocking Kv channels and BK channels become sensitive to iberiotoxin (16), opening the possibility that developmental changes in the expression or quantity of β4 subunits may occur at presynaptic terminals during postnatal development to regulate synaptic function.

BK channels have been involved in some forms of short-term plasticity (32, 38), and our present results demonstrated its involvement in long-lasting depression in the neonatal hippocampus. While the exact mechanisms by which BK channels can generate a LTD vs a short-term plasticity is unknown, it is possible that the localization of BKβ4 at the presynaptic nerve terminal likely modulates both the amplitude and duration of depolarization evoked calcium influx limiting vesicle fusion at active zones and decreased neurotransmitter release (16, 18) in a long-term manner. It is also possible that changes in kinase/phosphatase balance downstream of BK activation might also be involved (12, 39, 40). Another possibility is the transient presence of some molecular mediator or pathway that interacts with the β4 auxiliary unit of the BK channel, as has been reported for some proteins in the postsynaptic domain (41). While further investigations are required to fully understand the contribution of presynaptic BK channels to regulate short vs long-term synaptic plasticity, it has been suggested that synaptic plasticity mechanisms have been implicated to synaptic maturation and circuitry formation (42). Particularly, LTD has been related to structural changes and a decrease in synaptic contacts (43, 44). Thus, a functional relevance of this BK-mediated plasticity can be related to the circuitry wiring, where LTD has been associated with pruning and a decrease in synaptic contacts (43, 44). Thus, synaptic plasticity could be relevant for establishing the hippocampal circuit, and BK channels could play a key role in its development, acting as a frequency filter, allowing high transmission rates to propagate but suppressing synapses that rely on low rates of transmission. In this way, BK channels may drive neuronal wiring in early development by enabling active synapses to undergo synaptic potentiation. However, whether BK channels' contribution to synaptic plasticity plays a role in synaptic wiring requires further investigations.

Materials and Methods

Hippocampal Slice Electrophysiology. Wild-type (WT) and TRPV1 null mice ($TRPV1^{-/-}$) were raised in the animal facility of the Universidad de Valparaiso and held at 20 to 25 °C under a 12-h light/dark cycle with water and food ad libitum. Animal handling and use followed a protocol approved by the bioethics committee of the Universidad de Valparaiso (CBC39/2022), in accordance with the bioethics and biosafety regulation of the Chilean Research Council (CONICYT).

Acute transverse hippocampal slices (400 μm thick) were prepared from Postnatal day (P) 7 to P13 mice of either gender as previously described (45, 46). Briefly, hippocampi were isolated and cutting using a DKT or Leica TS1200 vibratome in a solution containing the following (in mM): 215 sucrose, 2.5 KCl, 26 $NaHCO_3$, 1.6 NaH_2PO_4, 1 $CaCl_2$, 4 $MgCl_2$, 4 $MgSO_4$, and 20 glucose. After 30-min recovery, slices were incubated in an artificial CSF (ACSF) recording solution containing the following (in mM): 124 NaCl, 2.5 KCl, 26 $NaHCO_3$, 1 NaH_2PO_4, 2.5 $CaCl_2$, 1.3 $MgSO_4$, and 10 glucose equilibrated with 95% O_2/5% CO_2, pH 7.4. Slices were incubated for 30 min before recordings.

Downloaded from https://www.pnas.org by Andrés Eduardo Chávez on January 8, 2025 from IP address 186.78.166.3.

All experiments, except where indicated, were performed at 28 ± 1 °C in a submersion-type recording chamber perfused at 1 to 2 mL/min rate with ACSF supplemented with the $GABA_A$ receptor antagonist picrotoxin (PTX; 50 μM). Extracellular field potentials (fEPSPs) were recorded with a patch pipette filled with 1 mM NaCl and placed in the CA1 stratum radiatum (100 μm deep). Whole-cell voltage-clamp recordings (Multiclamp 700B Molecular Devices, USA) were made from CA1 pyramidal neurons voltage-clamped at −60 mV using patch-type pipette electrodes (3 to 4 M) containing the following intracellular solution (in mM): 131 Cs-gluconate, 8 NaCl, 1 $CaCl_2$, 10 EGTA, 10 glucose, 10 HEPES, pH 7.2, and 292 mmol/kg osmolality. For current clamp experiments, CA1 pyramidal neurons were recorded using a KCl-based intracellular solution (in mM): 130 KCl, 5 NaCl, 1 $MgCl_2$, 0.2 EGTA, 10 HEPES, 2 MgATP, and 0.1 NaGTP (adjusted to pH 7.2 with KOH).

fEPSPs and EPSCs were evoked by stimulating Schaffer collateral inputs with a monopolar electrode filled with ACSF and positioned ~100 to 150 μm away from the recording pipette. Two pulses (100 ms interstimulus interval) were used to calculate PPR that was defined as the ratio of the slope or amplitude of the second EPSP/EPSC to the slope or amplitude of the first EPSP/EPSC, respectively. The coefficient of variation ($1/CV^2$) was calculated as the squared mean EPSP/EPSC slope/amplitude divided by EPSP/EPSC variance. Both PPR and 1/CV were calculated 10 min before and 15 to 20 min after application of the LTD induction protocol. mGluR-LTD was evoked using a standard low-frequency stimulation (5 Hz, 900 pulses, 3 min) as previously described (2) or by bath application of 50 mM DHPG, a specific mGluR agonist. LFS- or DHPH-induced LTD was typically induced after 10 min of stable baseline and the magnitude of mGluR-LTD was compared 30 to 40 min after LTD protocol in the absence or presence of the pharmacological agents. In some experiments (Fig. 4*A*), puff application of L-glutamate (1 mM, 25 ms, 1 to 2 PSI bar) onto CA1 pyramidal neurons was delivered while neurons were voltage clamped at −60 mV. Reagents were obtained from Sigma, Tocris, and Ascent Scientific, prepared in stock solutions (water or DMSO), and added to the ACSF as needed. Total DMSO in the ACSF was maintained less than 0.01%. For whole cell experiments, series resistance (range, 8 to 12 MΩ) was monitored throughout the experiment with a 5 mV, 80 ms voltage step, and cells that exhibited significant change in series resistance (>20%) were excluded from analysis. Data were elicited at 15 to 20-s intervals, filtered at 2.2 kHz, and acquired at 10 kHz using a custom-made routine written in Igor Pro 6.37 (WaveMetrics, Portland, OR), whereas statistical comparisons were made using paired Student's *t* test at $P < 0.05$ significance level, using Origin 8.5 Pro software (OriginLab).

Channel Expression and Recordings. BK channels were expressed in *X. laevis* oocytes. The cDNA coding for the WT human BK α -subunit (Gen bank U11058), the human β_2-subunit (Gen bank AF099137) without inactivation domain (β_2IR) (47), and β_4-subunit (Gen Bank AF160967) were provided by L. Toro (University of California, Los Angeles, CA). The mRNA was prepared in vitro by using the mMESSAGE mMACHINE (Ambion) kit. The oocytes were injected with 50 ng of mRNA and incubated in an ND96 solution (96 mM NaCl, 2 mM KCl, 1.8 mM $CaCl_2$, 1 mM $MgCl_2$, and 5 mM HEPES, pH adjusted to 7.4 with NaOH) at 18 °C for 3 to 5 d before electrophysiological recordings. All the recordings were acquired by using the patch-clamp technique in the inside-out configuration. Data were acquired with an Axopatch 200B (Molecular Devices) amplifier and the Clampex 10 (Molecular Devices) acquisition software. Both, the voltage command, and current output were filtered at 10 kHz with an 8-pole Bessel low-pass filter (Frequency Devices). Current signals were sampled with a 16-bit A/D converter (Digidata 1550B; Molecular Devices), using a sampling rate of 500 kHz. Unless otherwise stated, linear membrane capacitance and leak subtraction were performed based on a P/-8 protocol (48). Borosilicate capillary glasses (1B150F-4, World Precision Instruments) were pulled in a horizontal pipette puller (Sutter Instruments). After fire-polishing, pipette resistance was typically 1 to 2 MΩ. An agar bridge with Cl^- as the main anion was used as the ground electrode. All experiments were performed at room temperature (18 to 20 °C).

Postassium currents (I_K) were elicited by 10-ms voltage steps of 10 mV, except for $\alpha + \beta_2$IR or $\alpha + \beta_4$ channel currents, that were elicited by 40-ms pulse durations. The holding voltage was -100 mV for all channels and the final voltage was 300 mV. The pipette and bath solutions were almost the same and typically contained 110 mM KOH, 10 mM HEPES, and 5 mM EGTA (free Ca^{2+} ~0.8 nM) (49), while the pipette external solution contained extra 2 mM $MgCl_2$. The pH for both cases was adjusted to 7.4 with about 108 mM $HMeSO_3$. For test solutions using Ca^{2+} (3 μM), $CaCl_2$ was added to reach the desired free [Ca^{2+}], and 2 mM EGTA was used as calcium buffer. Free calcium concentration was estimated using the WinMaxChelator Software and checked with a Ca^{2+}-electrode (Hanna Instruments).

Data Analysis. For ionic current experiments, the instantaneous $I_{tail,i}(V)$ data for each *i* experiment were fitted by using a Boltzmann function,

$$I_{tail,i}(V) = \frac{I_{tail,i,max}}{1 + e^{\left(\frac{-z\delta F\left(V - V_{h,i}\right)}{RT}\right)}}(X),$$

where $I_{tail,max}$ is the maximum tail current, $z\delta$ is the voltage dependency for channel activation, V_h is the half-activation voltage, T is the absolute temperature (294 K), F is the Faraday's constant, and R is the universal gas constant. The best values for $I_{tail,max}$, V_h, and $z\delta$ were determined by using the Matlab´s function *lsqnonlin*. The averaged half activation voltage ($< V_h >$) and the averaged voltage dependency ($< z\delta >$) were reported as mean ± SEM of the *n* experiments. Each individual $I_{tail,i}(V)$ curve was normalized by dividing by its specific $I_{tail,i,max}$ value and then aligned by shifting along the voltage axis by $\left(< V_h > - V_{h,i} \right)$. A further shift of the $I_{tail,i}(V)$ curves was done by rounding each voltage value to the nearest ten. This procedure allowed generating an averaged $I_{tail,i}(V)$ curve with a voltage dependence representative of the *n* experiments (50).

Data, Materials, and Software Availability. All study data are included in the article and/or *SI Appendix*.

ACKNOWLEDGMENTS. This work was supported by the Chilean government through FONDECYT Regular #1201848 (A.E.C.), #1230265 (R.L.), #1171840 (C.Q.C.), ANID Millennium Science Initiative Program (P09-022F to R.L, C.Q.C., and A.E.C.), and the National Institute Award RO1GM030376 (R.L.). C.A.-G. and A.A. were supported by PhD fellowship from ANID #21201603 (C.A.-G.) and #21202136 (A.A.). R.C.M. was supported by ANID-FONDECYT postdoctorado Grant #3190793.

Author affiliations: [a]Programa de Doctorado en Ciencias Mención Neurociencia, Facultad de Ciencias, Universidad de Valparaíso, Valparaíso 2340000, Chile; and [b]Instituto de Neurociencias, Centro Interdisciplinario de Neurociencia de Valparaíso, Facultad de Ciencias, Universidad de Valparaíso, Valparaíso 2340000, Chile

1. C. Luscher, K. M. Huber, Group 1 mGluR-dependent synaptic long-term depression: Mechanisms and implications for circuitry and disease. *Neuron* **65**, 445–459 (2010).
2. S. J. Feinmark *et al.*, 12-lipoxygenase metabolites of arachidonic acid mediate metabotropic glutamate receptor-dependent long-term depression at hippocampal CA3-CA1 synapses. *J. Neurosci.* **23**, 11427–11435 (2003).
3. V. Y. Bolshakov, S. A. Siegelbaum, Postsynaptic induction and presynaptic expression of hippocampal long-term depression. *Science* **264**, 1148–1152 (1994).
4. V. Y. Bolshakov, S. A. Siegelbaum, Regulation of hippocampal transmitter release during development and long-term potentiation. *Science* **269**, 1730–1734 (1995).
5. R. C. Hardie, TRP channels and lipids: From *Drosophila* to mammalian physiology. *J. Physiol.* **578**, 9–24 (2007).
6. F. J. Taberner *et al.*, TRP channels interaction with lipids and its implications in disease. *Biochim. Biophys. Acta* **1848**, 1818–1827 (2015).
7. H. E. Gibson *et al.*, TRPV1 channels mediate long-term depression at synapses on hippocampal interneurons. *Neuron* **57**, 746–759 (2008).
8. L. M. Boland, M. M. Drzewiecki, Polyunsaturated fatty acid modulation of voltage-gated ion channels. *Cell Biochem. Biophys.* **52**, 59–84 (2008).
9. M. L. Roberts-Crowley *et al.*, Regulation of voltage-gated Ca^{2+} channels by lipids. *Cell Calcium* **45**, 589–601 (2009).
10. A. Besana, R. B. Robinson, S. J. Feinmark, Lipids and two-pore domain K^+ channels in excitable cells. *Prostaglandins Other Lipid Mediat.* **77**, 103–110 (2005).
11. M. Carta *et al.*, Membrane lipids tune synaptic transmission by direct modulation of presynaptic potassium channels. *Neuron* **81**, 787–799 (2014).
12. C. Ancaten-Gonzalez *et al.*, Ca(2+)- and voltage-activated K(+) (BK) channels in the nervous system: One gene, a myriad of physiological functions. *Int. J. Mol. Sci.* **24**, 3407 (2023).
13. J. R. Montgomery, A. L. Meredith, Genetic activation of BK currents in vivo generates bidirectional effects on neuronal excitability. *Proc. Natl. Acad. Sci. U.S.A.* **109**, 18997–19002 (2012).
14. M. H. Zink *et al.*, 12-lipoxygenase in porcine coronary microcirculation: Implications for coronary vasoregulation. *Am. J. Physiol. Heart Circ. Physiol.* **280**, H693–H704 (2001).

Downloaded from https://www.pnas.org by Andrés Eduardo Chávez on January 8, 2025 from IP address 186.78.166.3.

15. F. M. Faraci *et al.*, Arachidonate dilates basilar artery by lipoxygenase-dependent mechanism and activation of K(+) channels. *Am. J. Physiol. Regul. Integr. Comp. Physiol.* **281**, R246–R253 (2001).
16. H. Hu *et al.*, Presynaptic Ca^{2+}-activated K^+ channels in glutamatergic hippocampal terminals and their role in spike repolarization and regulation of transmitter release. *J. Neurosci.* **21**, 9585–9597 (2001).
17. H. Misonou *et al.*, Immunolocalization of the Ca^{2+}-activated K^+ channel Slo1 in axons and nerve terminals of mammalian brain and cultured neurons. *J. Comp. Neurol.* **496**, 289–302 (2006).
18. G. Raffaelli *et al.*, BK potassium channels control transmitter release at CA3-CA3 synapses in the rat hippocampus. *J. Physiol.* **557**, 147–157 (2004).
19. C. A. Sailer *et al.*, Immunolocalization of BK channels in hippocampal pyramidal neurons. *Eur. J. Neurosci.* **24**, 442–454 (2006).
20. V. Y. Bolshakov, S. A. Siegelbaum, Hippocampal long-term depression: Arachidonic acid as a potential retrograde messenger. *Neuropharmacology* **34**, 1581–1587 (1995).
21. S. S. Zakharenko, L. Zablow, S. A. Siegelbaum, Altered presynaptic vesicle release and cycling during mGluR-dependent LTD. *Neuron* **35**, 1099–1110 (2002).
22. M. Normandin *et al.*, Involvement of the 12-lipoxygenase pathway of arachidonic acid metabolism in homosynaptic long-term depression of the rat hippocampus. *Brain Res.* **730**, 40–46 (1996).
23. C. A. Rice, R. W. Stackman Jr., The small conductance Ca(2+)-activated K(+) channel activator GW542573X impairs hippocampal memory in C57BL/6J mice. *Neuropharmacology* **252**, 109960 (2024).
24. R. Brenner *et al.*, BK channel beta4 subunit reduces dentate gyrus excitability and protects against temporal lobe seizures. *Nat. Neurosci.* **8**, 1752–1759 (2005).
25. C. Contet *et al.*, BK channels in the central nervous system. *Int. Rev. Neurobiol.* **128**, 281–342 (2016).
26. J. Zhang *et al.*, Glutamate-activated BK channel complexes formed with NMDA receptors. *Proc. Natl. Acad. Sci. U.S.A.* **115**, E9006–E9014 (2018).
27. Y. Zhou, C. J. Lingle, Paxilline inhibits BK channels by an almost exclusively closed-channel block mechanism. *J. Gen. Physiol.* **144**, 415–440 (2014).
28. P. E. Castillo *et al.*, Endocannabinoid signaling and synaptic function. *Neuron* **76**, 70–81 (2012).
29. W. G. Regehr, M. R. Carey, A. R. Best, Activity-dependent regulation of synapses by retrograde messengers. *Neuron* **63**, 154–170 (2009).
30. Y. Wu *et al.*, TRPV1 channels are functionally coupled with BK(mSlo1) channels in rat dorsal root ganglion (DRG) neurons. *PLoS ONE* **8**, e78203 (2013).
31. M. S. Hunsberger, M. Mynlieff, BK potassium currents contribute differently to action potential waveform and firing rate as rat hippocampal neurons mature in the first postnatal week. *J. Neurophysiol.* **124**, 703–714 (2020).
32. P. Y. Deng *et al.*, FMRP regulates neurotransmitter release and synaptic information transmission by modulating action potential duration via BK channels. *Neuron* **77**, 696–711 (2013).
33. S. Shruti *et al.*, The brain-specific Beta4 subunit downregulates BK channel cell surface expression. *PLoS ONE* **7**, e33429 (2012).
34. L. R. Shao *et al.*, The role of BK-type Ca^{2+}-dependent K^+ channels in spike broadening during repetitive firing in rat hippocampal pyramidal cells. *J. Physiol.* **521**, 135–146 (1999).
35. T. Hoshi *et al.*, Mechanism of the modulation of BK potassium channel complexes with different auxiliary subunit compositions by the omega-3 fatty acid DHA. *Proc. Natl. Acad. Sci. U.S.A.* **110**, 4822–4827 (2013).
36. A. M. Dopico, A. N. Bukiya, Lipid regulation of BK channel function. *Front. Physiol.* **5**, 312 (2014).
37. J. T. King *et al.*, Beta2 and beta4 subunits of BK channels confer differential sensitivity to acute modulation by steroid hormones. *J. Neurophysiol.* **95**, 2878–2888 (2006).
38. T. Zaman *et al.*, BK channels mediate synaptic plasticity underlying habituation in rats. *J. Neurosci.* **37**, 4540–4551 (2017).
39. A. G. Leenders, Z. H. Sheng, Modulation of neurotransmitter release by the second messenger-activated protein kinases: Implications for presynaptic plasticity. *Pharmacol. Ther.* **105**, 69–84 (2005).
40. P. E. Castillo, Presynaptic LTP and LTD of excitatory and inhibitory synapses. *Cold Spring Harb. Perspect. Biol.* **4**, a005728 (2012).
41. C. Lohmann, H. W. Kessels, The developmental stages of synaptic plasticity. *J. Physiol.* **592**, 13–31 (2014).
42. S. Chaudhury *et al.*, Activity-dependent synaptic plasticity modulates the critical phase of brain development. *Brain Dev.* **38**, 355–363 (2016).
43. N. Becker *et al.*, LTD induction causes morphological changes of presynaptic boutons and reduces their contacts with spines. *Neuron* **60**, 590–597 (2008).
44. C. Piochon, M. Kano, C. Hansel, LTD-like molecular pathways in developmental synaptic pruning. *Nat. Neurosci.* **19**, 1299–1310 (2016).
45. A. E. Chavez, C. Q. Chiu, P. E. Castillo, TRPV1 activation by endogenous anandamide triggers postsynaptic long-term depression in dentate gyrus. *Nat. Neurosci.* **13**, 1511–1518 (2010).
46. A. E. Chavez *et al.*, Compartment-specific modulation of GABAergic synaptic transmission by TRPV1 channels in the dentate gyrus. *J. Neurosci.* **34**, 16621–16629 (2014).
47. M. Wallner, P. Meera, L. Toro, Molecular basis of fast inactivation in voltage and Ca^{2+}-activated K^+ channels: A transmembrane beta-subunit homolog. *Proc. Natl. Acad. Sci. U.S.A.* **96**, 4137–4142 (1999).
48. C. M. Armstrong, F. Bezanilla, Currents related to movement of the gating particles of the sodium channels. *Nature* **242**, 459–461 (1973).
49. D. H. Cox, J. Cui, R. W. Aldrich, Separation of gating properties from permeation and block in MSLO large conductance Ca-activated K^+ channels. *J. Gen. Physiol.* **109**, 633–646 (1997).
50. F. T. Horrigan, R. W. Aldrich, Coupling between voltage sensor activation, Ca^{2+} binding and channel opening in large conductance (BK) potassium channels. *J. Gen. Physiol.* **120**, 267–305 (2002).

Downloaded from https://www.pnas.org by Andrés Eduardo Chávez on January 8, 2025 from IP address 186.78.166.3.

scientific reports

Check for updates

OPEN

Impact of KDM6B mosaic brain knockout on synaptic function and behavior

Bastian Brauer[1,7], Carlos Ancatén-González[2,3,7], Constanza Ahumada-Marchant[1], Rodrigo C. Meza[3], Nicolas Merino-Veliz[1], Gino Nardocci[4,5], Lorena Varela-Nallar[1,6], Gloria Arriagada[1], Andrés E. Chávez[3]✉ & Fernando J. Bustos[1,6]✉

Autism spectrum disorders (ASD) are complex neurodevelopmental conditions characterized by impairments in social communication, repetitive behaviors, and restricted interests. Epigenetic modifications serve as critical regulators of gene expression playing a crucial role in controlling brain function and behavior. Lysine (K)-specific demethylase 6B (KDM6B), a stress-inducible H3K27me3 demethylase, has emerged as one of the highest ASD risk genes, but the precise effects of *KDM6B* mutations on neuronal activity and behavioral function remain elusive. Here we show the impact of KDM6B mosaic brain knockout on the manifestation of different autistic-like phenotypes including repetitive behaviors, social interaction, and significant cognitive deficits. Moreover, KDM6B mosaic knockout display abnormalities in hippocampal excitatory synaptic transmission decreasing NMDA receptor mediated synaptic transmission and plasticity. Understanding the intricate interplay between epigenetic modifications and neuronal function may provide novel insights into the pathophysiology of ASD and potentially inform the development of targeted therapeutic interventions.

Keywords KDM6B, ASD, Gene editing, NMDA, Behavior

Autism spectrum disorders (ASD) and neurodevelopmental disorders are a group of clinically heterogeneous conditions that are characterized by changes in social skills, attention deficits, hyperactivity and cognition. These disorders can cause difficulties with social communication and interaction, as well as restricted, repetitive, and stereotyped patterns of behavior[1]. People with ASD often have co-occurring conditions including epilepsy, depression, anxiety, and hyperactivity[2], having significant impact on the individual's everyday life. The complexity and heterogeneity of ASD pathogenesis is mainly due to the large number of ASD-related genetic variations including copy number variants, single nucleotide polymorphism, deletions and duplications according to SFARI gene database[3]. Moreover, the target gene function is quite diverse leading to abnormalities in neuronal communication, cytoskeleton formation and dynamics, chromatin regulation, and gene expression[4–8]. Over the last decade, special emphasis has been given to mutations in chromatin regulating genes where new gene variants have been described that could explain the genetic complexity of ASD[9]. However, the precise mechanisms through which these mutations contribute to ASD phenotypes remain largely elusive.

Several studies have focused on unraveling the role that mutations or knockout (KO) of chromatin associated genes have on the appearance of ASD phenotypes, including Chromodomain helicase DNA binding protein 8 (CHD8), Lysine demethylase 6A (KDM6A), and Lysine methyltransferase 2C (KMT2C)[10–12]. Recently, one of the largest whole exome sequencing studies, showed that one of the highest risk genes for ASD is lysine demethylase 6b (KDM6B), also known as JMJD3 (Jumonji domain-containing protein-3)[9]. KDM6B functions as a histone tail demethylase specifically targeting histone H3 lysine 27 trimethylation (H3K27me3)[13]. In its role as a demethylase of H3K27, it counteracts the repressive function of the Polycomb repressive complex 2 (PRC2)[14],

[1]Constantine-Paton Research Laboratory, Instituto de Ciencias Biomédicas, Facultad de Medicina y Facultad de Ciencias de la Vida, Universidad Andres Bello, Santiago, Chile. [2]Programa de Doctorado en Ciencias, Mención Neurociencia, Universidad de Valparaíso, Valparaíso, Chile. [3]Instituto de Neurociencias, Centro Interdisciplinario de Neurociencia de Valparaíso (CINV), Facultad de Ciencias, Universidad de Valparaíso, 2340000 Valparaiso, Chile. [4]School of Medicine, Faculty of Medicine, Universidad de los Andes, Santiago, Chile. [5]Molecular Biology and Bioinformatics Lab, Program in Molecular Biology and Bioinformatics, Center for Biomedical Research and Innovation (CIIB), Universidad de Los Andes, Santiago, Chile. [6]Millennium Nucleus of Neuroepigenetics and Plasticity (EpiNeuro), Santiago, Chile. [7]These authors contributed equally: Bastian Brauer and Carlos Ancatén-González. ✉email: andres.chavez@uv.cl; fernando.bustos@unab.cl

thereby facilitating the induction of gene expression[15]. KDM6B has been widely studied for its role associated with cancer aggressiveness and progression, as well as its involvement in brain neurogenesis, neuron differentiation, maturation, survival, and in neurological disorders[16–19]. Full KDM6B KO animals die at birth due to respiratory deficits[20], thus most studies have used conditional or heterozygous animals. Heterozygous KDM6B KO mice reportedly display hyperactivity, social and cognitive deficits[21]. However, the synaptic mechanisms underlying these observed behaviors were not investigated[21]. Using conditional KO in cerebellar granule neurons, it has been shown that the correct control and dynamics of H3K27me3 deposition is needed for neuronal maturation[22]. In addition, conditional knockout of KDM6B in excitatory neurons causes loss of synaptic activity, spine density, and synaptic vesicle number likely by dysregulation of VGLUT1/2 gene expression[21,21].

Given its critical role in regulating chromatin structure and gene transcription, dysregulation of KDM6B has been implicated in various neurodevelopmental disorders, including ASD [21,24,25]. Human genetic studies have identified over 130 likely pathogenic rare variants in the *KDM6B* gene, highlighting its significance in neurodevelopment, however only 3 confirmed variants with ASD phenotype have been validated[3]. Notably, studies of more than 85 variants across the *KDM6B* gene in humans have shown a myriad of phenotypes. However, a common denominator in all of them is the presence of cognitive deficits[26]. This underscores the importance of gaining insight into the mechanisms and behavioral outcomes of KDM6B mutations and how they relate to autistic-like behaviors and brain function.

Here we utilized the CRISPR/Cas9 system delivered via AAV to create a whole-brain mosaic knockout (mKO) of *Kdm6b* at postnatal day 1, with the aim of investigating its role in controlling behavior and the functional consequence on synaptic mechanisms associated with these behaviors. As anticipated, KDM6B mKO animals exhibited reduced KDM6B expression, consequently leading to an increase in H3K27me3. Additionally, we observed hyperactivity, repetitive behaviors, social impairment, and cognitive deficits. Notably, these findings correlate with a significant impairment of synaptic plasticity in the hippocampus, and more specifically a significant disruption in NMDA receptor (NMDAR)-mediated excitatory post-synaptic currents, which may underlie the observed cognitive effects. Our results demonstrate the feasibility of modeling *Kdm6b* loss-of-function mutations using CRISPR/Cas9, providing an additional platform to study the cellular and molecular mechanisms underlying mutations associated with ASD.

Results

Editing of the *Kdm6b* gene to generate mosaic brain knockout

To elucidate the role of KDM6B in the pathogenesis of ASD, we employed the CRISPR/Cas9 system to knock out its expression in cultured neurons and animal brain, as previously described[10,27,28]. We designed four sgRNAs targeting exon 6 of *Kdm6b* (Fig. 1A), considering its conservation across all isoforms. These sgRNAs (KDM6B KO1-4) were tested in cultured neurons from Cas9KI animals transducing with AAVs coding for CRISPR/Cas9 at 3 days in vitro (DIV). At 10 DIV, RT-qPCR from these neurons was conducted to assess KO efficiency revealing that all of them downregulated *Kdm6b* expression (Fig. 1B). KDM6B KO4 showed the best efficiency downregulating KDM6B expression in vitro by approximately 70%. Subsequently, we utilized this sgRNA to conduct our in vivo experiments.

To evaluate whether CRISPR/Cas9 induced *Kdm6b* KO produces autistic-like behaviors and explore potential underlying mechanisms, we utilized intracerebroventricular delivery of AAV encoding KDM6B KO4 and TdTomato as fluorescence marker to determine transduction efficiency. This methodology ensures efficient transduction of brain cells as previously described[10,27,28]. Cas9KI animals received injections at P1 to produce KDM6B mKO, and behavioral testing started at eight weeks. For inclusion in the analyses, animals had to meet three criteria: 1. Display a widespread fluorescent label throughout the entire brain, 2. Exhibit a positive T7 endonuclease I assay confirming gene editing, and 3. Demonstrate a reduction in KDM6B expression of at least 50%. Nine control and KDM6B mKO animals met the criteria and were included in the final analyses. Following behavioral or electrophysiological analyses, animals were imaged to determine transduction efficiency, revealing widespread transduction including CA1, CA3 and DG in the hippocampus (Fig. 1C). Using hippocampal tissue from transduced animals, the T7 endonuclease I assay for gene editing showed that all nine KDM6B mKO animals were positive for editing at the locus (Fig. 1D). Furthermore, RT-qPCR revealed that transduced animals exhibited an approximate 70% reduction in mRNA levels (Fig. 1E), and western blot analyses of mKO animals show a significant reduction in KDM6B protein expression (Fig. 1F). In addition, digital PCR assay shows a significant reduction in the number of copies of KDM6B cDNA in hippocampal tissue of KDM6B mKO animals (Fig. 1G), confirming the reduction of the expression of *Kdm6b* after gene editing.

KDM6B is an enzyme responsible for catalyzing histone H3 lysine 27 demethylation, leading to the activation of gene targets, counteracting the repressive role of the PRC2 complex[13,15]. Consequently, we hypothesized that knocking out *Kdm6b* would result in an increase in total H3K27me3 in brain tissue. As anticipated, our observations confirmed that KDM6B mKO animals exhibit a global increase in this histone tail modification (Fig. 1H-I). These results indicate that our strategy targeting *Kdm6b* can efficiently reduce its expression in the entire brain and consequently increase global H3K27me3.

KDM6B mKO animals show hyperactivity and repetitive behaviors

It has been demonstrated that heterozygous KDM6B animals exhibit behaviors resembling those observed in ASD, including reduced anxiety[21]. Furthermore, studies using KDM6B conditional KO animals have shown impaired memory but no signs of anxiety[23]. Our approach to knocking out KDM6B in the animal brain to produce KDM6B mKO helps us study behaviors and could help shed light on the mechanisms behind KDM6B loss-of-function mutations. Eight weeks after infection, both control (tdTomato injected) and KDM6B mKO animals were subjected to a battery of behavioral tests. First, we examined the locomotion activity of KDM6B

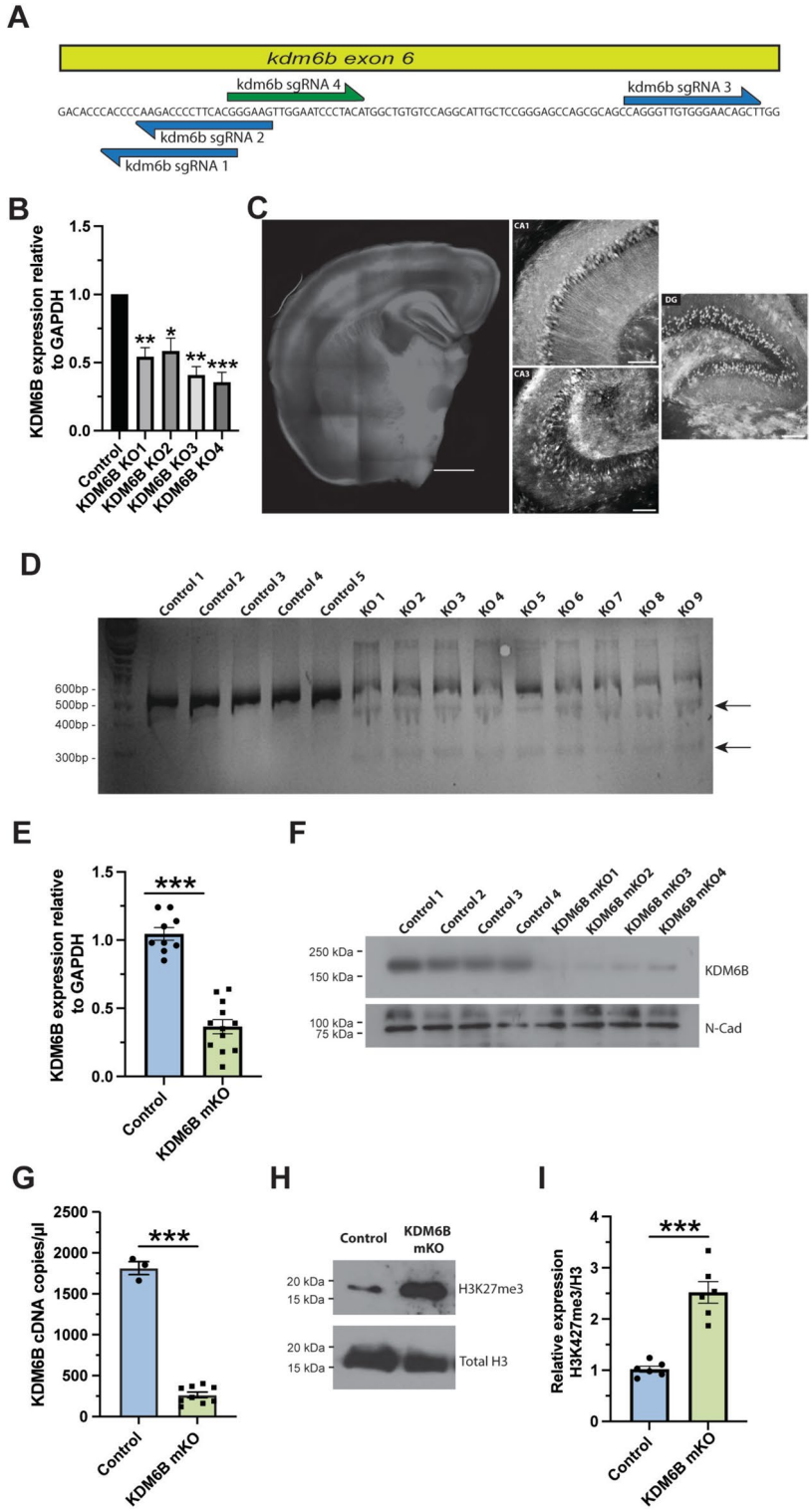


Fig. 1. Knockout of *Kdm6b* by gene editing. (**A**) Scheme showing exon 6 of *Kdm6b* genomic sequence and the position where the designed sgRNAs bind to the genomic sequence. In green is sgRNA-4 that is used for all in vivo experiments. (**B**) Cultured cortical neurons were transduced with sgRNAs and Cas9 to determine sgRNA efficiency. At 10 DIV RT-qPCR was conducted to determine expression levels of KDM6B relative to GAPDH. (**C**) Representative image of brain slice and high magnification of CA1, CA3 and DG of the hippocampus after transduction by intracerebroventricular injection of CRISPR/Cas9. (**D**) T7 endonuclease I assay from transduced cortical tissue of injected animals. (**E**) RT-qPCR to determine expression levels of KDM6B relative to GAPDH in transduced cortical tissue of injected animals. (**F**) Representative western blot of KDM6B and N-Cadherin as loading control in WT and KDM6B mKO animals. (**G**) Digital PCR assay to determine KDM6B cDNA copies/µl in WT and KDM6B mKO animals (WT n = 3; KDM6B mKO n = 9) (**H**) Representative image of western blot analysis of total H3 histone, and H3K27me3. (**I**) Quantification of the relative expression of H3K27me3 from cortical tissue extracted from 6 control or KDM6B mKO animals**.** Bars represents mean ± SEM; $*p < 0.05$, $**p < 0.01$, $***p < 0.001$. Students t-test was used to determine significance compared to control condition. Scale bar = 1000µm and 100µm for high magnification images.

mKO animals using the accelerated rotarod apparatus. We found that KDM6B mKO animals spent more time on the rotarod than control animals (Fig. 2A). The presence of anxiety-like behaviors is recognized as a distinctive feature in both human and animal cases of ASD[1,10,27,29,30]. Therefore, we investigated whether KDM6B mKO animals exhibited this phenotype. Using the open field test, we allowed the animals to freely explore for 10 min and measured their location and movements in the arena (Fig. 2B). Like the rotarod test, KDM6B mKO animals traveled a significantly longer distance than control animals in the arena (Fig. 2C). However, KDM6B mKO animals spent a similar amount of time than control animals in the center of the arena (Fig. 2D) and in the periphery (Fig. 2E), indicating that KDM6B mKO animals do not exhibit anxiety behaviors. To confirm this finding, we conducted the light and dark, and zero maze tests. In the light–dark apparatus, animals were placed in the dark box and allowed to explore for 10 min (Fig. 3A). The test revealed no differences in total entries (Fig. 3B) or time spent (Fig. 3C) in the illuminated zone between KDM6B mKO and controls. However, we did find a significant difference in the distance traveled in the illuminated zone (Fig. 3D). Moreover, in the zero maze (Fig. 3E), KDM6B mKO and control animals spent a similar amount of time in the open zone (Fig. 3F) but KDM6B mKO mice exhibited an increased number of entries to the open zone compared to control animals (Fig. 3G). Such difference can be attributed to the hyperactivity displayed by the animals, leading them to cover longer distances and enter open zones more frequently. Then, animals underwent the marble burying test to assess repetitive behaviors and anxiety where KDM6B mKO animals buried a significantly greater number of marbles compared to control animals (Fig. 3H). Lastly, when grooming episodes were quantified, KDM6B mKO animals displayed a significantly higher count of grooming episodes compared to control animals (Fig. 3I). Altogether these findings suggest that KDM6B mKO animals exhibit limited anxiety as shown in the marble burying test and in addition animals show significant hyperactivity and repetitive behaviors.

KDM6B mKO animals exhibit deficiencies in social behaviors

Given that individuals with ASD commonly face challenges in social interaction, often demonstrating a deficit or lack of proficiency in engaging socially[1,29], we sought to assess the social interaction capabilities of KDM6B mKO mice. We started by analyzing the behavior of animals in the tube dominance test to determine social hierarchy and interaction between animals. Test revealed that KDM6B mKO animals win the challenge significantly more times that the control animals in days 1–4 (Fig. 4A), showing an increase in social dominance behavior. Next, we employed the 3-chamber social interaction test to assess the capacity for social interaction, allowing the animals to interact in the chambers for 10 min. While control animals spent a greater amount of time interacting with the novel animal compared to the object, KDM6B mKO animals spent similar amounts of time interacting with both the novel animal and the object (Fig. 4B), indicating a social deficit in mutant mice. To better understand

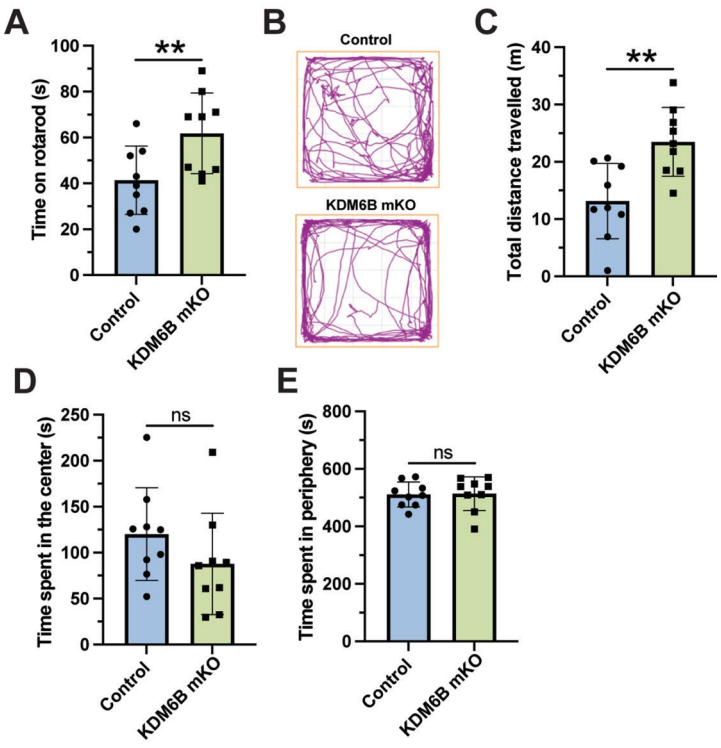


Fig. 2. Hyperactivity in KDM6B mKO animals. (**A**) Time spent on the rotarod apparatus. (**B**) Representative trace plots of open field test in Control and KDM6B mKO animals. (**C–E**) Quantification of the total distance travelled (**C**), time spent in the center area (**D**), time spent in the periphery (**E**). Bars represents mean ± SEM. Students t-test was used to determine significance compared to control condition. $^{**}p < 0.01$, n = 9 animals for Control and KDM6B mKO animals. ns = non-significant.

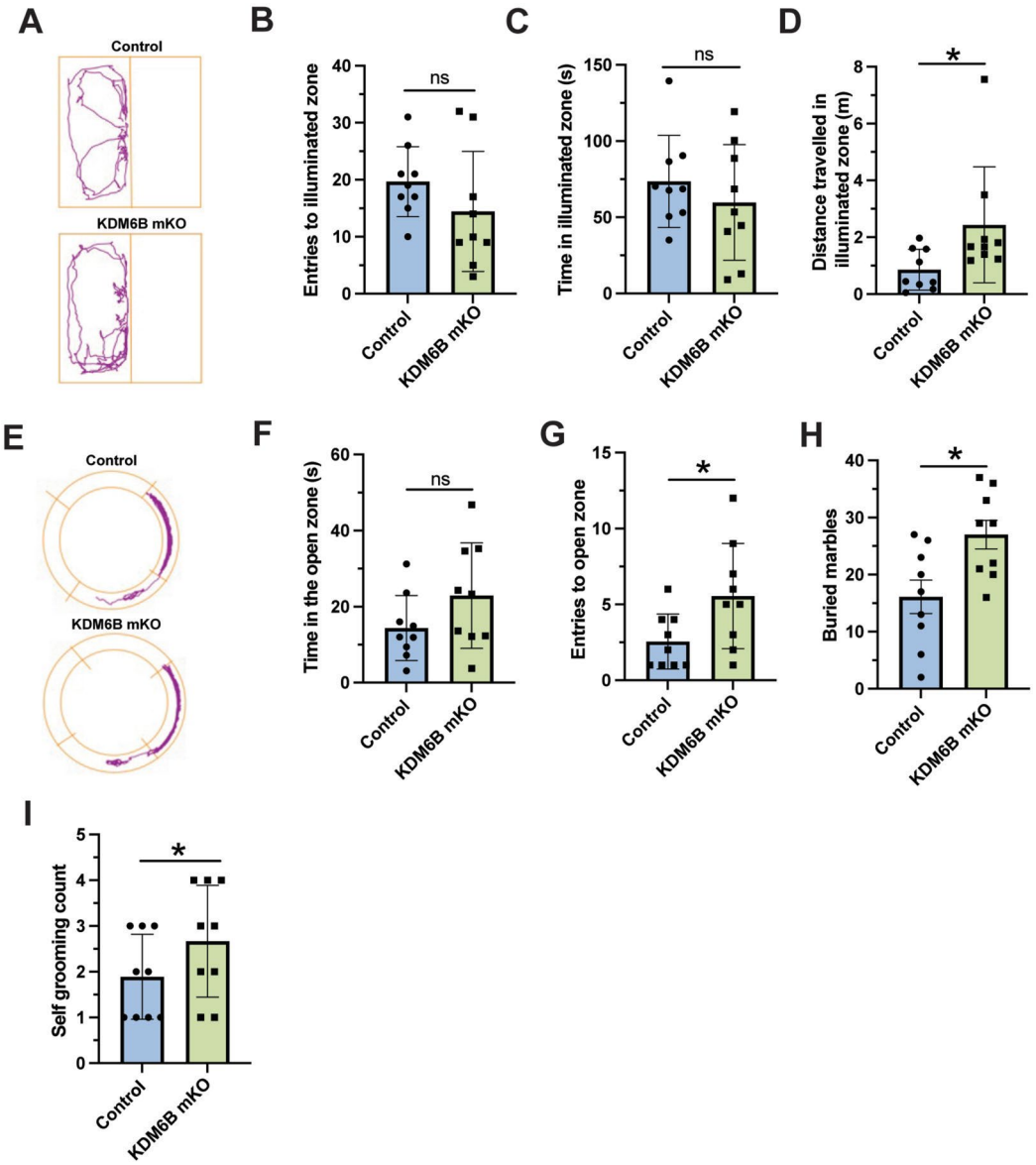


Fig. 3. KDM6B mKO animals display repetitive behaviors. (**A**) Representative trace plots of dark and light test (top = Control; bottom = KDM6B mKO). (**B–D**) Quantification of the number of entries to illuminated zone (**B**), the time spent in the illuminated zone (**C**), and the distance travelled in the illuminated zone (**D**). (**E**) Representative trace plots of the zero-maze test (top = Control; bottom = KDM6B mKO). (**F–G**) Quantification of the time spent in the open zone (**F**), and the total entries to the open zone (**G**) in the zero maze. (**H**) Quantification of the number of marbles buried during the marble burying test. (**I**) Quantification of the self-grooming behavior shown by Control or KDM6B mKO animals. Bars represents mean ± SEM. Students t-test was used to determine significance compared to control condition. $*p < 0.05$, n = 9 animals for Control and KDM6B mKO animals. ns = non-significant.

the social deficits observed in the 3-chamber test, we employed the direct social interaction paradigm. During this test, KDM6B mKO and control animals were given the opportunity to interact within a clear box for 10 min, and their interactions were recorded for evaluation. Specifically, we focused on observing sniffing and grooming behaviors during this time. Our analysis revealed that social sniffing between animals showed no significant differences in nose-nose (N–N) interactions (Fig. 4C) or nose–head (N–H) interactions (Fig. 4D). However, upon evaluating nose–anogenital (N–A), a significant decrease in KDM6B mKO animals was observed (Fig. 4E), demonstrating a reduction in social investigative activity. Together, this data demonstrates that KDM6B mKO animals show increased social dominance and exhibit social deficits, as evidenced by decreased social interaction with other animals and behaviors indicative of avoiding direct interaction, as observed in the direct social interaction paradigm.

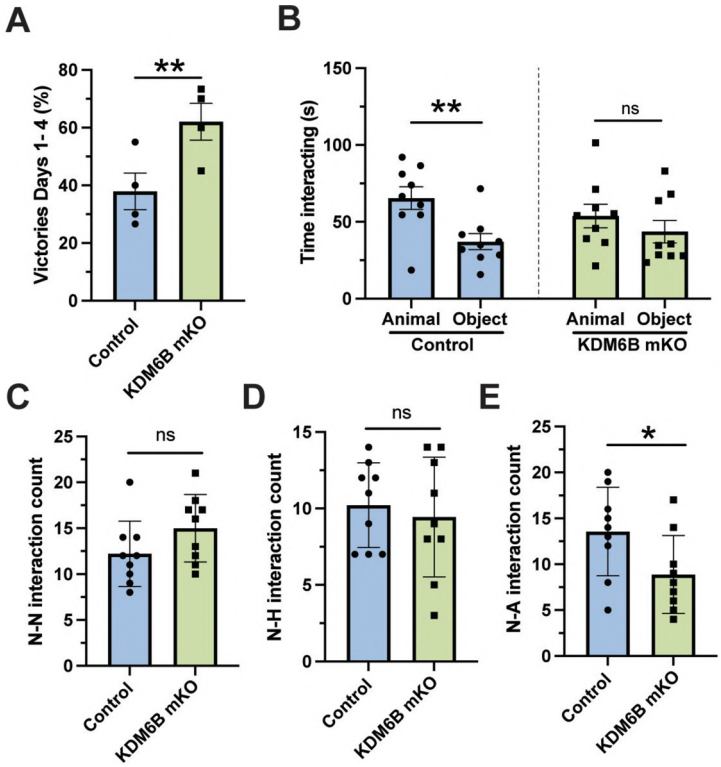


Fig. 4. Impaired social behaviors of KDM6B mKO animals. (**A**) Quantification of the number of victories in the tube dominance test. Each point represents the mean of victories per day 1–4. (**B**) Quantification of the time spent in the 3-chamber social interaction test with the novel animal or novel object in Control and KDM6B mKO animals. (**C**-**E**) Direct social interaction test to quantify (**C**) nose-nose (N–N), (**D**) nose-head (N–H), and (**E**) nose-anogenital (N-A) interactions between Control or KDM6B mKO animals. Bars represents mean ± SEM. Students t-test was used to determine significance compared to control condition. $^{*}p < 0.05$, $^{**}p < 0.01$, n = 9 animals for Control and KDM6B mKO animals. ns = non-significant.

Impaired cognitive function in KDM6B mKO mice

Human patients with mutations in *KDM6B* have exhibited varying degrees of intellectual disability[21,24,25]. Moreover, studies involving knockdown of the Drosophila ortholog of KDM6B and KDM6A, UTX, which plays a similar role in removing H3K27me3, have shown that deficits in UTX lead to cognitive impairments[26]. Consequently, we investigated whether KDM6B mKO animals display deficits in memory formation. To assess spatial learning and memory, we employed the Barnes maze paradigm[31]. Measuring the total distance traveled by the animals over 5 days revealed that KDM6B mKO animals covered a longer distance each day in the apparatus compared to control animals (Fig. 5A). This aligns with our previous observations in the rotarod, open field apparatus, and light–dark test, highlighting the hyperactivity of KDM6B mKO animals. Additionally, we analyzed the time it took for the animals to find the escape hole for the first time, termed primary latency. KDM6B mKO animals experienced difficulties locating the escape hole, resulting in a greater primary latency in all days compared to control animals (Fig. 5B). To evaluate spatial memory formation, the escape hole was removed, and we monitored the time the animals spent in the zone of interest where the escape hole was previously located. We found that KDM6B mKO animals spent significantly less time in the zone of interest, indicating cognitive deficits (Fig. 5C). Lastly, we assessed long-term memory formation using the contextual fear conditioning paradigm. During the 5 min test period, KDM6B mKO animals exhibited a significantly reduced percentage of time freezing compared to control animals (Fig. 5D). Collectively, our data indicate that KDM6B mKO animals display severe cognitive impairments.

NMDA receptor mediated synaptic function and plasticity are diminished in KDM6B mKO mice

To investigate the physiological consequences of KDM6B ablation in brain function, we used acute brain slices from KDM6B mKO animals to perform an electrophysiological characterization of excitatory synaptic activity at the Schaffer-collateral to CA1 synapse in the hippocampus (Fig. 6A). We first characterized spontaneous AMPA receptor (AMPAR)-mediated excitatory synaptic activity and found a significant decrease in the frequency but not in the amplitude of spontaneous excitatory postsynaptic currents (sEPSCs) in KDM6B-deficient synapses compared to control (Fig. 6B). Likewise, a significant decrease in the frequency of miniature excitatory postsynaptic currents (mEPSCs) was observed in KDM6B-deficient synapses (Fig. 6C), suggesting that ablation of KDM6B impact spontaneous excitatory synaptic activity. To further determine whether KDM6B mKO impacts

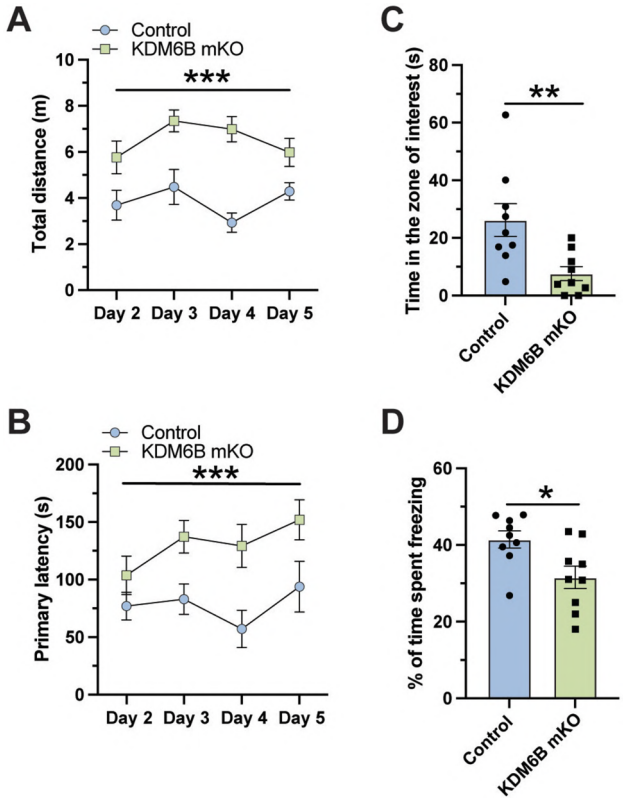


Fig. 5. KDM6B mKO animals display cognitive deficits. (**A**) Quantification of the total distance travelled in the Barnes maze apparatus. (**B**) Primary latency of Control and KDM6B mKO animals in the Barnes maze apparatus. (**C**) Quantification of the time spent in the zone of interest where the escape hole was formerly located. (**D**) Percentage of time spent freezing by Control and KDM6B mKO animals in the contextual fear conditioning test. Bars represents mean ± SEM. Students t-test was used to determine significance compared to control condition. $^{*}p < 0.05$, $^{**}p < 0.01$, $^{***}p < 0.001$, n = 9 animals for Control and KDM6B mKO animals.

evoked neurotransmitter release probability, we perform paired-pulse ratio measurements at different interstimulus intervals. No differences between control and KDM6B mKO animals were observed (Fig. 6D), suggesting normal release probability in KDM6B-deficient synapses compared to control synapses. Moreover, no differences between control and KDM6B mKO animals were observed in AMPAR-mediated fEPSP input–output function (Fig. 6E), indicating that KDM6B ablation does not affect evoked glutamate release probability and AMPAR-mediated synaptic transmission in the hippocampus.

Next, we analyzed NMDAR/AMPAR ratios by recording AMPAR-mediated EPSCs at -60 mV and isolated NMDAR-mediated EPSCs at + 40 mV in the continuous presence of 10 µM NBQX (Fig. 7A). A significant decrease in the NMDAR/AMPAR ratio was observed in KDM6B mKO deficient synapse compared to control (Fig. 7A), suggesting a decrease in the total number of NMDARs. To confirm this possibility, we measure isolated NMDAR-EPSCs input–output curve and found a significant decrease in KDM6B mKO compared to control animals (Fig. 7B). Moreover, we found that NMDAR-EPSC display significantly slower decay kinetics in KDM6B mKO mice (Fig. 7C), which could reflect a change in synaptic NMDAR subunit composition[32–34]. To test this possibility, we first analyzed the expression of the NMDA receptor subunits NR2A and NR2B in hippocampal tissue using digital PCR. We found a significant reduction in the number of copies of NR2A cDNA (Fig. 7D) and an increase in the number of copies of NR2B cDNA (Fig. 7E) in hippocampal tissue of KDM6B mKO animals compared to control. Second, we performed electrophysiological recording of isolated NMDARs-EPSCs and used Ro25-6981 (500 nM) to selectively block NR2B-containing NMDARs. We found that NMDAR-EPSCs in KDM6B mKO mice were more sensitive to Ro25-6981 than controls mice (Fig. 7F). Altogether these results strongly suggest that KDM6B ablation alters NMDAR-mediated synaptic transmission by decreasing the total number and the subunit composition of NMDAR present at the Schaffer-collateral to CA1 synapse.

Due to the widespread infection in the animal brain, we also analyzed the effect of KDM6B mKO on synaptic function from layer V pyramidal neurons in the medial prefrontal cortex (Supplementary Fig. 1). As in the hippocampus, we found a significant decrease in the frequency but not in the amplitude of sEPSC in KDM6B-deficient synapses compared to control (Supplementary Fig. 1). Moreover, NMDAR-mediated EPSC recorded from KDM6B mKO animals are more sensitive to Ro25-6981 than control cells (Supplementary Fig. 1B), consistent with the idea that KDM6B mKO impact synaptic function and NMDARs subunit composition in both the cortex and the hippocampus.

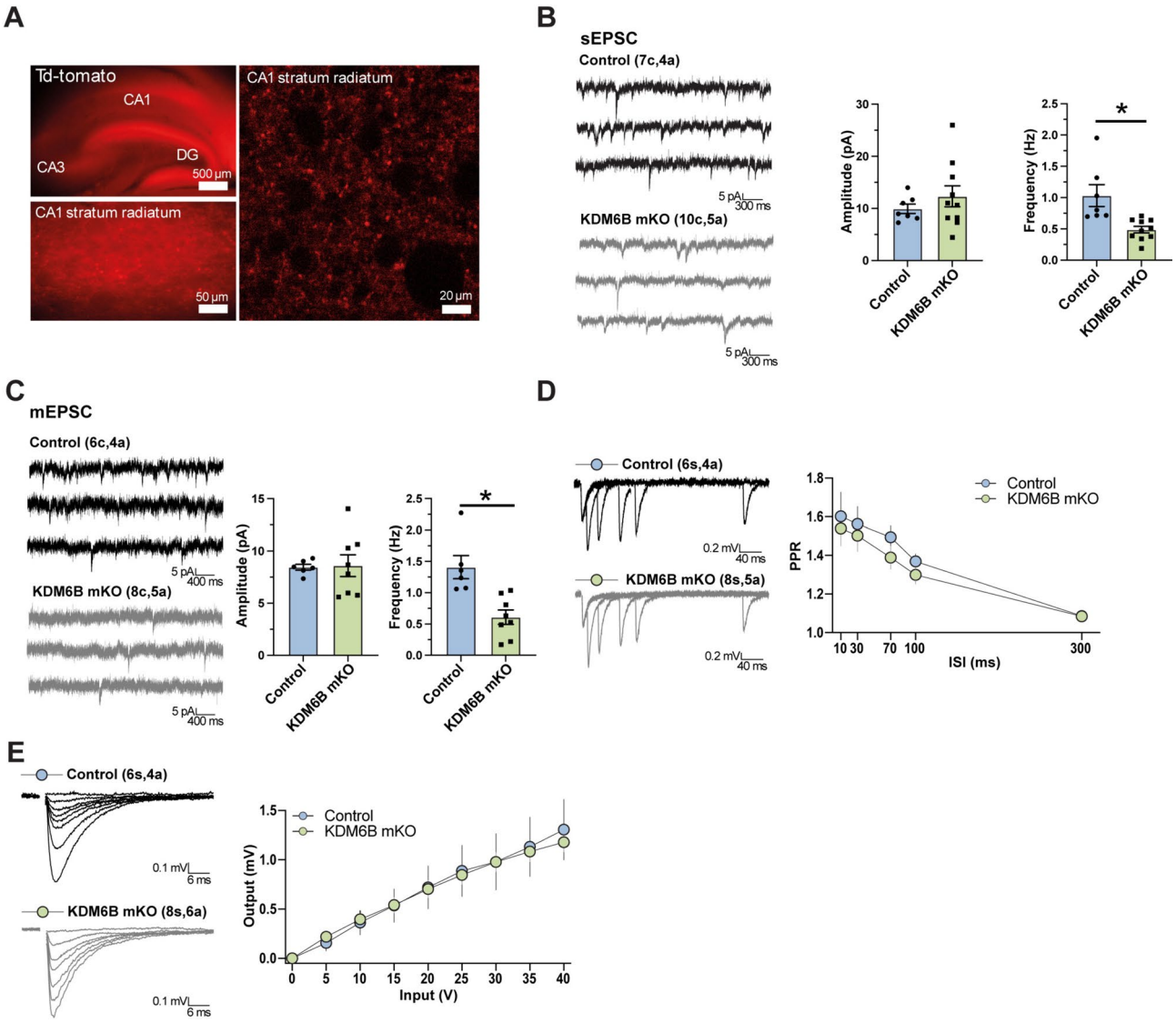


Fig. 6. AMPAR-mediated excitatory transmission is normal at hippocampal Sch–CA1 synapses in KDM6B mKO mice. (**A**) Representative image of acute hippocampal slice showing the expression of Td-tomato as infection control for KDM6B mKO in the hippocampus and in the CA1 field. (**B**) Representative AMPAR-mediated sEPSC traces (left) and summary plots (right) showing a decrease in frequency (Control: 1.03 ± 0.46 Hz vs KDM6B mKO: 0.48 ± 0.05 Hz, $p = 0.03$) but no in the amplitude of AMPAR-sEPSC in KDM6B mKO neurons. (**C**) Loss of KDM6B also significantly decrease the frequency (Control: 1.41 ± 0.2 Hz vs KDM6B mKO: 0.61 ± 0.11 Hz, $p = 0.03$) but not the amplitude of mEPSC. (**D**) Representative traces (*left*) and summary data (*right*) showing that ablation of KDM6B did not alter AMPAR-mediated paired-pulse ratio (PPR) measured at 10, 30, 70, 100, and 300 ms interstimulus intervals (ISI) or (**E**) input–output function. In all panels, summary data represent the mean ± SEM. Number of cells (c), slices (s), and animals (a) are indicated in parentheses. Student t-test was used for statistical analysis, $^{*}p < 0.05$.

Changes in NMDARs function has been associated with alteration in the induction of NMDAR-dependent long-term potentiation (NMDAR-LTP;[34]). Thereby, we evaluated if NMDAR-LTP is altered by the ablation of KDM6B and found a strong reduction in the magnitude of LTP in KDM6B mKO mice compared to control (Fig. 7G). These results indicate that KDM6B plays an important role in NMDAR-dependent synaptic plasticity in the hippocampus likely by regulating NMDAR expression and activity.

Discussion

Although numerous ASD-related genetic variations are reported, we aimed to deepen our understanding of the role of KDM6B in regulating chromatin structure and gene transcription in the pathophysiology of ASD by investigating its effects on behavior and synaptic function. KDM6B is a lysine demethylase responsible for removing methyl groups from histone H3 lysine 27[13], thereby counteracting the repressive effects of the PRC2[14] hence facilitating gene expression. In agreement with previous reports in cKO KDM6B[23] and heterozygous

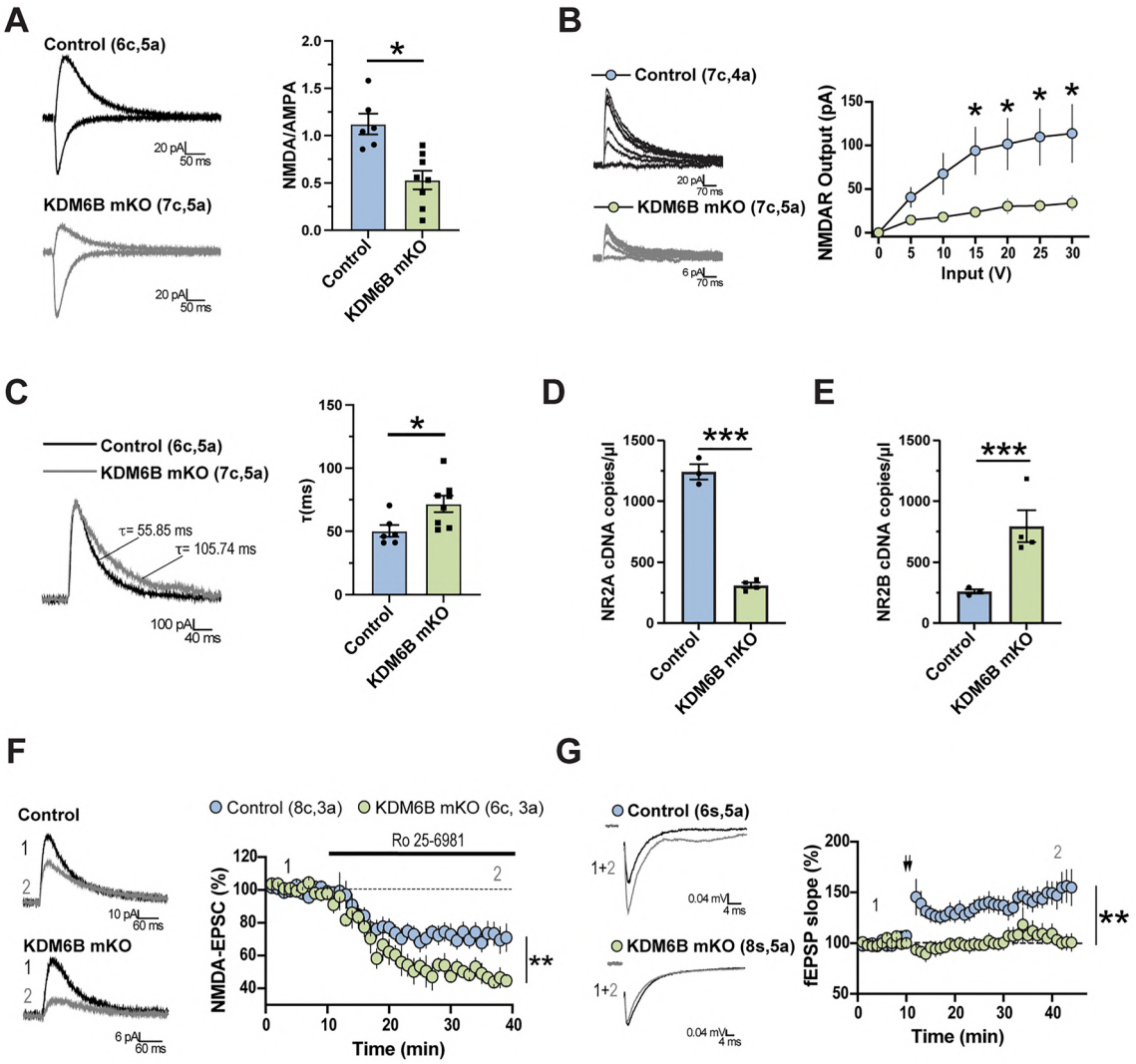


Fig. 7. NMDAR-mediated synaptic transmission is altered at hippocampal Sch–CA1 synapses in KDM6B mKO mice. (**A**) Representative traces (*left*) and summary data (*right*) showing that the NMDAR/AMPAR ratio is lower in KDM6B mKO compared to control (Control, 1.12 ± 0.10; KDM6B mKO, 0.53 ± 0.09, $p = 0.02$). (**B**) NMDAR-EPSCs input output curve is decrease in KDM6B mKO compared to control. (**C**) Normalized NMDAR-EPSCs (*left*) and summary data (*right*) showing slower NMDAR decay kinetics in KDM6B mKO compared with control (Control, 50.30 ± 11.30; KDM6B mKO, 71.70 ± 18.36, $p = 0.04$). (**D–E**) Digital PCR assay to determine NR2A (**D**) or NR2B (**E**) cDNA copies/µl in WT and KDM6B mKO animals (WT n = 3; KDM6B mKO n = 4). (**F**) Averaged NMDAR-EPSCs (left) and summary data (right) showing more sensitivity to the selective NR2B antagonist Ro25-6981 (500 nM) in KDM6B mKO animals compared to control (Control, 71.24 ± 4.67; KDM6B mKO, 44.69 ± 4.65, $p = 0.002$) (**G**) Representative traces (left) and summary data (right) showing that NMDA-dependent LTP induced by high frequency stimulation (arrows) is impaired in KDM6B mKO compared with control animal. Averaged sample traces were taken at times indicated by numbers in the summary plot. In all panels, summary data represent the mean ± SEM and the number of cells (**c**), and animals (**a**) are indicated in parentheses. Student t-test was used for statistical analysis, $^{*}p < 0.05$, $^{**}p < 0.01$, $^{***}p < 0.001$.

KDM6B KO animals[21], our findings reveal that ablation of brain KDM6B play a critical role in controlling different ASD phenotype including hyperactivity, repetitive behaviors, social interaction, and cognitive deficits. Synaptic dysfunction is suggested as a core mechanism underlying ASD pathophysiology[35]. Accordingly, our results demonstrated that ablation of KDM6B strongly impact NMDAR-mediated synaptic function and plasticity in the hippocampus, an observation that could explain the cognitive impairments observed in KDM6B mKO animal. These findings highlight a critical role of KDM6B in the pathophysiology of ASD phenotypes.

Here we utilized CRISPR/Cas9-mediated gene editing to generate KDM6B mKO animals, allowing us to investigate the behavioral and synaptic consequences of KDM6B deficiency, similarly to what we have previously done for KMT2C, a histone methyltransferase associated to ASD[10]. Genetic editing of *Kdm6b* leads to an enrichment of H3K27me3, reflecting the deficiency of KDM6B in cells. This dysregulation of histone methylation suggests a potential mechanism by which KDM6B deficiency may disrupt normal gene expression patterns.

Specifically, the increased H3K27me3 levels observed after gene editing likely result in the aberrant silencing of genes that are normally upregulated by KDM6B-mediated demethylation, as it has been shown in cerebellar granule neurons where KDM6B deficiency show deficient expression of genes needed for synaptic maturation, including the predominant NMDA receptor subunit *Grin2c*[36].

The behavioral characterization of the mKO animals reveals the absence of anxiety, as evidenced by results from the open field, light and dark, and zero maze tests. Surprisingly, in tests such as the rotarod and those previously mentioned, KDM6B mKO animals exhibited increased locomotion, traveling a longer distance compared to control animals. Given the absence of anxiety-related behaviors, this heightened activity can be attributed to hyperactivity in the animals, a trait reminiscent of observations in heterozygous KDM6B animals[21]. In contrast to findings in *Kdm6b* heterozygous models, our model system reveals the manifestation of repetitive behaviors observed in the marble burying and grooming tests. These differences might be a consequence of the different approach used to induce KDM6B KO and the extent of KO in different brain areas and cell types. Notably, KDM6B mKO animals also exhibit significant social impairments, a hallmark trait associated with ASD phenotypes that has also been observed in human patients carrying *KDM6B* mutations[25].

Although *KDM6B* mutants in humans have highly variable phenotypes, all of them present cognitive deficits as a common feature[26]. In agreement, KDM6B mKO animals display cognitive deficits, as evidenced by impairments in spatial learning and memory formation in the Barnes maze and fear conditioning paradigms. These findings are in line with existing genetic studies in both humans and mice, which have implicated KDM6B in intellectual disability and cognitive impairment[21,24,25,37]. It is worth highlighting that, contrary to previous observations, our study did not identify differences between male and female mice in terms of behavioral outcomes, thus all our data shows the average obtained from both sexes. This discrepancy could potentially be attributed to differences in methodology, including the approach used to induce gene editing in both alleles, as opposed to haploinsufficiency observed in KDM6B heterozygous models.

To gain insight into the mechanisms by which KDM6B deficiency produced autistic-like behaviors, we conducted electrophysiological recording from acute hippocampal slices as this region is mainly implicated in cognitive function. We found that KDM6B mKO has a significant reduction on the frequency of excitatory postsynaptic currents, however the amplitude was not changed, similarly to what has been observed in other ASD models including TSC2[38],CNTNAP2, and AHI1[39]. Furthermore, we looked deeper into the impact on AMPAR-mediated synaptic transmission, revealing no significant differences compared to control animals. However, a significant reduction in the AMPAR/NMDAR ratio, indicating a decrease in the total number of NMDAR at the synapse was found in KDM6B mKO. This characteristic aligns with observations from other animal models of ASD, where a reduction in NMDAR expression has been documented including neuroligin-1 (NL1) and Shank2 mutants[40,41]. To determine the extent to which NMDARs affect synaptic transmission in KDM6B mKO animals, we induced NMDAR-dependent LTP and found that its induction is severely impaired. This phenomenon has been observed in other ASD animal models such as TSC2[38], NL1[40], and Shank2[41] mutants among others[42].

In addition, our experiments also show that the decay time of NMDA currents is significantly slower in KDM6B mKO animals in both the hippocampus and medial prefrontal cortex, suggesting a change in the subunit composition of the NMDARs from the faster NR2A subunit to the slower NR2B kinetics[32,43]. This was supported by digital PCR analyses showing that NR2A subunit expression is reduced while NR2B subunit expression is increased. Future experiments will try to unravel the mechanisms behind this change in NMDA currents.

It has been demonstrated that NMDARs composed of the NR2A subunit are preferentially anchored by PSD95 to the postsynaptic site, whereas NR2B-composed NMDARs are anchored by SAP102[44–47]. As the expression of PSD95 is regulated by H3K27me3[48,49], it is possible to suggest a link between KDM6B deficiency and altered PSD95 expression. Since PSD95 serves as the primary anchor for NR2A at the postsynaptic density, the absence of KDM6B may disrupt the expression of PSD95, consequently impacting the localization of NR2A/PSD95 complexes. Therefore, the disruption of KDM6B function may lead to an imbalance in NMDAR subunit composition, thereby influencing synaptic transmission and plasticity. Alternatively, it has been shown that NMDAR subunits expression during post-natal development is regulated by H3K27me3[50], thus KDM6B deficiency may directly affect the expression of NMDAR subunits impacting synaptic transmission and plasticity. These aspects warrant further investigations.

Our use of CRISPR/Cas9 to induce a mosaic knockout of KDM6B leads to a significant reduction in KDM6B expression, likely occurring across a wide range of brain cells as the approach we used is not cell-type specific. As we are unable to differentiate between cell types or confirm complete knockout in all targeted cells, we acknowledge that our experimental design does not allow us to definitively determine whether the observed effects are cell-autonomous (neurons) or non-cell-autonomous (e.g. mediated by KDM6B KO in glial cells). Moreover, it is possible that these effects may arise from a combination of cell-autonomous and non-cell-autonomous mechanisms. For instance, the disruption of KDM6B in one cell type could indirectly affect neighboring cells and contribute to the overall phenotype. This limitation is inherent in our approach and should be considered when interpreting our findings. To address this limitation in future studies, more refined techniques such as single-cell RNA sequencing or cell-type-specific knockouts would be required to elucidate the precise contributions of cell-autonomous versus non-cell-autonomous effects.

In conclusion, our approach and mouse model successfully recapitulated the phenotypes observed in humans, shedding light on the mechanisms through which KDM6B deficiency contributes to ASD phenotypes. Consequently, targeting NMDARs as a therapeutic strategy to address KDM6B brain deficiencies could pave the way for novel treatments for neurodevelopmental disorders resulting from *KDM6B* mutations.

Methods

Primary neuronal cultures

Postnatal day 1 Cas9 KI mice (C57BL/6J; JAX 026179) were euthanized by decapitation and the whole brain was extracted in ice cold Ca2+/Mg2+ -free Hank's balanced salt solution (HBSS). Meninges were removed, the tissue was minced and incubated with Papain (20 U) for 15 min at 37 °C. Cells were rinsed twice with HBSS, resuspended by mechanical agitation through fire-polished glass Pasteur pipettes of decreasing diameters, and plated over poly-L-lysine-coated culture plates or cover slips. Cultures were maintained at 37 °C in 5% CO2 in growth media [Neurobasal-A (Life technologies 1088802) supplemented with B27 (Life technologies 17504044), 2 mM L-glutamine (Life technologies 25030-081), 100 U/ml penicillin/streptomycin (Life technologies 15070–063)]. Half of the media was replaced every 3 days. Neuronal cultures were transduced at 3 days in vitro (DIV) using concentrated AAV particles.

Animals and injections

All animal procedures and experiments were performed according to the NIH and ARRIVE guidelines and were approved by the animal ethics committee from Universidad Andrés Bello (020/2018). Newborn Cas9 KI mice (C57BL/6J; JAX 026179) were cryoanesthetized in a cold aluminum plate and injected with 1 µL of concentrated AAV (1×10^{11} vg), containing sgRNA or empty vector, in each cerebral ventricle at a depth of 3 mm in the animal's head at 2/5 of the intersection between lambda and the eye with a 10 µL HAMILTON syringe (Hamilton, 7653-01) and a 32 G needle (Hamilton, 7803-04). After the injection, P1 mice were placed in an infrared heating pad until they recovered their color and temperature, then they were returned to their cage with the mother[10,51,52]. Three weeks after birth, mice from both conditions were weaned off and separated by sex in cages with a 12/12 light/dark cycle with free access to food and water. A chip (p-chips, Pharmaseq) was put in the tail of each animal for easy tracking during behavioral test. Behavior tests were performed between 9:00 am and 6:00 pm. At the end of the battery of behavioral tests, the animals were euthanized using isoflurane for subsequent molecular analyses.

Plasmids

For the expression of CRISPR/Cas9, plasmids were generated in AAV backbones. For sgRNAs 20nt target sequences were selected contiguous to a 5′-NGG photospacer-adjacent motif (PAM). sgRNAs for *Kdm6b* were designed against exon 6. sgRNA used for in vivo experiments (5′ GGGAAGTTGGAATCCCTACA 3′) were cloned into a custom AAV plasmid under the control of the U6 promoter, and coding for tdTomato under the control of the human synapsin1 promoter, as in[10]. For viral packaging we used a plasmid coding for the PHP.eB capsid and pAdDeltaF6 plasmid to express adenovirus E4, E2A and VA genes. pUCmini-iCAP-PHP.eB was a gift from Viviana Gradinaru (Addgene plasmid # 103005; http://n2t.net/addgene:103005; RRID: Addgene_103005), pAdDeltaF6 was a gift from James M. Wilson (Addgene plasmid # 112867; http://n2t.net/addgene:112867; RRID:Addgene_112867).

AAV Production

AAVs were prepared as in[10,27]. Briefly, AAV particles coding for sgRNA against *Kdm6b* under the control of a U6 promoter, together with the red fluorescent protein tdTomato controlled by the hSyn1 promoter were packed using the PHP.eB capsid to obtain high titer viral particles[10,27,49,53]. HEK 293T were transfected with PEI and PHP.eB capsid plasmids, the vector with *Kdm6b* sgRNA-tdTomato, and the helper plasmid DF6. After 24 h of transfection, the media was replaced for DMEM 1% FBS. 72 h later, medium was collected from the plates and replaced with fresh DMEM 1% FBS. The collected medium was stored at 4 °C. To collect the viruses, 120 h after transfection, the cells were detached from the plate and transferred to 250 mL conical tubes, as well as the collected media. They were centrifuged for 10 min at 2000*g*, the supernatant was removed and saved for later use. The pellet was resuspended in SAN digestion buffer (5 mL of 40 mM Tris, 500 mM NaCl and 2 mM MgCl2 pH 8.0) containing 100U/mL of Salt Active Nuclease (SAN) from Arcticzymes and incubated at 37 °C for 1 h. To the supernatant that was saved, a 5 × stock solution of 40% PEG 8000 (Sigma Aldrich, USA) in 2.5M NaCl was added, incubated on ice for 2 h and centrifuged at 4000*g* for 30 min in 250 mL bottles. The supernatant was collected and was placed in an Optiprep gradient and ultracentrifuged at 41.000*g* for 4 h. The phase containing the AAV was recovered and frozen at – 80 °C for later use.

Genomic DNA extraction and T7 endonuclease I assay

Genomic DNA from transduced brain tissue was extracted using Quick-DNA Miniprep Kit (Zymo Research, USA) following manufacturer recommendations. To test *Kdm6b* edition, PCR with primers encompassing the edited region (5′ CAGGCATTTCTCTCCCAGTC 3′, 5′ GCAAAGGGCAGAGGAAGATT 3′) were used. PCR products were run in agarose gels and purified by Gel extraction kit (Qiagen). 300 ng of amplified gDNA was used for T7 endonuclease I assay (NEB Cat#M0302). Assays were run in TBE polyacrylamide gels and visualized using Gel Red (Biotium).

RNA extraction and RT-qPCR

RNA was isolated from the tissues using TRIzol (Life Technologies, USA) according to manufacturer's instructions as in[10,27,48,49]. To obtain complementary DNA (cDNA), 400 ng of RNA was used with iScript cDNA synthesis kit (Biorad, USA). Quantification was performed by qPCR using 3 µL of the cDNA mix, 6 µL Fast Evagreen qPCR Master Mix (Biotium, 31003). The relative abundance was measured by the ddCt method using the GAPDH gene as housekeeping control. Transcript detection was performed with specific primers for messenger RNA (mRNA):

Kdm6b: Fw 5′ TGAAGAACGTCAAGTCCATTGTG 3′; Rv 5′ TCCCGCTGTACCTGACAGT 3′; *Gapdh*: Fw 5′ ATGGTGAAGGTCGGTGTGAA 3′; Rv 5′ CATTCTCGGCCTTGACTGTG 3′.

Digital PCR (dPCR)

Undiluted cDNA was used for dPCR detection using a Qiacuity One dPCR system (Qiagen, Germany). An 8.5K 24-well Qiacuity Nanoplate was used to detect KDM6B, NR2A, NR2B, and GAPDH as reference control for even cDNA content. dPCR was run for 2 min at 95 °C for activation, 15 s 95 °C denaturation, 15 s 60 °C annealing, 15 s 72 °C extension for 40 cycles. Imaging was set to 500 ms exposure and gain of 4. For *Kdm6b* and *Gapdh* the same primers as in qPCR were used. In addition, primers used for dPCR were: *Grin2b* Fw 5′ GCCAAACTGGAA GAACATGG 3′; Rv 5′ TCTGCTCAGACTCTCACCCC 3′; *Grin2a* Fw 5′ TGGAAGCTCCAAACTGGAAG 3′; Rv 5′ CCTCACAGACTTTCATCCCC 3′.

Nuclear protein extraction

Nuclear extracts were used to determine histone tail modification by western blot as in[10]. Briefly, tissues were washed with cold PBS, centrifuged at 5000 g for 5 min and the pellet was resuspended in 5 volumes of cell lysis buffer (50 mM Hepes pH 7.9, 3 mM MgCl2, 20 mM KCl, 0.1% NP-40, 1 mM DTT and protease inhibitor cocktail) and incubated on ice for 10 min. Solution was homogenized with 30 strokes in a dounce homogenizer and centrifuged at 6000 g for 15 min at 4 °C to separate the cytosolic and nuclear fractions. The pellet was resuspended in 1 volume of Buffer C (10 mM Hepes pH 7.9, 420 mM NaCl, 1.5 mM MgCl2, 25% Glycerol, 0.2 mM EDTA, 1 mM DTT and protease inhibitor cocktail) and incubated for 1 h. Extracts were sonicated at 50% amplitude in cycles of 30 s ON/ 30 s OFF, centrifuged at 12,000*g* for 15 min at 4 °C. Supernatant was recovered and frozen at − 80 °C to be subsequently quantified by Bradford.

Western blot analysis

Nuclear fractions or total extracts were separated on polyacrylamide gels and transferred to PVDF membranes (Millipore, USA). Membranes were blocked using 5% milk or 3% BSA and incubated overnight at 4 °C with primary antibodies. After rinsing, the membranes were incubated with secondary antibodies for 30 min at room temperature, rinsed and developed using chemiluminescence (Cell Signaling Technology, USA). Primary antibodies used: KDM6B (Sigma-Aldrich, 07-1533), N-Cadherin (Santa Cruz Biotechnology, SC-7939), H3K27me3 (Sigma-Aldrich, 07-449), and H3pan (Diagenode C15410324). For detection HRP-conjugated secondary antibodies were used (Cell Signaling Technology, USA).

Behavioral overview

All behavioral tests on mice were carried out 8 weeks after AAV injection as in[10,27,28]. Before each test, mice cages were transported to the behavior room and habituated for 30 min in the dark. After completing a test, equipment and devices used were cleaned with 70% ethanol. Tests were recorded and analyzed with ANY-Maze software (Stoelting, USA).

Rotarod: Mice were placed on an elevated accelerating rod for three trials. Each trial lasted for a maximum of 3 min, during which the Rotarod underwent a linear acceleration of 4 rpm per min. Mean time and speed from each animal were registered before falling off.

Open Field: Mice were tested in an open field (45 × 45 cm) virtually divided into central and peripheral regions with ANY-Maze software. Apparatus was illuminated from above with 300 lx in center and 250 lx in periphery. Animals were allowed to roam freely for 10 min. The total distance traveled and time in center and periphery were analyzed.

Light and Dark: The apparatus used for this test is a 40 cm box split in half with 390 lx on light side and 0–2 lx on the dark side. Mice were placed in the dark chamber and were allowed to freely explore both chambers for 10 min. Distance traveled, time spent and number of entrances to the light side were analyzed.

Elevated zero-maze: The apparatus consisted of a 46 cm diameter circular runway and raised 54 cm off the ground. The runway was divided equally into four alternating quadrants of open arcs and closed arcs, with 15 cm walls. Mice started in the center of an open arm and were recorded by video tracking for 10 min. Measures of cumulative open and closed arc times, total open arm entries, distance in each arm and total distance traveled were analyzed.

Marble burying test: Mice were tested in a 45 × 45 cm box filled with 5 cm deep wood chips and 49 marbles distributed in a 7 × 7 pattern. Animals were placed in the test cage and allowed to explore and bury the marbles during a 30 min session that was videotaped. At the end of the session the subject was removed and the number of marbles buried (2/3 marble covered by wood chip) were counted.

Contextual fear conditioning: Equipment consisted of a sound attenuating box, fan, light (visible/I.R.), a speaker, a USB camera, a single on-board controller, and a mouse cage. All trials were recorded, and all mice underwent a habituation, conditioning and testing phase. During the habituation (day 1): mice were placed in the fear conditioning cage to explore freely for 5 min and then returned to their cage. During the conditioning phase (day 2): subject mouse was placed in the fear conditioning cage, let explore freely for 2 min and then subjected to an electric shock of 0.75 mA for 2 s. Next, animal was allowed to explore freely for 3 min and returned to its cage. On the test phase (day 3): Twenty-four hours after the conditioning phase, the animals were tested for contextual memory. Each mouse was placed in the fear conditioning box, allowed to freely explore for 5 min, and returned to its cage. The number and time of freezing episodes was registered.

Barnes Maze: A non-reflective gray circular platform (91 cm diameter) with 20 holes (5 cm diameter) evenly distributed along the perimeter, with one hole containing a metal escape tunnel was used. Three exogenous visual cues (length/width ~ 30 cm) were used around the platform: black circle, blue triangle and a yellow square.

The light was adjusted to 1000 lx in the center of the platform. All animals underwent a phase of habituation, spatial acquisition and testing[31]. For habituation (day 1): each mouse was placed in the center of the platform, directed towards the escape hole, and allowed to remain there for 1 min. Then it was taken and allowed to freely explore the maze for 5 min and was again allowed to spend 1 min inside the escape hole. If the mouse did not enter within 5 min, it was gently guided near the escape hole selected randomly on the table. During training phase (day 2–4): each animal was introduced into the start box, left in the center of the platform for 10 s and the start box was removed, and simultaneously a 16,000 Hz sound was played. The test ended at 3 min or when the mouse has found the escape hole. This procedure was repeated 2 times per day. During those days the following was recorded: Primary latency: Time to review the escape hole for the first time; Time in the zone of interest; Total distance traveled. In the test phase (day 5): the position of the escape tunnel was changed, and the animal was brought in the start box to the center of the platform, left for 10 s and sound reproduction was started. The test ended at 90 s or when the mouse found the escape tunnel. The number of primary and total errors, primary and total latency, and total distance before finding the gap were recorded. The number of visits to each hole was also measured to show preference.

Three-Chamber Sociability and Social Novelty Test: This was performed in a transparent acrylic three-chambered apparatus with the following dimensions: 61.5 × 43.5 × 22 cm. Each outer chamber was 20 × 43.5 cm. We used small cages of 8 cm diameter and 18 cm height to put the social (unknown WT mice of the same sex and similar age) and nonsocial stimulus (plastic block of 8 × 4 × 4 cm). A 20 lx illumination was used in this test. On the habituation phase (day 1): stimulus holders were placed in the center of outer chambers. The subject mouse was placed in the central chamber and allowed to explore freely for 10 min. Apparatus and stimulus holders were cleaned between mice with 70% ethanol. During pre-test (day 2): two clean paper balls were prepared and introduced inside each stimulus holder. The mouse was placed in the central chamber and allowed to explore freely for 10 min. Apparatus and stimulus holders were cleaned between mice with 70% ethanol. For the social preference test (day 3): a control mouse was placed in a stimulus holder to be used as a social stimulus and changed for another one every 2 test runs to avoid burnout or social fatigue[54]. A plastic block was placed in the stimulus holder as a nonsocial stimulus. Once social and nonsocial objects were put in the outer chambers, mouse was placed in the central chamber and allowed to explore freely for 10 min. Behavior was video recorded. Time amount and distance traveled in the social and nonsocial chamber was registered, as well as the interaction time with each stimulus. Discrimination index was calculated by (time with novel animal – time with novel object) / (time with novel animal + time with novel object).

Social Interactions: In this test, an animal from the control condition or KDM6B mKO with a control animal of the same sex and similar age, were placed in a 30 × 30 × 30 cm box for 10 min. Social interactions (nose-nose sniffing, nose-face, nose-anogenital area, and grooming) between them were quantified.

Tube dominance: Tube test apparatus consisted of a smooth transparent acrylic tube of 30 cm length and internal diameter of 2.5 cm. Mice were habituated for 3 days. On day 1, each animal interacted and explored the tube freely for 30 min. On day 2 and 3, tube inlet was closed, and gel food was placed at the end. Animals were allowed to explore freely for 30 min. On the training phase (day 4 and 5) mice were taken by the tail and allowed to freely explore for approximately 1 min on the table where the tube was located. Then they were taken from the tail and put on one end of the tube and when the animal entered the tail, it was released. If the animal did not move for several seconds, it was gently prodded with a wooden stick. This step was repeated 5 times per side, so that the mouse passed through the tube a total of 10 times. The same procedure was repeated on day 4 and 5. On the test phase (day 6–9): two mice, one control and one KDM6B mKO, were taken and brought to the ends of the tube by the tail. When they entered completely and reached the middle of the tube, their tails were released to begin the confrontation. The test was repeated for 4 days. The mouse that pushes and removes its opponent from the tube was considered the winner and the one that is removed from the tube was considered the loser. All confrontations were video recorded to analyze the times each animal won and lost. The test stopped when the loser had all 4 paws out of the tube. The total number of wins and the number of wins per day were compared between control and KDM6B mKO conditions.

Brain sectioning and mounting

To assess brain transduction, after behaviors animals were deeply anesthetized, and half of the brain was extracted and fixed by immersion in PBS + 4% PFA + 4% Sucrose into 30 mL flasks for 24 h. After fixation, a Leica VT1000s vibratome was used to cut 100 µm coronal sections. Slices were kept in PBS and mounted using Fluoromont G (EMS, Hatfield, PA) to preserve the fluorescence signal. Brain images were captured with a Nikon Eclipse TE2000 epifluorescence microscope (Nikon, USA) or a Nikon C2 plus confocal microscope (Nikon, USA).

Slice electrophysiology

Acute coronal hippocampal slices (400 µm thick) were prepared from control and KDM6B mKO at postnatal day (P) 30 to P45 as previously described[27,30,49,55,56]. Animal handling and use was conducted following a protocol approved by the Animal Care and Use Committee of the Universidad de Valparaiso (CBC 92-2023) in accordance with the bioethics regulation of the Chilean Research Council (ANID). Briefly, the brain was isolated and cut using a DKT vibratome in a solution containing the following (in mM): 215 sucrose, 2.5 KCl, 26 $NaHCO_3$, 1.6 NaH_2PO_4, 1 $CaCl_2$, 4 $MgCl_2$, 4 $MgSO_4$, and 20 glucose. After 30 min recovery, slices were incubated in an artificial CSF (ACSF) recording solution containing the following (in mM): 124 NaCl, 2.5 KCl, 26 $NaHCO_3$, 1 NaH_2PO_4, 2.5 $CaCl_2$, 1.3 $MgSO_4$, and 10 glucose equilibrated with 95% O2/5% CO2, pH 7.4. Slices were incubated in this solution for 30 min before recordings. For medial prefrontal cortex (mPFC) slices (300 µm thick), brain was cut in an ice-cold high-choline solution containing (in mM): 110 Choline-Cl, 2.5 KCl, 1.25 NaH_2PO_4, 7 $MgCl_2$, 25 $NaHCO_3$, 15 glucose, 0.5 $CaCl_2$, 11.6 ascorbate, 3.1 pyruvate (290–305 mmol/Kg) as previously described[57].

mPFC slices were kept at room temperature for at least 30 min before recording in ACSF containing (in mM): 124 NaCl, 2.69 KCl, 1.25 KH2PO4, 1.3 MgSO4, 26 NaHCO3, 10 glucose, 2.5 CaCl2, pH 7.4 (300–305 mmol/Kg).

All experiments, except where indicated, were performed at 28 ± 1 °C in a submersion-type recording chamber perfused at 1–2 ml/min rate with ACSF supplemented with the GABAA receptor antagonist picrotoxin (PTX; 100 μM). Extracellular field potentials (fEPSPs) were recorded with a patch pipette filled with 1 mM NaCl and placed in the CA1 stratum radiatum. Whole-cell voltage-clamp recordings (Multiclamp 700B, Molecular Devices, USA) were acquired from CA1 pyramidal neurons or layer V pyramidal neurons voltage-clamped at -60 mV or + 40 mV using patch pipette electrodes (3–4 M) containing the following intracellular solution (in mM): 131 Cs-gluconate, 8 NaCl, 1 $CaCl_2$, 10 EGTA, 10 glucose, 10 HEPES, pH 7.2, 292 mmol/kg osmolality. Reagents were obtained from Sigma, Tocris and Ascent Scientific, prepared in stock solutions and added to the ACSF as needed.

fEPSPs and excitatory postsynaptic currents (EPSCs) were evoked by stimulating Schaffer collateral inputs in the hippocampus and layer 2/3 in the mPFC with a monopolar electrode filled with ACSF and positioned ~ 100 to 150 mm away from the recording pipette. Miniature EPSCs (mEPSCs) were recorded at 32 ± 1 °C in the continuous present of tetrodotoxin (TTX, 500 nM) to block action potential dependent release, whereas spontaneous EPSC (sEPSCs) were recorded in the absence of TTX. Short-term synaptic plasticity was induced by two pulses at different interstimulus interval (10, 30, 70 100 and 300 ms) and were used to calculated paired-pulse ratio (PPR) that was defined as the ratio of the slope of the second fEPSP to the slope of the first fEPSP, respectively. Long-term potentiation (LTP) was induced by 4 trains of 100 pulses at 100 Hz repeated two times, separated by 10 s. The magnitude of LTP was compared with baseline 30–35 min after applying the stimulation protocol. To assess cell stability, series and input resistances were monitored with test pulses (− 4 mV, 50 ms) throughout all experiments. Cells with > 20% change in series resistance were excluded from analysis. All recordings were elicited at 15–20-s intervals, filtered at 2.4 kHz, and acquired at 10 kHz, using custom made software written in Igor Pro 6.36 (WaveMetrics). Statistical comparisons were made using two samples Student's t-test at $p < 0.05$ significance level, using Origin 8.5 Pro software (OriginLab). Unless otherwise indicated, all electrophysiological values are provided as mean ± S.E.M and illustrated traces are average of 31–40 responses.

Statistical analysis

Values are presented as mean ± standard error of mean (SEM) for 3 or more independent experiments. Statistical analyzes with Student's *t*-test or Two-samples student t-test was performed. Values of $p < 0.05$ were considered statistically significant. All statistical analyzes were performed using Graphpad Prism (GraphPad Software Inc.) or Origin 9.3 Pro (Origin Lab).

Data availability

All data supporting our conclusions are incorporated in the original manuscript. Other data and material are available from the corresponding authors upon request.

Received: 3 April 2024; Accepted: 20 August 2024
Published online: 02 September 2024

References

1. Lord, C. *et al.* Autism spectrum disorder. *Nat. Rev. Dis. Prim.* **6**, 5 (2020).
2. Parenti, I., Rabaneda, L. G., Schoen, H. & Novarino, G. Neurodevelopmental disorders: From genetics to functional pathways. *Trends Neurosci.* **43**, 608–621 (2020).
3. Banerjee-Basu, S. & Packer, A. SFARI Gene: An evolving database for the autism research community. *Dis. Model Mech.* **3**, 133–135 (2010).
4. Iossifov, I. *et al.* De novo gene disruptions in children on the autistic spectrum. *Neuron* **74**, 285–299 (2012).
5. Rubeis, S. D. *et al.* Synaptic, transcriptional and chromatin genes disrupted in autism. *Nature* **515**, 209–215 (2014).
6. Stessman, H. A. F. *et al.* Targeted sequencing identifies 91 neurodevelopmental-disorder risk genes with autism and developmental-disability biases. *Nat. Genet.* **49**, 515–526 (2017).
7. Grove, J. *et al.* Identification of common genetic risk variants for autism spectrum disorder. *Nat. Genet.* **51**, 431–444 (2019).
8. Ruzzo, E. K. *et al.* Inherited and de novo genetic risk for autism impacts shared networks. *Cell* **178**, 850-866.e26 (2019).
9. Satterstrom, F. K. *et al.* Large-scale exome sequencing study implicates both developmental and functional changes in the neurobiology of autism. *Cell* **180**, 568-584.e23 (2020).
10. Brauer, B., Merino-Veliz, N., Ahumada-Marchant, C., Arriagada, G. & Bustos, F. J. KMT2C knockout generates ASD-like behaviors in mice. *Front. Cell Dev. Biol.* **11**, 1227723 (2023).
11. Platt, R. J. *et al.* Chd8 mutation leads to autistic-like behaviors and impaired striatal circuits. *Cell reports* **19**, 335–350 (2017).
12. Tang, G.-B. *et al.* The histone H3K27 demethylase UTX regulates synaptic plasticity and cognitive behaviors in mice. *Front. Mol. Neurosci.* **10**, 267 (2017).
13. Agger, K. *et al.* UTX and JMJD3 are histone H3K27 demethylases involved in HOX gene regulation and development. *Nature* **449**, 731–734 (2007).
14. Cao, R. *et al.* Role of histone H3 lysine 27 methylation in polycomb-group silencing. *Science* **298**, 1039–1043 (2002).
15. Nottke, A., Colaiácovo, M. P. & Shi, Y. Developmental roles of the histone lysine demethylases. *Development* **136**, 879–889 (2009).
16. Burgold, T. *et al.* The histone H3 lysine 27-specific demethylase jmjd3 is required for neural commitment. *PLoS ONE* **3**, e3034 (2008).
17. Wijayatunge, R. *et al.* The histone lysine demethylase Kdm6b is required for activity-dependent preconditioning of hippocampal neuronal survival. *Mol. Cell. Neurosci.* **61**, 187–200 (2014).
18. Park, D. H. *et al.* Activation of neuronal gene expression by the JMJD3 demethylase is required for postnatal and adult brain neurogenesis. *Cell Rep.* **8**, 1290–1299 (2014).
19. Shi, Y. Histone lysine demethylases: Emerging roles in development, physiology and disease. *Nat. Rev. Genet.* **8**, 829–833 (2007).
20. Burgold, T. *et al.* The H3K27 demethylase JMJD3 is required for maintenance of the embryonic respiratory neuronal network, neonatal breathing, and survival. *Cell Rep.* **2**, 1244–1258 (2012).

21. Gao, Y., Aljazi, M. B. & He, J. Kdm6b haploinsufficiency causes ASD/ADHD-like behavioral deficits in mice. *Front. Behav. Neurosci.* **16**, 905783 (2022).
22. Ramesh, V., Liu, F., Minto, M. S., Chan, U. & West, A. E. Bidirectional regulation of postmitotic H3K27me3 distributions underlie cerebellar granule neuron maturation dynamics. *eLife* **12**, e86273 (2023).
23. Wang, Y. *et al.* KDM6B cooperates with Tau and regulates synaptic plasticity and cognition via inducing VGLUT1/2. *Mol. Psychiatry* **27**, 5213–5226 (2022).
24. Pineda, I. I. & González, C. L. G. The KDM6B mutation: Phenotype and clinical characteristics—Report of a case. *Rev. Psiquiatry Salud Ment.* **15**, 88–93 (2022).
25. Stolerman, E. S. *et al.* Genetic variants in the KDM6B gene are associated with neurodevelopmental delays and dysmorphic features. *Am. J. Méd. Genet. Part A* **179**, 1276–1286 (2019).
26. Rots, D. *et al.* The clinical and molecular spectrum of the KDM6B-related neurodevelopmental disorder. *Am. J. Hum. Genet.* **110**, 963–978 (2023).
27. Bustos, F. J. *et al.* Removal of a partial genomic duplication restores synaptic transmission and behavior in the MyosinVA mutant mouse Flailer. *BMC Biol.* **21**, 232 (2023).
28. Ahumada-Marchant, C. *et al.* Deletion of VPS50 protein in mouse brain impairs synaptic function and behavior. *BMC Biol.* **22**, 142 (2024).
29. Silverman, J. L., Yang, M., Lord, C. & Crawley, J. N. Behavioural phenotyping assays for mouse models of autism. *Nat. Rev. Neurosci.* **11**, 490–502 (2010).
30. Pandian, S. *et al.* Myosin va brain-specific mutation alters mouse behavior and disrupts hippocampal synapses. *eNeuro* **7**, ENEURO.0284-20.2020 (2020).
31. Pitts, M. Barnes maze procedure for spatial learning and memory in mice. *BIO-Protoc.* **8**, e2744 (2018).
32. Sepulveda, F. J. *et al.* Differential roles of NMDA receptor subtypes NR2A and NR2B in dendritic branch development and requirement of RasGRF1. *J. Neurophysiol.* **103**, 1758–1770 (2010).
33. Tindi, J. O. *et al.* ANKS1B gene product AIDA-1 controls hippocampal synaptic transmission by regulating GluN2B subunit localization. *J. Neurosci.* **35**, 8986–8996 (2015).
34. Paoletti, P., Bellone, C. & Zhou, Q. NMDA receptor subunit diversity: Impact on receptor properties, synaptic plasticity and disease. *Nat. Rev. Neurosci.* **14**, 383–400 (2013).
35. de la Torre-Ubieta, L., Won, H., Stein, J. L. & Geschwind, D. H. Advancing the understanding of autism disease mechanisms through genetics. *Nat. Med.* **22**, 345–361 (2016).
36. Wijayatunge, R. *et al.* The histone demethylase Kdm6b regulates a mature gene expression program in differentiating cerebellar granule neurons. *Mol. Cell. Neurosci.* **87**, 4–17 (2018).
37. Feliciano, P. *et al.* Exome sequencing of 457 autism families recruited online provides evidence for autism risk genes. *NPJ Genom Med.* **4**, 19 (2019).
38. Costa, V. *et al.* mTORC1 inhibition corrects neurodevelopmental and synaptic alterations in a human stem cell model of tuberous sclerosis. *Cell Rep.* **15**, 86–95 (2016).
39. Sacai, H. *et al.* Autism spectrum disorder-like behavior caused by reduced excitatory synaptic transmission in pyramidal neurons of mouse prefrontal cortex. *Nat. Commun.* **11**, 5140 (2020).
40. Budreck, E. C. *et al.* Neuroligin-1 controls synaptic abundance of NMDA-type glutamate receptors through extracellular coupling. *Proc. Natl. Acad. Sci.* **110**, 725–730 (2013).
41. Won, H. *et al.* Autistic-like social behaviour in Shank2-mutant mice improved by restoring NMDA receptor function. *Nature* **486**, 261–265 (2012).
42. Guang, S. *et al.* Synaptopathology involved in autism spectrum disorder. *Front. Cell. Neurosci.* **12**, 470 (2018).
43. van Zundert, B., Yoshii, A. & Constantine-Paton, M. Receptor compartmentalization and trafficking at glutamate synapses: A developmental proposal. *Trends Neurosci.* **27**, 428–437 (2004).
44. Bustos, F. J. *et al.* PSD95 suppresses dendritic arbor development in mature hippocampal neurons by occluding the clustering of NR2B-NMDA receptors. *PLoS ONE* **9**, e94037 (2014).
45. Elias, G. M., Elias, L. A. B., Apostolides, P. F., Kriegstein, A. R. & Nicoll, R. A. Differential trafficking of AMPA and NMDA receptors by SAP102 and PSD-95 underlies synapse development. *Proc. Natl. Acad. Sci. USA* **105**, 20953–20958 (2008).
46. Sans, N. *et al.* A developmental change in NMDA receptor-associated proteins at hippocampal synapses. *J. Neurosci.* **20**, 1260–1271 (2000).
47. Elias, G. M. *et al.* Synapse-specific and developmentally regulated targeting of AMPA receptors by a family of MAGUK scaffolding proteins. *Neuron* **52**, 307–320 (2006).
48. Henriquez, B. *et al.* Ezh1 and Ezh2 differentially regulate PSD-95 gene transcription in developing hippocampal neurons. *Mol. Cell. Neurosci.* **57**, 130–143 (2013).
49. Bustos, F. J. *et al.* Epigenetic editing of the Dlg4/PSD95 gene improves cognition in aged and Alzheimer's disease mice. *Brain* **140**, 3252–3268 (2017).
50. Rodenas-Ruano, A., Chávez, A. E., Cossio, M. J., Castillo, P. E. & Zukin, R. S. REST-dependent epigenetic remodeling promotes the developmental switch in synaptic NMDA receptors. *Nat. Neurosci.* **15**, 1382–1390 (2012).
51. Kim, J.-Y., Grunke, S. D., Levites, Y., Golde, T. E. & Jankowsky, J. L. Intracerebroventricular viral injection of the neonatal mouse brain for persistent and widespread neuronal transduction. *J. Vis. Exp.* **91**, 51863 (2014).
52. Passini, M. A. & Wolfe, J. H. Widespread Gene delivery and structure-specific patterns of expression in the brain after intraventricular injections of neonatal mice with an adeno-associated virus vector. *J. Virol.* **75**, 12382–12392 (2001).
53. Chan, K. Y. *et al.* Engineered AAVs for efficient noninvasive gene delivery to the central and peripheral nervous systems. *Nat. Neurosci.* **20**, 1172–1179 (2017).
54. Rein, B., Ma, K. & Yan, Z. A standardized social preference protocol for measuring social deficits in mouse models of autism. *Nat. Protoc.* **15**, 3464–3477 (2020).
55. Delgado-Acevedo, C. *et al.* Behavioral and synaptic alterations relevant to obsessive-compulsive disorder in mice with increased EAAT3 expression. *Neuropsychopharmacology* **44**, 1163–1173 (2019).
56. Plaza-Briceño, W. *et al.* N-Methyl-d-aspartate receptor modulation by nicotinamide adenine dinucleotide phosphate oxidase type 2 drives synaptic plasticity and spatial memory impairments in rats exposed pre- and postnatally to ethanol. *Antioxid. Redox Signal.* **32**, 602–617 (2020).
57. Cortés, B. I. *et al.* Loss of protein tyrosine phosphatase receptor delta PTPRD increases the number of cortical neurons, impairs synaptic function and induces autistic-like behaviors in adult mice. *Biol. Res.* **57**(1), 40 (2024).

Acknowledgements

This work was supported by: ANID Fondecyt Iniciacion 11180540 (FJB), ANID PAI 77180077 (FJB), Exploración-ANID 13220203 (FJB), ANID-MILENIO (NCN2023_32, FJB, LVN), UNAB DI-02-22/REG (FJB), Fondequip EQM230028 (FJB), UNAB DI-06-24/REG (FJB), ANID-FONDECYT 1220480 (GA), ANID-FONDECYT 1201848 (A.E.C), ANID-FONDECYT 1230454 (LVN), DI-03-21/APP UNAB (BB), Fondequip EQM160154

(A.E.C) and by ANID Millennium Science Initiative Program (P09-022F to A.E.C). R.C.M was supported by ANID-FONDECYT postdoctorado grant #3190793. CA-G and NM-V were supported by PhD fellowship from ANID #21201603 (to CA-G) and #21211967 (to NM-V).

Author contributions

B.B, N.M-V, and C.A-M performed all behavioral experiments and analyzed the results. C.A-G, and R.C.M performed all slices electrophysiological experiments and analyzed the results. F.J.B, G.N, L.V–N, G.A, and A.E.C designed experiments, guided the research, provided resources, and interpreted all the results. F.J.B, and A.E.C., wrote the paper.

Competing interests

The authors declare no competing interests.

Additional information

Supplementary Information The online version contains supplementary material available at https://doi.org/10.1038/s41598-024-70728-5.

Correspondence and requests for materials should be addressed to A.E.C. or F.J.B.

Reprints and permissions information is available at www.nature.com/reprints.

Publisher's note Springer Nature remains neutral with regard to jurisdictional claims in published maps and institutional affiliations.

Open Access This article is licensed under a Creative Commons Attribution-NonCommercial-NoDerivatives 4.0 International License, which permits any non-commercial use, sharing, distribution and reproduction in any medium or format, as long as you give appropriate credit to the original author(s) and the source, provide a link to the Creative Commons licence, and indicate if you modified the licensed material. You do not have permission under this licence to share adapted material derived from this article or parts of it. The images or other third party material in this article are included in the article's Creative Commons licence, unless indicated otherwise in a credit line to the material. If material is not included in the article's Creative Commons licence and your intended use is not permitted by statutory regulation or exceeds the permitted use, you will need to obtain permission directly from the copyright holder. To view a copy of this licence, visit http://creativecommons.org/licenses/by-nc-nd/4.0/.

© The Author(s) 2024

BMC Biology

RESEARCH ARTICLE

Open Access

Deletion of VPS50 protein in mouse brain impairs synaptic function and behavior

Constanza Ahumada-Marchant[1], Carlos Ancatén-Gonzalez[4,5], Henny Haensgen[1], Bastian Brauer[1], Nicolas Merino-Veliz[1], Rita Droste[2], Felipe Arancibia[1], H. Robert Horvitz[2], Martha Constantine-Paton[3], Gloria Arriagada[1], Andrés E. Chávez[5] and Fernando J. Bustos[1,6*]

Abstract

Background The VPS50 protein functions in synaptic and dense core vesicle acidification, and perturbations of VPS50 function produce behavioral changes in *Caenorhabditis elegans*. Patients with mutations in VPS50 show severe developmental delay and intellectual disability, characteristics that have been associated with autism spectrum disorders (ASDs). The mechanisms that link VPS50 mutations to ASD are unknown.

Results To examine the role of VPS50 in mammalian brain function and behavior, we used the CRISPR/Cas9 system to generate knockouts of VPS50 in both cultured murine cortical neurons and living mice. In cultured neurons, KO of VPS50 did not affect the number of synaptic vesicles but did cause mislocalization of the V-ATPase V1 domain pump and impaired synaptic activity, likely as a consequence of defects in vesicle acidification and vesicle content. In mice, mosaic KO of VPS50 in the hippocampus altered synaptic transmission and plasticity and generated robust cognitive impairments.

Conclusions We propose that VPS50 functions as an accessory protein to aid the recruitment of the V-ATPase V1 domain to synaptic vesicles and in that way plays a crucial role in controlling synaptic vesicle acidification. Understanding the mechanisms controlling behaviors and synaptic function in ASD-associated mutations is pivotal for the development of targeted interventions, which may open new avenues for therapeutic strategies aimed at ASD and related conditions.

Keywords ASD, VPS50, Synaptic vesicles, Gene editing, Vesicle acidification

*Correspondence:
Fernando J. Bustos
fernando.bustos@unab.cl
[1] Constantine-Paton Research Laboratory, Institute of Biomedical Sciences (ICB), Faculty of Medicine and Faculty of Life Sciences, Universidad Andres Bello, Santiago, Chile
[2] Department of Biology, Howard Hughes Medical Institute, Massachusetts Institute of Technology, McGovern Institute for Brain Research, Cambridge, MA 02139, USA
[3] Department of Biology, Massachusetts Institute of Technology, McGovern Institute for Brain Research, Cambridge, MA 02139, USA
[4] Programa de Doctorado en Ciencias, Universidad de Valparaíso, Mención Neurociencia, Valparaíso, Chile
[5] Instituto de Neurociencias, Centro Interdisciplinario de Neurociencia de Valparaíso (CINV), Facultad de Ciencias, Universidad de Valparaíso, Valparaíso, Chile
[6] Millennium Nucleus of Neuroepigenetics and Plasticity (EpiNeuro), Santiago, Chile

© The Author(s) 2024. **Open Access** This article is licensed under a Creative Commons Attribution 4.0 International License, which permits use, sharing, adaptation, distribution and reproduction in any medium or format, as long as you give appropriate credit to the original author(s) and the source, provide a link to the Creative Commons licence, and indicate if changes were made. The images or other third party material in this article are included in the article's Creative Commons licence, unless indicated otherwise in a credit line to the material. If material is not included in the article's Creative Commons licence and your intended use is not permitted by statutory regulation or exceeds the permitted use, you will need to obtain permission directly from the copyright holder. To view a copy of this licence, visit http://creativecommons.org/licenses/by/4.0/. The Creative Commons Public Domain Dedication waiver (http://creativecommons.org/publicdomain/zero/1.0/) applies to the data made available in this article, unless otherwise stated in a credit line to the data.

Background

Thousands of mutations have been implicated in promoting neurodevelopmental disorders, with different degrees of certainty and a myriad of phenotypes [1–6]. An understanding of the consequences of specific gene mutations will be crucial to identifying common pathways and potential therapies for these disorders. Autism spectrum disorders (ASDs) are neurodevelopmental disorders characterized by deficits in social interaction, repetitive behaviors, and anxiety [7]. In addition, memory performance involving working and spatial memory is severely reduced in ASD patients [8, 9]. ASD can be driven by mutations that cause changes in brain wiring, structure, and function. Mutations in more than 1300 genes—including single-nucleotide polymorphisms (SNPs), copy-number variations (CNVs), deletions, and duplications—are associated with ASD, reflecting the complexity of its multifactorial genetics [1–6]. In particular, mutations that affect the function, loading, or availability of synaptic vesicles have been strongly associated with the manifestation of ASD-like phenotypes [10]. For instance, mice carrying mutations in Syn1, a synaptic vesicle component, cause limited synaptic vesicle release and, in Nhe9, a Na + /H + exchanger, cause hyper-acidification of vesicles; both mice mutants show phenotypes associated with ASD [11–13].

The evolutionarily conserved VPS50 protein functions in synaptic and dense-core vesicle maturation and acidification both in *Caenorhabditis elegans* and in murine cultured neurons and controls behavioral state in *C. elegans;* VPS50 is widely expressed in both the *C. elegans* and the murine nervous system [14]. VPS50 is associated with components of the Golgi-associated retrograde protein (GARP) complex and more specifically with the endosome-associated recycling protein (EARP) complex, suggesting a role in endocytosis of synaptic vesicles by early endosomes [15, 16]. In *C. elegans* VPS50 physically interacts with the protein VHA-15, a component of the V-ATPase complex pump responsible for acidifying both dense core and synaptic vesicles, and knockdown of VPS50 in cultured murine neurons causes a robust decrease in synaptic vesicle acidification [14]. In humans, a deletion spanning the *Vps50* gene, and the calcitonin receptor, has been reported in an ASD patient [17]. More recently, two patients with a neurodevelopmental disorder including severe developmental delays and intellectual disability were reported to carry homozygous loss-of-function mutations in *Vps50* [18]. These findings implicate VPS50 in ASD. However, no mechanisms have been identified that link the phenotypes shown by these patients to their deficits in *Vps50* function.

Below we describe our use of the CRISPR/Cas9 system to produce VPS50 knockouts (KO) in cultured murine neurons and mosaic knockouts (mKOs) in living mice, allowing us to analyze the role of VPS50 in synaptic function and mouse behavior. Our findings suggest mechanisms through which VPS50 mutations contribute to ASD phenotypes in general and to cognitive impairment in particular. In addition, our brain mosaic VPS50 mKO animal model should enable further investigations into the cellular and molecular mechanisms underlying the function of VPS50 and its relationship to ASD.

Results

VPS50 modulates synaptic vesicle acidification and V-ATPase V1 domain pump localization in cortical neurons

In *C. elegans*, VPS50 KO causes changes in behavior state, likely as a consequence of defects in synaptic and dense core vesicle acidification [14]. In mice, VPS50 is highly expressed in the central nervous system, and its knockdown in culture causes dysregulation of synaptic vesicle acidification [14]. To further investigate the role of VPS50 in regulating mammalian synaptic function and behavior, we used the CRISPR/Cas9 technology to generate VPS50 KO murine neurons. Cortical neuron cultures from Cas9 KI mice were transduced at 3 DIV with AAV encoding tdTomato as an infection marker alone or together with sgRNAs targeting the *Vps50* gene. The transduction efficiency reached > 90% of cultured neurons. Genomic DNA was extracted 10 days after infection, and a T7 endonuclease I assay was performed to determine the efficiency of gene editing. We tested different combinations of sgRNAs targeting the *Vps50* genomic locus and observed the highest editing efficiency when the pair sgRNA1 and sgRNA6 were used together (Additional file 1: Fig. S1A).

Next, we performed a series of experiments using together sgRNA1 and sgRNA6 (hereafter referred to as "VPS50 KO" in culture and "VPS50 mKO" in mice). T7 endonuclease I assay revealed that in cultured neurons VPS50 KO allows efficient gene editing (Fig. 1A). Editing of the *Vps50* locus caused a ~ 70% reduction in VPS50 mRNA and protein levels in cortical neurons (Fig. 1B–D), confirming an efficient KO of VPS50 after gene editing. Locus-specific sequencing showed the resulting edited genomic sequences that were introduced by CRISPR/Cas9 as evidenced by the presence of deletions represented by dashes when compared to the WT sequence (Additional file 1: Fig. S1B). Since VPS50 has been related to synaptic vesicle acidification, we next evaluated if the number of vesicles was changed in VPS50 KO neurons. Importantly, VPS50 KO neurons showed no significant difference in the total number of synaptic vesicles as assessed by electron microscopy (Fig. 1E, F). To determine changes in synaptic vesicle acidification, we used the ratio-SyPhy probe, which in red signal shows all

synaptic vesicles and in green the vesicles with basic pH, we observed a robust reduction in vesicle acidification in VPS50 KO neurons (Fig. 1G). Quantification using a Mander's coefficient to show the ratio of red clusters (vesicles) that are also green (high pH) shows a reduction in the coefficient (Fig. 1H), consistent with previous observations showing that VPS50 modulates synaptic vesicle acidification [14].

As VPS50 is enriched in synaptic and dense core vesicles and appears as a soluble protein in mouse brain extracts [14], we next performed proximity ligation assays (PLA) to evaluate its approximate location within the synapse. PLA assesses the proximity between two proteins of interest by generating a positive fluorescent signal. In this study, the positive signal is observed as puncta in the red channel (550 nm), indicating that the targeted proteins are within a distance of < 40 nm. First, we tested in control neurons whether VPS50 was proximal to either the post-synaptic protein PSD95 or the presynaptic protein in synaptic vesicles Synapsin1. We observed the PLA signal only in proximity to Synapsin1, confirming that VPS50 is near or within synaptic vesicles (Fig. 2A). This interaction was quantified showing high PLA puncta only in the VPS50/Syn1 condition (Fig. 2B). As controls, we performed PLA reactions using Synapsin1/Synaptophysin and PSD95/Synaptophysin (Additional file 1: Fig. S2A-B). Since VPS50 interacts directly with ATP6V1H in murine tissue [14] and synaptic vesicle acidification is reduced in VPS50 KO neurons [14] (Fig. 1G, H), it is possible that VPS50 facilitates the sorting or assembly of the V-ATPase complex in synaptic vesicles to acidify them for neurotransmitter filling. To test this possibility, we used PLA to evaluate the proximity of VPS50 and the V-ATPaseV1 domain of the pump in control neurons and observed PLA signal, indicating proximity between VPS50 and the V-ATPaseV1 domain (Fig. 2C; top). Importantly, in VPS50 KO neurons, this PLA signal was absent, confirming the reduced expression of VPS50 and a consequent lack of interaction between VPS50 and the V-ATPaseV1 domain of the pump (Fig. 2C; bottom). Quantification of the PLA signal between VPS50/v-ATPaseV1 shows a significant decrease in the number of puncta per field in VPS50 KO neurons (Fig. 2D). We then asked if the localization of the V-ATPaseV1 domain is disrupted in VPS50 KO neurons. While PLA experiments examining the V-ATPaseV1 domain and Synaptophysin showed that they are in proximity in control neurons (Fig. 2E; top), no corresponding signal was observed in VPS50 KO neurons (Fig. 2E; bottom), strongly suggesting that KO of VPS50 causes a mislocalization of the V-ATPaseV1 domain. Quantification of PLA signal between v-ATPaseV1/Syn shows a significant decrease in VPS50 KO neurons (Fig. 2F). As a control to show that there are no changes in the expression of the interacting proteins, in all PLA experiments, we imaged in the blue channel (633 nm) the proteins of interest that were used to test interaction (Fig. 2). As an additional control for PLA experiments, we carried out western blot analyses of PSD95 and Synaptophysin in VPS50 KO neurons. As expected, we found a small reduction in PSD95 expression and no change in Synaptophysin expression levels (Additional file 1: Fig. S2I). Together, these results indicate that KO of VPS50 does not affect the total number of synaptic vesicles but produces a mislocalization of the V-ATPaseV1 domain that could in turn prevent the correct assembly of the v-ATPase complex and as a consequence could be likely responsible for the observed impairment in synaptic vesicle acidification [14] (Fig. 1G, H).

VPS50 KO impairs synaptic activity in cortical neurons

To further evaluate the effect of VPS50 KO on synaptic function, murine cortical neurons were infected at 3 DIV and miniature and spontaneous excitatory postsynaptic currents (mEPSC and sEPSC, respectively) were recorded at 12–13 DIV. Compared to control neurons, VPS50 KO neurons showed a strong reduction in both the amplitude and frequency of sEPCS (Fig. 3A–C). To determine if the amplitude and frequency of sEPSC decreased with time, we performed continuous sEPSC recordings for 30 min. While in control neurons we observed no significant changes, VPS50 KO neurons displayed a significant reduction in the amplitude of the sEPSCs over time (Additional file 1: Fig. S3A-C), consistent with the idea

(See figure on next page.)

Fig. 1 VPS50 gene editing causes a decrease in synaptic vesicle acidification but no change in synaptic vesicle number. Cortical neurons from Cas9KI mice were transduced with sgRNA targeting VPS50 at 3 DIV to produce VPS50 KO. **A** T7 endonuclease I assay of control or VPS50 KO cortical neurons. **B** RT-qPCR to quantify relative mRNA expression of VPS50. **C** VPS50 protein expression in VPS50 KO and control neurons. N-cadherin was used as loading control. **D** Quantification of VPS50 expression in western blots ($n = 6$ biological replicates). **E**, **F** Representative images of synaptic terminals as visualized by electron microscopy and quantification of the number of synaptic vesicles in control and VPS50 KO neurons ($n = 50$ cells per condition from 3 independent experiments). **G** Representative images of the Ratio-SyPhy signal used to determine synaptic vesicle acidification in control and VPS50 mKO neurons. Red signal shows all synaptic vesicles and green signal shows vesicles with basic pH. **H** Quantification of Ratio-SyPhy signal showing Mander's coefficient. Thirteen samples from 3 biological replicates were used for Ratio-SyPhy quantification. Scale bar: 400 nm (**E**); 25 µm (**G**). Unpaired *t*-test was used for statistical analysis; ***$p < 0.001$. Error bars represent ± SEM. ***$p < 0.001$

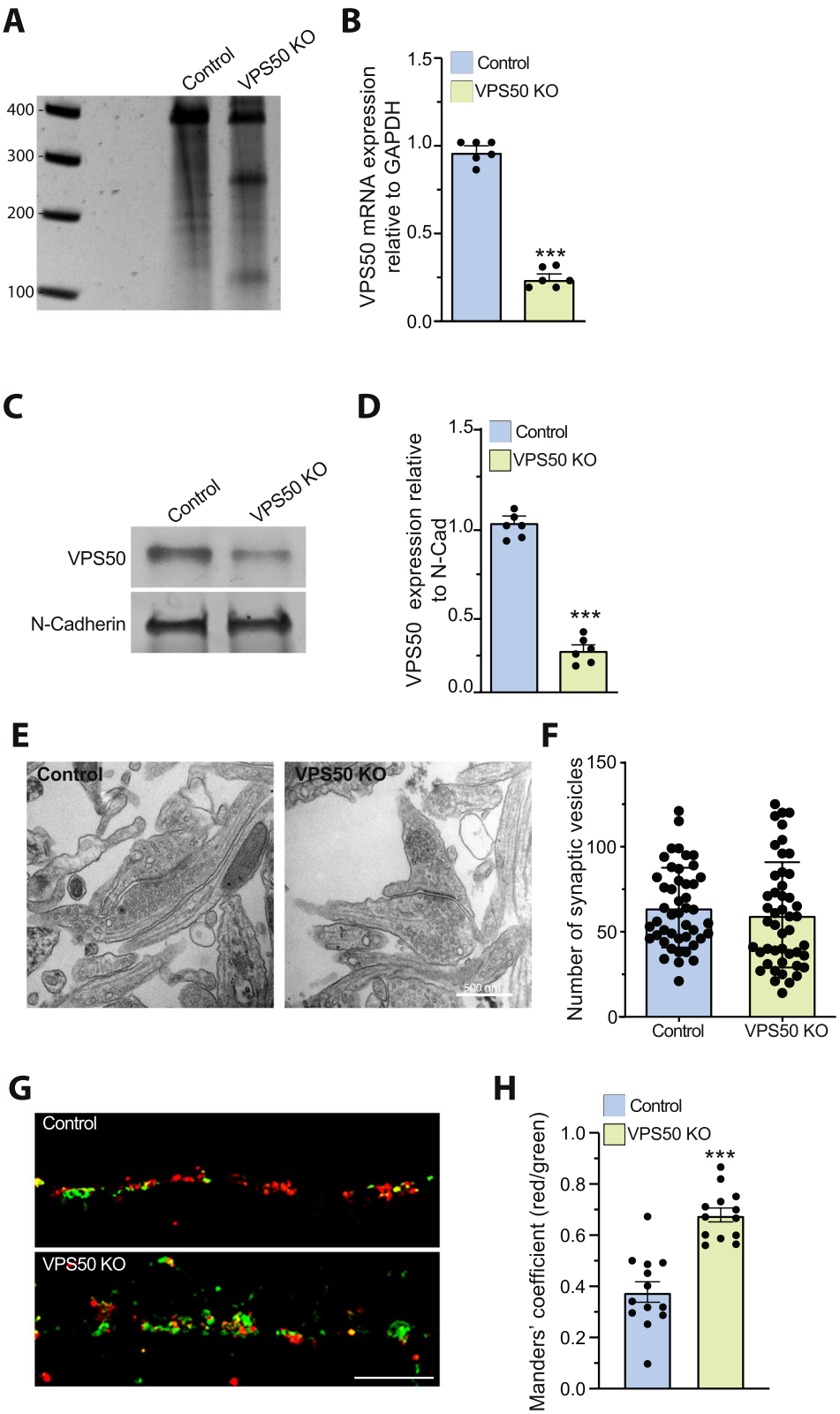


Fig. 1 (See legend on previous page.)

that vesicular content might be reduced in VPS50 KO neurons. Moreover, VPS50 KO neurons showed a drastic reduction in the frequency but not in the amplitude of mEPSCs (Fig. 3D–F), an effect that could reflect an increase in the exocytosis of empty vesicles. This reduction in synaptic strength correlates with a decrease in neuronal activity, as the spontaneous spike frequency was decreased in VPS50 KO neurons compared to control neurons (Fig. 3G, H). In addition, calcium imaging using the genetically encoded GCaMP7 probe showed that VPS50 KO neurons were reduced in calcium event frequency, confirming deficient spiking (Additional file 1: Fig. S3D-E). To further evaluate if synaptic vesicle acidification was partly responsible for the reduction in vesicle content and neuronal activity, we used pHoenix, a genetically encoded proton pump targeted to synaptic vesicles [19]. Spontaneous spiking of pHoenix-infected control and VPS50 KO neurons was recorded for 1 min as baseline, and then, 532 nm light was used to activate pHoenix (yellow line under traces). During the 2-min activation period, we observed a partial recovery of spiking in VPS50 KO neurons close to control levels (Fig. 3I, J; yellow line). Moreover, after stimulation, we observed no significant differences from control neurons (Fig. 3K). Altogether, our results strongly indicate that the reduction in synaptic activity in VPS50 KO requires synaptic vesicle acidification, since this reduction can be rescued by artificially acidifying synaptic vesicles.

VPS50 mKO impacts synaptic function and memory formation

Having demonstrated that VPS50 KO causes a deficit in vesicle acidification as shown by Ratio-SyPhy (Fig. 1G, H), and synaptic function in cultured cortical neurons (Fig. 3), we next aimed to evaluate whether VPS50 mKO in mice can cause changes in synaptic transmission and behavior in vivo, as observed previously for *C. elegans* [14] and as suggested for humans [18]. Toward this end, we used the CRISPR/Cas9 system to induce VPS50 mKO in the intact mouse brain. We delivered high titer AAVs at postnatal day 1 (P1) intracerebroventricularly to Cas9 KI mice. Animals were injected with the same sgRNAs tested previously in culture together with tdTomato as a fluorescence marker under the control of the human synapsin1 promoter; tdTomato alone was used as control. Post-mortem analyses showed high AAV infection in multiples brain areas (Fig. 4A, B), including the cortex and the hippocampus (Fig. 4C). In those brain areas, VPS50 protein expression was significantly reduced > 70% (Fig. 4D–F), confirming efficient mKO of VPS50 after gene editing in the mouse brain. In addition, the expression of VPS50 mRNA was also significantly reduced in VPS50 mKO animals (Fig. 4G, H). No changes were observed in the brain length of VPS50 mKO mice; however, a significant difference in brain weight was found compared to the control group (Additional file 1: Fig. S4A-D). We then monitored basal synaptic function at Schaffer collateral-to-CA1 synapses in acute hippocampal slices. We observed a significant decrease in the frequency but not in the amplitude of miniature excitatory postsynaptic currents (mEPSCs) in VPS50 mKO synapses (Fig. 5A–C). Similarly, we observed a strong reduction in the frequency and amplitude of spontaneous EPSCs (sEPSCs) in VPS50 mKO synapses (Fig. 5D–F). Moreover, input/output curves revealed a large decrease in the amplitudes of evoked EPSC at all stimulus intensities tested for VPS50 mKO synapses (Fig. 6A, B). Importantly, paired-pulse facilitation remained unchanged (Fig. 6C, D), suggesting that the decrease in evoked EPSC amplitude cannot be explained by changes in release probability, but rather could be a consequence of a decrease in vesicle content and/or vesicle refilling caused by a change in the level of acidification, as observed for cultured neurons (Fig. 1G). To further evaluate whether the filling state of vesicles might be involved in this synaptic change, we used high-frequency stimulation to assess the response of VPS50 mKO synapses. High-frequency stimulation promotes full fusion of synaptic vesicles and posterior fast endocytosis for neurotransmitter filling. Thus, during high-frequency stimulation, a neuron with

(See figure on next page.)

Fig. 2 VPS50 KO causes mislocalization of v-ATPaseV1 domain in cortical neurons. Proximity-ligation assays (PLAs) was used to determine proximity between studied proteins as indicated in each case. A positive PLA signal, thus proximity between the proteins, is observed as red puncta in images (red channel, 546 nm). In all experiments, an antibody against the microtubule-associated protein 2 (MAP2) was used to stain processes of all neurons (green channel, 488 nm). Merge shows superimposed images of MAP2 (green), PLA signals (red), and the signal for a protein of interest as shown in the figure (blue, 633 nm). **A** PLA using PSD95 or Synapsin1 (Syn1) antibodies to define pre- or post-synaptic localization of VPS50 in control neurons. **B** Quantification of PLA puncta per field of VPS50/PSD95 and VPS50/Syn1. **C** PLA to assess proximity of VPS50 and v-ATPAseV1 domain in control and VPS50 KO neurons. **D** Quantification of PLA puncta per field of VPS50/v-ATPaseV1 in control and VPS50 KO neurons. **E** PLA to determine proximity of v-ATPaseV1 domain and Synaptophysin (Syn) in control and VPS50 KO neurons. **F** Quantification of PLA puncta per field of v-ATPaseV1 domain/Syn in Control and VPS50 KO neurons. Six low magnification (20×) fields from 3 independent biological samples were used for quantification in each condition. Scale bars, 25 µm. Unpaired *t*-test was used for statistical analysis; ***$p < 0.001$. Error bars represent ± SEM

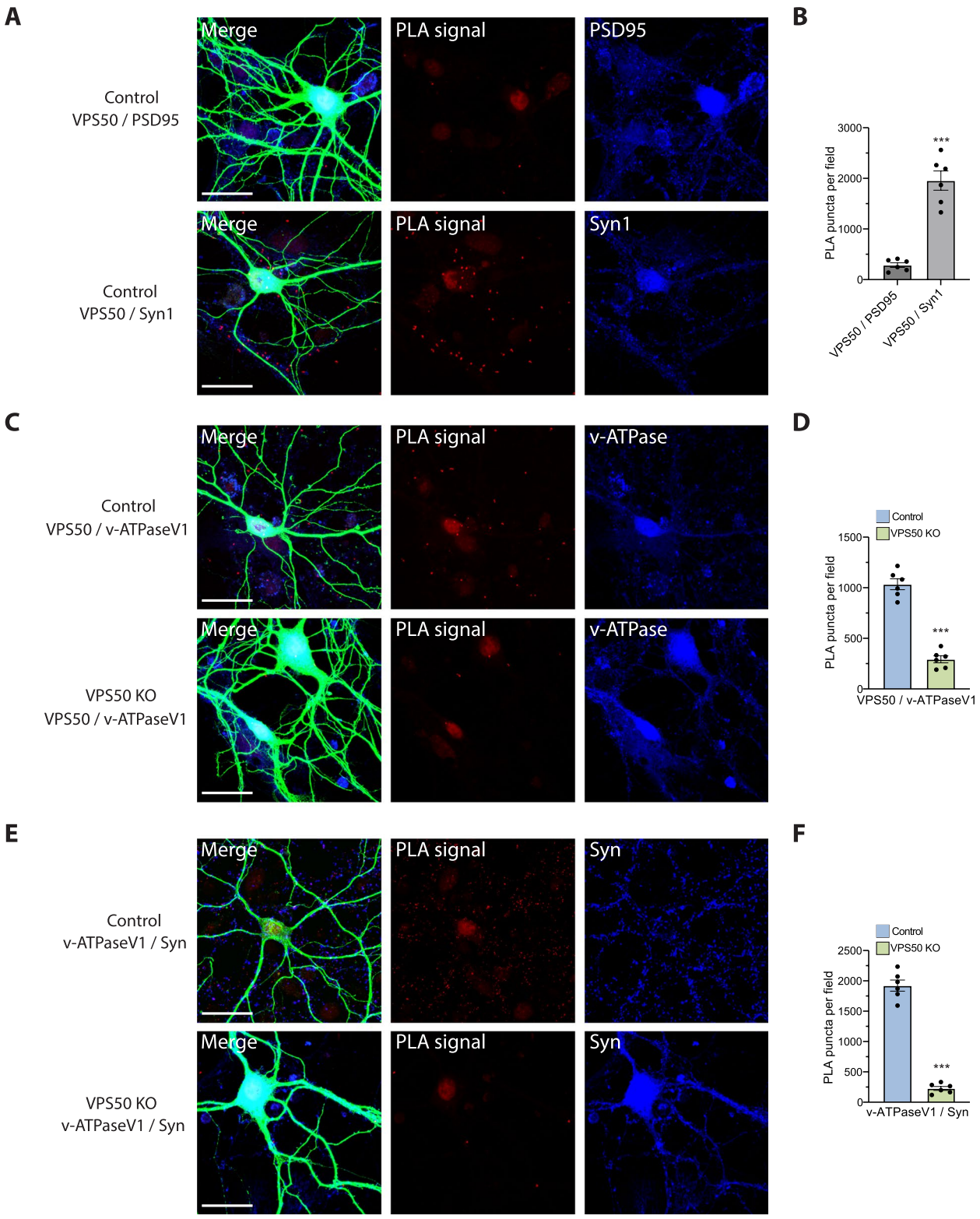


Fig. 2 (See legend on previous page.)

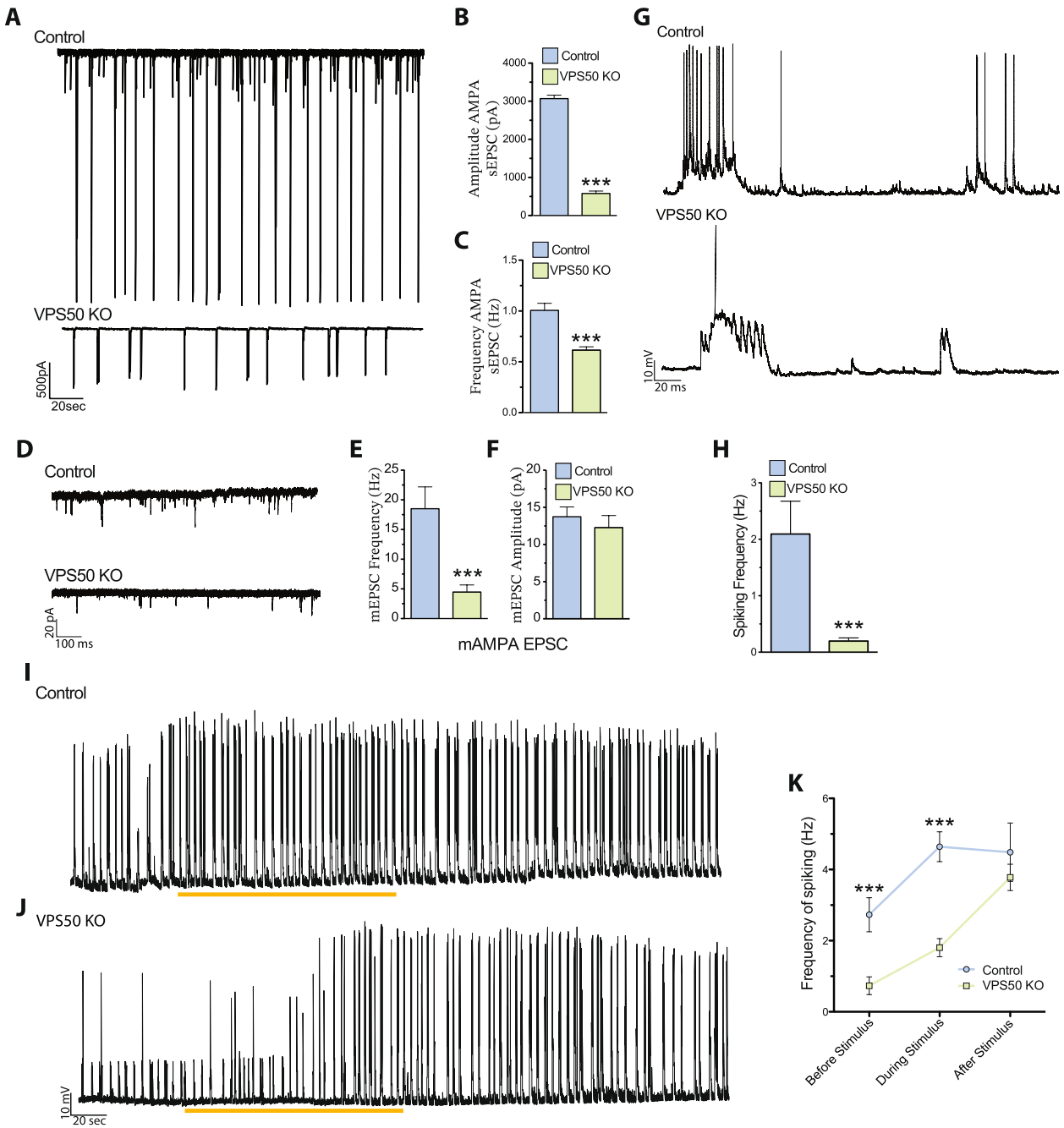


Fig. 3 VPS50 KO neurons show a reduction in synaptic activity that can be recovered by inducing synaptic vesicle acidification. Cortical neuronal cultures from Cas9KI animals were transduced at 3DIV and at 12–13 DIV used for electrophysiology or calcium imaging. **A** Representative traces and **B**, **C** quantification of amplitude (**B**) and frequency (**C**) of spontaneous AMPA-mediated EPSCs. **D** Representative traces and **E**, **F** quantification of the frequency (**E**) and amplitude (**F**) of miniature AMPA-mediated currents. **G** Representative traces and quantification of the frequency (**H**) of current clamp recordings of control and VPS50 KO neurons. **I**–**K** Representative traces of current clamp recordings of control and VPS50 KO neurons expressing pHoenix. Orange bars under the traces show the periods pHoenix was activated. **K** Quantification of the frequency of spiking of control and VPS50 KO neurons before, during, and after stimulus with pHoenix to artificially acidify synaptic vesicles. For all experiments, at least 18 neurons from 3 independent experiments were analyzed. Unpaired *t*-test was used for statistical analysis; ***$p < 0.001$. Error bars represent mean ± SEM

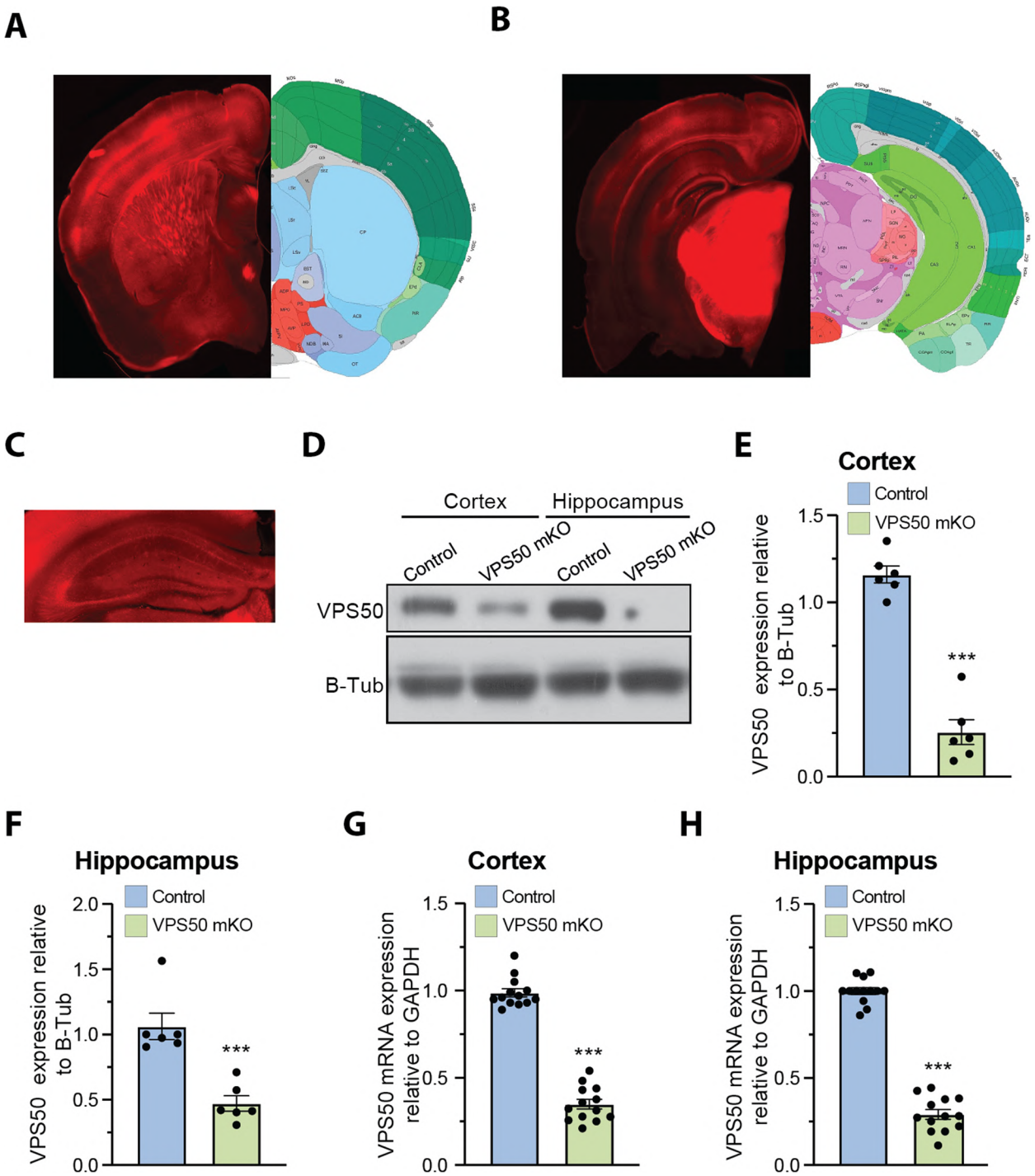


Fig. 4 Systemic injection of AAV at P1 to produce VPS50 mKO. **A**, **B** Representative image of coronal sections of a mouse brain (VPS50 mKO) injected at P1 with AAV after 15 weeks to show infection efficiency by tdTomato fluorescent signal. Two different sections are shown to show broad infection. **A**, **B** (right) Anatomical annotations from the Allen Reference Atlas – Mouse Brain (atlas.brain-map.org), at the same slice position as A and B (left). Scheme of the relative positions are shown to identify brain areas. **C** Higher magnification image of a hippocampus section showing transduction efficiency. **D** Representative western blot analyses for the detection of VPS50 expression in control and VPS50 mKO animals in both cortex and hippocampus. B-tubulin was used as loading control. **E**, **F** Quantification of VPS50 expression in western blots from cortex (**E**) or hippocampus (**F**) $n = 6$ animals per condition. **G**, **H** RT-qPCR to quantify expression of VPS50 in cortex (**G**) or hippocampus (**H**), $n = 13$ animals per condition. Scale bar, 500 µm. Unpaired *t*-test was used for statistical analysis; ***$p < 0.001$. Error bars represent ± SEM

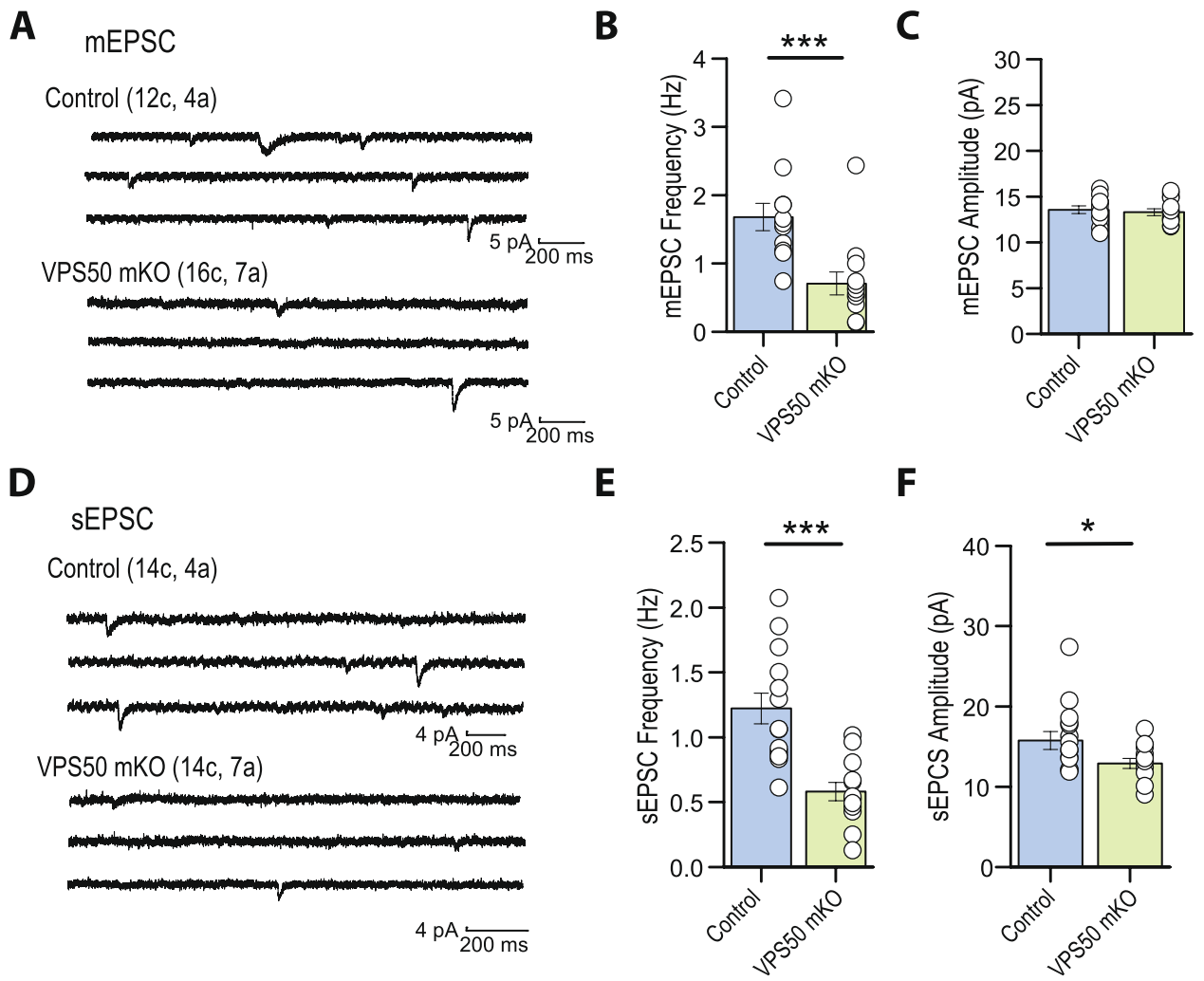


Fig. 5 Hippocampal spontaneous excitatory synaptic activity is impaired in VPS50 mKO mouse. **A** Representative traces of mEPSCs recorded from CA1 pyramidal neurons in acute hippocampal slices of control and VPS50 mKO animals. **B**, **C** Quantification of the frequency (**B**) and amplitude (**C**) of mEPSCs. **D** Representative traces of sEPSCs in hippocampal slices of control and VPS50 mKO animals. **E**, **F** Quantification of the frequency (**E**) and amplitude (**F**) of mEPSCs. In each representative trace (**A**–**D**), the numbers of cells (c) and animals (a) are indicated in parentheses. Two-samples Student *t*-test was used for statistical analysis; $*p < 0.05$, $***p < 0.001$. Summary data consist of mean ± SEM

partial or null synaptic vesicle filling would be detected as a decrease in quantal size. Under this condition, the responses of VPS50 mKO to high-frequency stimulation synapses were greatly reduced compared to control synapses (Fig. 6E, F), strongly suggesting that vesicle content is reduced in VPS50 mKO synapses. Next, we investigated the impact of VPS50 mKO on hippocampal long-term synaptic plasticity (LTP), the cellular mechanism underlying learning and memory. We found that the magnitude of LTP induced by high-frequency stimulation

(See figure on next page.)

Fig. 6 Hippocampal synaptic function and plasticity are impaired in VPS50 mKO mice. Electrophysiological recordings characterizing Schaffer collateral-to-CA1 synapses in acute hippocampal slices of control and VPS50 mKO animals. **A** Representative traces fEPSP of input–output curve elicited at different stimulus intensities. **B** Input–output curves reveal a strong reduction in the amplitude of fEPSC at all stimulus intensities tested. **C** Representative traces and **D** quantification of paired-pulse facilitation at different inter-stimulus intervals. **E** Representative synaptic responses and **F** quantification showing a strong synaptic depression in response to a single high-frequency stimulus train (100 pulses at 100 Hz) that likely reflect a reduce vesicular content in VPS50 mKO synapses compared to control synapses. **G** Representative traces before and after LTP induction elicited by four trains of high-frequency stimulation. Sample traces were taken at times indicated by numbers in summary plot. **H** Summary plot showing that the magnitude of LTP is reduced in VPS50 mKO animals. In each representative trace, the number of slices (s) or cells (c) and animals (a) are indicated in parenthesis. Two-samples Student *t*-test was used for statistical analysis; $*p < 0.05$. Summary data consist of mean ± SEM

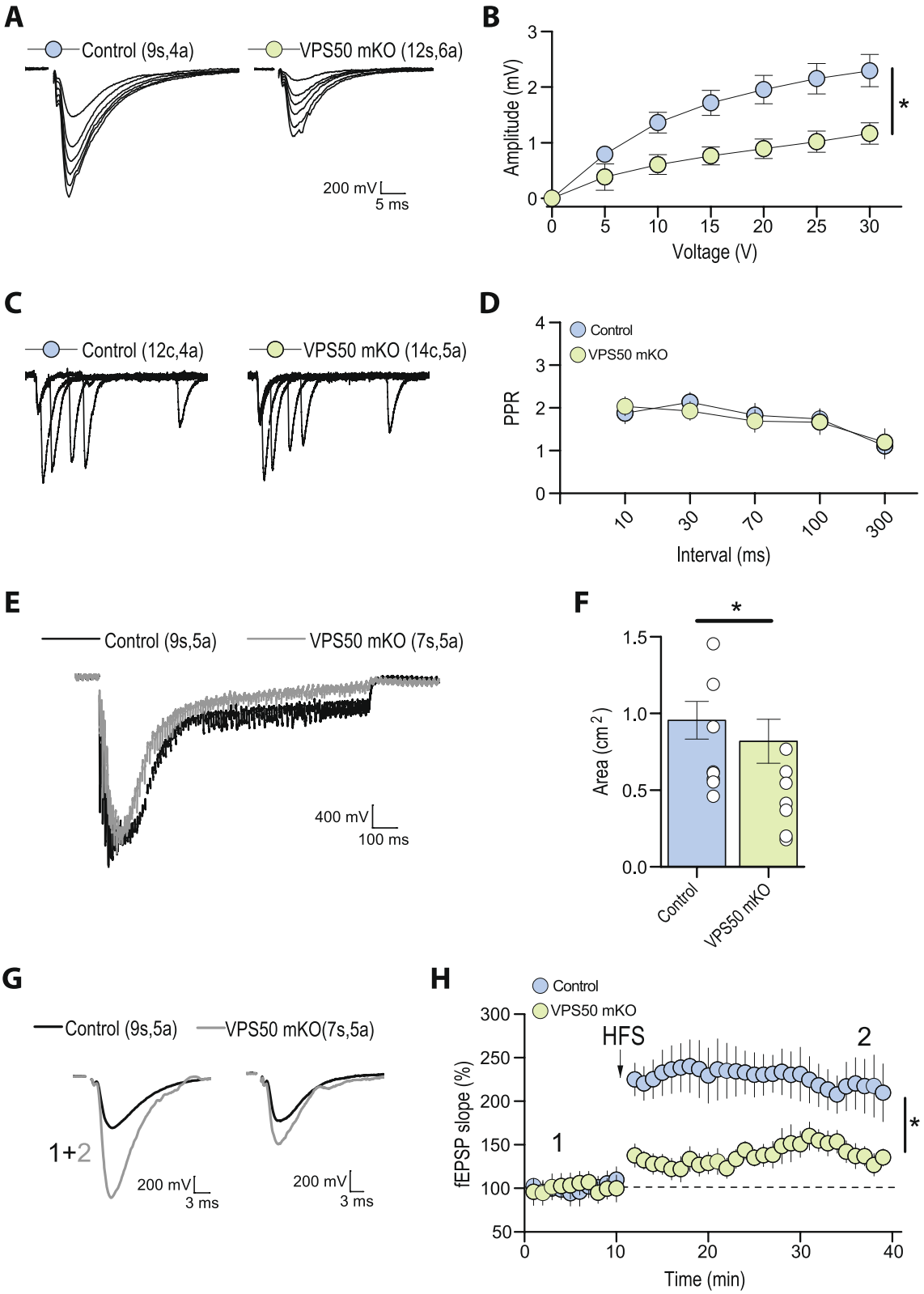


Fig. 6 (See legend on previous page.)

was reduced in mice with disrupted VPS50 compared to controls (Fig. 6G, H), suggesting that there might be cognitive deficits in the context of memory formation in VPS50 mKO mice.

Finally, we evaluated the cognitive performance of VPS50 mKO mice in the Barnes maze and a fear-conditioning apparatus (Fig. 7), two memory formation paradigms dependent on the hippocampus. First, we asked if VPS50 mKO mice had locomotor problems that might affect their performance in behavioral testing. Accelerated rotarod test showed that VPS50 mKO animals spent more time on the ramp, evidencing better motor function than control animals (Fig. 7A). In the Barnes maze (Fig. 7B), VPS50 mKO animals made a significantly higher number of primary errors (holes checked before finding the escape hole) on days 1 and 2 (Fig. 7C) but behaved similarly to control error numbers on days 3 and 4. Also, primary latency, the time the animal takes to find the escape hole, was significantly affected in VPS50 mKO, but only on the first day (Fig. 7D), and VPS50 mKO animals spent significantly less time in the escape zone on days 1–3 compared to control littermates (Fig. 7E). These data indicate that VPS50 mKO animals have deficits in the short-term acquisition of spatial learning. Using the context-dependent fear-conditioning paradigm, we found that VPS50 mKO animals significantly decreased

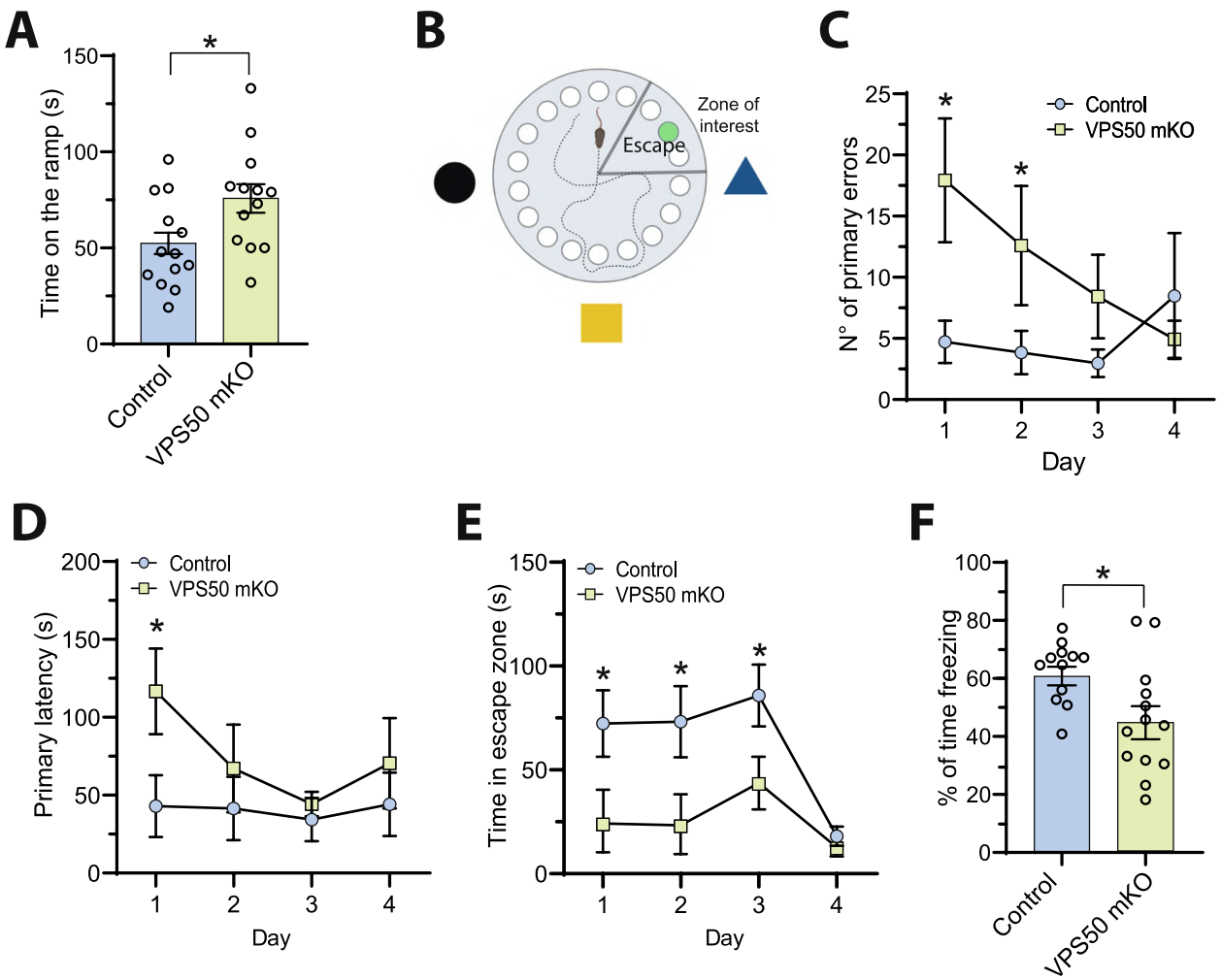


Fig. 7 VPS50 mKO animals show impaired hippocampal memory formation. Brain-wide control and VPS50 mKO animals were subjected to behavioral testing. **A** Quantification of the time spent on the ramp on the accelerated rotarod apparatus. **B** Scheme of the Barnes maze memory paradigm in which clues attached to the wall, escape hole, and escape zone are shown. **C** Quantification of the numbers of primary errors made by control and VPS50 mKO animals before finding the escape hole. **D** Quantification of the primary latency of control and VPS50 mKO animals to find the escape hole. **E** Quantification of the time control and VPS50 mKO animals spent in the escape zone. **F** Quantification of freezing percentage time shown by control and VPS50 mKO animals in the fear conditioning paradigm. For behavioral experiments, a total of $N = 13$ animals per condition were assayed. Unpaired *t*-test was used for statistical analysis; $*p < 0.05$. Error bars represent ± SEM

in freezing compared to control littermates (Fig. 7F). Together, these results indicate that VPS50 mKO mice display alterations in hippocampal synaptic function and memory deficits dependent on this brain area.

Discussion

The VPS50 protein is evolutionarily conserved, with homologs in *C. elegans, M. musculus*, and humans, reflecting its fundamental importance in cellular function [14, 18]. VPS50 has been associated with the EARP complex (endosome-associated recycling protein) and more specifically with dense core and synaptic vesicles [20]. Studies of *C. elegans* revealed that VPS50 controls locomotion and behavioral state by controlling vesicle acidification and function, likely by regulating the assembly of the V-ATPase pump [14]. The V-ATPase pump is recruited to synaptic vesicles after recycling to facilitate neurotransmitter filling [21]. *C. elegans* mutants in the gene unc-32, which encodes the homolog of the human V-ATPase pump, have severe deficits in motoneuron neurotransmission [22]. Interestingly, the V-ATPase pump acidifies cellular compartments broadly in the cell; specificity is conferred by the differential formation of the complex by different isoforms and protein interactions [23].

Our findings reveal a critical role of VPS50 in synaptic function and behavior in mammals and demonstrate that this role likely involves synaptic vesicle acidification. Using CRISPR/Cas9 to produce KO of VPS50 in cultured cortical neurons, we showed that VPS50 KO neurons exhibited mislocalization of the V-ATPaseV1 domain, lacking proximity to synaptic vesicles, without affecting the total number of synaptic vesicles. Instead, this mislocalization impedes the correct assembly of the v-ATPase complex affecting vesicle acidification, thereby influencing vesicular content and/or vesicle refilling. The limited acidification of synaptic vesicles is known to reduce neurotransmitter filling and cause a consequent decline in synaptic activity [10, 21, 24]. Our findings strongly indicate that VPS50 plays a crucial role in facilitating the proper sorting of the v-ATPaseV1 domain near synaptic vesicles or the assembly of the v-ATPase complex that permits synaptic vesicle acidification.

Our data further demonstrate that in cultured neurons the reduction of VPS50 impairs synaptic transmission and that these deficiencies can be recovered by artificially acidifying synaptic vesicles. Electrophysiological recordings using hippocampal slices showed a strong decrease in the frequency of spontaneous synaptic events, a reduction of the amplitude after high-frequency stimulation, and a severe deficit in LTP formation. These observations strongly support the idea that the changes observed in synaptic activity were a consequence of the exocytosis of empty or partially filled synaptic vesicles, similar to what has been shown in cultured hippocampal neurons in which the v-ATPase pump had been pharmacologically blocked [25]. These synaptic transmission defects likely caused the impaired memory formation of VPS50 mKO animals, linking the deficits in synaptic vesicle acidification and/or synaptic filling to complex cognitive behaviors such as learning and memory formation. Deficits in working and spatial memory have been described as one of the phenotypes of ASD patients [8, 9], a phenotype that has also been described for patients with VPS50 mutations [18].

In summary, our data demonstrate that VPS50 modulates synaptic transmission by facilitating the recruitment of the V-ATPase pump to synaptic vesicles, thereby enabling vesicle acidification and modulating vesicle content. Deficits in this process, as exhibited by VPS50 mKO mice, result in cognitive impairment. Future studies of VPS50 mKO mice should provide a comprehensive understanding of the behavioral consequences of VPS50 mKO and provide insights into how mutations in the VPS50 gene can lead to ASD.

Conclusions

Our study provides compelling evidence for the critical role of the evolutionarily conserved VPS50 protein in synaptic function and behavior across mammalian species. Utilizing CRISPR/Cas9 knockout techniques, we have elucidated the involvement of VPS50 in regulating synaptic vesicle acidification, a process crucial for neurotransmitter filling and synaptic activity. Our findings shed light on the molecular mechanisms underlying VPS50's function and highlight the significance of VPS50 in maintaining synaptic transmission integrity, as evidenced by the impaired synaptic activity and cognitive deficits observed in VPS50 mKO mice. These results not only deepen our understanding of synaptic function but also provide valuable insights into the etiology of neurodevelopmental disorders such as ASD.

Methods

Animals and injections

All animal procedures and experiments were performed according to NIH and ARRIVE guidelines and were approved by MIT Committee on Animal Care (CAC) and the animal ethics committee from Universidad Andrés Bello (020/2018). Animal injections were performed as in [26, 27]. Briefly, newborn Cas9 KI mice (C57BL/6J; JAX 026179) were cryoanesthetized in a cold aluminum plate and injected with 1 µL of concentrated AAV (1×10^{11} vg) in each cerebral ventricle at a depth of 3 mm in the animal's head at 2/5 of the intersection between lambda and the eye with a 10-µL HAMILTON syringe (Hamilton,

7653–01) and a 32-G needle (Hamilton, 7803–04). After the injection, mice were placed in an infrared heating pad at 37 °C until they recovered their pink color, at which point they were returned to the cage with their mother [26–28]. In the third week after birth, mice were weaned and separated by sex into cages with a 12 h/12 h light/dark cycle with free access to food and water. An electronic chip (p-chips, Pharmaseq) with a unique identifier was put in the tail of each injected animal to facilitate animal tracking. After behavioral testing, mice were anesthetized with isoflurane (3% in 0.8 L/min air flow) in an induction chamber for 3 min and decapitated for molecular analyses.

Neuronal cultures

At P1, neonatal mice were quickly decapitated and dissected in ice-cold HBSS to obtain cerebral cortices as described by [26, 27, 29, 30]. Cortices were minced and incubated for 20 min at 37 °C with papain (Worthington, USA) for enzymatic digestion. Then, cells were transferred to a 15-ml tube containing plating media (D-MEM supplemented with 10% fetal bovine serum and 100 U/ml penicillin/streptomycin; Life technologies 15,070–063). Cells were resuspended by mechanical agitation through fire-polished glass Pasteur pipettes of decreasing diameters. Cells were plated on freshly prepared poly-L-lysine-coated plates. After 2 h, plating media were replaced with growth media (Neurobasal-A (Life technologies 1,088,802) supplemented with B27 (Life technologies 17,504,044), 2 mM L-glutamine (Life technologies 25,030–081), 100 U/ml penicillin/streptomycin (Life technologies 15,070–063)). Half of the media was replaced every 3 days.

AAV production

AAV viral particles containing sgRNA directed to VPS50, red fluorescent protein tdTomato under the control of the human Synapsin1 promoter (hSyn), and packaged with the PHP.eB capsid [31] were obtained from HEK 293T cells and purified as described by [26, 27]. AAVs were also prepared using transfer plasmids encoding GCamP7f to measure calcium transients (Addgene Cat#104,488), and custom AAV plasmids for enhanced Cas9 (eCas9) [32], SyPhy to assess synaptic vesicle acidification [33], plus pHoenix to artificially acidify synaptic vesicles [19]. Briefly, HEK 293T cells were grown to approximately 6×10^4 cells/cm^2 with DMEM 10% FBS. Cultures were transfected using the PEI "MAX" reagent (Polysciences, Cat 24,765) with PHP.eB capsid plasmids, the vector with transfer plasmids, and the helper plasmid DF6. After 24 h of transfection, the media was exchanged for DMEM 1% FBS. After 72 h, media was collected from the plates and replaced with fresh DMEM 1% FBS. The collected media was stored at 4 °C, and 120 h after transfection cells were detached from the plate and transferred to 250-mL conical tubes, together with the collected media and centrifuged for 10 min at 2000*g*. The supernatant was removed and saved for later use, and the pellet was resuspended in SAN digestion buffer (5 mL of 40 mM Tris, 500 mM NaCl, and 2 mM MgCl2 pH 8.0) containing 100 U/mL of Salt Active Nuclease (Arcticzymes, USA) and incubated at 37 °C for 1 h. The supernatant was precipitated using 8% PEG 8000 and 500 mM NaCl, incubated on ice for 2 h, and centrifuged at 4000*g* for 30 min in 250-mL bottles. Pellet was resuspended with SAN digestion buffer and the complete solution was placed in an iodixanol gradient (15 to 60%) and centrifuged at 350,000*g* for 2.5 h. The phase containing the AAV was rescued and frozen at − 80 °C for later use.

Proximity ligation assays

Assays were conducted using the Duolink PLA Fluorescence kit (Sigma-Aldrich) following the manufacturer's instructions. Briefly, cortical cultured neurons were fixed using 4% paraformaldehyde for 20 min at RT, washed 3 times with PBS, permeabilized using 0.05% Triton X-100 for 5 min, and rinsed 3 times with PBS. Samples were incubated with blocking solution for 1 h at 37 °C and incubated with primary antibodies (VPS50, Sigma Aldrich, HPA026679, rabbit 1:100; PSD95, Neuromabs, 75–348, mouse 1:250; Synapsin1, Synaptic Systems, 106,011, mouse 1:1000; Synaptophysin, Zymed, 180,130, rabbit 1:1200; v-ATPase H, Santa Cruz Biotechnology, SC-166227, mouse 1:100) overnight at 4 °C. Samples were washed twice with buffer A for 5 min, incubated with plus-minus probes for 1 h at 37 °C, washed twice with buffer A, and incubated with ligation mixture for 30 min at 37 °C. Samples were washed twice with buffer A, incubated with an amplification mixture for 2 h at 37 °C, and washed twice for 10 min with buffer B. Lastly, samples were mounted, and images were acquired using a Nikon C2 + confocal microscope (Nikon, USA).

Brain sectioning and mounting

To assess brain infection, half of the brains were submerged in PBS + 4% PFA + 4% Sucrose into 30-mL flasks and fixed for a minimum of 24 h. After fixation, a Leica VT1000 vibratome was used to cut 100-µm coronal sections. Slices were kept in PBS 1X and mounted using Fluoromount G (EMS, Hatfield, PA) to preserve the fluorescence signal. Brain images were captured with a Nikon Eclipse TE2000 epifluorescence microscope (Nikon, USA).

Protein extraction and electrophoresis

For immunodetection tests, proteins were extracted from the cortex and hippocampus of mice brains. Fifty milligrams of tissue was ground in N-PER lysis buffer (ThermoFisher Product No. 23225) with protease and phosphatase inhibitors (cOmplete Protease Inhibitor Cocktail 11,697,498,001, Roche Diagnostics) until a homogeneous solution was achieved and incubated for 10 min on ice. This extract was centrifuged at 10,000*g* for 10 min at 4 °C. The supernatant with extracted proteins was collected and quantified using the BCA method, following the manufacturer's recommendations (Perkin-Elmer). For electrophoresis, the proteins were denatured in loading buffer (NuPAGE LDS Sample buffer 4X; NP0007) and heated at 95 °C for 10 min. Forty micrograms of the sample was loaded onto an SDS 6% acrylamide-bisacrylamide gel to visualize proteins larger than 100 kDa and a 10% gel for proteins smaller than 100 kDa. Electrophoresis was performed at 80–150 V constant voltage in running buffer (25 mM Tris·Cl, 250 mM glycine, 0.1% SDS) in a minichamber (MiniPROTEAN System, BIO-RAD).

Western blots

After electrophoresis, proteins were transferred to an activated PDVF membrane in transfer buffer (250 mM glycine, 25 mM Tris–Cl, 20% methanol) at 400 mA constant current for 1.5 h. To verify protein transfer, the membrane was incubated with Ponceau red S (0.1% Ponceau S, 5% acetic acid). The membrane was washed with TBS/Tween 20 0.05% until the Ponceau red staining was removed. Next, the membrane was blocked for 1 h to eliminate non-specific protein binding sites in a 0.05% TBS/Tween 20 solution with 5% skim milk. The membrane was then incubated with the specific primary antibody VPS50 (Sigma, HPA026679-100UL, Rabbit, 1/500 dilution) in 0.05% TBS/Tween 20 solution with 5% skim milk at 4 °C overnight. The membrane was washed with TBS/Tween 20 0.05% five times for 5 min each. Then, the membrane was incubated with a second antibody directed against the first antibody and coupled to horseradish peroxidase (HRP) (anti-rabbit HRP, CS7074, Cell Signaling Technology, USA) in TBS/Tween 20 0.05% with 5% skim milk at room temperature for 1 h. The membrane was washed with TBS/Tween 20 0.05% five times for 5 min each. Detection was performed with chemiluminescence reagents (SignalFire™ Elite ECL Reagent). Protein expression was normalized to β-Tubulin expression (Abcam, ab6046, Rabbit, 1/500) or N-Cadherin (Santa-Cruz Biotechnology, SC-7939, rabbit. 1/500).

DNA and RNA extraction

Thirty to 50 mg of tissue were weighed for DNA and RNA extractions with Quick-DNA/RNA Miniprep kit (Zymo Research, D7001). Briefly, the tissue was homogenized with a Dounce homogenizer in lysis buffer and centrifuged for 30 s at 14,000*g*. The supernatant was collected and transferred to a Zymo-Spin IIICR column in a collection tube and centrifuged at 14,000*g* for 30 s. The filtrate was used for RNA extraction, and the column for DNA extraction. For RNA extraction, the same volume of 100% ethanol was added and homogenized, transferred to a Zymo-Spin IICR column, and centrifuged at 14,000*g* for 30 s. The column was then treated with DNase I, 400 µL DNA/RNA Prep Buffer was added, and the column was centrifuged and washed twice with wash buffer. To elute the RNA, 25 µL of nuclease-free water was added, incubated for 3 min, quantified, and stored at − 80 °C for later use. For DNA extraction, 400 µL DNA/RNA Prep Buffer was added to the Zymo-Spin IIICR column, and the column was centrifuged and washed twice with wash buffer. To elute the DNA, 50 µL of nuclease-free water was added, incubated for 5 min, quantified, and stored at − 80 °C for later use.

RT-qPCR

RT-qPCR assays were performed using 400 ng of extracted total RNA. To obtain complementary DNA (cDNA), each sample was mixed with 0.25 µg Oligo-dT (New England Biolab S1316S) in 10 µL of nuclease-free water, denatured at 75 °C for 5 min and then quickly transferred to 4 °C for 5 min. Reverse transcription (RT) was performed in a final 20 µL volume containing: 10 µL denatured RNA, 100 U of M-MLV Reverse Transcriptase (NEB; M0253S), M-MLV RT buffer (NEB; B0253S) 1X, 20 U of RNase Inhibitor (NEB; M0314S), and 0.5 mM of dNTPs (Biotechnology N557-0.5ML). The mixture was incubated at 42 °C for 1 h, then at 95 °C for 5 min, and the reaction was stopped at 4 °C and then diluted five times with nuclease-free water. Three microliters of the diluted cDNA were used for real-time PCR reactions, using relative abundance by the ddCt method, and GAPDH transcript as a loading control. Transcript detection was performed with specific primers for VPS50 mRNA (Sense: TGTTACTTCTC CGAGGCAGG, Antisense: GCTCTCAAAGGACCAAGAT) and GAPDH mRNA (Sense: ATGGTGAAGGTCGGTGTG AA, Antisense: CATTCTCGGCCTTGACTGTG).

Transmission electron microscopy

Electron microscopy was conducted as described in [34]. Briefly, cortical neurons were grown on sterilized Aclar pieces (EMS, Cat#50,425) and infected at 3 DIV with AAVs to produce VPS50 KO. Ten days after infection, cultures were fixed with 4% Glutaraldehyde in 0.1M Cacodylate Buffer for 1 h at RT, and a secondary fix in 1% Osmium tetroxide in 0.1M Cacodylate buffer

on ice 1 h. Samples were dehydrated using increasing concentrations of ethanol and embedded in Epon resin using an aluminum weighing dish at 60 °C for 48 h. After polymerization the resin was taken out of the aluminum dish, pieces were sawed out and mounted for sectioning at 50 nm and imaged using a transmission electron microscope (JEOL JEM-1200 ExII) and CCD camera (AMT XR-41).

Calcium imaging

Control and VPS50 KO cortical neurons were co-infected at 3 DIV with GCaMP7f. At 10 days in vitro (DIV), neurons were imaged using a Nikon Eclipse TE-2000 microscope (Nikon, USA) equipped with a CO2/temperature chamber (Tokai-Hit). Pictures were acquired every 30 ms for 5 min. Using ImageJ (NIH) regions of interest were selected in neuronal somas to determine fluctuations of fluorescence over time to calculate calcium transient frequency. The Kolmogorov–Smirnov test was used to test for significance.

Electrophysiology of cultured neurons

Whole-cell patch-clamp recordings of infected cortical neurons were performed and analyzed as previously described [27, 30, 35]. The external solution contained 150 mM NaCl, 5.4 mM KCl, 2.0 mM CaCl2, 2.0 mM MgCl2, 10 mM HEPES (pH 7.4), and 10 mM glucose. Patch electrodes (5–7 MΩ) were filled with 120 mM CsCl, 10 mM BAPTA, 10 mM HEPES (pH 7.4), 4 mM MgCl2, and 2 mM ATP-Na2. After the formation of a high resistance seal and break-in (>1 GΩ), whole-cell voltage and current signals were recorded with an Axopatch 700B amplifier (Molecular Devices). Signals were low-pass filtered (5 kHz) and digitized (5–40 kHz) using a PC with pClamp10 software. Cells were held at −60 mV.

To analyze synaptic function, we recorded isolated AMPA-mediated synaptic currents using a mixture of antagonists against NMDA receptors (NMDARs; 20 μM d-APV) and $GABA_A$ receptors (GABAARs; 2 μM bicuculline). In some experiments, the sodium channel blocker tetrodotoxin (TTX; 500 nM) was added to the bath to record miniature AMPA-mediated currents. For current-clamp analyses, cells were patched, and spontaneous spiking of cells was recorded. MiniAnalysis software (Synaptosoft) was used to analyze synaptic events. The frequency and amplitude of currents were automatically calculated and plotted.

Hippocampal slice electrophysiology

Electrophysiological recording from hippocampal slices was conducted as previously described [27, 30, 36–38]. Briefly, acute coronal hippocampal slices (400 mm thick) were prepared from control and VPS50 mKO mice at postnatal day (P) 30 to P45. Mice were anesthetized with isoflurane (3% in 0.8 L/min air flow) in an induction chamber for 3 min and decapitated. Brain slices were cut using a DKT vibratome in a solution containing the following: 215 mM sucrose, 2.5 mM KCl, 26 mM NaHCO3, 1.6 mM NaH2PO4, 1mM CaCl2, 4 mM MgCl2, 4 mM MgSO4, and 20 mM glucose. After 30-min recovery, slices were incubated in an artificial CSF (ACSF) recording solution containing the following: 124 mM NaCl, 2.5 mM KCl, 26 mM NaHCO3, 1 mM NaH2PO4, 2.5 mM CaCl2, 1.3 mM MgSO4, and mM 10 glucose equilibrated with 95% O2/5% CO2, pH 7.4. Slices were incubated in this solution for 30 min before recordings.

Except as otherwise indicated, all electrophysiological experiments were performed at 28 ± 1 °C using a submersion-type recording chamber perfused at 1–2 ml/min rate with ACSF supplemented with the $GABA_A$ receptor antagonist picrotoxin (PTX; 100 μM). Extracellular field potentials (fEPSPs) were recorded with a patch pipette filled with 1 mM NaCl and placed in the CA1 stratum radiatum. Whole-cell voltage-clamp recordings (Multiclamp 700B Molecular Devices, USA) were made from CA1 pyramidal neurons voltage-clamped at −60 mV using patch pipette electrodes (3–4 MΩ) containing the following intracellular solution: 131 mM Cs-gluconate, 8 mM NaCl, 1 mM CaCl2, 10 mM EGTA, 10 mM glucose, 10 mM HEPES, pH 7.2, 292 mmol/kg osmolality. fEPSPs and EPSCs were evoked by stimulating Schaffer collateral inputs with a monopolar electrode filled with ACSF and positioned ~ 100–150 μm away from the recording pipette. mEPSCs were recorded at 32 ± 1 °C in the continuous presence of tetrodotoxin (TTX, 500 nM) to block action potential-dependent release, whereas sEPSCs were recorded in the absence of TTX. Short-term synaptic plasticity was induced by two pulses (100 ms interstimulus interval) to calculate a paired-pulse ratio (PPR) that was defined as the ratio of the slope or amplitude of the second fEPSP/EPSC to the slope or amplitude of the first fEPSP/EPSC, respectively. Long-term potentiation (LTP) was induced by 4 trains of 100 pulses at 100 Hz repeated four times, separated by 10 s. The magnitude of LTP was compared with baseline 30–40 min after applying the stimulation protocol. Reagents were obtained from Sigma, Tocris, and Ascent Scientific; prepared in stock solutions (water or DMSO); and added to the ACSF as needed. Total DMSO in the ACSF was maintained at less than 0.01%. For the whole-cells experiments, series resistance (range, 8–12 MΩ) was monitored throughout the experiment with a 5 mV, 80 ms voltage step, and cells that exhibited significant changes in series resistance (20%) were excluded from analysis. All recordings were elicited

at 15–20-s intervals, filtered at 2.4 kHz, and acquired at 10 kHz, using custom-made software written in Igor Pro 6.36 (WaveMetrics). Statistical comparisons were made using two samples Student's *t*-test at $p < 0.05$ significance level, using Origin 9.3 Pro software (OriginLab). Unless otherwise indicated, all slice electrophysiological values are provided as mean ± S.E.M and illustrated traces are average of 15–20 responses.

Behavioral analyses

All behavioral tests of mice were performed 8 weeks after AAV injection and conducted as previously described [26, 27, 30, 38]. Before each test, mouse cages were transported to the behavior room and habituated for 30 min in the dark. After completing a trial, the equipment and devices used were cleaned with 70% ethanol. Tests were recorded and analyzed with ANY-Maze software (Stoelting, USA). Behavior tests were performed between 9:00 am and 6:00 pm. At the end of the battery of behavioral tests, the animals were sacrificed for subsequent molecular analyses.

Contextual fear conditioning

An UGO-BASILE apparatus controlled by ANY-Maze was used. This equipment consists of a sound attenuating box, fan, light (visible/IR), a speaker, a USB camera, a single onboard controller, and a mouse cage. All trials were recorded, and all mice underwent habituation, conditioning, and testing phase. Twenty-four hours after training, the animals were tested for contextual memory. Each mouse was placed in the fear-conditioning box, allowed to explore for 5 min freely, and returned to its cage. The number of freezing episodes and freezing time were recorded.

Barnes maze

A non-reflective gray circular platform (91 cm diameter) with 20 holes (5 cm diameter) evenly distributed along the perimeter, with one hole containing a metal escape tunnel, was used. Three exogenous visual cues (length/width ~ 30 cm) were used around the platform: a black circle, a blue triangle, and a yellow square. The light was adjusted to 1000 lx in the center of the platform. All animals underwent a phase of habituation, spatial acquisition, and testing. On test day, the position of the escape tunnel was changed, and the animal was brought in the start box to the center of the platform, left for 10 s, and sound reproduction was started. The test ended at 90 s or when the mouse found the escape tunnel. The number of primary and total errors, primary and total latency, and total distance before finding the gap were recorded. The number of visits to each hole was also measured to show preference.

Data analysis

All values are presented as means ± standard errors (SE) for three or more independent experiments. Most statistical analyses were performed using the Student's *t*-test, whereas slice electrophysiological data were compared using two-tailed Student's *t*-test. For calcium imaging analyses, the Kolmogorov–Smirnov test was used to test for significance. Values of $p < 0.05$ are considered statistically significant. Statistical analyses were performed using OriginPro 9.3 software (OriginLab Corporation) or Graphpad Prism 10 (Dotmatics).

Abbreviations

ASD	Autism spectrum disorders
CRISPR	Clustered regularly interspaced short palindromic repeats
KO	Knockout
mKO	Mosaic knockout
SNPs	Single nucleotide polymorphism
CNVs	Copy number variants
GARP	Golgi-associated retrograde protein
EARP	Endosome-associated recycling protein
WT	Wild-type
PLA	Proximity ligation assay
DIV	Days in vitro
mEPSC	Miniature excitatory postsynaptic currents
sEPSC	Spontaneous excitatory postsynaptic currents
AAV	Adeno-associated virus
LTP	Long-term potentiation
PPR	Paired-pulse ratio
fEPSPs	Extracellular field potentials

Supplementary Information

The online version contains supplementary material available at https://doi.org/10.1186/s12915-024-01940-y.

Additional file 1: Fig. S1. Cortical neurons were infected at 3 DIV with AVV encoding TdTomato as control and a combination of sgRNAs (1–6 / 2–4 / 1–4 / 2–6) targeting Vps50, as indicated. 10 days later genomic DNA was extracted, and the T7 endonuclease I assay was performed. (A) T7 endonuclease I assay for sgRNA combinations showing successful editing of the VPS50 locus with all sgRNA combinations as shown by lower size bands in the treated samples. (B) Sequences of VPS50 locus edited with sgRNAs in VPS50 KO cultured neurons showing the changes in the DNA sequence after gene editing using locus-specific sequencing. **Fig S2.** Proximity ligation assay (PLA) in Control and VPS50 KO neurons. PLA was performed using specific antibodies to determine proximity between proteins of interest. Low magnification (20x) for each condition are shown. Microtube-associated protein 2 (MAP2) was used to stain all neurons. (A) PLA for Synapsin1 (Syn1)-Synaptophysin (Syn) (pre-presynaptic) or (B) Synaptophysin-PSD95 (pre-post synaptic). Reaction controls where PLA signal was observed only for the Synapsin1-Synaptosophysin pair, the two proteins known to be in proximity. Lower magnification of PLA reactions in Fig. 2 to show different combinations of PLA reactions to determine proximity between (C) VPS50/PSD95, (D) VPS50/Syn1, (E) VPS50/v-ATPaseV1, (F) VPS50/v-ATPaseV1 in VPS50 KO neurons, (G) v-ATPaseV1/Syn, and (H) v-ATPaseV1/Syn in VPS50 KO neurons. (I) PSD95 and Synaptophysin protein expression in VPS50 KO and control neurons. N-cadherin was used as loading control. Scale bars, 25 µm. **Fig. S3.** VPS50 KO neurons show deficits in synaptic transmission. (A) Representative traces of AMPA-mediated EPSCs followed for 30 min for control and VPS50 KO neurons. VPS50 KO neurons show a robust reduction in both Amplitude (B) and Frequency (C) of AMPA EPSCs. (D-E) Cortical neurons were co-transduced with GCaMP7 to measure calcium events by changes in fluorescence over time. (D) Representative traces and quantification (E) of changes of fluorescence over time in control and VPS50 KO neurons. A significant reduction is observed

in VPS50 KO neurons compared to control. Control $n = 1214$; VPS50 mKO $n = 1175$ cells from 3 independent experiments; Kolmogorov–Smirnov test was used to test for significance. For electrophysiology recordings at least 18 neurons from 3 independent experiments were analyzed. Unpaired t-test was used for statistical analysis; $*p < 0.05$, $***p < 0.001$. Error bars represent ± SEM. **Fig. S4.** Anatomical changes of Control and VPS50 mKO brains. (A-B) Representative images of full brains from Control and VPS50 mKO animals. (C-D) Quantification of the total length (C) and weight (D) of brains extracted from Control or VPS50 mKO animals. (E–F) Representative bright field images of brain slices from Control (E) and VPS50 mKO (F) brains.

Additional file 2. Original gels/blots.

Acknowledgements
We especially thank Dr. Martha Constantine-Paton for her support and generous donations.

Authors' contributions
Investigation: C.A-M., C.A-G., H.H., F.A., B.B., N.M-V., and R.D.; conceptualization, resources, funding acquisition, writing: H.R.H., M.C-P.; supervision, writing, funding: G.A., A.C.; conceptualization, supervision, writing, investigation, funding: F.J.B. All authors read and approved the final manuscript.

Author's X handle
Fernando J. Bustos, @fjbustosf.

Funding
This work was supported by the Chilean government through ANID FONDECYT Iniciacion #11180540 (to FJB), PAI #77180077 (to FJB), Exploración-ANID #13220203 (to FJB), ANID-MILENIO (NCN2023_32, to FJB), FONDECYT Regular # 1220480 (to GA), #1201848 (to AEC), UNAB DI-02–22/REG and DI-06–24/REG (to FJB), Fondequip # EQM160154 (to AEC), and ANID Millennium Science Initiative Program (P09-022F to AEC) and by a grant from the Simons Foundation to the MIT Simons Center for the Social Brain (to HRH and MCP), NIH grant R01-GM024663 (to HRH), and NIH grant R01-EY014420 (to MCP). HRH is an Investigator of the Howard Hughes Medical Institute. CA-G and NM-V were supported by PhD fellowship from ANID #21201603 (to CA-G) and #21211967 (to NM-V).

Availability of data and materials
All data generated or analyzed during this study are included in this published article and its supplementary information files.

Declarations

Ethics approval and consent to participate
All animal protocols were approved by the MIT Committee on Animal Care (CAC) and Ethical and Bio-security Committees of Universidad Andres Bello (020/2018).

Consent for publication
Not applicable.

Competing interests
The authors declare that they have no competing interests.

Received: 17 November 2023 Accepted: 17 June 2024
Published online: 26 June 2024

References

1. Banerjee S, Riordan M, Bhat MA. Genetic aspects of autism spectrum disorders: insights from animal models. Front Cell Neurosci. 2014;8:58.
2. Chahrour M, O'Roak BJ, Santini E, Samaco RC, Kleiman RJ, Manzini MC. Current perspectives in autism spectrum disorder: from genes to therapy. The Journal of neuroscience : the official journal of the Society for Neuroscience. 2016;36(45):11402–10.
3. Satterstrom FK, Kosmicki JA, Wang J, Breen MS, Rubeis SD, An JY, et al. Large-scale exome sequencing study implicates both developmental and functional changes in the neurobiology of autism. Cell. 2020;180(3):568-584.e23.
4. Rubeis SD, He X, Goldberg AP, Poultney CS, Samocha K, Cicek AE, et al. Synaptic, transcriptional and chromatin genes disrupted in autism. Nature. 2014;515(7526):209–15.
5. de la Torre-Ubieta L, Won H, Stein JL, Geschwind DH. Advancing the understanding of autism disease mechanisms through genetics. Nat Publ Group. 2016;22(4):345–61.
6. Sanders SJ, Ercan-Sencicek AG, Hus V, Luo R, Murtha MT, Moreno-De-Luca D, et al. Multiple recurrent de novo CNVs, including duplications of the 7q11.23 Williams syndrome region, are strongly associated with autism. Neuron. 2011;70(5):863–85.
7. Miles JH. Autism spectrum disorders—a genetics review. Genet Med. 2011;13(4):278–94.
8. Liu J, Chen L, Chang H, Rudoler J, Al-Zughoul AB, Kang JB, et al. Replicable patterns of memory impairments in children with autism and their links to hyperconnected brain circuits. Biol Psychiatry: Cogn Neurosci Neuroimaging. 2023;8(11):1113–23.
9. Williams DL, Goldstein G, Minshew NJ. The profile of memory function in children with autism. Neuropsychology. 2006;20(1):21–9.
10. Zoghbi HY, Bear MF. Synaptic dysfunction in neurodevelopmental disorders associated with autism and intellectual disabilities. Csh Perspect Biol. 2012;4(3):a009886.
11. Greco B, Managò F, Tucci V, Kao HT, Valtorta F, Benfenati F. Autism-related behavioral abnormalities in synapsin knockout mice. Behav Brain Res. 2013;251:65–74.
12. Fassio A, Patry L, Congia S, Onofri F, Piton A, Gauthier J, et al. SYN1 loss-of-function mutations in autism and partial epilepsy cause impaired synaptic function. Hum Mol Genet. 2011;20(12):2297–307.
13. Ullman JC, Yang J, Sullivan M, Bendor J, Levy J, Pham E, et al. A mouse model of autism implicates endosome pH in the regulation of presynaptic calcium entry. Nat Commun. 2018;9(1):330.
14. Paquin N, Murata Y, Froehlich A, Omura DT, Ailion M, Pender CL, et al. The conserved VPS-50 protein functions in dense-core vesicle maturation and acidification and controls animal behavior. Curr Biol. 2016;26(7):862–71.
15. Schindler C, Chen Y, Pu J, Guo X, Bonifacino JS. EARP is a multisubunit tethering complex involved in endocytic recycling. Nat Cell Biol. 2015;17(5):639–50.
16. Gillingham AK, Sinka R, Torres IL, Lilley KS, Munro S. Toward a comprehensive map of the effectors of Rab GTPases. Dev Cell. 2014;31(3):358–73.
17. Gai X, Xie HM, Perin JC, Takahashi N, Murphy K, Wenocur AS, et al. Rare structural variation of synapse and neurotransmission genes in autism. Mol Psychiatr. 2012;17(4):402–11.
18. Schneeberger PE, Nampoothiri S, Holling T, Yesodharan D, Alawi M, Knisely AS, et al. Biallelic variants in VPS50 cause a neurodevelopmental disorder with neonatal cholestasis. Brain. 2021;144(10):3036–49.
19. Rost BR, Schneider F, Grauel MK, Wozny C, Bentz CG, Blessing A, et al. Optogenetic acidification of synaptic vesicles and lysosomes. Nat Neurosci. 2015;18(12):1845–52.
20. Gershlick DC, Ishida M, Jones JR, Bellomo A, Bonifacino JS, Everman DB. A neurodevelopmental disorder caused by mutations in the VPS51 subunit of the GARP and EARP complexes. Hum Mol Genet. 2019;28(9):ddy423.
21. Südhof TC. The synaptic vesicle cycle. Annu Rev Neurosci. 2004;27:509–47.
22. Pujol N, Bonnerot C, Ewbank JJ, Kohara Y, Thierry-Mieg D. The Caenorhabditis elegans unc-32 gene encodes alternative forms of a vacuolar ATPase asubunit. J Biol Chem. 2001;276(15):11913–21.
23. Toei M, Saum R, Forgac M. Regulation and isoform function of the V-ATPases. Biochemistry. 2010;49(23):4715–23.
24. Gowrisankaran S, Milosevic I. Regulation of synaptic vesicle acidification at the neuronal synapse. IUBMB Life. 2020;72(4):568–76.
25. Zhou Q, Petersen CCH, Nicoll RA. Effects of reduced vesicular filling on synaptic transmission in rat hippocampal neurones. J Physiol. 2000;525(1):195–206.
26. Brauer B, Merino-Veliz N, Ahumada-Marchant C, Arriagada G, Bustos FJ. KMT2C knockout generates ASD-like behaviors in mice. Front Cell Dev Biol. 2023;11:1227723.

27. Bustos FJ, Pandian S, Haensgen H, Zhao JP, Strouf H, Heidenreich M, et al. Removal of a partial genomic duplication restores synaptic transmission and behavior in the MyosinVA mutant mouse Flailer. BMC Biol. 2023;21(1):232.
28. Passini MA, Wolfe JH. Widespread gene delivery and structure-specific patterns of expression in the brain after intraventricular injections of neonatal mice with an adeno-associated Virus Vector. J Virol. 2001;75(24):12382–92.
29. Henriquez B, Bustos FJ, Aguilar R, Becerra A, Simon F, Montecino M, et al. Ezh1 and Ezh2 differentially regulate PSD-95 gene transcription in developing hippocampal neurons. Mol Cell Neurosci. 2013;57:130–43.
30. Bustos FJ, Ampuero E, Jury N, Aguilar R, Falahi F, Toledo J, et al. Epigenetic editing of the Dlg4/PSD95 gene improves cognition in aged and Alzheimer's disease mice. Brain. 2017;140(12):3252–68.
31. Chan KY, Jang MJ, Yoo BB, Greenbaum A, Ravi N, Wu WL, et al. Engineered AAVs for efficient noninvasive gene delivery to the central and peripheral nervous systems. Nat Neurosci. 2017;20(8):1172–9.
32. Slaymaker IM, Gao L, Zetsche B, Scott DA, Yan WX, Zhang F. Rationally engineered Cas9 nucleases with improved specificity. Science. 2016;351(6268):84–8.
33. Granseth B, Odermatt B, Royle SJ, Lagnado L. Clathrin-mediated endocytosis is the dominant mechanism of vesicle retrieval at hippocampal synapses. Neuron. 2006;51(6):773–86.
34. Chen X, Levy JM, Hou A, Winters C, Azzam R, Sousa AA, et al. PSD-95 family MAGUKs are essential for anchoring AMPA and NMDA receptor complexes at the postsynaptic density. Proc Natl Acad Sci. 2015;112(50):E6983–92.
35. Sepulveda FJ, Bustos FJ, Inostroza E, Zuniga FA, Neve RL, Montecino M, et al. Differential roles of NMDA receptor subtypes NR2A and NR2B in dendritic branch development and requirement of RasGRF1. J Neurophysiol. 2010;103(4):1758–70.
36. Chávez AE, Chiu CQ, Castillo PE. TRPV1 activation by endogenous anandamide triggers postsynaptic long-term depression in dentate gyrus. Nat Neurosci. 2010;13(12):1511–8.
37. Park J, Chávez AE, Mineur YS, Morimoto-Tomita M, Lutzu S, Kim KS, et al. CaMKII phosphorylation of TARPγ-8 is a mediator of LTP and learning and memory. Neuron. 2016;92(1):75–83.
38. Pandian S, Zhao JP, Murata Y, Bustos FJ, Tunca C, Almeida RD, et al. Myosin Va brain-specific mutation alters mouse behavior and disrupts hippocampal synapses. eNeuro. 2020;7(6):ENEURO.0284-20.2020.

Publisher's Note

Springer Nature remains neutral with regard to jurisdictional claims in published maps and institutional affiliations.

Cortés *et al. Biological Research* (2024) 57:40
https://doi.org/10.1186/s40659-024-00522-0

Biological Research

RESEARCH ARTICLE Open Access

Loss of protein tyrosine phosphatase receptor delta PTPRD increases the number of cortical neurons, impairs synaptic function and induces autistic-like behaviors in adult mice

Bastián I. Cortés[1], Rodrigo C. Meza[2], Carlos Ancatén-González[2,3], Nicolás M. Ardiles[2], María-Ignacia Aránguiz[1], Hideaki Tomita[4,11], David R. Kaplan[4,5], Francisca Cornejo[6], Alexia Nunez-Parra[7], Pablo R. Moya[8,9], Andrés E. Chávez[2,10] and Gonzalo I. Cancino[1*]

Abstract

Background The brain cortex is responsible for many higher-level cognitive functions. Disruptions during cortical development have long-lasting consequences on brain function and are associated with the etiology of brain disorders. We previously found that the protein tyrosine phosphatase receptor delta Ptprd, which is genetically associated with several human neurodevelopmental disorders, is essential to cortical brain development. Loss of *Ptprd* expression induced an aberrant increase of excitatory neurons in embryonic and neonatal mice by hyper-activating the pro-neurogenic receptors TrkB and PDGFRβ in neural precursor cells. However, whether these alterations have long-lasting consequences in adulthood remains unknown.

Results Here, we found that in *Ptprd+/-* or *Ptprd-/-* mice, the developmental increase of excitatory neurons persists through adulthood, affecting excitatory synaptic function in the medial prefrontal cortex. Likewise, heterozygosity or homozygosity for *Ptprd* also induced an increase of inhibitory cortical GABAergic neurons and impaired inhibitory synaptic transmission. Lastly, *Ptprd+/-* or *Ptprd-/-* mice displayed autistic-like behaviors and no learning and memory impairments or anxiety.

Conclusions These results indicate that loss of *Ptprd* has long-lasting effects on cortical neuron number and synaptic function that may aberrantly impact ASD-like behaviors.

Keywords Protein tyrosine phosphatase receptor delta, Medial prefrontal cortex, Synaptic transmission, Anxiety, Learning, Memory, ASD

*Correspondence:
Gonzalo I. Cancino
gcancino@uc.cl

Full list of author information is available at the end of the article

© The Author(s) 2024. **Open Access** This article is licensed under a Creative Commons Attribution 4.0 International License, which permits use, sharing, adaptation, distribution and reproduction in any medium or format, as long as you give appropriate credit to the original author(s) and the source, provide a link to the Creative Commons licence, and indicate if changes were made. The images or other third party material in this article are included in the article's Creative Commons licence, unless indicated otherwise in a credit line to the material. If material is not included in the article's Creative Commons licence and your intended use is not permitted by statutory regulation or exceeds the permitted use, you will need to obtain permission directly from the copyright holder. To view a copy of this licence, visit http://creativecommons.org/licenses/by/4.0/. The Creative Commons Public Domain Dedication waiver (http://creativecommons.org/publicdomain/zero/1.0/) applies to the data made available in this article, unless otherwise stated in a credit line to the data.

Introduction

The cerebral cortex is responsible for processing complex sensory and cognitive behaviors, requiring an extraordinary control over the generation of neurons and their connections during the development of the nervous system [1]. Typically, cortical circuits are assembled from different glutamatergic and GABAergic neuron lineages, each with unique morphological and physiological characteristics [2, 3]. Indeed, disruption in the generation of neurons or their connectivity has long-lasting consequences affecting behavior that can result in brain disorders. In this regard, it has been proposed that the number, diversity, and function of glutamatergic and GABAergic neurons are essential to maintain the balance between different cerebral circuits and to avoid the onset of multiple neuropsychiatric conditions [4]. Perturbation of cellular processes such as neural precursor cell proliferation, neurogenesis, and neuronal migration during brain development may, in part, cause structural brain alterations that lead to the onset of brain disorders [5]. Gain or loss of expression or activity of genes involved in these processes are associated with the onset of several brain disorders, including autism spectrum disorder (ASD), schizophrenia, bipolar disorder, attention-deficit/hyperactivity disorder (ADHD), and intellectual disability [5–10]. We reported that alterations in the expression of one of these genes, protein tyrosine phosphatase receptor delta (PTPRD), impairs cerebral cortex development in mice [11, 12].

Ptprd is a receptor protein tyrosine phosphatase type II family member. Structurally, it contains extracellular immunoglobulin and fibronectin III domains and two cytoplasmic tyrosine phosphatase domains [13–15]. We reported that *Ptprd* hetero- or homozygosity during cortical development triggered dysregulation of TrkB and PDGFRβ tyrosine kinase activity in embryonic and neonatal cortical neural precursor cells. Ptprd acted as a TrkB and PDGFRβ phosphatase, fine tuning kinase activity and preventing their hyperactivation. Loss of *Ptprd* resulted in aberrantly increased proliferation of neural precursor cells and concomitant mispositioning of their progeny, embryonic and newborn excitatory neurons [11, 12]. Ptprd regulation of receptor tyrosine kinases like TrkB thus ensures the generation of appropriate numbers of neural precursor cells and neurons postnatally. Ptprd also performs a critical function at synapses, regulating cell adhesion important for synaptic formation and differentiation [15]. Given the role of Ptprd in assuring appropriate numbers of postnatal cortical neuron subtypes and its role at synapses, we asked if alterations of cortical neuron numbers observed embryonic and postnatally persist into adulthood, and if they perturb cortical synaptic function and ultimately, behavior.

Studies of how *Ptprd* deficiency alters excitatory and inhibitory synaptic transmission have yielded contradictory results [16–19]. For example, in hippocampal neuron cultures, Ptprd is involved in inhibitory synaptic formation and transmission but not in the development of excitatory synaptic transmission [16]. More recently, the loss of *Ptprd* expression differentially suppressed excitatory synaptic transmission in the stratum lacunosum moleculare in the hippocampus but not in the stratum radiatum [17]. Moreover, deletion of *Ptprd* in cultured neurons did not alter the development or number of synapses [18] and did not interfere with excitatory or inhibitory synaptic development and transmission [19]. It is important to note that these findings focused on hippocampal neurons. Whether the absence of PTPRD alters synaptic transmission in cortical neurons has not yet been addressed.

Here we address these issues by assessing in adult *Ptprd-/-* mice the number of glutamatergic and GABAergic neurons in the brain cortex, recording both excitatory and inhibitory synaptic function and analyzing animal behavior. Our results indicate that ablation of *Ptprd* results in an increase in both glutamatergic and GABAergic neurons in adult cortex leading to changes in excitatory and inhibitory synaptic transmission. Moreover, *Ptprd+/-* or *Ptprd-/-* mice show deficits in sociability and social novelty, and repetitive behavior characteristic of ASD-like behaviors when compared to *Ptprd+/+* mice. These findings indicate that loss of one or both alleles of *Ptprd* during the formation of the cerebral cortex leads to profound structural changes that affect the assembly and functioning of glutamatergic and GABAergic circuits and synaptic transmission, likely contributing to ASD-like behaviors in adulthood.

Methods

Animals

The C57BL/6 N-A<tm1Brd>*Ptprd*<tm2a(KOMP)Wtsi>/WtsiOrl mice strain was purchased from Wellcome Trust Sanger Institute and maintained as heterozygous. The cross between heterozygous mice allowed the *Ptprd+/+*, *Ptprd+/-*, and *Ptprd-/-* mice to be obtained. The following primers were used to identify the three genotypes mentioned above: Ptprd_111547_F: 5'-TCAC CTCGCTGTTCTTCCTG-3'; Ptprd_111547_R:5'-CTT CTCAGTGCCCAACCCTC-3'; CAS_R1_Term: 5'-TCG TGGTATCGTTATGCGCC-3'. In addition, for sociability and social novelty tests, BALB/c wild-type mice were used as "old mouse" and "new mouse". All mice had free access to rodent chow and water in a 12-hour dark-light cycle room with temperature controlled at 20–22 °C.

Perfusion of mice and brain extraction

Ptprd+/+, *Ptprd+/-*, and *Ptprd-/-* mice were perfused transcardially at 3 months old. The mice were first placed in an isoflurane chamber to be lightly anesthetized. Once the animal was numb, the heart was exposed, and a saline solution (0.9% NaCl) was injected gradually through the right ventricle. Once the blood flow stopped, the brains were extracted and fixed in a 4% PFA solution overnight at 4 °C. The next day, the brains were dehydrated in 20%, 25%, and 30% sucrose (Merk, 107,651,100) solutions at 4 °C for 24 h each incubation. Subsequently, brains were embedded in the optimal cutting temperature compound (OCT; Sakura, 4583) and stored at -80 °C until cut. Next, 18 µm coronal slices were obtained by cryostat (Leica, CM1850) at a temperature of -20 °C and stored at -80 °C until use.

Immunofluorescence and quantification

For morphometric analysis, immunostaining of tissue sections was performed as described [11, 12, 20]. Briefly, brain sections were washed with 1X TBS for immunostaining. Then were permeabilized with TBS −0.3% Triton X-100 for 30 min. The tissues were then incubated in TBS with 5% BSA 0.3% Triton X-100 for 1 h as a blocking solution. Brain slices were incubated overnight with primary antibodies in a blocking solution at 4 °C. The next day, the sections were washed with TBS and then incubated with secondary antibodies in a blocking solution for 1 h at room temperature. After TBS washes, sections were counterstained with Hoechst 33,258 for 10 min and mounted. To evaluate the number of GABAergic neurons in the somatosensory cortex and medial prefrontal cortex (mPFC), rabbit anti-parvalbumin antibody (1:100; Swant, PV 25) and mouse anti-somatostatin antibody (1:500; Santa Cruz, sc-55,565) were used. To evaluate the number of glutamatergic neurons in the somatosensory cortex and mPFC, rabbit anti-Tbr1 antibody (1:400; Abcam, ab31940) and rabbit anti-Satb2 antibody (1:500; Abcam, ab92446) were used. To quantify the specific neuronal types, the somatosensory cortex and mPFC boundaries were established using the mouse brain Atlas [21] and Adobe Photoshop CC 2015. Then, the images were quantified using the Cell Counter tool of the Fiji program.

Prefrontal cortex slice preparation

Acute coronal brain slices (300 µm thick) were obtained as previously described [22]. Briefly, the brain was removed and slices containing the mPFC were cut using a DTK-1000 Microslicer (Ted Pella, Inc.) in an ice-cold high-choline solution (110 mM Choline-Cl, 2.5 mM KCl, 1.25 mM NaH_2PO_4, 7 mM $MgCl_2$, 25 mM $NaHCO_3$, 15 mM glucose, 0.5 mM $CaCl_2$, 11.6 mM ascorbate, 3.1 mM pyruvate (290–305 mmol/Kg)). Thirty minutes post-sectioning, coronal slices were gradually switched to artificial cerebral spinal fluid (aCSF) solution (124 mM NaCl, 2.69 mM KCl, 1.25 mM KH_2PO_4, 1.3 mM $MgSO_4$, 26 mM $NaHCO_3$, 10 mM glucose, 2.5 mM $CaCl_2$, pH 7.4 (300–305 mmol/Kg)). All solutions were equilibrated with 95% O_2 and 5% CO_2 (pH 7.4), and slices were kept at room temperature for at least 30 min before recording.

Electrophysiology

All experiments, unless otherwise stated, were performed at 28±1 °C in a submersion-type recording chamber perfused at ~2 mL/min with aCSF supplemented with either the GABAA receptor antagonist picrotoxin (PTX; 50 µM) or the AMPA/Kainate and NMDA receptor antagonists CNQX (25 µM) and D-APV (50 µM) to block fast inhibitory and excitatory transmission, respectively. Coronal slices were visualized using infrared differential interference contrast on a Nikon Eclipse FN1 microscope, and layer 2/3 pyramidal neurons from prelimbic (PrL) and infralimbic (IL) subdivisions of mPFC were morphologically identified. Whole-cell voltage-clamp recordings using a Multiclamp 700B amplifier (Molecular Devices, Sunnyvale, CA, USA) were made from 2/3 pyramidal neuron somas located ~200 mm from pia and voltage-clamped at -60 or 0 mV (unless otherwise stated) using patch-type pipette electrodes (~3.0–4.5 MΩ) containing 131 mM Cs-gluconate, 8 mM NaCl, 1 mM $CaCl_2$, 10 mM EGTA, 10 mM glucose, 10 mM HEPES, 5 mM MgATP, and 0.4 mM Na_3GTP; pH 7.2–7.4 (285 mmol/kg). To assess cell stability, series, and input resistances were monitored with test pulses (-4mV, 80 ms) throughout all experiments. Cells with >20% change in series resistance were excluded from the analysis.

To elicit excitatory and inhibitory postsynaptic currents (EPSCs and IPSCs, respectively), a bipolar-stimulating patch pipette filled with aCSF was placed in layer 2/3 around 100–150 µm from the recording neuron and voltage pulses (1–15 V, 100–200 ms pulse width) were delivered through a stimulus isolator (DS2A-Mk.II, Digitimer Ltd). Typically, stimulation was adjusted to obtain comparable magnitude synaptic response across experiments (e.g., 100–150 pA EPSC and IPSC). Two different protocols were used to evaluate short-term synaptic plasticity: First, two pulses at different interstimulus intervals (10, 30, 70, 100, and 300 ms) were used to calculate the paired-pulse ratio (PPR) that was defined as the ratio of the amplitude of the second response to the amplitude of the first response. Second, synaptic depression was evaluated using a burst of 25 (for EPSC) and 20 (for IPSC) stimuli at 14 and 10 Hz, respectively, and delivered every 60 s; 5 burst-evoked responses were averaged for each experiment. Miniature EPSCs (mEPSCs) were recorded at 32±1 °C from neurons voltage-clamped at -60 mV in the continuous presence of tetrodotoxin (TTX, 500 nM).

In contrast, isolated miniature IPSCs were recorded at 0 mV in the continuous presence of TTX, CNQX (25 μM), and D-APV (50 μM). mEPSCs and mIPSC were identified using a minimal threshold amplitude (≥5 pA) and analyzed using the mini-analysis software Synaptosoft (Synaptosoft). Spontaneous excitatory and inhibitory currents (sEPSCs/sIPSCs) were recorded without TTX, whereas AMPAR/NMDAR ratios were analyzed by recording AMPAR-mediated EPSCs at -60 mV. In contrast, NMDAR-mediated EPSCs were recorded at +40mV in the continuous presence of CNQX (25 μM) to isolate NMDA-mediated EPSC. All drugs were obtained from Sigma and Tocris, prepared in stock solutions in milli-Q water or DMSO, and added to the ACSF as needed. Total DMSO in the aCSF was maintained at >0.1%. Synaptic EPSCs and IPSCs were elicited at 10-sec intervals (0.16 Hz), filtered at 2.2 kHz, and acquired at 10 kHz using custom-made software written in Igor Pro 4.09 A (WaveMetrics).

Morris water maze test

Morris water maze navigation task was performed to evaluate spatial learning and memory as previously described [23]. Briefly, in the learning phase, the animals were trained to locate a hidden 9-cm-diameter white platform (1 cm below the surface of the water) for 4 consecutive days following 4 external cues, 4 times per day per animal in a 1.2-m-diameter circular pool filled with 23±2 °C painted white water. Each trail ended when the animals found the platform and remained there for 10 s. If the animal did not find the platform at the end of 60 s, they were gently guided there for the remaining 10 s. Later in each trial, the animals were gently removed from the maze, dried with a tissue paper towel, and put in a similar housing cage with additional tissue paper towels to continue drying. On the fifth day, in the memory phase, the test was performed by removing the platform and allowing the free swimming for 60 s. The behavior was monitored during all tasks using an automatic tracking system (ANY-maze video tracking software, Stoelting Co, Wood Dale, IL, USA). The learning phase measured latency and path length to the platform, while the memory test measured the time spent in each quadrant and the target quadrant and the traveled distance within the target quadrant.

Y-Maze test

Memory was also evaluated with the Y-maze as previously described [24]. Briefly, Y-Maze tests were performed using a maze with 3 arms of 8 cm width x 35 cm long and walls of 20 cm height, connected at a 120° angle, shaping a Y and assigned as arms A, B, and C. Each animal was placed in the arm (A), looking to the center of the maze, and tracked for 8 min by the ANY-maze software. Four clues were put on the maze walls to guide the animals. Alternation was defined as a visit to 3 different arms (ABC, ACB, BCA, BAC, CAB, CBA), and % spontaneous alternation was determined by the following formula:

% Spontaneous alternation = (Total alternations / (Total arm entries-2) x 100.

Open field test

Anxiety was evaluated with the open field test as described previously [25]. Briefly, mice were exposed to a free exploration in an open field chamber of 40 cm (l) x 40 cm (w) x 40 cm (h). This arena is divided into two areas by a line: the peripheral and central regions. The time in each chamber area was recorded for 10 min by ANY-maze software.

Elevated plus maze test

Anxiety was also evaluated with the evaluated plus maze as described previously [26]. Briefly, the test was performed using a maze with 4 arms of 7.5 cm width x 35 cm long, shaping a cross with a 7.5×7.5 cm center and 50 cm from the floor. 2 arms (closed arms) had walls of 20 cm height, and the others (open arms) were uncovered. The animals were placed in the center of the maze and tracked for 5 min by ANY-maze software.

Self-grooming test

Repetitive behavior was measured by the self-grooming test as previously described [25, 27]. Briefly, mice were recorded for 10 min through a 20×20 cm transparent box to allow visualization of the animal. The cumulative time spent by the animals performing the self-grooming process was quantified.

Marble burying test

Repetitive behavior was also evaluated by the marble burying test as previously described [22, 25]. Briefly, the animals were exposed to a free exploration arena of 23×33 cm in the presence of 20 proportionally distributed black marbles. The marbles were placed in a 5 cm thick layer of dry sawdust to allow the animal to perform the digging behavior. After 30 min, the number of buried marbles was quantified. A marble was considered buried if 2/3 were covered.

Three-chamber test

The three-chamber social novelty and sociability test was used to evaluate deficits in social behavior as previously described [25, 27, 28]. First, the animals were subjected to 10 min of habituation in the three chambers. Then, to assess the sociability of the animals, mice were placed in a context in which they chose to interact with either a caged mouse (old mouse) or an inanimate object, each

in a different chamber for 10 min. Subsequently, to assess the social novelty, the inanimate object was replaced by a second unfamiliar mouse (new mouse), and the experimental mouse was placed in a context in which it had to choose between interacting with a familiar or an unfamiliar mouse for 10 min. ANY-maze software recorded the time the experimental animals spent with each option.

Statistical analyses

Statistical analyses were performed using the one-way ANOVA test with unpaired data to compare data between *Ptprd*+/+, *Ptprd*+/-, and *Ptprd*-/- genotypes. Unless otherwise indicated, all electrophysiological results were statistically analyzed using paired and unpaired two-tailed Student's t-test and One- or Two-way ANOVA at the $p<0.05$ significance level in OriginPro 7.0 and 8.6 (OriginLab). In the figures illustrated, traces are averages of 25–30 responses. In the case of the statistical analysis used to evaluate the sociability and social novelty test, the 2-way ANOVA test was used. Corrections for multiple comparisons were performed using Tukey's post hoc test. All statistical tests were performed with Prism 6 software. In all cases, the bars indicate the standard error of the mean.

Results

Ptprd+/- or *Ptprd*-/-mice display an increase in glutamatergic neurons and impaired synaptic function in the adult cortex

We previously reported that *Ptprd*+/- and *Ptprd*-/- embryos have more excitatory cortical neurons [11]. To determine whether this phenotype persisted until adulthood, we performed immunostaining for Tbr1 (Fig. 1A) and Satb2 (Fig. 1C), markers of deep- and upper-layer excitatory cortical neurons, respectively, in coronal sections of the mPFC, a brain area involved in different cognitive processes, from 3-month-old *Ptprd*+/+, *Ptprd*+/-, and *Ptprd*-/- mice. While heterozygous mice showed no differences as compared to control littermates, *Ptprd*-/- mice had 20% more Tbr1-positive neurons than control and *Ptprd*+/+ littermates in the mPFC (Fig. 1B). However, we did not observe any changes in the number of Satb2-positive neurons (Fig. 1D), suggesting that only early born neurons are affected at the mPFC. To complement this result, we analyzed the somatosensory cortex, another cortical region commonly disrupted in brain disorders associated with *PTPRD* mutations. We found that *Ptprd*-/- and *Ptprd*+/- mice had more Tbr1-(Fig. 1E, F) and Satb2-positive excitatory neurons (Fig. 1G, H).

The brain cortex has 6 layers which are connected to different brain circuits. To determine if this increase in excitatory neurons is cortical layer specific [1, 3, 29], the mPFC and somatosensory cortex were divided into their respective layers as previously described [21, 30–33]. In the mPFC, there were no differences in the number of Tbr1- or Satb2-positive excitatory neurons per cortical layer (Fig. 1I, J). However, in the somatosensory cortex, the increase in Tbr1-positive neurons was specific to layers IV and VI in 3-month-old *Ptprd*+/- or *Ptprd*-/- mice compared to *Ptprd*+/+ mice (Fig. 1K). For Satb2-positive neurons, the increase was observed in all cortical layers in the somatosensory cortex of 3-month-old *Ptprd*-/- mice compared to *Ptprd*+/+ mice, except for cortical layer V, where *Ptprd*+/- mice had more Satb2-positive neurons compared to *Ptprd*+/+ mice (Fig. 1L). These results indicate that loss of *Ptprd* in adult mice results in an increase in excitatory cortical neurons in brain areas associated with cognition.

As an increased number of glutamatergic neurons is associated with altered synaptic function [33], we characterized the impact of the *Ptprd* ablation on the spontaneous synaptic activity in layer 2/3 pyramidal neurons in the mPFC. Firstly, we recorded spontaneous excitatory synaptic currents (sEPSCs) and found a significant increase in the frequency but not amplitude of sEPSCs in *Ptprd*-/- and not *Ptprd*+/- mice when compared to *Ptprd*+/+ littermates (Fig. 2A). Similarly, an increase in the frequency of miniature excitatory synaptic currents (mEPSCs) but not in the amplitude was observed in *Ptprd*+/- or *Ptprd*-/- mice compared to *Ptprd*+/+ mice (Fig. 2B). Secondly, we analyzed the evoked synaptic transmission mediated by AMPA receptors by generating input–output curves. We observed an increased response at high voltage inputs in *Ptprd*-/- mice compared to *Ptprd*+/+ (Fig. 2C), suggesting that excitatory transmission is augmented in the *Ptprd*-/- mice. Thirdly, we examined whether the effect of the PTPRD ablation alters synaptic release probability by estimating two principal forms of short-term synaptic plasticity: paired-pulse ratio (PPR) and use-dependent depression. However, both PPR (Fig. 2D) and synaptic depression in response to a stimulus train of 25 stimuli at 14 Hz (Fig. 2E) remained unchanged between genotypes. Finally, we measured the AMPA/NMDA ratio and found no significant differences between genotypes (Fig. 2F). Together, these results suggest that the increase in excitatory transmission cannot be accounted for by changes in postsynaptic receptor numbers or changes in release probability, but rather, could be due to an increase in the number of synaptic contacts in *Ptprd*-/- mice.

Ptprd+/- or *Ptprd*-/- mice display an increase in GABAergic neurons and aberrant inhibitory synaptic transmission in the adult cortex

Ptprd is expressed in subcortical structures during brain development [34] and is important for GABAergic synaptic differentiation [35–37]. However, its role in regulating the generation of GABAergic neurons has not been described. We therefore evaluated whether loss of

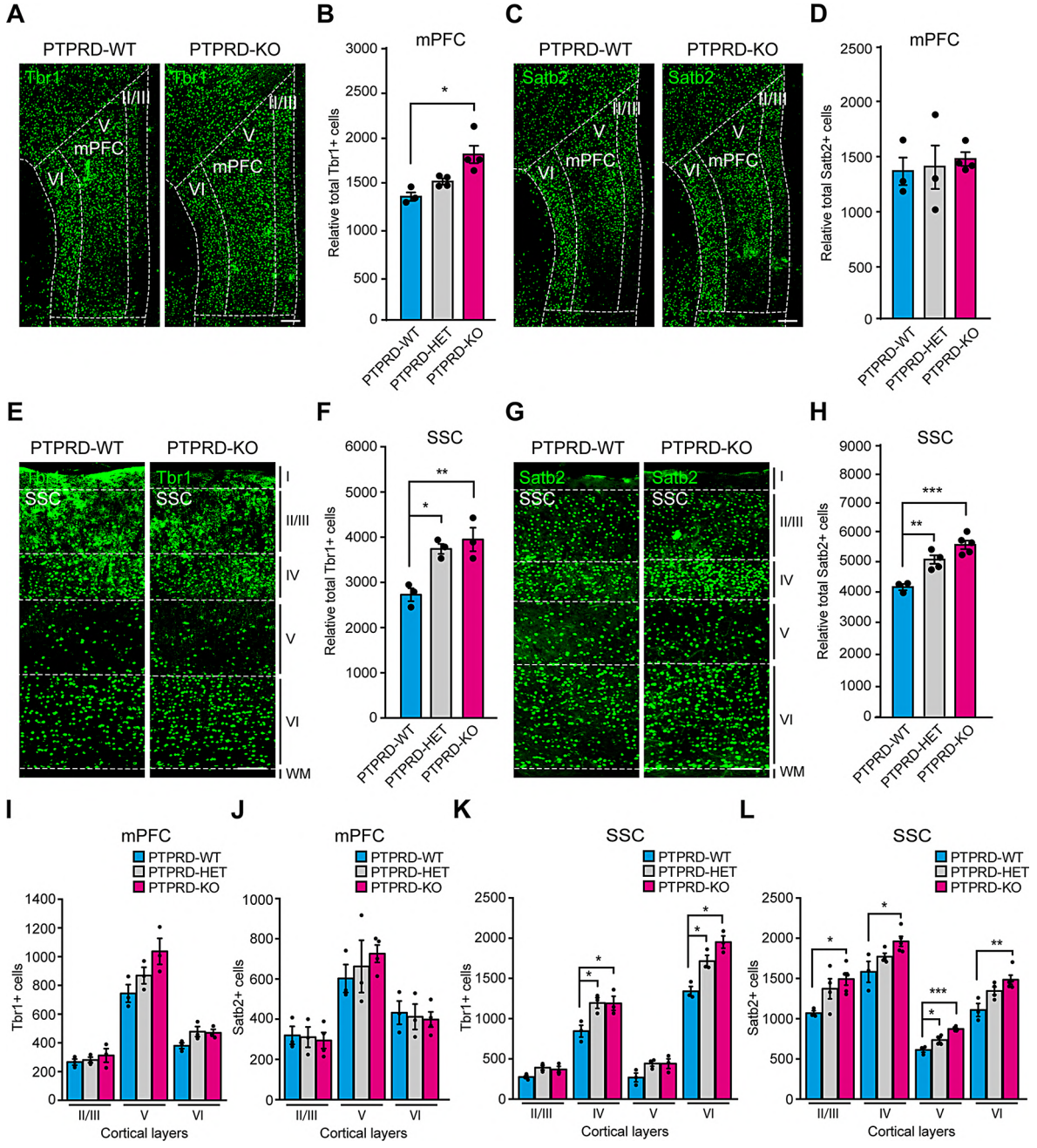


Fig. 1 Adult *Ptprd+/-* or *Ptprd-/-* mice show an increase of glutamatergic neurons in the mPFC and somatosensory cortex. (**A-H**) Coronal sections of mPFC (**A, C**) or somatosensory cortex (**E, G**) of *Ptprd+/+* (PTPRD-WT) and *Ptprd-/-* (PTPRD-KO) 3-month-old animals were immunostained against Tbr1 (**A, E**) or Satb2 (**C, G**). Relative total Tbr1-positive cells in the mPFC **(**for **B**, PTPRD-WT, $n = 3$; PTPRD-HET, $n = 4$; PTPRD-KO, $n = 4$**)** or somatosensory cortex **(**for **F**, PTPRD-WT, $n = 3$; PTPRD-HET, $n = 5$; PTPRD-KO, $n = 5$**)** of *Ptprd+/+*, *Ptprd+/-* (PTPRD-HET), and *Ptprd-/-* 3-month-old mice were quantified. Relative total Satb2-positive cells in the mPFC **(**for **D**, PTPRD-WT, $n = 3$; PTPRD-HET, $n = 3$; PTPRD-KO, $n = 4$**)** or somatosensory cortex **(**for **H**, PTPRD-WT, $n = 3$; PTPRD-HET, $n = 4$; PTPRD-KO, $n = 5$**)** of *Ptprd+/+*, *Ptprd+/-*, and *Ptprd-/-* 3-month-old mice were quantified. In (**A**) and (**C**), the dotted line shows mPFC and specific cortical layers. **(I, J)** Tbr1 (**I**) or Satb2 (**J**) positive neurons were quantified per cortical layers II/III, V and VI in the mPFC. **(K, L)** Tbr1 (**K**) or Satb2 (**L**) positive neurons were quantified per cortical layers II/III, IV, V and VI in the somatosensory cortex. mPFC = medial prefrontal cortex. SSC = somatosensory cortex. WM = white matter. $^{*}p < 0.05$; $^{**}p < 0.01$; $^{***}p < 0.001$. In all the images, scale bars represent 200 µm. In all graphs, the error bars denote SEMs

Ptprd expression could also alter the number of GABAergic neurons in the adult mouse cortex. To address this, we performed immunostaining for parvalbumin (Fig. 3A) and somatostatin (Fig. 3C), two major types of cortical GABAergic neurons [2], at the mPFC. We found that *Ptprd-/-* mice had more parvalbumin-positive (Fig. 3B) and somatostatin-positive neurons (Fig. 3D) than wild-type littermates in the mPFC. Additionally,

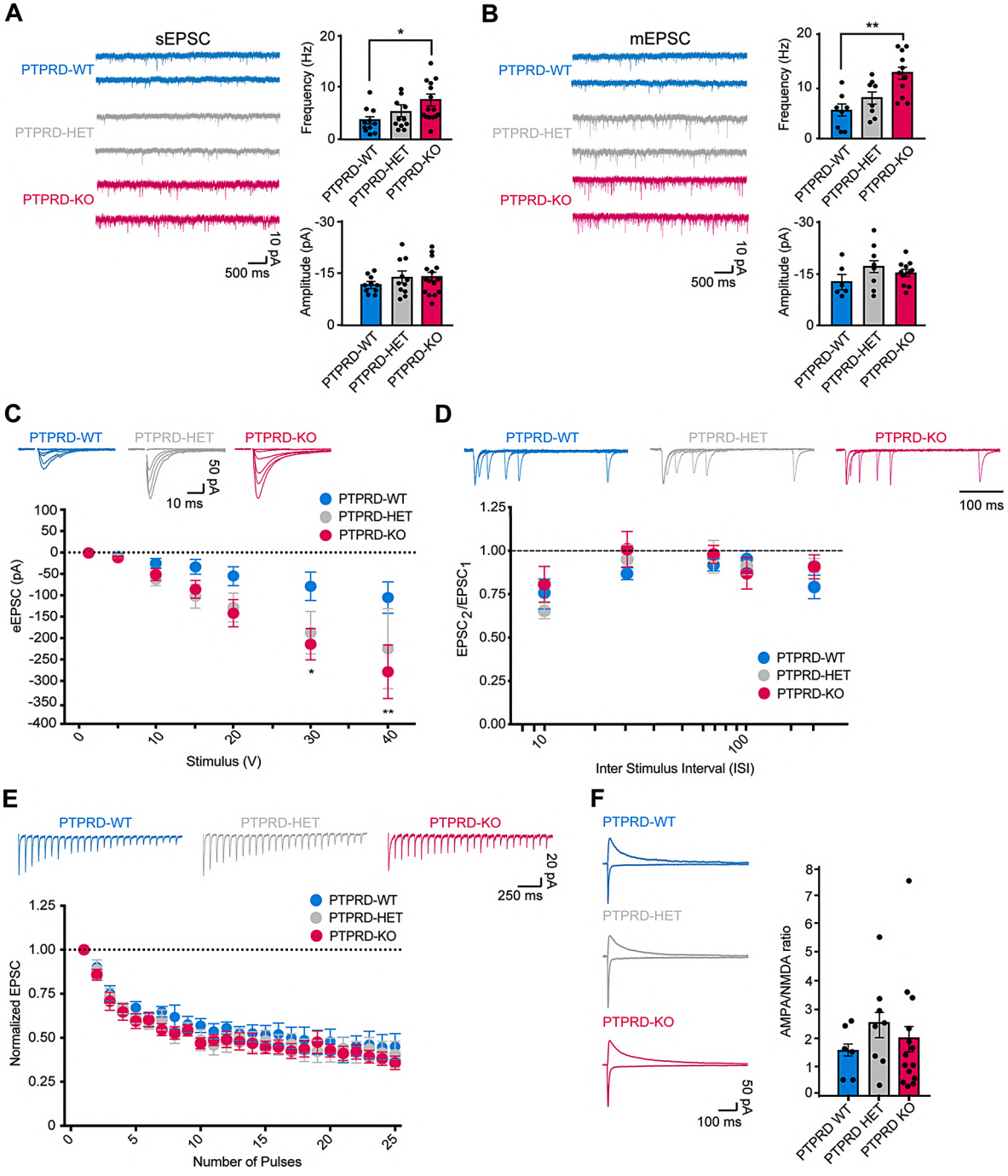


Fig. 2 Excitatory synaptic transmission in layer 2/3 of the mPFC is disrupted in the *Ptprd-/-* mice. (**A**) Sample traces (left) and quantitative analysis (right) of sEPSC activity recorded from layer 2/3 pyramidal neurons in the mPFC in *Ptprd*+/+ (PTPRD-WT), *Ptprd*+/- (PTPRD-HET), and *Ptprd-/-* (PTPRD-KO) mice. A significant increase in the frequency but not in the amplitude of sEPSC in PTPRD-KO was detected. PTPRD-WT, $n=4$ animals, 10 cells; PTPRD-HET, $n=5$ animals, 11 cells; PTPRD-KO, $n=8$ animals, 15 cells. $^{**}p<0.01$. (**B**) Miniature excitatory synaptic current (mEPSC) also shows an increase in the frequency but not in the amplitude in *Ptprd-/-* compared to *Ptprd*+/+ and *Ptprd*+/- mice. PTPRD-WT, $n=5$ animals, 8 cells; PTPRD-HET, $n=5$ animals, 8 cells; PTPRD-KO, $n=6$ animals, 11 cells. $^{*}p<0.05$. (**C**) Input/output function measured as the EPSP amplitude as a function of stimulus intensity also is increased in *Ptprd-/-* compared to *Ptprd*+/+ and *Ptprd*+/- mice. PTPRD-WT, $n=3$ animals, 6 cells; PTPRD-HET, $n=5$ animals, 9 cells; PTPRD-KO, $n=5$ animals, 7 cells. (**D**) Paired-pulse responses superimposed after subtraction of the first pulse at 10, 30, 70, 100, and 300 ms interstimulus intervals (ISI) are similar between genotyping. PTPRD-WT, $n=4$ animals, 6 cells; PTPRD-HET, $n=6$ animals, 8 cells; PTPRD-KO, $n=5$ animals, 8 cells. (**E**) Short-term synaptic responses (top) and normalized summary data (bottom) evoked by a burst of 25 stimuli at 14 Hz are also similar between genotyping. PTPRD-WT, $n=3$ animals, 6 cells; PTPRD-HET, $n=4$ animals, 8 cells; PTPRD-KO, $n=4$ animals, 9 cells. (**F**) AMPA/NMDA ratio shows no significant differences between genotyping. PTPRD-WT, $n=3$ animals, 6 cells; PTPRD-HET, $n=3$ animals, 8 cells; PTPRD-KO, $n=5$ animals, 14 cells. In all graphs, the error bars denote SEMs

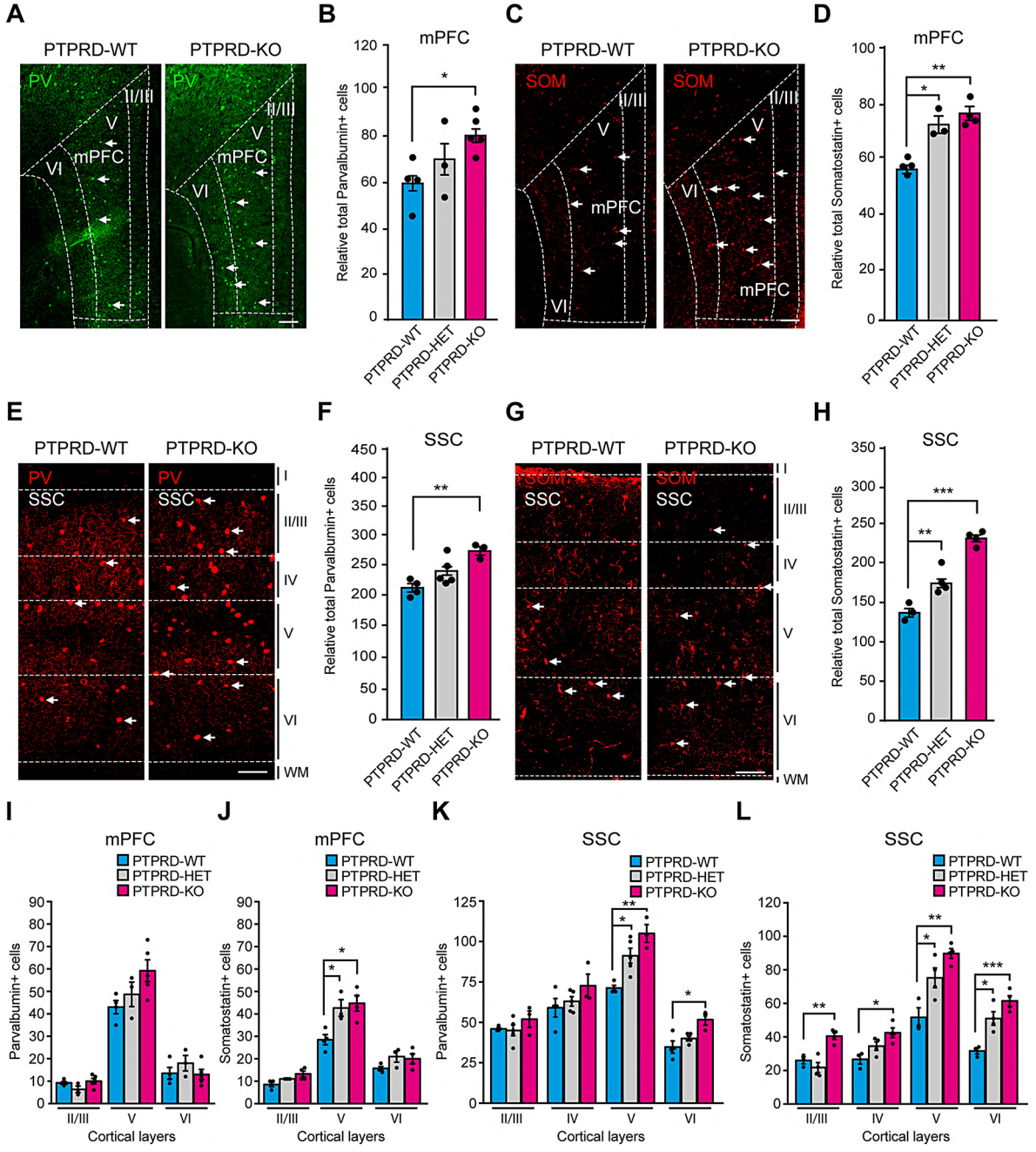


Fig. 3 *Ptprd+/- or Ptprd-/-* mice show an increase of GABAergic neurons in the mPFC and somatosensory cortex at 3 months. (**A-H**) Coronal sections of the mPFC or somatosensory cortex of *Ptprd*+/+ (PTPRD-WT) and *Ptprd-/-* (PTPRD-KO) 3-month-old animals were immunostained against parvalbumin (**A, E**) or somatostatin (**C, G**). Relative total parvalbumin-positive cells in the mPFC **(**for **B**, PTPRD-WT, $n=4$; PTPRD-HET, $n=3$; PTPRD-KO, $n=5$**)** or somatosensory cortex **(**for **F**, PTPRD-WT, $n=4$; PTPRD-HET, $n=5$; PTPRD-KO, $n=3$**)** of *Ptprd*+/+, *Ptprd*+/- (PTPRD-HET), and *Ptprd-/-* 3-month-old mice. Relative total of somatostatin-positive cells (arrows head) in the mPFC **(**for **D**, PTPRD-WT, $n=4$; PTPRD-HET, $n=3$; PTPRD-KO, $n=4$**)** or somatosensory cortex **(**for **H**, PTPRD-WT, $n=3$; PTPRD-HET, $n=4$; PTPRD-KO, $n=4$**)** of *Ptprd*+/+, *Ptprd*+/- and *Ptprd-/-* 3-month-old mice. In (**A**) and (**C**), the dotted line shows mPFC and specific cortical layers. **(I, J)** Parvalbumin (**I**) or Somatostatin (**J**) positive neurons were quantified per cortical layers II/III, V and VI in the mPFC. **(K, L)** Parvalbumin (**K**) or Somatostatin (**L**) positive neurons were quantified per cortical layers II/III, IV, V and VI in the somatosensory cortex. mPFC = medial prefrontal cortex. SSC = somatosensory cortex. PV = parvalbumin. SOM = somatostatin. WM = white matter. In all the images, scale bars represent 200 µm, and arrows show positive cells. *$p<0.05$; **$p<0.01$; ***$p<0.001$. In all graphs, the error bars denote SEMs

we immunostained for parvalbumin (Fig. 3E) and somatostatin (Fig. 3G) at the somatosensory cortex. Quantification showed that *Ptprd-/-* mice had more parvalbumin- (Fig. 3F) and somatostatin-positive neurons (Fig. 3H). In addition, *Ptprd* heterozygous mice had more somatostatin-positive neurons (Fig. 3H), indicating that GABAergic neurons are increased in the cortex of 3-month-old *Ptprd-/-* mice.

We then evaluated the number of inhibitory neurons per layer. We found no differences in the number of parvalbumin-positive neurons in the mPFC per layer across genotypes (Fig. 3I). However, when we analyzed the somatostatin-positive neurons, we found that they were increased specifically in the mPFC layer V of 3-month-old *Ptprd+/-* or *Ptprd-/-* compared to *Ptprd+/+* mice (Fig. 3J). Next, we performed a similar analysis in the somatosensory cortex and found that parvalbumin-positive neurons were specifically increased in layers V and VI (Fig. 3K). For somatostatin-positive neurons, the increase was observed in all cortical layers in the somatosensory cortex of 3-month-old *Ptprd-/-* compared to *Ptprd+/+* mice, except for cortical layers V and VI, where *Ptprd+/-* mice also had more somatostatin-positive neurons compared to *Ptprd+/+* mice (Fig. 3L).

As the increase in glutamatergic neurons was coupled with increase synaptic activity, we evaluated whether the increase in GABAergic neurons observed in *Ptprd-/-* mice was associated with an increase in inhibitory synaptic transmission by recording spontaneous inhibitory synaptic currents. As we found with excitatory synaptic transmission (Fig. 2), we observed an increase in the frequency but not amplitude of spontaneous inhibitory synaptic currents (sIPSCs) in *Ptprd-/-* but not *Ptprd+/-* mice when compared to *Ptprd+/+* littermates (Fig. 4A). Similarly, there was an increase in the frequency but not amplitude of miniature synaptic currents (mIPSCs) in *Ptprd-/-* mice (Fig. 4B). Next, we evaluated evoked inhibitory input-output curves and found an enhancement in evoked IPSCs in *Ptprd-/-* compared to *Ptprd+/+* mice (Fig. 4C), suggesting an increase in GABAergic synaptic transmission. To further evaluate the effect of the PTPRD ablation on GABAergic synaptic function, we measured PPR and use-dependent depression and found that both PPR and synaptic depression in response to a stimulus train of 20 stimuli at 10 Hz remained unchanged between genotypes (Fig. 4D, E), indicating that the increase in GABAergic function is independent of changes in release probability.

Finally, we tested whether the enhanced excitatory and inhibitory inputs onto layer 2/3 pyramidal neurons in *Ptprd-/-* mice altered the excitatory/inhibitory balance of these neurons. We recorded simultaneously evoked EPSC and IPSCs by holding pyramidal neurons at −35 mV and found no significant differences in the excitation/inhibitory ratio among genotypes (Fig. 4F), indicating that the increase in synaptic function observed in *Ptprd-/-* mice does not alter the excitatory/inhibitory balance in the mPFC.

Ptprd+/- or *Ptprd-/-* mice do not show impairments in learning and memory or increased anxiety

Mutation or aberrant expression of genes associated with neuroanatomical alterations are thought to have profound consequences in adulthood as they affect the connectivity between neurons, promoting brain disorders [5]. As *PTPRD* mutations have been associated with brain disorders that include cognitive impairments, we evaluated whether *Ptprd+/-* or *Ptprd-/-* mice have learning and memory deficits by performing the Morris Water Maze test. We found that *Ptprd-/-* or *Ptprd+/-* exhibited normal latency escape (Fig. 5A). Also, they showed normal time spent (Fig. 5B) and distance (Fig. 5C) in the target quadrant as well as in the time spent (Fig. 5D) and distance (Fig. 5E) in the area where the platform was located compared to *Ptprd+/+ mice*. To confirm these observations, we performed the Y-maze test, and found that *Ptprd+/-* or *Ptprd-/-* mice showed no difference in the percentage of spontaneous alternation preference as compared to *Ptprd+/+* animals (Fig. 5F). These results indicate that *Ptprd+/-* or *Ptprd-/-* mice do not present with spatial learning and memory deficits.

As individuals with *PTPRD* variants exhibit anxiety [38] we evaluated if *Ptprd+/-* or *Ptprd-/-* mice showed increased anxiety using the open-field and elevated plus maze tests [26, 39]. In the open field test, we observed no differences between *Ptprd+/-* or *Ptprd-/-* and *Ptprd+/+* animals in the time spent in the central zone (Fig. 6A) and the number of times that mice entered this area (Fig. 6B). In addition, none of the animal groups presented differences in the distance covered, indicating that the mice did not have motor deficits (Fig. 6C). In the elevated plus maze test, there were no differences between genotypes in terms of the percentage of time spent in the open (Fig. 6D) and closed arms (Fig. 6E) or in the number of entries to these arms (Fig. 6F, G). Together, these results suggest that losing one or both alleles of *Ptprd* does not result in learning and memory impairment or aberrant anxious behavior.

Ptprd+/- or *Ptprd-/-* mice exhibit autistic-like behaviors

PTPRD variants have also been associated with ASD [40–43]. Therefore we asked whether the loss of one or both *Ptprd-/-* alleles induces autistic-like behaviors. To address this, we evaluated social behavior using the three-chamber test for social interaction and novelty [44]. In this test, wild-type rodents prefer to spend more time with another rodent (sociability) and will investigate a novel intruder more than a familiar one (social novelty).

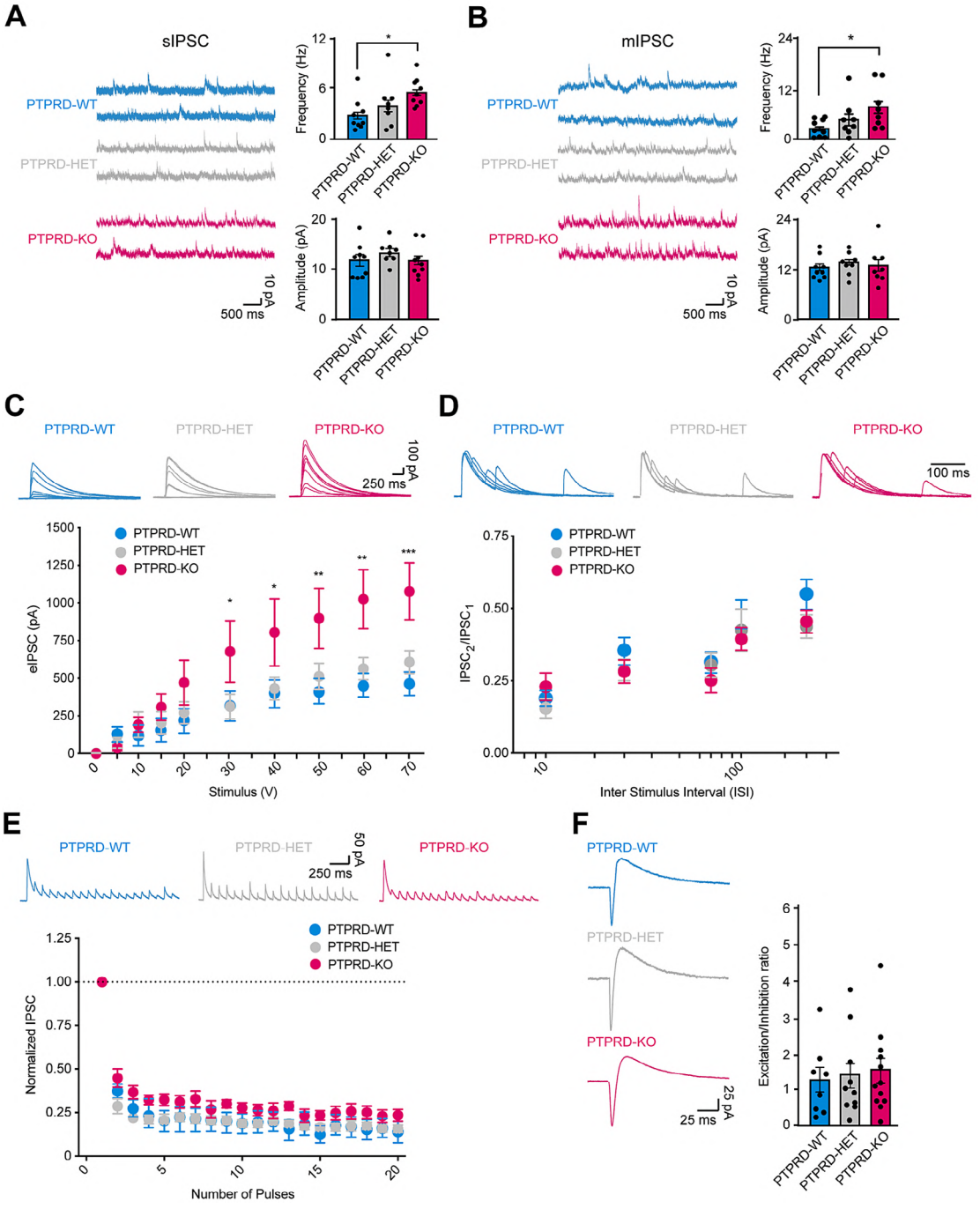


Fig. 4 Inhibitory synaptic transmission in layer 2/3 of the mPFC is impaired in the *Ptprd-/-* mice. (**A**) Representative traces (left) and quantitative analysis (right) of sIPSC activity recorded from layer 2/3 pyramidal neurons in the mPFC in *Ptprd+/+* (PTPRD-WT), *Ptprd+/-* (PTPRD-HET), and *Ptprd-/-* (PTPRD-KO). PTPRD-WT, $n=5$ animals, 9 cells; PTPRD-HET, $n=6$ animals, 8 cells; PTPRD-KO, $n=4$ animals, 9 cells. *$p<0.05$. (**B**) Representative traces (left) and quantitative analysis (right) of mIPSC activity recorded from layer 2/3 pyramidal neurons in the mPFC in *Ptprd+/+* (PTPRD-WT), *Ptprd+/-* (PTPRD-HET), and *Ptprd-/-* (PTPRD-KO). PTPRD-WT, $n=4$ animals, 9 cells; PTPRD-HET, $n=4$ animals, 8 cells; PTPRD-KO, $n=4$ animals, 8 cells. *$p<0.05$. (**C**) Evoked IPSC amplitudes as a function of stimulus intensity plotted as input/output curves show an increase in *Ptprd-/-* compared to *Ptprd+/+* and *Ptprd+/-* mice. Significant changes between *Ptprd+/+* and *Ptprd-/-* groups are as "*". *$p<0.05$, **$p<0.01$, and ***$p<0.001$. PTPRD-WT, $n=4$ animals, 7 cells; PTPRD-HET, $n=5$ animals, 9 cells; PTPRD-KO, $n=4$ animals, 8 cells. (**D**) Paired-pulse responses at 10, 30, 70, 100, and 300 ms interstimulus intervals (ISI) are similar between genotyping. PTPRD-WT, $n=4$ animals, 6 cells; PTPRD-HET, $n=4$ animals, 6 cells; PTPRD-KO, $n=5$ animals, 8 cells. (**E**) Short-term synaptic responses (top) and normalized summary data (bottom) evoked by a burst of 20 stimuli at 10 Hz are also similar between genotyping. PTPRD-WT, $n=4$ animals, 7 cells; PTPRD-HET, $n=6$ animals, 10 cells; PTPRD-KO, $n=4$ animals, 7 cells. (**F**) Excitatory and inhibitory balances show no significant differences between genotyping. PTPRD-WT, $n=4$ animals, 8 cells; PTPRD-HET, $n=4$ animals, 10 cells; PTPRD-KO, $n=5$ animals, 12 cells. In all graphs, the error bars denote SEMs

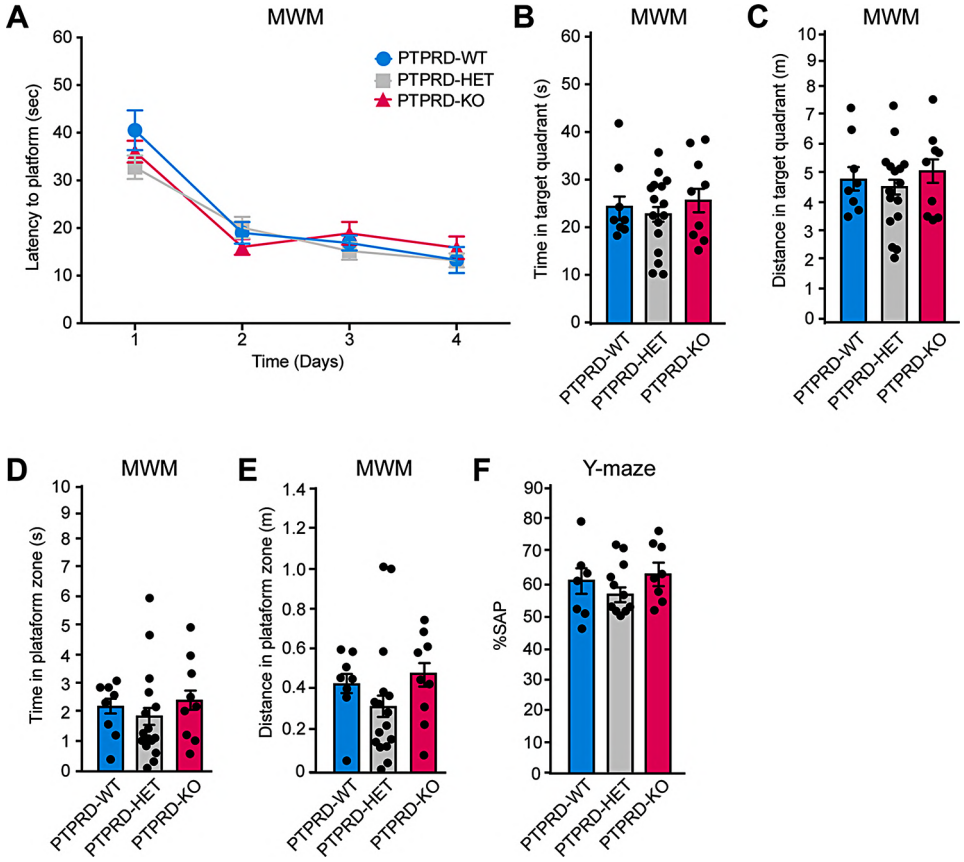


Fig. 5 Heterozygous or homozygous *Ptprd* mice showed no learning and memory deficits. (**A-E**) 3-month-old *Ptprd*+/+ (PTPRD-WT), *Ptprd*+/- (PTPRD-HET), and *Ptprd-/-* (PTPRD-KO) mice were tested in the Morris water maze (MWM) test. **(A)** Latency escape during the 4 training days. **(B)** Time spent by the animals swimming in the target quadrant area on test day (day 5). **(C)** Distance traveled in the target quadrant zone on test day. **(D)** Time spent by the animals swimming in the platform area on test day. **(E)** Distance traveled in the platform zone on test day. PTPRD-WT, $n=8$; PTPRD-HET, $n=16$; PTPRD-KO, $n=9$. **(F)** 3-month-old *Ptprd*+/+, *Ptprd*+/-, and *Ptprd-/-* mice were tested in the Y-maze test. Percentage of preference for spontaneous alternations (SAP). PTPRD-WT, $n=6$; PTPRD-HET, $n=11$; PTPRD-KO, $n=8$. In all graphs, the error bars denote SEMs

To evaluate the sociability of *Ptprd-/-* mice, they were placed in a context where they could interact with a caged mouse or an inanimate object, each in a different chamber. We observed that *Ptprd-/-* or *Ptprd*+/- mice, unlike *Ptprd*+/+ animals, did not show a preference to spend more time exploring the chamber containing the caged mouse, indicating a social deficit (Fig. 7A). The inanimate object was then replaced by another mouse (new mouse) and the caged mouse was kept in the same chamber (old mouse). *Ptprd-/-* or *Ptprd*+/- mice did not discriminate between the old and new mouse, indicating a deficit in social novelty compared to *Ptprd*+/+ mice (Fig. 7B).

Next, we evaluated repetitive and stereotyped behaviors. Self-grooming behavior is often altered in mouse models of ASD [45]. Thus, we recorded mice from below through a transparent box to allow the visualization and further analysis of self-grooming. *Ptprd-/-* mice increased their time self-grooming as compared to *Ptprd*+/+ mice (Fig. 7C). Finally, we used the marble burying test, a test widely used to assess repetitive behavior in mouse models of compulsive disorder and ASD [46, 47]. The test assesses the percentage of marbles that mice bury in 30 min, which indirectly reflects the degree of repetitive digging behavior. We found that *Ptprd-/-* or *Ptprd*+/- mice showed a significant increase in buried marbles as compared to *Ptprd*+/+ mice (Fig. 7D). Therefore, our behavioral results suggest that loss of one or both *Ptprd* alleles induces autistic-like behaviors.

Discussion

Here, we analyzed how loss of *Ptprd* expression impacts the generation of glutamatergic and GABAergic neurons and synaptic transmission in the cerebral cortex, potentially contributing to the emergence of behavioral impairments in adulthood. Mutations or aberrant expression of this gene have previously been associated with various neurodevelopmental disorders such as obsessive-compulsive disorder, schizophrenia, and ASD [14]. In this regard, we reported that *Ptprd* is a key regulator of mouse embryonic neurogenesis, controlling the numbers of neurogenic intermediate progenitor cells and, ultimately, the number of neonatal cortical neurons [11,

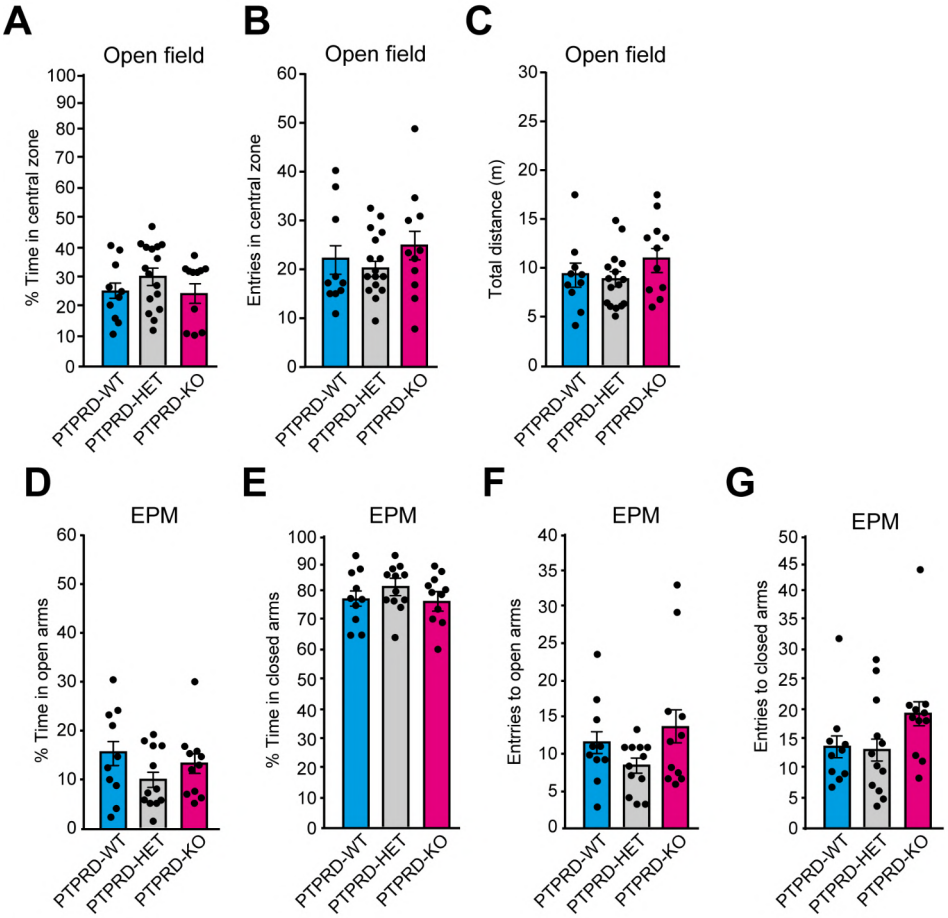


Fig. 6 Loss of one or both *Ptprd* alleles does not induce anxious behavior. (**A-C**) 3-month-old *Ptprd*+/+ (PTPRD-WT), *Ptprd*+/- (PTPRD-HET), and *Ptprd*-/- (PTPRD-KO) mice were tested in open-field anxiety test. **(A)** Percentage of the total time that the mice spent in the central zone. (**B**) Number of times that the animals enter the central zone. (**C**) Total distance traveled. PTPRD-WT, $n = 10$; PTPRD-HET, $n = 16$; PTPRD-KO, $n = 11$. (**D-G**) 3-month-old *Ptprd*+/+, *Ptprd*+/-, and *Ptprd*-/- mice were tested in the elevated plus maze test (EPM). (**D**) Percentage of the total time spent in open arms. (**E**) Percentage of the total time spent in closed arms. **(F)** Number of times that the animals enter the open arms. (**G**) Number of times that the animals enter the closed arms. PTPRD-WT, $n = 10$; PTPRD-HET, $n = 12$; PTPRD-KO, $n = 11$. In all graphs, the error bars denote SEMs

12]. Here, we found that the developmental increase of excitatory neurons persisted through adulthood, affecting excitatory synaptic function in the mPFC. Moreover, loss of *Ptprd* expression resulted in an increase in inhibitory GABAergic neurons and inhibitory synaptic function. Finally, adult *Ptprd-/-* mice displayed autistic-like behaviors, suggesting that ablation of *Ptprd* not only influences the number and function of cortical neurons but also behavior.

What accounts for the increase in glutamatergic neurons in adult *Ptprd-/-* mice? We propose that it is directly related to the increase in Tbr2-positive intermediate precursor cells in these mice during embryogenesis that we previously reported [11, 12]. There is abundant evidence that ASD-associated genes exhibit cell cycle changes in neural precursor cells during brain development, culminating in an alteration in the total number of glutamatergic neurons [48]. For example, Fang et al. [33], reported that the increase in Tbr2-positive intermediate precursors that in turn produces increased amounts of glutamatergic neurons, was sufficient to elicit alterations in synaptic function, interneuron mislocalization, and the appearance of ASD-like behaviors. The genes affected in animal models of ASD in which the number of Tbr2-positive cells is increased are many [48]. Therefore, given that the pathophysiological mechanisms that trigger the onset of ASD-like behaviors include alterations in the production of glutamatergic neurons [33, 48] like those observed in the mPFC and somatosensory cortex of *Ptprd*+/- or *Ptprd-/-* mice, this could, at least in part, explain the ASD-like behavior in these animals.

Ptprd participates both as an adhesion molecule promoting synaptic formation and differentiation, and a phosphatase regulating the activity of receptors involved in synaptic transmission such as TrkB [14]. The role of Ptprd in synaptic function in cultured hippocampal neurons is conflicting, as the absence of *Ptprd* has been reported to either not alter synaptic formation or

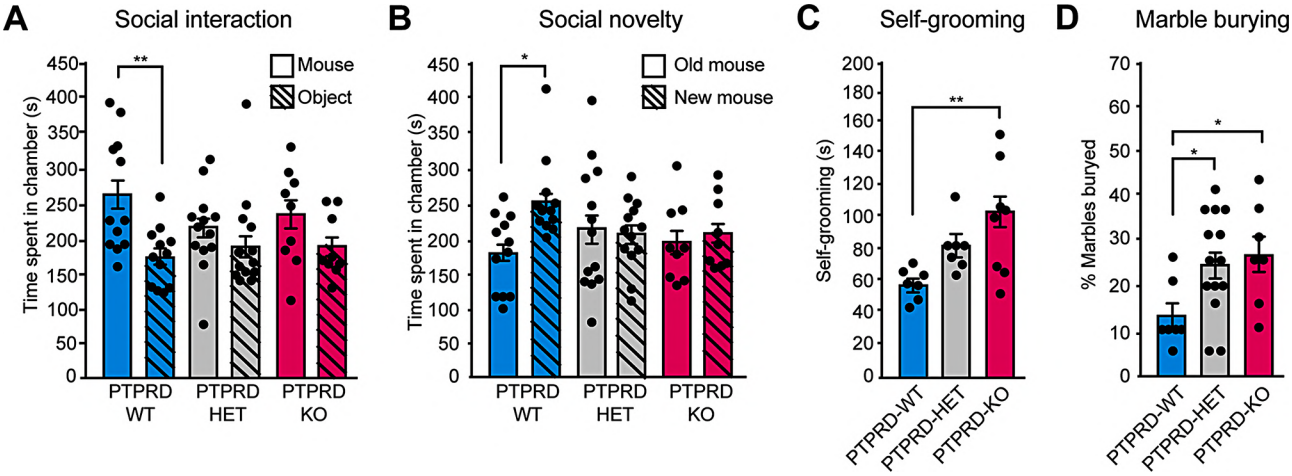


Fig. 7 *Ptprd*+/- or *Ptprd*-/-mice showed autistic-like behaviors. (**A-D**) 3-month-old *Ptprd*+/+ (PTPRD-WT), *Ptprd*+/- (PTPRD-HET), and *Ptprd*-/- (PTPRD-KO) mice were tested for sociability (**A**) and social novelty (**B**), self-grooming (**C**) or marble burying (**D**). (**A**) Social Interaction Test was measured in the three-chamber test. The graph shows the cumulative duration of *Ptprd*+/+, *Ptprd*+/-, and *Ptprd*-/- mice in the mouse or object chambers. PTPRD-WT, $n=12$; PTPRD-HET, $n=13$; PTPRD-KO, $n=9$. (**B**) Social Novelty Test was assessed in the three-chamber test. The graph shows the cumulative duration of *Ptprd*+/+, *Ptprd*+/-, and *Ptprd*-/- mice in the old mouse and new mouse chambers. PTPRD-WT, $n=12$; PTPRD-HET, $n=13$; PTPRD-KO, $n=9$. *$p<0.05$; **$p<0.01$. **(C, D)** Repetitive behavior was evaluated by the time spent in spontaneous self-grooming **(C)** or marble-burying behaviors (**D**). (**C**) Cumulative time in which *Ptprd*+/+, *Ptprd*+/-, and *Ptprd*-/- mice did self-grooming behavior in a total of 10 min. PTPRD-WT, $n=7$; PTPRD-HET, $n=7$; PTPRD-KO, $n=8$. (**D**) Percentage of marbles buried by *Ptprd*+/+, *Ptprd*+/-, and *Ptprd*-/- mice after 30 min. PTPRD-WT, $n=7$; PTPRD-HET, $n=14$; PTPRD-KO, $n=7$. *$p<0.05$; **$p<0.01$. In all graphs, the error bars denote SEMs

transmission [18, 19] or decrease excitatory synaptic transmission [17]. Our results obtained in acute mPFC slices from adult *Ptprd*-/- mice indicate an increase in both excitatory and inhibitory synaptic activity. While this increase was not due to changes in the number of postsynaptic receptors or release probability, it is possible that these differences could be due to increased number of synaptic contacts in the *Ptprd*-/- mPFC.

Ptprd+/- or *Ptprd*-/- mice showed autistic-like behaviors. ASD is characterized by social deficits and repetitive behavior [49]. Consistent with this idea, *Ptprd*+/- or *Ptprd*-/- mice present deficits in sociability with a conspecific and the preference for interaction with a new individual, supporting findings of mutations in *PTPRD* linked to ASD risk [40–43]. Moreover, *Ptprd*-/- mice have increased self-grooming and marble-burying behavior, core symptoms of ASD. However, our findings do differ from those reported by Ho et al. [50] that did not report changes in the time invested in self-grooming. These differences likely reflect the different experimental paradigms used. We evaluated instinctively self-grooming behavior without stimuli to promote it. Ho et al. [50] quantified self-grooming time after spraying the animals with a sucrose solution to encourage the indicated behavior. We propose that artificially stimulating self-grooming could mask normal behavior in *Ptprd*+/+ animals. We also evaluated the number of the marbles buried that represents the occurrence of repetitive behavior, while Ho et al. [50] evaluated the time and number of times the experimental animals spent performing the digging process. While the experimental paradigms used by both groups are valid, our findings of increased repetitive behavior in the *Ptprd*-/- mice do indeed indicate that they exhibit ASD-like behavior.

Uetani et al. [51] and Drgonova et al. [52] reported impairments of spatial learning and memory in *Ptprd*-/- mice which we did not observe. While the Uetani et al. [51], Drgonova et al. [52], and our mice were in the same C57BL/6J genetic background, there were evident differences in the mouse models. The mice of those groups showed growth retardation and weight loss attributed to problems in food intake. While their *Ptprd*-/- mice lived for approximately one year, our animals aged normally. To confirm the lack of spatial learning and memory impairments, we also evaluated our animals in the Y-maze test, which showed no cognitive deficits associated with learning and memory. Our findings regarding the lack of anxious behavior in *Ptprd*-/- mice were similar to the results reported by Park et al. [17] and Ho et al. [50], who used the same *Ptprd*-/- model as that by Uetani et al. [51] and Drgonova et al. [52]. The findings will need to be resolved in future studies with neural precursor specific knockouts of *Ptprd*.

Conclusions

Our data, together with previous findings [11, 12], show that several phenotypic features normally associated with ASD were present in mice lacking *Ptprd*, including deficits in neural precursor cell proliferation, increased neurogenesis, neuronal mislocalization [48, 53], alterations

in the number and function of glutamatergic and GABAergic neurons [54], and social deficits and repetitive behavior [55]. These findings lead us to propose that the absence of *Ptprd* expression disrupts the generation and functioning of glutamatergic and GABAergic cortical neurons, inducing the appearance of ASD-like behavior in adulthood in mice. Our results suggest a possible explanation for why variants in *PTPRD* result in brain disorders.

Acknowledgements
We thank the technical support of Jessica Molina, Sebastián Bondi, María Beatriz Lazen, Ale Frene, Gloria Lucero, and Luis Lopez.

Authors' contributions
BIC, MIA, GIC and FC performed the neuroanatomical studies and their analyzes. RCM, AEC and CAG performed the electrophysiological experiments and their analyses. PRM, GIC, BIC, NA and HT performed the behavioral experiments and their analyzes. ANP, AEC, PRM, DRK and GIC conceptualized all the experiments, analyzed the data, and wrote the manuscript. All authors participated in the writing of the manuscript. All authors read and approved the final manuscript.

Funding
This work was supported by the research grants ANID-FONDECYT Regular 1201848 (to AEC), 1210507 (to GIC), and 1231012 (to PRM); ANID-FONDECYT Iniciación 11220708 (to FC); ANID-FONDECYT postdoctorado grant 3190793 (to RCM); CIHR to DRK, and ANID-FONDEQUIP (EQM160154 to AEC). CAG was supported by a Ph.D. fellowship from ANID 21201603.

Data availability
The datasets used and/or analyzed during the current study are available from the corresponding author on reasonable request.

Declarations

Ethics approval and consent to participate
Animal use was approved by Universidad Mayor, Universidad de Valparaiso, and Pontificia Universidad Católica de Chile Bioethics and Animal Care Committees in accordance with the bioethics regulation of the Chilean Research Council (ANID).

Consent for publication
Not applicable.

Competing interests
The authors declare that they have no competing interests.

Author details
[1]Laboratorio de Neurobiología, Facultad de Ciencias Biológicas, Pontificia Universidad Católica de Chile, Santiago 8331150, Chile
[2]Centro Interdisciplinario de Neurociencia de Valparaíso (CINV), Facultad de Ciencias, Universidad de Valparaíso, Valparaíso 2340000, Chile
[3]Programa de Doctorado en Ciencias mención Neurociencias, Facultad de Ciencias, Universidad de Valparaíso, Valparaíso 2340000, Chile
[4]Program in Neuroscience and Mental Health, The Hospital for Sick Children, Toronto M5G 1X8, Canada
[5]Department of Molecular Genetics, University of Toronto, Toronto M5S 1X8, Canada
[6]Center for Integrative Biology, Facultad de Ciencias, Universidad Mayor, Santiago 8580745, Chile
[7]Cell Physiology Laboratory, Biology Department, Faculty of Science, Universidad de Chile, Santiago 7800003, Chile
[8]Centro de Estudios Traslacionales en Estrés y Salud Mental (C-ESTRES), Universidad de Valparaíso, Valparaíso 2340000, Chile
[9]Instituto de Fisiología, Facultad de Ciencias, Universidad de Valparaíso, Valparaíso 2340000, Chile
[10]Instituto de Neurociencias, Facultad de Ciencias, Universidad de Valparaíso, Valparaíso 2340000, Chile
[11]Ludna Biotech Co., Ltd, Suita, Osaka 565-0871, Japan

Received: 7 March 2024 / Accepted: 7 June 2024
Published online: 18 June 2024

References

1. Lodato S, Arlotta P. Generating neuronal diversity in the mammalian cerebral cortex. Annu Rev Cell Dev Biol. 2015;31:699–720.
2. Lim L, Llorca A, Marín O. Development and functional diversification of Cortical Interneurons. Neuron. 2018;100(2):294–313.
3. Matho KS, Huilgol D, Galbavy W, He M, Kim G, An X, et al. Genetic dissection of the glutamatergic neuron system in cerebral cortex. Nature. 2021;598(7879):182–7.
4. Sohal VS, Rubenstein JLR. Excitation-inhibition balance as a framework for investigating mechanisms in neuropsychiatric disorders. Mol Psychiatry. 2019;24(9):1248–57.
5. Juric-Sekhar G, Hevner RF. Malformations of cerebral cortex development: molecules and mechanisms. Annu Rev Pathol. 2019;14:293–318.
6. Courchesne E, Gazestani VH, Lewis NE. Prenatal origins of ASD- the when, what, and how of ASD Development. Trends Neurosci. 2020;43(5):326–42.
7. Zamanpoor M. Schizophrenia in a genomic era: a review from the pathogenesis, genetic and environmental etiology to diagnosis and treatment insights. Psychiatr Genet. 2019;30(1):1–9.
8. Faraone SV, Larsson H. Genetics of attention deficit hyperactivity disorder. Mol Psychiatry. 2018;24(4):562–75.
9. Bowling KM, Thompson ML, Amaral MD, Finnila CR, Hiatt SM, Engel KL, et al. Genomic diagnosis for children with intellectual disability and / or developmental delay. Genome Med. 2017;9(1):43.
10. Gazzellone MJ, Zarrei M, Burton CL, Walker S, Uddin M, Shaheen SM, et al. Uncovering obsessive-compulsive disorder risk genes in a pediatric cohort by high-resolution analysis of copy number variation. J Neurodev Disord. 2016;8(36):1–11.
11. Tomita H, Cornejo F, Kaplan DR, Miller FD, Cancino GI, Woodard CL, et al. The Protein Tyrosine Phosphatase Receptor Delta regulates Developmental Neurogenesis Article the protein tyrosine phosphatase receptor Delta regulates Developmental Neurogenesis. Cell Rep. 2020;30(1):215–28.
12. Cornejo F, Franchini N, Cortés BI, Elgueta D, Cancino GI. Neural conditional ablation of the protein tyrosine phosphatase receptor Delta PTPRD impairs gliogenesis in the developing mouse brain cortex. Front Cell Dev Biol. 2024;12:1357862.
13. Pulido R, Serra-Pagès C, Tang M, Streuli M. The LAR/PTP delta/PTP sigma subfamily of transmembrane protein-tyrosine-phosphatases: multiple human LAR, PTP delta, and PTP Sigma isoforms are expressed in a tissue-specific manner and associate with the LAR-interacting protein LIP.1. Proc Natl Acad Sci U S A. 1995;92(25):11686–90.
14. Cornejo F, Cortés BI, Findlay GM, Cancino GI. LAR Receptor Tyrosine Phosphatase Family in healthy and diseased brain. Front Cell Dev Biol. 2021;9:659951.
15. Takahashi H, Craig AM. Protein tyrosine phosphatases PTP D, PTP s, and LAR : presynaptic hubs for synapse organization. Trends Neurosci. 2013;36(9):522–34.
16. Han KA, Ko JS, Pramanik G, Kim JY, Tabuchi K. PTPσ drives excitatory presynaptic assembly via various extracellular and intracellular mechanisms. J Neurosci. 2018;18:6700–21.
17. Park H, Choi Y, Jung H, Kim S, Lee S, Han H, et al. Splice-dependent trans-synaptic PTP d – IL 1 RAPL 1 interaction regulates synapse formation and non-REM sleep. EMBO J. 2020;39(11):e104150.
18. Sclip A, Südhof TC. LAR receptor phospho-tyrosine phosphatases regulate NMDA-receptor responses. Elife. 2020;9:e53406.
19. Han KA, Lee HY, Lim D, Shin J, Yoon TH, Liu X, et al. Receptor protein tyrosine phosphatase delta is not essential for synapse maintenance or transmission at hippocampal synapses. Mol Brain. 2020;13(1):94.
20. Cancino GI, Fatt MP, Miller FD, Kaplan DR. Conditional ablation of p63 indicates that it is essential for embryonic development of the central nervous system. Cell Cycle. 2015;14(20):3270–81.
21. George P, Keith F. In. The mouse brain in Stereotaxis coordinates. 2004. p. 71–5.
22. Delgado-Acevedo C, Estay SF, Radke AK, Sengupta A, Escobar AP, Henríquez-Belmar F, et al. Behavioral and synaptic alterations relevant to

obsessive-compulsive disorder in mice with increased EAAT3 expression. Neuropsychopharmacology. 2019;44(6):1163–73.
23. Vorhees CV, Williams MT. Morris water maze: procedures for assessing spatial and related forms of learning and memory. Nat Protoc. 2006;1(2):848–58.
24. Kraeuter AK, Guest PC, Sarnyai Z. The Y-Maze for Assessment of spatial working and reference memory in mice. Methods Mol Biol. 2019;1916:105–11.
25. Yang G, Cancino GI, Zahr SK, Guskjolen A, Voronova A, Gallagher D, et al. A Glo1-Methylglyoxal pathway that is perturbed in maternal diabetes regulates embryonic and adult neural stem cell pools in murine offspring. Cell Rep. 2016;17(4):1022–36.
26. Kraeuter AK, Guest PC, Sarnyai Z. The elevated plus maze test for measuring anxiety-like Behavior in rodents. Methods Mol Biol. 2019;1916:69–74.
27. Gallagher D, Voronova A, Zander MA, Cancino GI, Bramall A, Krause MP, et al. Article Ankrd11 is a chromatin Regulator involved in Autism that is essential for neural development. Dev Cell. 2015;32(1):31–42.
28. Moya PR, Fox MA, Jensen CL, Laporte JL, French HT, Wendland JR, et al. Altered 5-HT2C receptor agonist-induced responses and 5-HT2C receptor RNA editing in the amygdala of serotonin transporter knockout mice. BMC Pharmacol. 2011;11:3.
29. Anastasiades PG, Carter AG. Circuit organization of the rodent medial prefrontal cortex. Trends Neurosci. 2021;44(7):550–63.
30. Pittaras EC, Faure A, Leray X, Moraitopoulou E, Cressant A, Rabat AA, et al. Neuronal nicotinic receptors are crucial for tuning of E/I balance in Prelimbic Cortex and for decision-making processes. Front Psychiatry. 2016;7:171.
31. Angenstein F, Niessen HG, Goldschmidt J, Lison H, Altrock WD, Gundelfinger ED, et al. Manganese-enhanced MRI reveals structural and functional changes in the cortex of Bassoon mutant mice. Cereb Cortex. 2007;17(1):28–36.
32. Perrenoud Q, Rossier J, Férézou I, Geoffroy H, Gallopin T, Vitalis T, et al. Activation of cortical 5-HT(3) receptor-expressing interneurons induces NO mediated vasodilatations and NPY mediated vasoconstrictions. Front Neural Circuits. 2012;6:50.
33. Fang WQ, Chen WW, Jiang L, Liu K, Yung WH, Fu AKY, et al. Overproduction of Upper-Layer neurons in the Neocortex leads to autism-like features in mice. Cell Rep. 2014;9(5):1635–43.
34. Sahin M, Dowling JJ, Hockfield S. Seven protein tyrosine phosphatases are differentially expressed in the developing rat brain. J Comp Neurol. 1995;351(4):617–31.
35. Takahashi H, Katayama K, Sohya K, Miyamoto H, Prasad T, Matsumoto Y, et al. Selective control of inhibitory synapse development by Slitrk3-PTP d transsynaptic interaction. Nat Neurosci. 2012;15(3):389–98.
36. Yoshida T, Yamagata A, Imai A, Kim J, Izumi I, Mishina M, et al. Canonical versus non-canonical transsynaptic signaling of neuroligin 3 tunes development of sociality in mice. Nat Commun. 2021;12(1):1848.
37. Yim YS, Kwon Y, Nam J, In H, Lee K, Goo D et al. Slitrks control excitatory and inhibitory synapse formation with LAR receptor protein tyrosine phosphatases. Proceedings of the National Academy of Sciences. 2013;110:4057–62.
38. Li W, Chen R, Feng L, Dang X, Liu J, Chen T, et al. Genome-wide meta-analysis, functional genomics and integrative analyses implicate new risk genes and therapeutic targets for anxiety disorders. Nat Hum Behav. 2024;8(2):361–79.
39. Kraeuter AK, Guest PC, Sarnyai Z. The Open Field Test for measuring locomotor activity and Anxiety-like Behavior. Methods Mol Biol. 2019;1916:99–103.
40. Pinto D, Delaby E, Merico D, Barbosa M, Merikangas A, Klei L, et al. Convergence of genes and Cellular pathways Dysregulated in Autism Spectrum disorders. Am J Hum Genet. 2014;94(5):677–94.
41. Levy D, Ronemus M, Yamrom B, Leotta A, Kendall J, Marks S, et al. Rare De Novo and Transmitted Copy-number variation in autistic Spectrum disorders. Neuron. 2011;70(5):886–97.
42. Gai X, Xie HM, Perin JC, Takahashi N, Murphy K, Wenocur AS, et al. Rare structural variation of synapse and neurotransmission genes in autism. Mol Psychiatry. 2011;17(14):402–11.
43. Liu X, Shimada T, Otowa T, Wu YY, Kawamura Y, Tochigi M, et al. Genome-Wide Association Study of Autism Spectrum Disorder in the east Asian populations. Autism Res. 2016;9(3):340–9.
44. Moy SS, Nadler JJ, Perez A. Sociability and preference for social novelty in five inbred strains: an approach to assess autistic-like behavior in mice. Genes Brain Behav. 2004;3(4):287–302.
45. Kalueff AV, Aldridge JW, Laporte JL, Murphy DL, Tuohimaa P. Analyzing grooming microstructure in neurobehavioral experiments. Nat Protoc. 2007;2(10):2538–44.
46. Gandhi T, Lee CC. Neural mechanisms underlying repetitive behaviors in Rodent models of Autism Spectrum disorders. Front Cell Neurosci. 2021;14(59):1–44.
47. Thomas A, Burant A, Bui N, Graham D, Yuva-Paylor LA, Paylor R. Marble burying reflects a repetitive and perseverative behavior more than novelty-induced anxiety. Psychopharmacology. 2009;204(2):361–73.
48. Packer A. Neocortical neurogenesis and the etiology of Autism Spectrum Disorder. Neurosci Biobehav Rev. 2016;64:185–95.
49. Chen JA, Peñagarikano O, Belgard TG, Swarup V, Geschwind DH. The emerging picture of Autism Spectrum Disorder: Genetics and Pathology. Annu Rev Pathol. 2015;10:111–44.
50. Ho EV, Welch A, Thompson SL, Knowles JA, Dulawa SC. Mice lacking Ptprd exhibit deficits in goal- directed behavior and female-specific impairments in sensorimotor gating. PLoS ONE. 2023;18(5):e0277446.
51. Uetani N, Kato K, Ogura H, Mizuno K, Kawano K, Mikoshiba K, et al. Impaired learning with enhanced hippocampal long-term potentiation in PTPδ-deficient mice. EMBO J. 2000;19(12):2775–85.
52. Drgonova J, Walther D, Wang KJ, Hartstein GL, Lochte B, Troncoso J. Mouse model for protein tyrosine phosphatase D (PTPRD) associations with restless Leg syndrome or Willis-Ekbom Disease and Addiction: reduced expression alters Locomotion, Sleep behaviors and Cocaine-conditioned place preference. Mol Med. 2015;21(1):717–25.
53. Casanova MF. Autism as a sequence: from heterochronic germinal cell divisions to abnormalities of cell migration and cortical dysplasias. Med Hypotheses. 2014;83(1):32–8. 2014/04/13.
54. Lee E, Lee J, Kim E. Excitation / inhibition imbalance in animal models of Autism Spectrum disorders. Biol Psychiatry. 2017;81(10):838–47.
55. Takumi T, Tamada K, Hatanaka F, Nakai N, Bolton PF. Behavioral neuroscience of autism. Neurosci Biobehav Rev. 2019;110:60–76.

Publisher's Note

Springer Nature remains neutral with regard to jurisdictional claims in published maps and institutional affiliations.